Mechanics and dynamics of biopolymer networks

Chase Paul Broedersz

Printed in the Netherlands by PrintPartners Ipskamp, Enschede.
A digital version of this thesis can be obtained at *www.ubvu.vu.nl/dissertations*.

© 2011, Chase Broedersz.

Cover design: Niels Smith.

The research was performed in the section Theoretical Physics of Complex Systems at the Vrije Universiteit, Amsterdam.

vrije Universiteit amsterdam

VRIJE UNIVERSITEIT

Mechanics and dynamics of biopolymer networks

ACADEMISCH PROEFSCHRIFT

ter verkrijging van de graad Doctor aan
de Vrije Universiteit Amsterdam,
op gezag van de rector magnificus
prof.dr. L.M. Bouter,
in het openbaar te verdedigen
ten overstaan van de promotiecommissie
van de faculteit der Exacte Wetenschappen
op maandag 16 mei 2011 om 11.45 uur
in de aula van de universiteit,
De Boelelaan 1105

door

Chase Paul Broedersz

geboren te Johannesburg, Zuid-Afrika

promotor: prof.dr. F.C. MacKintosh

To Kirsten

Table of contents

1 **A material cell living in a material world** **1**

1.1 Cytoskeletal biopolymers 5

1.2 Semiflexible polymers 5

1.3 Reconstituted biopolymer networks 6

1.4 Rheology: measuring the macroscopic dynamic mechanical response of biological gels 8

1.5 Outline of this thesis 9

Bibliography 13

2 **Cross-link governed dynamics** **17**

2.1 Introduction 18

2.2 Results and discussion 21

2.3 Implications for cross-link dynamics at high stress 26

2.4 Appendix 1: Materials and methods 32

2.5 Appendix 2: Evolution equations of the CGD model 33

2.6 Acknowledgments 35

Bibliography 36

3 **Flexibly cross-linked networks** **39**

3.1 Introduction 40

3.2 Effective Medium Approach 43

3.3 The Linear medium model 44

3.3.1 Hookean Finite Extendable cross-linkers 46

3.3.2 Worm Like Chain cross-Linkers 48

3.4 Self-Consistent medium model 49

3.4.1 Continuum elastic limit 50

3.5 3D Network calculation 51

3.5.1 Semiflexible polymer networks with rigid point-like cross-links 53

3.5.2 Stiff polymer networks with highly flexible cross-links 55

3.6 Tension profiles and single cross-linker force estimate . . . 56

3.7 Implications and discussion 61

3.8 Acknowledgments 64

Bibliography 65

4 Filament length tunes elasticity in actin-filamin gels 69
4.1 Introduction 70
4.2 Materials and methods 73
  4.2.1 Proteins 73
  4.2.2 Network formation 74
  4.2.3 Characterization of f-actin length distribution 74
  4.2.4 Imaging 74
  4.2.5 Rheology 75
4.3 Results and discussion 76
  4.3.1 F-actin length distribution in the presence of gelsolin 76
  4.3.2 Microstructure of filamin-gelsolin-F-actin networks 78
  4.3.3 Linear response 78
  4.3.4 Dependence of the modulus on filament length . . . 80
  4.3.5 Nonlinear response 83
  4.3.6 Dependence of maximum stress on filament length 87
4.4 Conclusions 94
4.5 Acknowledgements 95
Bibliography 96

5 Nonlinear rheology of biopolymer gels 101
5.1 Introduction 102
5.2 Materials and methods 104
5.3 Results 105
  5.3.1 Linear mechanical response 105
  5.3.2 Nonlinear response - Strain ramp protocol 105
  5.3.3 Nonlinear response - Prestress protocol 107
  5.3.4 Protocol comparison 110
  5.3.5 Simple model 110
5.4 Discussion and implications 115
5.5 Acknowledgements 116
Bibliography 118

6 Criticality and isostaticity in fiber networks 121
6.1 Introduction 122
6.2 Model 125

6.3 Results 128
6.3.1 Elastic response 128
6.3.2 Non-affine deformations 135
6.3.3 Finite size scaling 137
6.4 Discussion and implications 141
6.5 Appendix: Counting argument for rigidity threshold . . . 142
6.6 Acknowledgments 143
Bibliography 144

7 Motors stiffen non-affine fiber networks 147
7.1 Introduction 148
7.2 The model 149
7.3 Results and discussion 152
7.3.1 Passive networks 152
7.3.2 Active networks 155
7.4 Conclusions 161
7.5 Acknowledgments 162
Bibliography 163

8 Intermediate filament networks 167
8.1 Introduction 168
8.2 Materials and methods 169
8.3 Results and discussion 170
8.4 Conclusions 178
8.5 Acknowledgements 180
Bibliography 181

Summary 185

Samenvatting 189

Acknowledgements 193

Curriculum Vitae 195

List of publications 197

1

Introduction: A material cell living in a material world

All living organisms are built up of basic units called cells. Although some organisms such as bacteria consist of only one cell, the more complex organisms consist of a large number of varied cells, differentiated to perform specific vital functions. Even if we single out biological functions of a mechanical nature, the main function of cells is highly diverse; certain cells provide structural support (e.g., epithelial cells), others generate forces (e.g., muscle cells) and yet others are highly mobile such as the white blood cells of the immune system that track down and eliminate pathogens.

The mechanical properties of animal and plant cells are largely due to their cytoskeleton, an assembly of networks of various biopolymers and associated regulatory proteins [1], as illustrated in Fig. 1.1. The cytoskeleton plays a central role in various biological functions, ranging from forming the machinery for intercellular transport of cargo to the spatial and temporal organization of the cell on a wide range of length- and timescales. Here we focus on its mechanical function: the fibrous networks of the cytoskeleton form a scaffold that protects the structural integrity of the cell by resisting both internal and external stresses. Frequently, however, the cell has to adapt its shape or move around, requiring the cytoskeleton to generate forces and to remodel its structure dynamically. Over billions of years of evolution, this has resulted in a finely tunable network structure, controlled by the varying expression of hundreds of different regulatory proteins.

When considering the structural and mechanical properties of the cellular cytoskeleton, it is extremely useful to take a physical perspective and view it as a *material* [2–9]. We take this approach in this thesis and investigate the materials properties of various cytoskeletal networks as well as the extracellular matrix, a biopolymer network that forms a major component of the connective tissue surrounding cells. Biopolymer networks are highly disordered assemblies of a large number of components, and although the behavior of the individual constituents is understood in some cases, a comprehensive theoretical description of their collective behavior remains a formidable challenge.

What makes biopolymer networks particularly intriguing—apart from their biological relevance—is that they are fundamentally different from most other common materials. First of all, they are part of a living, active system. This is reflected, for example, through the action of motor proteins; fueled by chemical energy, they generate forces that drive the cytoskeleton away from thermal equilibrium [10–14]. Despite some recent theoretical progress [15–17], only little is understood theoretically of such out-of-equilibrium behavior. In chapter 7 of this thesis we discuss the effects of force-generating molecular motors on the mechanics of biopolymer networks.

A second important aspect of biopolymer networks is that the relevant interaction energies that hold the material together and preserve its shape are small and often comparable in magnitude to the thermal energy in the system. As a result, thermal fluctuations play an important role and mechanical interactions and entropic

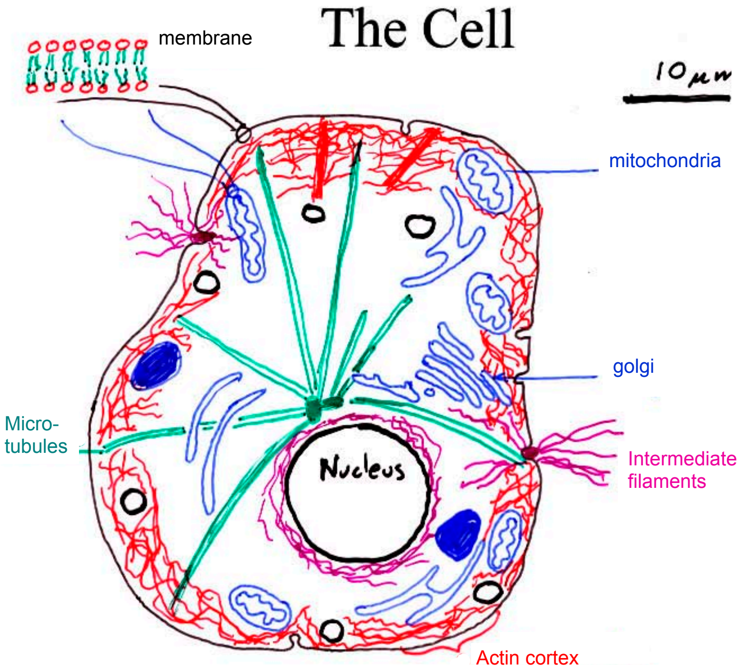
The Cell
membrane
10 μm
mitochondria
golgi
Micro-
tubules
Nucleus
Intermediate
filaments
Actin cortex

Figure 1.1 – Schematic of the eukaryotic cell highlighting the cytoskeleton, which contains three families of filaments, including filamentous actin (F-actin), intermediate filaments and microtubules along with various binding proteins for force generation, cross-linking and polymer growth regulation. The cytoskeleton largely controls the mechanical response and locomotion of living cells. Courtesy of Fred MacKintosh (Vrije Universiteit Amsterdam).

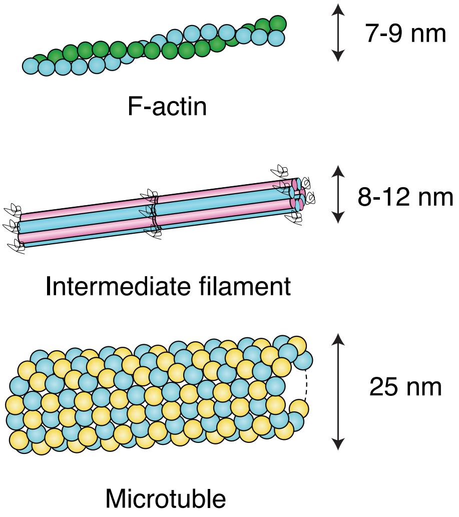

Figure 1.2 – (Color online) The three families of cytoskeletal filaments, including F-actin, intermediate filaments and microtubules.

effects often compete, resulting in a rich and finely tunable mechanical and dynamical network behavior. In this respect, cells and their cytoskeletal networks are *soft* materials [18] that only weakly resist deformation. Nonetheless, they exhibit numerous unique properties that contrast them with other soft materials such as foams, granular matter, synthetic polymer gels and emulsions. One striking example that will appear throughout this thesis is their dramatic stiffening under deformation [19–28]; even under small relative deformations of 10-50 percent, their elastic stiffness can increase dramatically, in some cases reaching stiffnesses a thousand times larger than their stiffness at small deformations.

These and other aspects lead to unusual materials behavior, as borne out by numerous experimental studies on reconstituted biopolymer networks (see section 1.3). Such *in vitro* biological gels form simplified modules of the cytoskeleton and the extracellular matrix. The study of these *in vitro* systems is very important since they facilitate a systematic and quantitative characterization of cytoskeletal networks. Such studies provide insight into the basic physical principles that govern the mechanical behavior of these systems, which may help elucidate their biological function and may inspire the development of novel biomemetic materials.

1.1 Cytoskeletal biopolymers

The main structural components of the cytoskeleton are fibrous networks consisting of three families of filaments: microtubules, filamentous actin (F-actin) and intermediate filaments (Fig. 1.2). These families of filaments fulfill distinct biological functions and most regulatory proteins are specific to a particular type of filament. From a physical point of view, the main differences between the different families of filaments are their dimensions and mechanical response (Table 1.1). The bending rigidity κ of these biopolymers is high compared to most synthetic polymers. Nonetheless, thermal fluctuations are capable of exciting weak, yet significant undulations in most biopolymers, such as F-actin and intermediate filaments. Comparing the bending rigidity κ to the thermal energy scale $k_{\mathrm{B}}T$ gives a lengthscale $\ell_p = \kappa / k_{\mathrm{B}}T$, where k_{B} is Boltzmann's constant and T is the temperature; this *persistence length* represents the distance measured along the filament over which the bending rigidity is sufficiently large to resist thermal fluctuations and keep the filament straight. More specifically, ℓ_p is the decay length of the angular correlations of a thermally fluctuating polymer. The persistence lengths of various biopolymers are listed in Table 1.1. An important aspect setting biopolymers apart from most synthetic polymers is that their persistence length is often comparable or larger than the relevant lengthscale on which the polymer is considered, such as its contour length or the cross-linking lengthscale of the network in which they are embedded. Such polymers are said to be *semiflexible*.

1.2 Semiflexible polymers

The minimal model for an inextensible semiflexible polymer is the worm-like chain (WLC) model [29–31]. In this model the filamentous protein structure is coarse-grained to a continuous space curve $\mathbf{r}(s)$ along the arc length s. The WLC Hamiltonian that captures the bending energy of a polymer of length L is given by

$$H_{\mathrm{WLC}} = \frac{\kappa}{2} \int_0^L \mathrm{d}s \left(\frac{\partial^2 \mathbf{r}}{\partial s^2} \right)^2 . \tag{1.1}$$

Thermal energy can excite Brownian undulations in a semiflexible polymer with a typical amplitude $\sim L/\ell_p^3$ [31]; this leads to a contraction of the polymer. A thermally contracted polymer can be extended by applying a tensile force, f, that stretches out these fluctuations. However, since such an extended state is entropically less favorable, the polymer will resist extensional deformations similar to a spring with an effective spring constant $\sim k_{\mathrm{B}}T\ell_p^2/L^4$ [31]. However, when the relative extension exceeds values $\sim L/\ell_p$, typically on the order of tens of percents, the system no longer responds as a simple Hookean spring. Instead the differential stiffness of

Table 1.1 – Persistence lengths and dimensions of various biopolymers [28, 32–35].

Type	approximate diameter	persistence length	contour length
Microtubule	25 nm	$\sim 1-5$ mm	10s of μm
F-actin	7 nm	17 μm	$\lesssim 20$ μm
Intermediate filament	9 nm	$0.2-1$ μm	$2-10$ μm
DNA	2 nm	50 nm	$\lesssim 1$ m

the polymer increases strongly with the applied forces as $f^{3/2}$ [19]. This entropic stiffening is the origin of the nonlinear stiffening response of cross-linked F-actin networks [19, 20], and in chapter 8 we provide evidence that intermediate filament networks cross-linked by divalent ions stiffen through a similar mechanism. Another interesting aspect of semiflexible polymers is their highly anisotropic response to a force. The ratio between the transverse and longitudinal spring constants is $\frac{L}{90\ell_p} \ll 1$.

Although the single-filament properties are fairly well understood, the behavior of entangled solutions and cross-linked networks of semiflexible polymers still remains to pose a significant theoretical challenge. Biopolymers provide an excellent experimental model system to study the behavior of semiflexible polymers and their networks.

1.3 Reconstituted biopolymer networks

The use of reconstituted biological gels as a bottom-up approach to cell mechanics has developed rapidly since the 1980s and has proven very successful in unravelling the basic properties of the various components of the cytoskeleton and their interactions under well-controlled conditions [2–9, 36, 37]. One particular type of biopolymer that has received much attention in these studies is F-actin, which forms one of the major structural components of the cytoskeleton. Typically, reconstituted F-actin gels consist of less than ~ 1 volume percent of protein in an aqueous solution. When purified monomeric actin is polymerized in the presence of the cross-linking protein filamin it can form isotropic networks of individual actin filaments, mimicking the structure of the actin cortex (Fig. 1.1), as shown in Fig. 1.3. In contrast, at large filamin concentrations the system adopts a qualitatively different network structure composed of curved bundles of F-actin (Fig. 1.3b). The precise type of cross-linking protein and its concentration relative to actin can have a dramatic effect on the network architecture, and experiments have further shown that the cross-linking protein can strongly affect the dynamic mechanical response as well as the nonlinear elastic response [9, 19, 23, 38]. A large part of this thesis is dedicated to understanding how

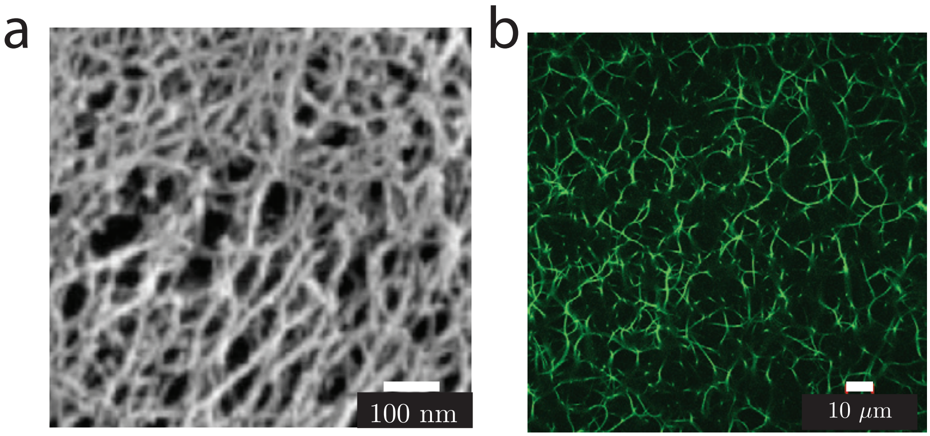

Figure 1.3 – (Color online) a) Electron micrograph of a fixed and rotary-shadowed filamin-F-actin network at an actin concentration 1 mg/ml, average filament length 15 μm, and a filamin:actin molar ratio of 0.005:1. b) Confocal microscopy image of a fluorescently labeled bundled filamin-F-actin network at high filamin concentrations. Courtesy of Karan Kasza (Harvard).

the microscopic properties of various types of cross-linkers control the mechanical behavior of actin and intermediate filament networks on the macroscopic scale.

Another important theme in this thesis concerns the mechanics of networks of fibers that are softer to bending than to stretching. Under shear, such networks exhibit highly nonuniform deformations. Both the linear mechanical response and the nonlinear elasticity at large shears of such systems remains poorly understood. Chapter 6 is dedicated to the elastic response of such non-affine stiff fiber networks. Examples of networks that exhibit such behavior may include bundled actin networks and collagen (one of the primary components of connective tissues). A microscopy image of a reconstituted network of collagen is shown in Fig. 1.4. These networks typically consist of thick fibers. One of the principle questions about such fiber networks is to what extent their behavior is governed by fiber stretching deformations. The entropic stretching stiffness of such fibers is likely to be very large. Consequently, the fibers may be much softer to bending deformations than stretching deformations.

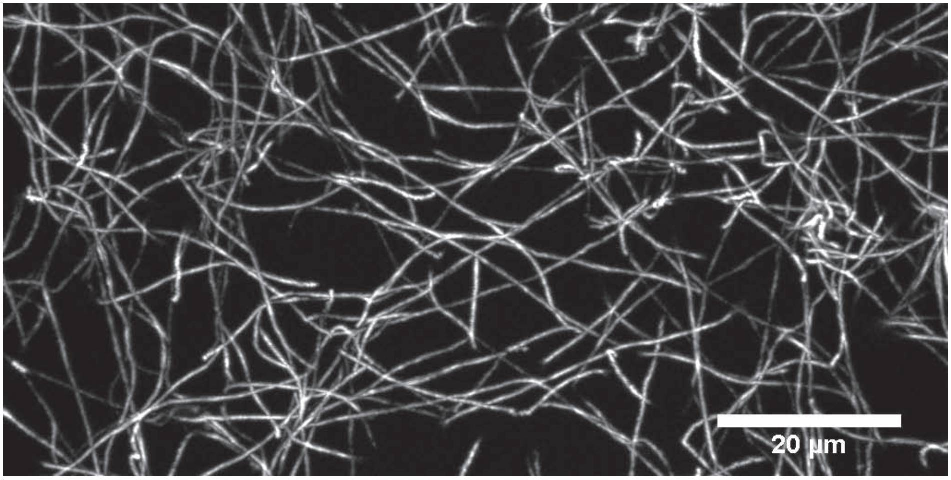

Figure 1.4 – Confocal microscopy image of a fluorescently labeled collagen network with a concentration of 0.4 mg/ml. Courtesy of Stefan Münster (Erlangen-Nurnberg).

1.4 Rheology: measuring the macroscopic dynamic mechanical response of biological gels

Biopolymer gels exhibit a mechanical response that in general depends on the timescale on which the system is probed. Furthermore, these gels often exhibit a highly nonlinear elastic response under shear. A careful and quantitative characterization of both the linear and nonlinear viscoelastic response is experimentally challenging. Various rheological methods have been developed to characterize the mechanical behavior of reconstituted biopolymer networks including both micro- and macrorheological methods. Microrheological methods are based on tracking one or multiple beads embedded within the network. The response of the system can be inferred directly by driving the beads with external fields or indirectly by monitoring their thermal fluctuations, although the latter relies on the assumption of the network being in thermal equilibrium. However, most of the experiments presented in this thesis have been performed using a macrorheological approach. With such an approach we can directly probe the macroscopic mechanical response by establishing the relation between the shear stress σ and the shear strain γ in a sample (Fig. 1.5). If the sample has a purely elastic response, and if network deformations are sufficiently small such that the response of the system is linear,

$$\sigma = G\gamma, \tag{1.2}$$

where G is the shear modulus. However, biopolymer gels exhibit both an elastic and a viscous component, which depends on the timescale on which the system is probed. To quantify such a viscoelastic response, the material is probed at a frequency ω, which allows us to determine the frequency dependent complex shear modulus $G(\omega) = G'(\omega) + iG''(\omega)$. The storage modulus G' captures the in-phase elastic-like response and the loss modulus G'' captures the out-of-phase viscous-like response.

Already at moderate strains ($\gamma \sim 0.1 - 1$) most cross-linked biopolymer networks stiffen dramatically. Various rheological protocols have been developed to determine this nonlinear response [19, 39–42]. Although these methods are discussed in more detail in chapter 5, we will here briefly introduce the prestress method since it is widely used throughout this thesis. In this protocol, the applied stress is the control variable and a differential measurement is used to determine the materials' differential stiffness. A steady prestress, σ_0, is applied on top of which a small amplitude oscillatory stress, $\delta\sigma(t) = \delta\sigma \mathrm{e}^{\mathrm{i}\omega \mathrm{t}}$ is superposed. For different frequencies ω one can determine the small oscillatory strain response, $\delta\gamma(t) = \delta\gamma \mathrm{e}^{\mathrm{i}\omega \mathrm{t}}$. The complex differential or tangent viscoelastic modulus is defined as $K = \frac{\delta\sigma}{\delta\gamma}$.

1.5 Outline of this thesis

Chapter 2: Cross-linked governed dynamics

One essential feature setting biopolymer networks apart from rubber-like materials is the intrinsic dynamics of their cross-links. This has important implications for cells, which have constantly remodeling internal networks, reflecting in part the dynamic nature of their cross-links. Recent experiments on actin networks with transient linkers provide evidence of a complex viscoelastic behavior.

To describe these systems we develop a microscopic model for the long time network relaxation that is controlled by cross-link dynamics. This cross-link governed dynamics (CGD) model describes the structural relaxation that results from many independent unbinding and rebinding events. We derive a set of nonlinear stochastic differential equations describing the time evolution of the dynamics of the polymers in the network. Using a combination of Monte Carlo simulations and a mean field approximation, we show that this type of cross-link dynamics yields a novel power-law regime in the rheology. Our model is in excellent quantitative agreement with experiments.

Chapters 3 and 4: Semiflexible polymer networks with flexible cross-links

Recent experiments on F-actin with the physiological cross-linker filamin have demonstrated several striking features; while their linear modulus is significantly lower than for rigidly cross-linked actin systems, they can nonetheless withstand remark-

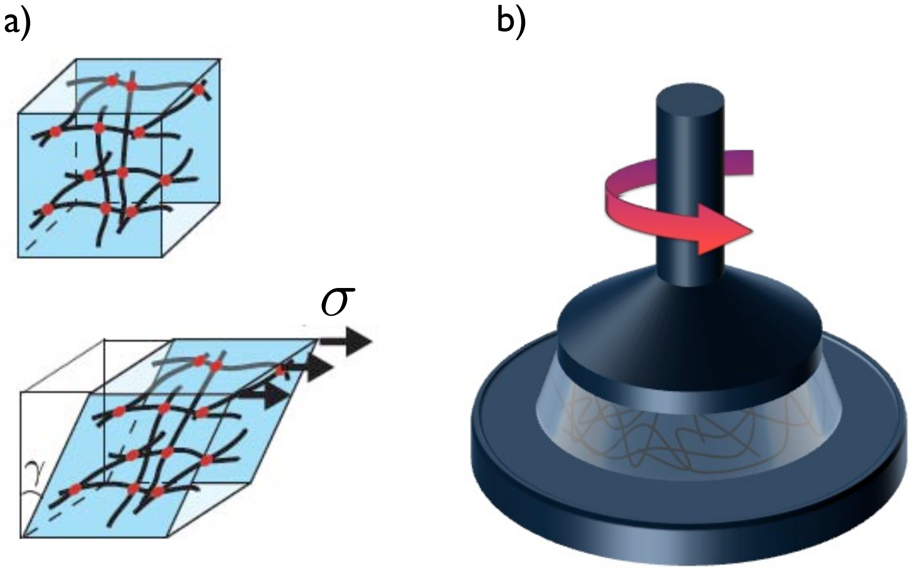

Figure 1.5 – (Color online) The viscoelastic response of reconstituted biological gels can be determined using macrorheological approaches. In such approaches, the resistance to a deformation is determined by probing the sample with an applied strain γ or stress σ to obtain the shear modulus $G = \sigma/\gamma$ (a). Most rheological experiments on biological gels use either a cone-plate (uniform strain) geometry (b) or a plate-plate geometry (non-uniform strain).

ably large stresses and can stiffen by a factor of 1000 with applied shear. We show quantitatively that this behavior can be accounted for by the highly flexible nature of the filamin cross-links. To describe these systems we develop a self-consistent mean field theory for the macroscopic nonlinear elasticity of these networks. The networks are modeled as a collection of randomly oriented rods connected by flexible linkers to a surrounding elastic continuum, which is required to self-consistently represent the behavior of the network. We have confirmed the main predictions of this model in close collaboration with the experimental group of D. Weitz.

Chapter 5: Nonlinear rheological methods for biopolymer gels

One of the hallmarks of biopolymer gels is their nonlinear viscoelastic response to stress, making the measurement of their mechanics very challenging. Using both strain ramp and differential prestress protocols, we investigate the nonlinear response of a variety of systems ranging from extracellular fibrin gels to intracellular F-actin solutions and F-actin cross-linked with permanent and physiological transient linkers. In particular, we designed a new protocol to investigate how both the linear and nonlinear mechanical response changes as the system creeps and deforms plastically under a large applied shear stress. In this protocol the differential response is determined under DC positive shear stresses of varying magnitude alternated with periods without load. The total strain and differential response are monitored continuously.

We find that the nonlinear response measured with the prestress protocol is remarkably insensitive to creep. This demonstrates that the nonlinear mechanical response of these biopolymer networks is robust, even when the network is flowing. To provide insight into these observations, we develop a simple, yet very general phenomenological model that includes the nonlinear elasticity of the network as well as network flow on long timescales.

Chapter 6: Criticality and isostaticity in fiber networks

The rigidity of elastic networks depends sensitively on their internal connectivity and the nature of the interactions between constituents. The isostatic point above which systems are rigid is captured by a classical argument introduced by Maxwell, which balances the degrees of freedom in the system against the number of constraints due to connectivity. Fibrous networks, such as those that form the cellular cytoskeleton or the extracellular matrix, exhibit rigidity at remarkably low connectivity, well bellow the Maxwell central force isostatic point. This rigidity is due to additional constraints provided by the fibers resistance to bending. However, the degree to which bending governs network mechanics remains a subject of considerable debate. We study disordered fibrous networks with variable coordination number, both above and below the central-force isostatic point. We find that this point controls a broad crossover from stretching- to bending-dominated elasticity. Strikingly, this crossover exhibits an anomalous power-law dependence of the shear modulus on both stretching and bending rigidities. At the central-force isostatic point—well above the rigidity threshold—we find divergent strain fluctuations together with a divergent correlation length ξ, implying a breakdown of continuum elasticity in this simple mechanical system.

Chapter 7: Motor generated stiffening in fiber networks

Reconstituted *active* filamentous F-actin networks with motor proteins form a good model system for cellular mechanics. The motor proteins generate forces that drive the network far from equilibrium and strongly affect the network mechanics. In some cases, the macroscopic nonlinear response of a passive network to an external shear is due to a transition between soft bending modes to stiffer stretching modes. The question arises how stress generating molecular motors couple to such a network and how they affect the macroscopic elastic response.

To address these issues, we develop a lattice-based approach to design networks with a connectivity of 4 or less, mimicking the architecture of biopolymer networks with binary cross-links. We showed how heterogeneous internal stresses generated by motors can lead to stiffening in networks that are governed by filament bending modes. The motors are modeled as force dipoles that cause muscle-like contractions. These contractions "pull out" the floppy bending modes in the system. Through this mechanism, motor activity can strongly stiffen the networks' mechanical response.

Chapter 8: Ionically cross-linked IF networks

Intermediate filament (IF) networks in the cytoplasm and nucleus are crucial for the mechanical integrity of metazoan cells. While filamentous actin and microtubules have been extensively studied, much less is known about IFs. In particular, the mechanism of cross-linking in these networks and the origins of their mechanical properties are not understood.

In close collaboration with the experimental group of D. Weitz, we have shown that divalent ions can mediate a cross-linking interaction between the negatively charged tail domains of intermediate filaments. We use an affine model for the nonlinear elastic response of these systems, which includes both the entropic stiffening and the enthalpic stretching of the individual filaments, as well as geometric affects that arise in networks under large shear deformations. This model allows us to extract microscopic parameters from the measured macroscopic rheological behavior, including the Young's modulus and the persistence length of the filaments, and the cross-linking lengthscale of the network.

Bibliography

[1] B. Alberts, A. Johnson, J. Lewis, M. Ra, K. Roberts,and P. Walter, *Molecular Biology of the Cell* (Garland Science, 2002), 4th ed.

[2] P. A. Janmey, U. Euteneuer, P. Traub, M. Schliwa. *Viscoelastic properties of vimentin compared with other filamentous biopolymer networks.* J. Cell Biol. **113**, 155 (1991).

[3] F. C. MacKintosh and P. A. Janmey. *Actin Gels*. Curr. Opin. Solid State Mater. Sci. **2**, 350 (1997).

[4] A. R. Bausch and K. Kroy. *A bottom-up approach to cell mechanics*. Nature Phys. **2**, 231 (2006).

[5] K. E. Kasza, A. C. Rowat, J. Liu, T. E. Angelini, C. P. Brangwynne, G. H. Koenderink and D. A Weitz. *The cell as a material*. Curr. Opin. Cell Biol. **19**:101-7 (2007).

[6] D. A. Weitz and P. A. Janmey. *The soft framework of the cellular machine*. Proc. Natl. Acad. Sci. USA **105**, 1105-1106 (2008).

[7] D. A. Fletcher, R. D. Mullins. *Cell mechanics and the cytoskeleton*. Nature **463**, 485-492 (2010).

[8] A.-S. Smith. *Physics challenged by cells*. Nature Phys. **6**, 726 (2010).

[9] O. Lieleg, M. M. A. E. Claessens and A. R. Bausch. *Structure and dynamics of cross-linked actin networks*. Soft Matter, **6**, 218-225 (2010).

[10] C. P. Brangwynne, G. H. Koenderink, F. C. MacKintosh, and D. A. Weitz. *Cytoplasmic diffusion: molecular motors mix it up*. J. Cell Biol. **183**, 583 (2008).

[11] F. C. MacKintosh and C. F. Schmidt. *Active cellular materials*. Curr. Opin. Cell Biol. **22**, 29 (2010).

[12] J. Joanny and J. Prost. *Active gels as a description of the actin-myosin cytoskeleton*. HFSP Journal **3**, 94 (2009).

[13] D. Mizuno, C. Tardin, C. F. Schmidt, and F. C. MacKintosh. *Nonequilibrium Mechanics of Active Cytoskeletal Networks*. Science **315**, 370 (2007).

[14] G. H. Koenderink, Z. Dogic, F. Nakamura, P. M. Bendix, F. C. MacKintosh, J. H. Hartwig, T. P. Stossel, and D. A. Weitz. *An active biopolymer network controlled by molecular motors* Proc. Natl. Acad. Sci. USA **106**, 15192 (2009).

[15] K. Kruse, J. F. Joanny, F. Jülicher, J. Prost, and K. Sekimoto. *Generic theory of active polar gels: a paradigm for cytoskeletal dynamics*. Eur. Phys. J. E **16**, 5 (2005).

[16] F. C. MacKintosh and A. J. Levine. *Non-equilibrium mechanics and dynamics of motor-activated gels*. Phy. Rev. Lett. **100**, 018104 (2008).

[17] T. B. Liverpool, M. C. Marchetti, J. Joanny, and J. Prost. *Mechanical response of active gels*. Europhys. Lett. **85**, 18007 (2009).

[18] T. C. Lubensky. *Soft condensed matter physics*. Solid State Commun. **102**, 187-197 (1997).

[19] M. L. Gardel, J. H. Shin, F. C. MacKintosh, L. Mahadevan, P. A. Matsudaira, D. A. Weitz. *Elastic Behavior of Cross-Linked and Bundled Actin Networks*. Science **304**, 1301 (2004).

[20] C. Storm, J. Pastore, F. C. MacKintosh, T. C. Lubensky and P. A. Janmey. *Nonlinear elasticity in biological gels*. Nature **435**: 191 (2005).

[21] O. Chaudhuri, S. H. Parekh and D. A. Fletcher. *Reversible stress softening of actin networks*. Nature **445**: 295 (2007).

[22] P. A. Janmey, M. E. McCormick, S. Rammensee, J. L. Leight, P. C. Georges, and F. C. MacKintosh. *Negative normal stress in semiflexible biopolymer gels*. Nature Materials **6**, 48 (2007).

[23] B. Wagner, R. Tharmann, I. Haase, M. Fischer and A.R. Bausch. *Cytoskeletal polymer networks: The molecular structure of cross-linkers determines macroscopic properties*. Proc. Nat. Acad. Sci. USA **103**, 13974 (2006).

[24] P. R. Onck, T. Koeman, T. van Dillen, and E. van der Giessen. *Alternative explanation of stiffening in cross-linked semiflexible networks*. Phys. Rev. Lett. **95**, 178102 (2005).

[25] E. M. Huisman, T. van Dillen, P. R. Onck, and E. Van der Giessen. *Three-Dimensional Cross-Linked F-Actin Networks: Relation between Network Architecture and Mechanical Behavior*. Phys. Rev. Lett. **99**, 208103 (2007).

[26] E. Conti, F. C. MacKintosh. *Cross-Linked Networks of Stiff Filaments Exhibit Negative Normal Stress*. Phys. Rev. Lett. **102**, 088102 (2009).

[27] K. E. Kasza, C. P. Broedersz, G. H. Koenderink, Y. C. Lin, W. Messner, E. A. Millman, F. Nakamura, T. P. Stossel, F. C. MacKintosh, D. A. Weitz. *Actin filament length tunes elasticity of flexibly crosslinked actin networks*. Biophys. J. **99**, 1091 (2010).

[28] Y. C. Lin, N. Y. Yao, C. P. Broedersz, H. Herrmann, F. C. MacKintosh, D .A. Weitz. *Origins of elasticity in intermediate filament networks*. Phys. Rev. Lett. **104**, 058101 (2010).

[29] C. Bustamante, J.F. Marko, E.D. Siggia and S. Smith. *Entropic elasticity of lambda-phage DNA*. Science **265**, 1599 (1994).

[30] J. F. Marko and E. D. Siggia. *Stretching DNA*. Macromolecules **27**, 981 (1995).

[31] F. C. MacKintosh, J. Käs, and P. Janmey. *Elasticity of Semiflexible Biopolymer Networks*. Phys. Rev. Lett. **75**, 4425 (1995).

[32] F. Gittes, B. Mickey, J. Nettleton, and J. Howard. *Flexural Rigidity of Microtubules and Actin Filaments Measured from Thermal Fluctuations in Shape*. J. Cell Biol. **120**:923 (1993).

[33] J. Howard, *Mechanics of motor proteins and the cytoskeleton* (Sinauer Press, Sunderland MA) 2001.

[34] Z. Dogic, J. Zhang, A. W. C. Lau, H. Aranda-Espinoza, P. Dalhaimer, D. E. Discher, P. A. Janmey, R. D. Kamien, T. C. Lubensky, and A. G. Yodh. *Elongation and Fluctuations of Semiflexible Polymers in a Nematic Solvent*. Phys. Rev. Lett. **92**, (2004).

[35] N. Mücke, L. Kreplak, R. Kirmse, T. Wedig, H. Herrmann, U. Aebi and J. Langowski1. *Assessing the Flexibility of Intermediate Filaments by Atomic Force Microscopy*. Journal of Mol. Bio. **335**, 1241 (2004).

[36] P. A. Janmey, J. Peetermans, K. S. Zaner, T. P. Stossel, and T. Tanaka. *Structure and mobility of actin filaments as measured by quasielastic light scattering, viscometry, and electron microscopy*. J. Biol. Chem. **261**, 8357 (1986).

[37] P. A. Janmey, S. Hvidt, J. Lamb, and T. P. Stossel. *Resemblance of actin-binding protein/actin gels to covalently crosslinked networks*. Nature **345**, 89 (1990).

[38] M. L. Gardel, F. Nakamura, J. H. Hartwig, J. C. Crocker, T. P. Stossel, and D. A. Weitz. *Prestressed F-actin networks cross-linked by hinged filamins replicate mechanical properties of cells*. Proc. Natl. Acad. Sci. **103**:1762-1767 (2006).

[39] C. Semmrich, R. J. Larsen, and A. R. Bausch. *Nonlinear mechanics of entangled F-actin solutions*. Soft Matter **4**, 1675-1680 (2008).

[40] R. H. Ewoldt, A. E. Hosoi, and G. H. McKinley. *New measures for characterizing nonlinear viscoelasticity in large amplitude oscillatory shear*. J. Rheol. **52**, 1427-1458 (2008).

[41] R. H. Ewoldt, A. E. Hosoi, and G. H. McKinley. *Nonlinear viscoelastic biomaterials: meaningful characterization and engineering inspiration*. Integrative and Comparative Biology **49**, 40-50 (2009).

[42] C. P. Broedersz, K. E. Kasza, L. M. Jawerth, S. Münster, D. A. Weitz, and F. C. MacKintosh. *Measurement of Nonlinear rheology of cross-linked biopolymer gels*. Soft Matter **6**, 4120 (2010).

2

Cross-link governed dynamics in F-actin gels

- C. P. Broedersz, M. Depken, N. Y. Yao, M. R. Pollak, D. A. Weitz and F. C. MacKintosh
  Cross-link governed dynamics of biopolymer networks,
  Physical Review Letters, **105**:238101 (2010)

18 N. Y. Yao, D. Becker, C. P. Broedersz, M. Depken, M. R. Pollak, F. C. MacKintosh and D. A. Weitz
Nonlinear Viscoelasticity of Actin Cross-linked with Mutant α-Actinin-4
(Under review, 2011)

- N. Y. Yao, C. P. Broedersz, M. Depken, M. R. Pollak, F. C. MacKintosh and D. A. Weitz
  Stress-enhanced Gelation of Biopolymer Networks,
  (to be submitted)

Abstract

Recent experiments show that networks of stiff biopolymers cross-linked by transient linker proteins exhibit complex stress relaxation, enabling network flow at long times. We present a model for the dynamics controlled by cross-links in such networks. We show that a single microscopic timescale for cross-linker unbinding leads to a broad spectrum of macroscopic relaxation times and a shear modulus $G \sim \omega^{1/2}$ for low frequencies ω. This model quantitatively describes the measured rheology of actin networks cross-linked with α-Actinin-4 over more than four decades in frequency. Furthermore, we demonstrate an unexpected mechanical behavior in these systems under large external stresses. Applied stress enhances gelation of these networks by delaying the onset of structural relaxation, thereby extending their solid-like behavior to lower frequencies.

2.1 Introduction

Reconstituted biopolymers such as actin are excellent models for semi-flexible polymers, with network mechanics and dynamics that are strikingly different from flexible polymer networks [1–8]. One essential feature setting biopolymer networks apart from rubber-like materials is the intrinsic dynamics of their cross-links. Such systems represent a distinct class of polymeric materials whose long-time dynamics are not governed by viscosity or reptation [9], but rather, by the transient nature of their cross-links. This can give rise to a complex mechanical response, particularly at long times, where the network is expected to flow. Such flow can have important implications for cells, where their internal networks are constantly remodeling, reflecting the transient nature of their cross-links [10]. The simplest possible description of a material that is elastic on short timescales while flowing on long timescales is that of a Maxwell fluid; this exhibits a single relaxation time τ, as depicted in Fig. 2.1. Indeed, some recent experiments on transient networks have been modeled with a single relaxation time [11, 12]; however, those experiments and others [13, 14]—probing longer relative time-scales compared to the linker unbinding time—evince a more complex viscoelastic behavior, indicative of multiple relaxation times. Thus, the basic physical principles governing transient networks remain unknown. A predictive theoretical model is essential to elucidate the effect of dynamic cross-linking, and to help explain the reported complex viscoelastic behavior.

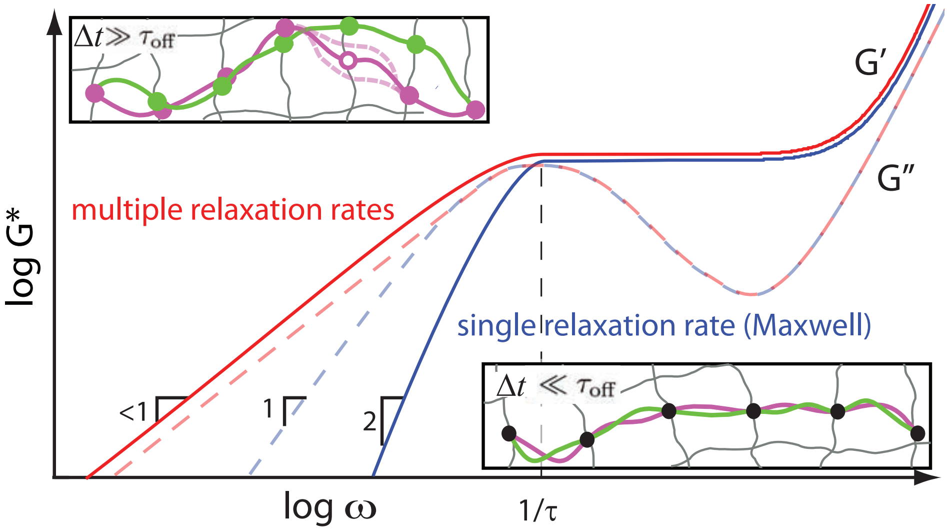
$\Delta t \gg \tau_{\rm off}$
G′
G″
log G*
multiple relaxation rates
single relaxation rate (Maxwell)
$\Delta t \ll \tau_{\rm off}$
<1
1
2
log ω
1/τ

Figure 2.1 – (color online) A schematic of the frequency dependent shear modulus $G^* = G' + \imath G''$. Non-permanent networks can exhibit a response ranging from a single timescale (τ) Maxwell-like behavior (blue lines) to a powerlaw regime with an exponent < 1 governed by a broad distribution of relaxation times ($> \tau$) (red lines). Upper inset: for times longer than the unbinding time $\tau_{\rm off}$, large scale conformational relaxation can occur via linker unbinding (open circle) and subsequent rebinding at a new location. Lower inset: for shorter times, only small-scale bend fluctuations between cross-links can relax, resulting in a plateau in G' for frequencies $> 1/\tau_{\rm off}$.

Here, we develop a microscopic model for long-time network relaxation that is controlled by cross-link dynamics. This *cross-link governed dynamics* (CGD) model describes the structural relaxation that results from many independent unbinding and rebinding events. Using a combination of Monte Carlo simulations and an analytic approach, we demonstrate that this type of cross-link dynamics yields power-law rheology arising from a broad spectrum of relaxation rates. Our predictions are in excellent quantitative agreement with experiments on actin networks with the transient linker protein α-Actinin-4.

The CGD model can be qualitatively understood in simple physical terms. We assume each filament is cross-linked to the network, with an average spacing ℓ_c. Only filament bending modes between cross-links can relax (Fig. 2.1, lower inset), and the thermalization of these modes results in an entropic, spring-like response. To account for transient cross-linking, we assume that the linkers unbind at a rate $1/\tau_{\text{off}}$ (Fig. 2.1,upper inset), which may depend on temperature [13]. This initiates the relaxation of long wavelength ($> \ell_c$) modes, giving rise to a reduced macroscopic modulus. However, the relaxation of successively longer wavelength modes becomes slower, as an increasing number of unbinding events are needed for such a relaxation. This simple physical picture suggests a broad spectrum of relaxation times, as opposed to the single relaxation time of the Maxwell model. As outlined below, both simulations and an analytic treatment of this model yield power-law behavior with $G \sim \omega^{1/2}$ below the characteristic frequency $\omega_0 = 2\pi/\tau_{\text{off}}$ (Figs. 2.2 A and B).

We compare the basic predictions of this model to the rheology of a representative transiently cross-linked actin network. As a cross-linker, we use α-Actinin-4 [14, 15], whose unbinding time τ_{off} is reported to be in the range $1 - 10$s. These gels (See section 2.4) [16] exhibit a low-frequency elastic shear modulus G' with a pronounced decay over three decades in frequency, while the viscous modulus G'' exhibits a broad local maximum located near the characteristic frequency of cross-link unbinding [11–13, 16] (Fig. 2.2B). In the asymptotic low-frequency range, both moduli exhibit power-law rheology with an approximate exponent of 1/2, in agreement with our predictions. Such behavior clearly indicates a more complex stress relaxation than captured by the Maxwell model, which is governed by a single relaxation time (Fig. 2.1). Taken together, the theoretical and experimental results demonstrate a distinct cross-link governed regime of network dynamics. Finally, we also provide experimental evidence of such dynamics for networks under large external loads. However, the applied stress does affect both the rate of linker unbinding dynamics and the stiffness of the networks, which results in a rich nonlinear viscoelastic response.

2.2 Results and discussion

To develop a predictive microscopic model, we first consider a single polymer within the network, and then extend the description to the macroscopic level. On length-scales longer than ℓ_c, the motion of the polymer is constrained by its cross-linking to the surrounding network (Fig. 2.1). When a linker unbinds, a local constraint is released, allowing for the relaxation of the freed segment. This thermal relaxation occurs within a time τ_eq, which is typically of order milliseconds [3, 4, 7]. We assume that this process is completed before the segment rebinds to the network at a new location; thus, $\tau_\mathrm{eq} \ll \tau_\mathrm{on}$, where τ_on is the rebinding time of the linkers. Furthermore, assuming $\tau_\mathrm{on} \ll \tau_\mathrm{off}$, only a small fraction of cross-links will be unbound at any given time, and simultaneous unbinding of neighboring cross-links can be neglected. This suggests a coarse-grained description on length-scales $> \ell_\mathrm{c}$, in which independent unbinding events occur at a rate $1/\tau_\mathrm{off}$. Since the relaxation of wavelengths $< \ell_\mathrm{c}$ occurs at a much faster rate $1/\tau_\mathrm{eq}$, we use the worm-like chain model, where the equilibrated short wavelength fluctuations manifest themselves as an entropic stretch modulus $\mu_\mathrm{th} \sim \kappa^2/\ell_\mathrm{c}^3 k_\mathrm{B}T$ [2, 4]. Here, κ is the bending rigidity, k_B is Boltzmann's constant and T is the temperature. In this description the coarse-grained energy is given by

$$H_{CG} = \frac{1}{\ell_\mathrm{c}} \sum_n \left[\frac{\kappa}{2} \left| \Delta \mathbf{t}_n \right|^2 + \frac{\mu_\mathrm{th}}{2} \left(\left| \Delta \mathbf{r}_n \right| - \ell_\mathrm{c} \right)^2 \right], \tag{2.1}$$

where the sum extends over all cross-link positions $\mathbf{r}_n$, $\mathbf{t}_n$ is the unit tangent vector and, e.g. $\Delta \mathbf{r}_n = \mathbf{r}_{n+1} - \mathbf{r}_n$.

Using the coarse-grained energy H_{CG}, we study the dynamics arising from multiple linker unbinding events, by performing 2D simulations of a single polymer. An initial chain conformation with periodic boundary conditions is randomly drawn from a Boltzmann distribution. Cross-link unbinding events are independent and result in the complete thermal equilibration of the two neighboring polymer segments. This is numerically implemented via a Metropolis Monte Carlo algorithm. These simulations allow us to determine the equilibrium fluctuations enabled by linker unbinding of a single polymer embedded in a network that is treated as a rigid medium. According to the fluctuation dissipation theorem (FDT), the linear mechanical response of the polymer is encoded in the fluctuations of the extension, $\delta\ell$, of the polymer. Interestingly, the simulations demonstrate that the power spectrum $C(\omega) = \langle |\delta\ell(\omega)|^2 \rangle$ depends on frequency as a fractional power-law consistent with an exponent $-3/2$, as shown in the inset of Fig. 2.2A, indicating a broad underlying distribution of relaxation times. Although this exponent also arises in the Rouse model for flexible polymers due to the viscous dynamics of *longitudinal* stretch modes [9], this is not the origin of the behavior found here. Our model does exhibit longitudinal modes; however, their contribution $C_{||}$ to full spectrum is subdominant (inset of Fig. 2.2A). This demonstrates

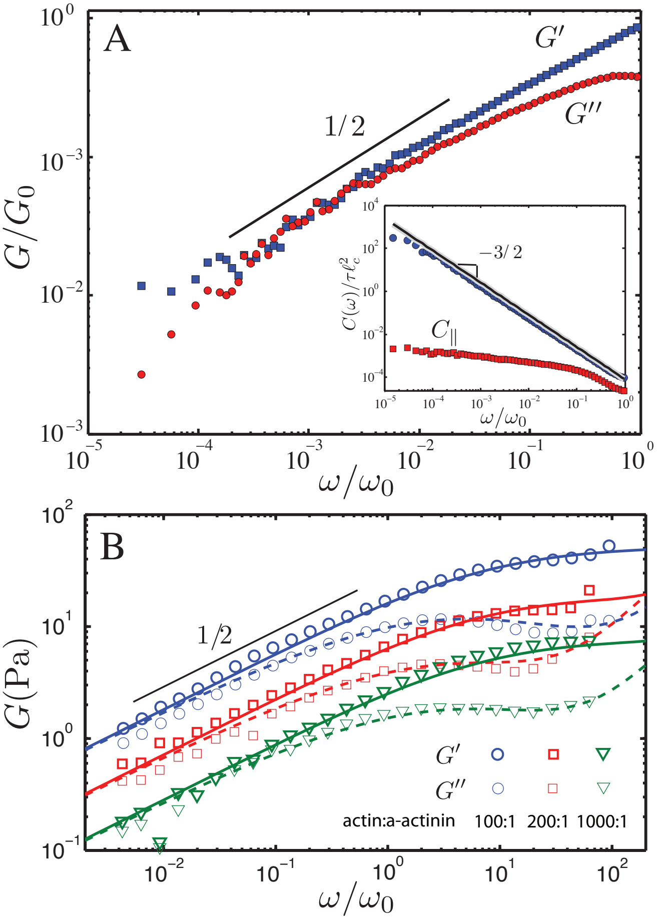

Figure 2.2 – (color online) A) The simulated rheology for frequencies below ω_0. The shear modulus is normalized by the elastic plateau value G_0 . The inset shows the total power spectrum $C(\omega)$ (blue circles) of distance fluctuations, as well as the fraction $C_{||}$ coming from effective stretch fluctuations originating in undulations on length scales shorter than the cross-linking distance. The distance fluctuations are determined over a length $16\ell_c$ of a polymer with a persistence length $\ell_p = 32\ell_c$ and a total length $32\ell_c$. The solid black line represents our analytical mean-field CGD prediction. B) Measured linear rheology of a 23.8 μM actin network cross-linked with various concentrations of α-Actinin-4. The low frequency behavior is consistent with $G \sim (\imath\omega)^{1/2}$. The solid and dashed lines are global fits utilizing our mean-field CGD model for the low frequency regime together with the known high frequency response [3, 4].

that the polymer's response to an applied tension is dominated by the dynamics of transverse modes.

The dynamical description of a single polymer can be extended to the network level by assuming that the network deforms affinely. The macroscopic shear modulus G^* is then related to the complex response function χ of relative length extension of a single polymer in response to a tensile force: $G^* = \rho/(15\chi)$, where ρ is the length of polymer per unit volume [3,4]. Ignoring end effects, the relative extension $\delta\ell/\ell$ of a polymer segment of length ℓ is conjugate to the uniform tension f, with $\delta\ell(\omega)/\ell = \chi(\omega)f(\omega)$. We use the FDT to calculate the imaginary part of the extensional response function $\ell\chi''(\omega) = \omega\langle\delta\ell^2(\omega)\rangle/2k_BT$. Using the Kramers-Kronig relation, we compute the response function χ and the network shear modulus [1]. Below ω_{off}, the shear modulus depends on frequency as a power-law with an exponent of 1/2 (Fig. 2.2A), consistent with experiments (Fig. 2.2B).

To obtain further insight, we develop a continuum analytical treatment of the CGD model. We calculate the polymer displacement due to the unbinding and subsequent rebinding of a linker to the n-th cross-link site. We separate the local equilibration step into a move to the minimum energy position, together with a stochastic thermal contribution set by the form of the energy around the mechanical equilibrium. The mechanical relaxation step $\mathbf{r}_n^{(\mathrm{i})} \to \mathbf{r}_n^{(\mathrm{meq})}$, from the initial (i) position to the local equilibrium position (meq), is determined by

$$\mathbf{0} = \left.\frac{\partial H_{CG}}{\partial \mathbf{r}_n}\right|_{\mathbf{r}_n=\mathbf{r}_n^{(\mathrm{meq})}}. \tag{2.2}$$

This condition replaces the usual force balance of drag and conservative terms in the low-Reynolds number regime. By performing the discrete calculation solving Eq. (2.2) and taking the continuum long-wavelength limit, the leading order evolution equations are (see section 2.5) [17]

$$\tau_{\text{off}}\partial_t r_{\parallel} = \frac{\ell_c^2}{2}\partial_x^2 r_{\parallel} + \hat{\boldsymbol{e}}_x \cdot \boldsymbol{\xi}_{\perp} \tag{2.3}$$

$$\tau_{\text{off}}\partial_t \mathbf{r}_{\perp} = \frac{\ell_c^2}{2}\partial_x^2 \mathbf{r}_{\perp} + \boldsymbol{\xi}_{\perp}. \tag{2.4}$$

Here $\mathbf{r}_\perp$ and $r_\parallel$ are the transverse and longitudinal deflections of the polymer with respect to its average direction $\hat{\boldsymbol{e}}_x$. The noise $\boldsymbol{\xi}_\perp$ captures both thermal effects and local bucking contributions due to thermally-induced compression (see section 2.5) [17]. While thermal contributions can be calculated from a quadratic expansion of H_{CG} around its local mechanical equilibrium, the state of the surrounding polymer influences the form of the Hessian, inducing correlations in the noise. In the inextensible limit, the longitudinal component of $\boldsymbol{\xi}$ is subdominant and is neglected.

---

[1] The Kramers-Kronig relation involves an integral over the whole frequency domain. Since we only simulate the low frequency part, we supplement this with the expected plateau above ω_0.

Importantly, the noise $\xi_\perp$ depends nonlinearly on the local state of the polymer and couples Eqs. (2.5,2.6). To explore this coupling, we artificially reduce the stretch modulus μ. In the limit $\mu \ll \mu_{\text{th}}$, the evolution equations decouple to leading order and become exactly solvable

$$\tau_{\text{off}}\partial_t r_{\|} = \frac{\ell_c^2}{2}\partial_x^2 r_{\|} + \xi_{\|} \tag{2.5}$$

$$\tau_{\text{off}}\partial_t \mathbf{r}_{\perp} = -\frac{\ell_c^4}{6}\partial_x^4 \mathbf{r}_{\perp} + \xi_{\perp}. \tag{2.6}$$

In this limit, both transverse and longitudinal noise are uncorrected in space and time. The resulting transverse contribution approaches $C_\perp \sim \omega^{-7/4}$. This can also be seen in our simulations with variable $\mu < \mu_{\text{th}}$ in Figs. 2.3 A and B. As μ is reduced below μ_{th}, $C_\perp$ evolves toward $C_\perp \sim \omega^{-7/4}$, which can be seen by the flattening of the normalized spectrum in Fig. 2.3B. In the limit $\mu \ll \mu_{\text{th}}$, the transverse bending dynamics are effectively those of a stiff filament fluctuating in a viscous solvent, for which the time-dependent fluctuations are $\langle|\delta\ell(t)|^2\rangle \sim t^{3/4}$ [3, 4, 18]. Only in this decoupled limit, can one understand the dynamics within the framework of an effective viscosity provided by the transient cross-links [17].

The nonlinear nature of the noise $\xi_\perp$ in the evolution Eqs. (2.5,2.6), in the limit of an inextensible polymer, precludes a full analytical solution of the model. Instead, further insight is gained by approximating the amplitude of the noise term by its mean-field value(see section 2.5) [17]. In the CGD model the noise term captures the width of the thermal distribution associated to a local relaxation event triggered by linker unbinding; in this mean-field approach the local deviations in the width of this thermal distribution are neglected; the width of the distribution used for *every* local relaxation event is then calculated by averaging over the equilibrium distribution of polymer conformations. In this approximation, the noise contributions are uncorrelated in both time and space, resulting in the response function

$$\chi_{\text{MF}}(\omega) \approx 0.0036\frac{k_B T \ell_c^3}{\pi\kappa^2}\int \mathrm{d}q \frac{1}{q^2 - 2\imath\omega\tau_{\text{off}}}.$$

This response function captures the cross-link governed dynamics dominating on timescales $> \tau_{\text{off}}$. Furthermore, we calculate the mean-field correlator, $C_{\text{MF}} \sim \omega^{-3/2}$, in good agreement with the simulations presented in the inset of Fig. 2.2A. As a further test, we perform simulations over a wide range of κ and polymer lengths L; the predicted amplitudes of the fluctuation spectrum are in good agreement with the simulated amplitudes, as shown in Fig. 2.3C. This further validates the assumptions made in our analytical approach.

To obtain a complete description of the behavior in the experimentally accessible range we include the viscous polymer dynamics relevant at high frequencies in our

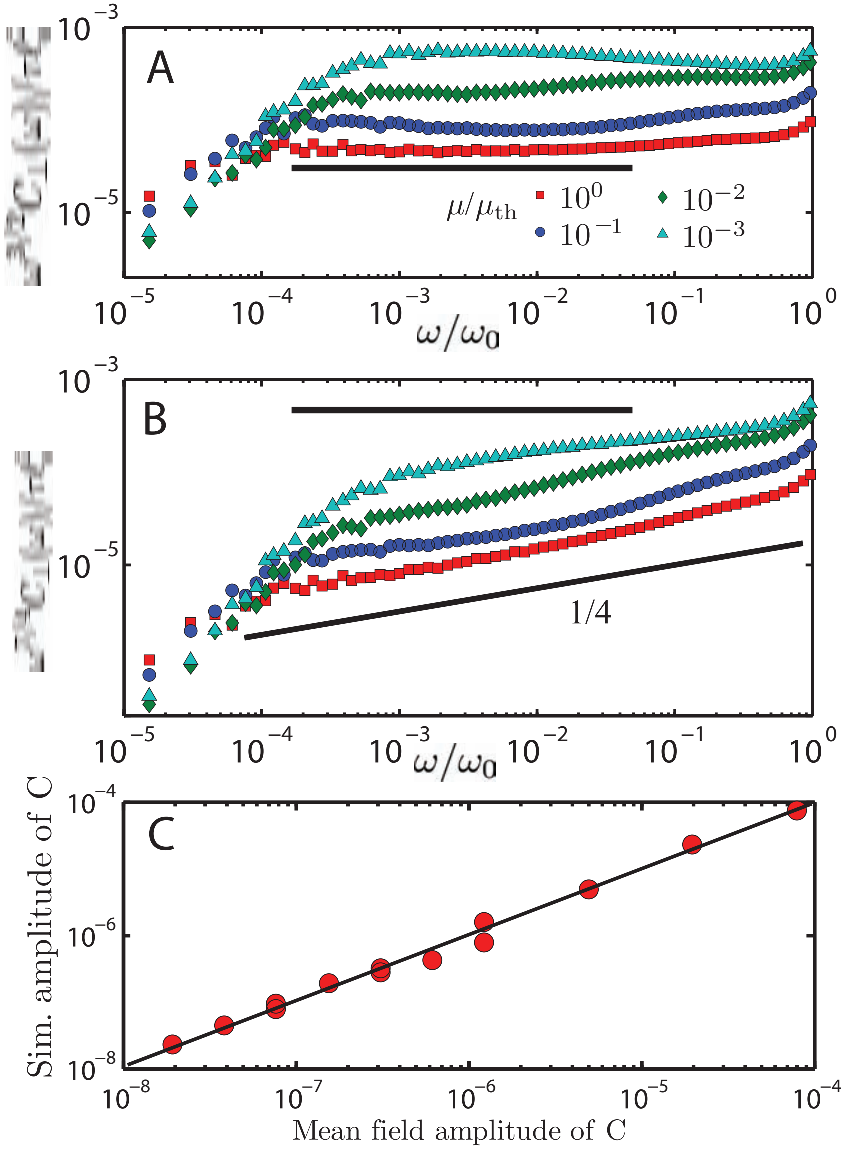

Figure 2.3 – (color online) The power spectrum $C_\perp(\omega)$ of end-to-end fluctuations originating from transverse undulations on length scales longer than ℓ_c, multiplied with $\omega^{3/2}$ (A) and $\omega^{7/4}$ (B) for a range of polymer backbone compliances. C) The simulated amplitude of the power spectrum $C(\omega)/\tau\ell_c^2$ plotted against the 2D mean-field prediction for a range of polymer lengths and bending rigidities.

model [3, 4]. This extension relies on the separation of timescales of the fast viscous polymer dynamics and the slow cross-link governed dynamics, which implies that their contributions to the fluctuation spectra add in quadrature. The model agrees with the experimental data—over the full range of frequencies—with just three parameters: the plateau modulus, the equilibration time τ_{eq} and the unbinding time τ_{off} (see Fig. 2.2). We have globally fitted all data over a decade of cross-linking concentrations with a single value for $\tau_{\mathrm{off}} = 2.7\mathrm{s}$. This provides strong evidence that the low-frequency rheology of actin networks with the physiological linker α-Actinin-4 is governed by the linker-controlled dynamics. Furthermore, the fitting procedure yields $\tau_{\mathrm{eq}} < 0.07\mathrm{s}$ consistent with $\tau_{\mathrm{eq}} \ll \tau_{\mathrm{off}}$; this, together with the quality of the fit, lends credence to the separation of timescales assumed in our model. Such a separation of timescales also implies that the fluid viscosity does not affect the rheology in the linker-governed regime, consistent with observations in other experiments [11, 12]. By contrast, for low enough cross-linking densities τ_{eq} becomes so large that the viscous dynamics and cross-link governed dynamics are no longer expected to be well separated. For an expected diffusive propagation of edge effects, we estimate a terminal relaxation time $\tau_{\mathrm{r}} \approx \tau_{\mathrm{off}}(L/\ell_c)^2$ [17]. As few as 10 cross-links per filament can account for the absence of a terminal relaxation in our experiments (Fig. 2.2). The possibility of observing a terminal relaxation for shorter filaments presents an interesting avenue for future experiments.

Many physiological actin cross-linking proteins are dynamic and should induce a $G^* \propto (\imath\omega)^{1/2}$ behavior at low frequencies. This may enable the cell to regulate its response; on timescales short compared to τ_{off}, the network is effectively permanently connected—thereby providing mechanical resilience—while on longer timescales, dynamic linkers allow for complex network flow. This ability to flow and remodel is required for many vital cellular functions, ranging from motility to division. The extent to which transient cross-linking affects the mechanical properties of the cell is, however, still unknown. Interestingly, some rheological measurements on living cells have suggested a 1/2 power-law behavior on time-scales ranging from several seconds to hours, consistent with our model for transient networks [19, 20]. Further experiments are needed to determine whether this regime is due to the transient nature of the cross-links.

2.3 Implications for cross-link dynamics at high stress

In this section we explore the effects of large external loads on transiently cross-linked F-actin/α-actinin-4 gels. To this end, we examine the nonlinear mechanics using the prestress protocol (see chapter 5). We apply a constant pre-stress, σ_0, while superposing a small amplitude oscillatory stress. We measure the resulting differential strain response, which allows us to determine the differential shear modulus as a function of frequency. Consistent with prior studied on cross-linked actin gels [6,21], the network stiffness increases with applied stress, as shown in Fig. 2.4. Surprisingly however, under applied stress we observe that the elastic plateau extends to significantly lower frequencies, which we characterize as *stress-enhanced gelation*. Together with the extension of the plateau, we observe a shift to lower frequencies of the local maximum in G'', which is identified as the onset of structural relaxation. Upon the removal of the external stress, the network response reverts back to the original linear behavior, indicating the reversible nature of stress enhanced gelation (data not shown). The behavior of these transiently cross-linked actin gels is diametrically opposed to the typical response of most materials, whereby an external stress leads to yielding and fluidization.

We obtain insight into this stress-enhanced gelation by investigating the dependence of the frequency for the onset of structural relaxation, ω_r, as a function of the applied steady stress, as shown in Fig. 2.6. At low stresses $\omega_r \approx 0.5$ Hz, independent of the applied stress. Beyond stresses of $\simeq 2$ Pa, however, the relaxation frequency decreases strongly after which it appears to level off at high stress to a value $\omega_r \approx 0.03$ Hz. Despite this dramatic shift in ω_r, the functional form of the nonlinear data appears to be remarkably similar to that of the linear data (Fig. 2.4). In particular, the shear moduli of the prestressed gel exhibit a dependence $G \sim \omega^{1/2}$ at low frequencies, suggesting that the viscoelasticity at large stresses is also governed by cross-link dynamics. Within this picture, the shift of the onset for structural relaxation to lower frequencies is interpreted as an increase of the unbinding time of the linkers τ_{off} with stress, characteristic of catch-bond behavior. This is in contrast with the expectation in which an applied load reduces the binding affinity of the linker [22]. However, our observations here are analogous to the observed behavior in actin gels cross-linked with the non-physiological linker heavy meromyosin [12].

We hypothesize that the microscopic origin of the apparent catch-bond behavior in the case of the physiological linker α-actinin-4 is due to a force-induced change in the protein conformation, which exposes an additional actin binding site with a high binding affinity. The binding head of α-Actinin-4 contains three actin-binding sites: ABS , ABS 2, and ABS 3, as illustrated in Fig. 2.5. In the wild-type conformation the actin binding domain is thought to be a closed structure in which the ABS 3 binding site is largely buried [23]. However, under load the actin binding domain may open up enabling accessibility to the ABS 1 binding site. Interestingly, in α-Actinin-4 proteins with a point mutation designated K255E, the hinge-like connection between the two CH domains is loosened and the structure is open, which indeed enhances the binding affinity of the linker [13,23]. In this case, the enhanced binding affinity is thought to be a consequence of the exposure of the high-affinity ABS 1 binding

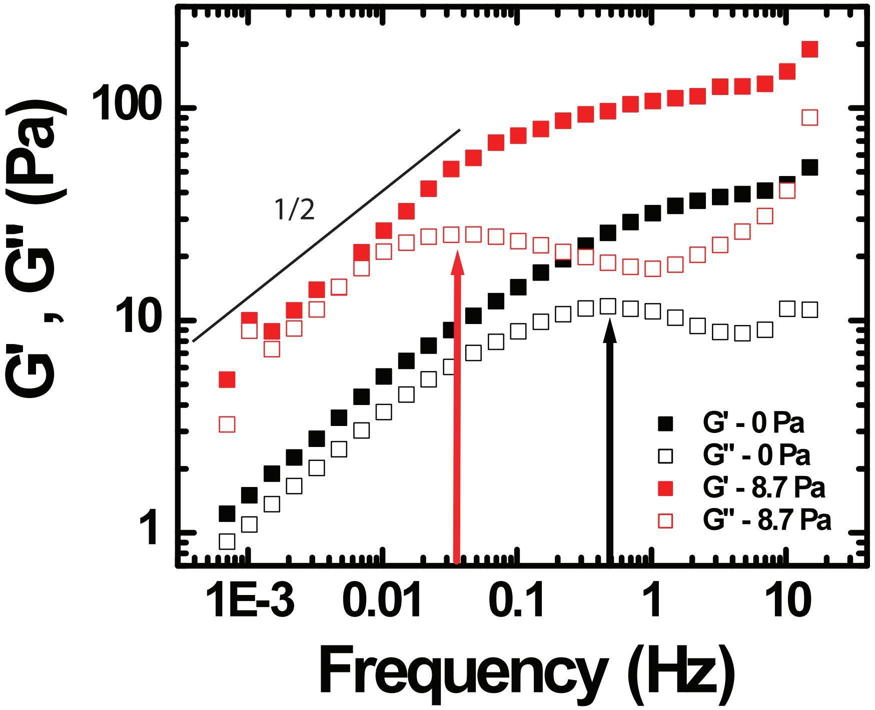

Figure 2.4 – (color online) B) Measured linear rheology of a 23.8 μM actin network cross-linked at an an actin:α-Actinin-4 molar ratio of 100:1 (black squares). The differential response under an applied steady prestress of 8.7 Pa is shown in red. In both cases the low frequency behavior is consistent with $G \sim (\imath\omega)^{1/2}$. Under stress, the plateau modulus of F-actin/α-Actinin-4 increases and the onset of structural relaxation (local maximum in G'') shifts to lower frequencies.

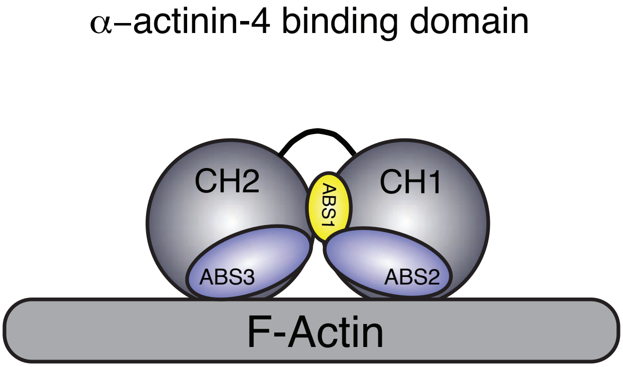

Figure 2.5 – (color online) Schematic of the binding domain of wild type α-actinin-4. In the wild type form the two domains are in a closed conformation and the ABS 2 and ABS 3 binding sites are largely responsible for the binding affinity of the linker [13,23]. We hypothesize that the conformation of the CH domains opens up under load exposing the high-affinity ABS 1 binding site; this mechanism can account for the load-induced reduction of the relaxation frequency we observe in the macroscopic rheological response of F-actin/α-actinin-4 gels.

site. Our macroscopic rheological data on actin gels with wild type α-actinin-4 under prestress has a relaxation frequency that appears to converge to $\omega_r \approx 0.03$ Hz at high loads, which is quantitatively consistent with the viscoelastic behavior of actin gels with K255E linkers in the absence of an applied load [13]. This supports the important role of the high affinity ABS 1 binding site in actin gels with wild type α-actinin-4 under load. Thus, stress-enhanced gelation—characterized by a reduction of the relaxation frequency—can be accounted for by a force-induced exposure of the otherwise sterically hindered ABS 1 binding site.

The stress dependent viscoelastic behavior depicts three distinct regimes as summarized in Fig. 2.6. At the lowest applied stresses, the behavior is linear and thus independent of stress; as stress increases, the differential plateau modulus remains unchanged, while the relaxation frequency decreases substantially. It is only at the highest stresses that differential plateau modulus also exhibits nonlinear behavior. Interestingly therefore, there is an extended range of stress where the network nonlinearity appears to be a consequence of only the force-dependent linker unbinding dynamics. By direct analogy to the structural relaxation observed in networks formed with mutant Actn4 cross-links, the change in relaxation frequencies under stress is consistent with a change in affinity induced by load, a defining feature of catch-bond-like behavior. However, this conclusion is based on macroscopic observations, and single molecular experiments are needed to confirm this mechanism. Furthermore, a nonlinear extension of the CGD model is required to quantitatively describe the nonlinear viscoelasticity of transiently cross-linked gels.

Our results may have interesting biological implications, relating to the mechanisms of intracellular remodeling and dynamic stress accommodation. In particular, we have identified a mechanism to independently control both the network stiffness and the onset time-scale for structural relaxation. This represents a novel design principle which may allow the cell to maintain structural integrity at longer time scales. While conventional network stiffening increases the elastic modulus, it does not prevent eventual network flow. By contrast however, stress-enhanced gelation may actually enables the cell to substantially delay network flow by extending the frequency range of solid-like behavior.

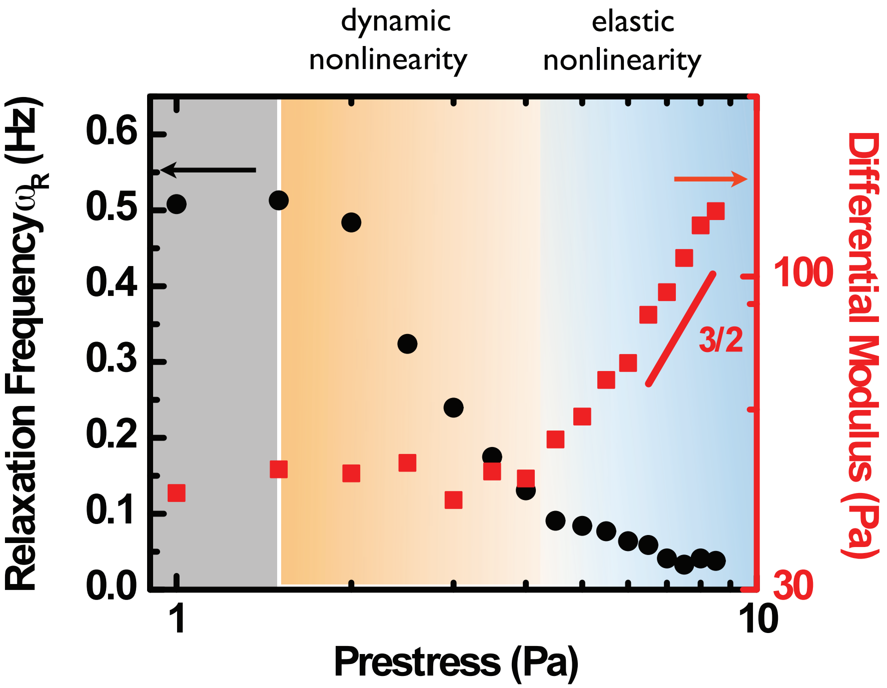

Figure 2.6 – The relaxation frequency for the onset of structural relaxation and the differential plateau modulus as a function of applied stress. There are three regimes with qualitatively different behavior. In the grey regime the viscoelasticity is independent of applied prestress, in the orange regime the applied prestress reduces the onset of structural relaxation shift and enhances gelation, and in the blue regime the plateau modulus increases strongly—characteristic of stiffening behavior. The stiffening behavior in which differential plateau modulus scales with stress as $\sim \sigma^{3/2}$, is consistent with prior experiments on cross-linked actin gels [6] and the affine entropic model [2, 21].

2.4 Appendix 1: Materials and methods

Networks of cross-linked actin are formed by mixing 23.8 μM (1mg/ml) G-actin solution with corresponding α-actinin-4 solutions ranging from 0.0238 μM to 0.238 μM. Polymerization was initiated by the addition of 5x polymerization buffer. The mechanical response of the cross-linked actin networks is measured after one hour of polymerization at a temperature of 25°C. We use a stress-controlled rheometer (AR-G2, TA Instruments) using a 20mm diameter 2 degree stainless steel cone plate geometry and a gap size of 50 μm. We utilize a home-made steel bottom plate to ensure that the networks do not slip and a solvent trap to prevent drying. To measure the linear viscoelastic moduli, we apply an oscillatory stress of the form $\sigma(\omega) = A \sin(\omega t)$, where A is the amplitude of the stress and ω is the frequency. The resulting strain is of the form $\gamma(\omega) = B \sin(\omega t + \delta)$ and yields the storage modulus $G'(\omega) = A/B \cos(\delta)$ and the loss modulus $G''(\omega) = A/B \sin(\delta)$. To determine the frequency dependence of the linear moduli, $G'(\omega)$, $G''(\omega)$ are sampled over a range of frequencies from 0.001 - 10 Hz.

2.5 Appendix 2: Evolution equations of the CGD model

Here we outline the basic steps used to derive the evolution equations of the CGD model presented in the main text. We describe the local relaxation of a polymer segment, upon unbinding of a cross-linker n at a position x_n along the average direction $\hat{\boldsymbol{e}}_x$ of the relaxed polymer. The release of cross-linker n lifts a constraint and enables the thermal relaxation of the two surrounding segments. To capture this local equilibration step, we approximate the thermal distribution as Gaussian and centered around the minimum energy position of the coarse-grained chain. This allows us to separate the equilibration step into a move to mechanical equilibrium and a stochastic thermal move.

The mechanical relaxation step of the cross-linker at an initial position $\boldsymbol{r}^{(\mathrm{i})}(x_n) = \boldsymbol{r}_\perp^{(\mathrm{i})}(x_n) + r_\parallel^{(\mathrm{i})}(x_n)\hat{\boldsymbol{e}}_x$ is written as

$$\boldsymbol{r}^{(\mathrm{i})}(x_n) \to \boldsymbol{r}^{(\mathrm{meq})}(x_n) = \boldsymbol{r}^{(\mathrm{i})}(x_n) + \Delta\boldsymbol{r}_\perp^{(\mathrm{meq})}(x_n) + \Delta r_\parallel^{(\mathrm{meq})}(x_n)\hat{\boldsymbol{e}}_x. \tag{2.7}$$

This step is determined through the local minimization condition

$$\mathbf{0} = \left.\frac{\partial H_{\mathrm{CG}}}{\partial \mathbf{r}_n}\right|_{\mathbf{r}_n=\mathbf{r}_n^{(\mathrm{meq})}}. \tag{2.8}$$

A discrete calculation gives a third-order equation for the mechanical relaxation and, using a convenient continuum notation for discrete differences over a length scale ℓ_{c}, we have

$$\ell_{\mathrm{b}}^2(\ell_{\mathrm{c}}^4\partial_x^4\boldsymbol{r}_\perp + 3\ell_{\mathrm{c}}^2\partial_x^2\boldsymbol{r}_\perp) = -\delta\boldsymbol{r}_\perp\left(2\ell_{\mathrm{c}}^2\partial_x\phi + 6\ell_{\mathrm{b}}^2 + \delta\boldsymbol{r}_\perp^2\right), \tag{2.9}$$

With $\delta r_\parallel = \hat{\boldsymbol{e}}_x \cdot \delta\boldsymbol{r}_\perp$ and $\ell_{\mathrm{b}} = \sqrt{\kappa/\mu_{\mathrm{th}}}$. Here we have decomposed the relaxation step into two sub-steps,

$$\Delta\boldsymbol{r}_{\perp,\parallel}^{(\mathrm{meq})}(x_n) = \frac{\ell_{\mathrm{c}}^2}{2}\partial_x^2\boldsymbol{r}_{\perp,\parallel}(x_n) + \delta\boldsymbol{r}_{\perp,\parallel}(x_n), \tag{2.10}$$

where the first term on the r.h.s. is a step to the midpoint between the still attached flanking cross-linkers, and the second term $\delta\boldsymbol{r}(x_n)$, which is small in the limit of an inextensible polymer considered here. We have further introduced

$$\partial_x\phi = \partial_x r_\parallel - 1 + \frac{1}{2}|\partial_x\boldsymbol{r}_\perp|^2, \tag{2.11}$$

as the differential state of strain along the polymer backbone. When the system evolves around equilibrium, we can estimate the typical size of the relevant terms in the relaxation equations. In the limit of an inextensible fiber, the dominant contribution to $\delta \boldsymbol{r}_\perp$ is of the same order of magnitude as the thermal noise and originates from local bucking,

$$|\delta \boldsymbol{r}_\perp| = \ell_c \sqrt{-2\partial_x \phi}\ \theta(-\partial_x \phi) \tag{2.12}$$

where the Heaviside step function θ is used since a fiber only buckles when under compression.
The full equilibration step, including a thermal contribution can thus be written as

$$\Delta \boldsymbol{r}_\perp = \frac{\ell_c^2}{2} \partial_x^2 \boldsymbol{r}_\perp + \delta \boldsymbol{r}_\perp + \xi_\perp^{\text{th}}, \tag{2.13}$$

$$r_\parallel = \frac{\ell_c^2}{2} \partial_x^2 r_\parallel + \hat{\boldsymbol{e}}_x \cdot \left(\delta \boldsymbol{r}_\perp + \xi_\perp^{\text{th}}\right). \tag{2.14}$$

In the parallel equation the transverse fluctuations, projected along $\boldsymbol{e}_x$, dominate over the longitudinal fluctuations, which are thus neglected.

The thermal noise term ξ^{th} can be calculated directly from the inverse Hessian of the coarse-grained energy function in the Gaussian approximation we use here. The dominating contribution to the noise originates in the transverse component of the Hessian,

$$H_\perp \sim k_B T \frac{\ell_p}{\ell_b^2 \ell_c} |\partial_x \phi|. \tag{2.15}$$

This makes explicit the non-linear dependence on the configuration of the polymer which introduces correlations in the thermal noise in both time and space. Since $\partial_x \phi$ depends explicitly on both $\partial_x r_\parallel$ and $\partial_x r_\perp$ (Eq. 2.11), the noise will couple the evolution equations (Eq. 2.14). The direction of the small buckling term is taken randomly from a continuously degenerate set of solutions and thus also acts effectively as a noise contribution.

We can treat this model using a mean field approach. By performing an equilibrium average of the state of the chain, we calculate the average projection on to $\hat{\boldsymbol{e}}_x$ for both the buckling contribution as well as the contributions of the thermal noise. We can also take the continuum limit in time by replacing the discrete steps $\Delta \boldsymbol{r}_{\perp,\parallel}$ occurring at a rate τ_{off}^{-1} with $\tau_{\text{off}} \partial_t \boldsymbol{r}_{\perp,\parallel}$. Here we are primarily interested in the parallel equation, from which the rheological behavior can be calculated. Within the mean-field picture we have

$$\partial_t r_\parallel = \frac{\ell_c^2}{2} \partial_x^2 r_\parallel + \xi_{\text{MF}}, \tag{2.16}$$

where the noise term can be calculated as

$$\langle \xi_{\text{MF}}(x,t) \xi_{\text{MF}}(x',t') \rangle \approx \frac{\tau_{\text{off}} L \ell_c^{5/2} \ell_b}{12 \ell_p^{3/2}} \delta(x-x') \delta(t-t'). \tag{2.17}$$

Here L is the length of the polymer. The unusual—stronger than linear—dependence on temperature originates in the back projection of local fluctuation on to the average direction of the polymer.

2.6 Acknowledgments

This work was performed in collaboration with M. Depken, N. Y. Yao (who performed the experiments), M. R. Pollak and D. A. Weitz. We thank G. Barkema for useful discussions.

Bibliography

[1] P. A. Janmey, S. Hvidt, J. Lamb, and T. P. Stossel. *Resemblance of actin-binding protein/actin gels to covalently crosslinked networks*. Nature, **345**:89–92 (1990).

[2] F. C. MacKintosh, J. Käs, and P. A. Janmey. *Elasticity of semiflexible biopolymer networks*. Phys. Rev. Lett., **75**:4425 (1995).

[3] F. Gittes and F. C. MacKintosh. *Dynamic shear modulus of a semiflexible polymer network*. Phys. Rev. E, **58**:R1241 (1998).

[4] D. C. Morse. *Viscoelasticity of concentrated isotropic solutions of semiflexible polymers. 2. linear response*. Macromolecules, **31**:7044–7067 (1998).

[5] B. Hinner, M. Tempel, E. Sackmann, K. Kroy, and E. Frey. *Entanglement, elasticity, and viscous relaxation of actin solutions*. Phys. Rev. Lett., **81**:2614–2617 (1998).

[6] M. L. Gardel, J. H. Shin, F. C. MacKintosh, L. Mahadevan, P. Matsudaira, and D. A. Weitz. *Elastic behavior of Cross-Linked and bundled actin networks*. Science, **304**:1301–1305 (2004).

[7] G. H. Koenderink, M. Atakhorrami, F. C. MacKintosh, and C. F. Schmidt. *High-Frequency stress relaxation in semiflexible polymer solutions and networks*. Phys. Rev. Lett., **96**:138307–4 (2006).

[8] R. Tharmann, M. M. A. E. Claessens, and A. R. Bausch. *Viscoelasticity of isotropically Cross-Linked actin networks*. Phys. Rev. Lett., **98**:088103–4, (2007).

[9] M. Doi and S. F. Edwards. *The Theory of Polymer Dynamics*. Clarendon Press, new edition edition, April 1999.

[10] D. Stamenovic. *Cell mechanics: Two regimes, maybe three?*. Nat Mater, **5**:597–598 (2006).

[11] O. Lieleg, M. M. A. E. Claessens, Y. Luan, and A. R. Bausch. *Transient binding and dissipation in Cross-Linked actin networks*. Phys. Rev. Lett., **101**:108101–4 (2008).

[12] O. Lieleg, K.M. Schmoller, M.M.A.E. Claessens, and A.R. Bausch. *Cytoskeletal polymer networks: Viscoelastic properties are determined by the microscopic interaction potential of cross-links*. Biophys. J., **96**:4725–4732 (2009).

[13] S. M. Volkmer Ward, A. Weins, M. R. Pollak, and D. A. Weitz. *Dynamic viscoelasticity of actin Cross-Linked with Wild-Type and Disease-Causing mutant alpha-Actinin-4*. Biophys. J., **95**:4915–4923 (2008).

[14] D. Wachsstock, W. Schwarz, and T. Pollard. *Cross-linker dynamics determine the mechanical properties of actin gels*. Biophys. J., **66**:801–809 (1994).

[15] H. Miyata, R. Yasuda, and K. Kinosita. *Strength and lifetime of the bond between actin and skeletal muscle [alpha]-actinin studied with an optical trapping technique*. Biochimica et Biophysica Acta (BBA) - General Subjects, **1290**:83–88 (1996).

[16] N. Y. Yao *et al.* (unpublished).

[17] M. Depken *et al.* (unpublished).

[18] R. Granek. *From Semi-Flexible polymers to membranes: Anomalous diffusion and reptation*. Journal de Physique II, **7**:28 (1997).

[19] D. R Overby, B. D Matthews, E. Alsberg, and D. E Ingber. *Novel dynamic rheological behavior of individual focal adhesions measured within single cells using electromagnetic pulling cytometry*. Acta Biomaterialia, **1**:295–303, (2005).

[20] N. Desprat, A. Richert, J. Simeon, and A. Asnacios. *Creep function of a single living cell*. Biophys. J., **88**:2224–2233 (2005).

[21] C. Storm, J. Pastore, F.C. MacKintosh, T.C. Lubensky and P.A. Janmey. *Nonlinear elasticity in biological gels*. Nature **435**:191 (2005).

[22] G. I. Bell. *Models for the specific adhesion of cells to cells*. Science **200**:618-627(1978).

[23] A. Weins, J. S. Schlöndorff, F. Nakamura, B. M. Denker, J. H. Hartwig, T. P. Stossel, M. R. Pollak. *A disease-associated mutant alpha-actinin-4 reveals a mechanism for regulating its F-actin binding affinity*. Proc. Natl. Acad. Sci. USA **104**:16080-5 (2007).

3

Elasticity of semiflexible polymer networks with flexible cross-links

- C. P. Broedersz, C. Storm and F. C. MacKintosh
  Nonlinear elasticity of composite networks of stiff biopolymers with flexible linkers,
  Physical Review Letters, **101**: 118103 (2008)

- C. P. Broedersz, C. Storm and F. C. MacKintosh
  Effective medium approach for stiff polymer networks with flexible cross-links,
  Phys. Rev. E **79**, 061914 (2009)

Abstract

Recent experiments have demonstrated that the nonlinear elasticity of *in vitro* networks of the biopolymer actin is dramatically altered in the presence of a flexible cross-linker such as the cytoskeletal protein filamin. The basic principles governing the mechanical properties of such networks, however, remain poorly understood. Here we describe an effective medium theory of flexibly cross-linked stiff polymer networks. The network is modeled as a collection of randomly oriented rods connected by flexible cross-links to an elastic continuum. This effective medium is treated in a linear elastic limit as well as in a more general framework, in which the medium self-consistently represents the nonlinear network behavior. This model predicts that the nonlinear elastic response sets in at strains proportional to cross-linker length and inversely proportional to filament length. Furthermore, we find that the differential modulus scales linearly with the stress in the stiffening regime. These results are in excellent agreement with bulk rheology data.

3.1 Introduction

The mechanical response and locomotion of living cells is mainly controlled by the cellular cytoskeleton. The cytoskeleton is a highly composite network of various stiff biopolymers, along with various binding proteins for force generation, cross-linking and polymer growth regulation. Understanding the basic physics that governs the mechanical properties of a composite biopolymer network represents an important biophysical challenge that will help elucidate the mechanics of a living cell. In addition to their importance for cell mechanics, cytoskeletal networks have also demonstrated novel rheological properties, especially in numerous *in vitro* studies [1–10]. However, there have been few theoretical or experimental studies that address the composite nature of the cytoskeleton [11–16]. Recent experiments on F-actin networks with the highly compliant cross-linker filamin, in particular, have demonstrated several striking features: These networks can have a linear modulus as low as 1 Pa, which is significantly lower than for actin gels with incompliant cross-links, and yet they can withstand stresses of 100 Pa or more and can stiffen dramatically by up to a factor of 1000 under applied shear [10, 11]. Both the linear and nonlinear elastic properties of actin-filamin gels appear to be dramatically affected by the flexible nature of the cross-links, resulting in novel behavior as compared to actin-networks with incompliant cross-links, and to synthetic polymer gels. This suggests new network design principles that may be extended to novel synthetic materials with engineered cross-links [12]. However, the basic physics of networks with flexible cross-links remain unclear.

In this chapter we provide a detailed description of an effective medium approach to describe the nonlinear elastic properties of composite networks consisting of stiff filaments linked by highly flexible cross-links [15]. A schematic image of the network we aim to model is shown in Fig. 3.1. The network is composed of randomly oriented filaments/rods of length L, which are linked together by highly flexible cross-linkers. The cross-links consist of two binding domains interconnected by a thermally fluctuating flexible polymer chain of length ℓ_0. The compliance of such a cross-linker is entropic in nature. Adopting the WLC model, we can fully characterize the cross-linkers with a contour length ℓ_0 and a persistence length ℓ_p [17, 18]. The WLC force-extension curve becomes highly nonlinear when the cross-linker reaches its full extension, as shown in Fig. 3.2 c). Indeed, atomic force microscope (AFM) measurements show that an actin cross-linker such as filamin exhibits strain stiffening and can be accurately described as a wormlike chain (WLC) [24, 25]. At large mechanical loads, however, the experimental force-extension curve deviates significantly from WLC behavior. The polymer chain in cross-linkers such as filamin consists of repeated folded protein domains, which unfold reversibly at sufficiently large mechanical loads. The experiments by Furuike et al. [25] show that after an initial stiffening regime at a force-threshold of ≈ 100 pN, one of the protein domains unfolds. The accompanied increase in contour length results in a strong decrease in the cross-linkers stiffness. This softening is immediately followed by WLC stiffening as the thermal undulations of the lengthened cross-linker are stretched out. This leads to an elastic response that alternates between entropic stiffening and softening caused by domain unfolding, resulting in a sawtooth force-extension curve.

It has been suggested that the unfolding behavior of filamin plays an important role in the mechanical properties of networks with such cross-linkers [11, 13, 25]. Simulations of stiff polymer networks, assuming a sawtooth force-extension curve for the unfoldable cross-links, reveal that such networks exhibit a fragile state in which a significant fraction of cross-linkers is at the threshold of domain unfolding [13]. This results in strain softening of the network under shear, inconsistent with the pronounced stiffening response observed experimentally in actin-filamin gels [10, 11]. We estimate, however, that under typical *in vitro* experimental conditions, domain unfolding in the cross-links is highly unlikely. For domain unfolding to occur with multiple filamin crosslinks experiencing forces of order 100 pN, the resulting tension in the actin filaments is likely to exceed rupture forces of order 300 pN of F-actin [26]. Also, a simple estimate of the macroscopic stress corresponding to even a small fraction of filamins under 100 pN tensions is larger than the typical limit of shear stress

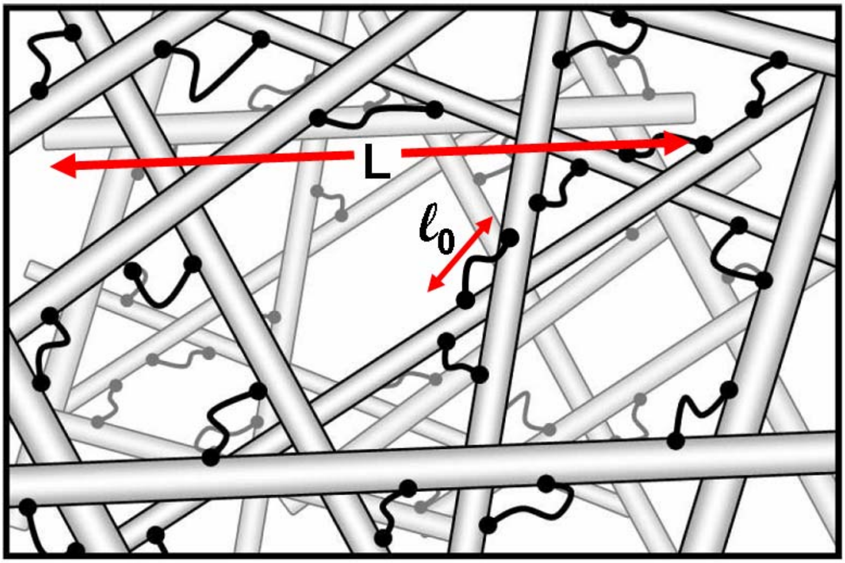

Figure 3.1 – (Color online) Schematic figure of an isotropic stiff polymer network with highly compliant cross-linkers.

before network failure is observed. Therefore, we do not expect domain unfolding to occur. Rather, it seems likely that cross-link unbinding occurs before sufficiently large sufficiently large forces are reached for domain unfolding. Detailed estimates based on experiments suggest filamin tensions only of order 1-5 pN at network failure [16]. It has also been shown in single molecule experiments [27] that filamin unbinds from F-actin at forces well below the forces required for unfolding, which indicates that cross-linker unfolding is unlikely to occur in typical network conditions. Therefore, we consider only the initial stiffening of the cross-links, which we show can account well for the observed nonlinear elasticity of actin-filamin gels.

Our model consists of a network of stiff filaments connected by flexible cross-linkers. The compliance of such a network is expected to be governed by the cross-linkers. The stiff filaments provide connectivity to the network and constrain the deformation of the cross-linkers, thereby setting the length scale of the effective unit cell of the network. Thus, we expect that the elasticity of the network will be controlled by the filament length L and network connectivity, which is expressed in terms of the number of cross-link per filament n. Therefore, we describe the network with a model in which the basic elastic element consists of a single stiff rod and many compliant cross-linkers that connect the rod to a surrounding linear elastic medium.

3.2 Effective Medium Approach

Networks of semiflexible polymers with point-like incompliant cross-links have been studied extensively [4, 5, 28–31]. These systems exhibit two distinct elastic regimes: one in which the deformation of the network is affine and a regime that is characterized by highly non-affine deformations. The network is said to deform affinely if the strain field is uniform down to the smallest length scale of the network. Simulations have shown that the deformation of these networks becomes more affine with increasing cross-link concentration and polymer length [32, 33], which has been borne out by experiments [4, 34]. The elastic response of the network can fully be accounted for by the stretching modes of the polymers in the affine regime. In addition to stretching modes, stiff polymers can also store energy in a non-affine bending mode. Indeed, it has been shown that in sparser networks, in which there are fewer constraints on the constituting polymers, non-affine bending modes dominate the elastic response [29, 32, 33]. We will, however, not consider this sparse network limit here.

In a dense network of stiff polymers with highly flexible cross-links, we expect the soft stretching modes of the linkers to govern the network elasticity. However, the large separation in size and stiffness between cross-links and filaments does imply a non-uniform deformation field for the cross-links at the sub-filament level. On a coarse-grained level the network deforms affinely and stretches the cross-links as depicted in Fig. 3.2 b. The network surrounding this particular rod is shown here as a grey background. The deformation of the cross-links increases linearly from 0 in the center towards a maximum value at the boundaries of the rod. At small strains the cross-links are very soft and follow the deformation of the stiffer surrounding medium. However, at a strain $\gamma_c \sim \ell_0/L$ the outer-most cross-links reach their full extension and, consequently, stiffen dramatically. This suggest the existence of a characteristic strain γ_c, for the onset of the nonlinear response of the network.

The macroscopic elasticity of the network results from the tensions in all the constituting filaments. The tension in a particular filament can be determined by summing up the forces exerted by the cross-links on one side of the midpoint of the filament. We will employ an effective medium approach to calculate these forces as a function of filament orientation and the macroscopic strain. Thus, we model the network surrounding one particular rod, as an affinely or uniformly deforming continuum, which effectively represents the elasticity of the network, as depicted in Fig. 3.2 a and b. We then proceed by considering contributions from rods over all orientations to calculate the macroscopic response of the network.

The remainder of this chapter is organized as follows. First we discuss a model in which the effective medium is treated as a linear elastic continuum. In this model we describe the cross-links both as linear springs with finite extension and as WLC cross-links. We analyze our model in both a fully 3D network, as well as a simplified 1D representation, which already captures the essential physics of the nonlinear behavior. At large strains, when many of the cross-linkers are extended well into their nonlinear regime, it is no longer realistic to model the surrounding network as a linear medium. Therefore, we extend our linear medium model in a self-consistent manner, replacing the embedding medium by a nonlinear effective medium whose elastic properties are determined by those of the constituent rods and linkers. This self-consistent model can quantitatively account for the nonlinear response found in prior experiments on actin filamin networks [11, 16]. Finally, we can compute the tension profiles along the filaments and we demonstrate how to use these to express the macroscopic stress in terms of the maximum force experienced by a single cross-link, which may set the failure stress of the network.

3.3 The Linear medium model

We first develop a one dimensional representation of our model, which will be used in section 3.5 to construct a more realistic three dimensional model. Also we will restrict the treatment here to a linear description of the effective medium, a constraint that is lifted in section 3.4.

Consider a rigid rod of length L connected by n flexible cross-links to an elastic medium. We shall refer to this configuration—consisting of a rod decorated by flexible linkers—as the basic elastic unit (BEU). The medium is stretched by an externally imposed extensional strain ϵ parallel to the orientation of the rod. Throughout this chapter we denote a 1D extensional strain with ϵ and a 3D shear strain with γ. The presence of the BEU in the medium reduces the deformation of the medium at a position x in the rest frame of the rod by an amount $u_{EM}(x,\epsilon) = \epsilon x - u_{cl}(x,\epsilon)$, where $u_{cl}(x,\epsilon)$ is the extension of a cross-linker at a distance x from the center of the rod. The magnitude of $u_{cl}(x,\epsilon)$ and $u_{EM}(x,\epsilon)$ are set by requiring force balance between the cross-links and the medium.

$$f_{cl}(u_{cl}(x,\epsilon)) = K_{EM} u_{EM}(x,\epsilon), \tag{3.1}$$

where $f_{cl}(u)$ is the force-extension curve of a single cross-linker and where K_{EM} is the elastic constant of the medium. The tension τ_0 in the center of the rod is found by summing up the forces exerted by the stretched cross-links on one side of the midpoint of the rod. Assuming a high, uniform line density n/L of cross-links along the rod, we can write the sum as an integral

$$\tau_0(\epsilon) = \frac{n}{L}\int_0^{L/2} dx' f_{cl}\big(u_{cl}(x',\epsilon)\big). \tag{3.2}$$

where $u_{cl}(x',\epsilon)$ is obtained by solving Eqn. (3.1). The full tension profile $\tau(\epsilon, x)$ is

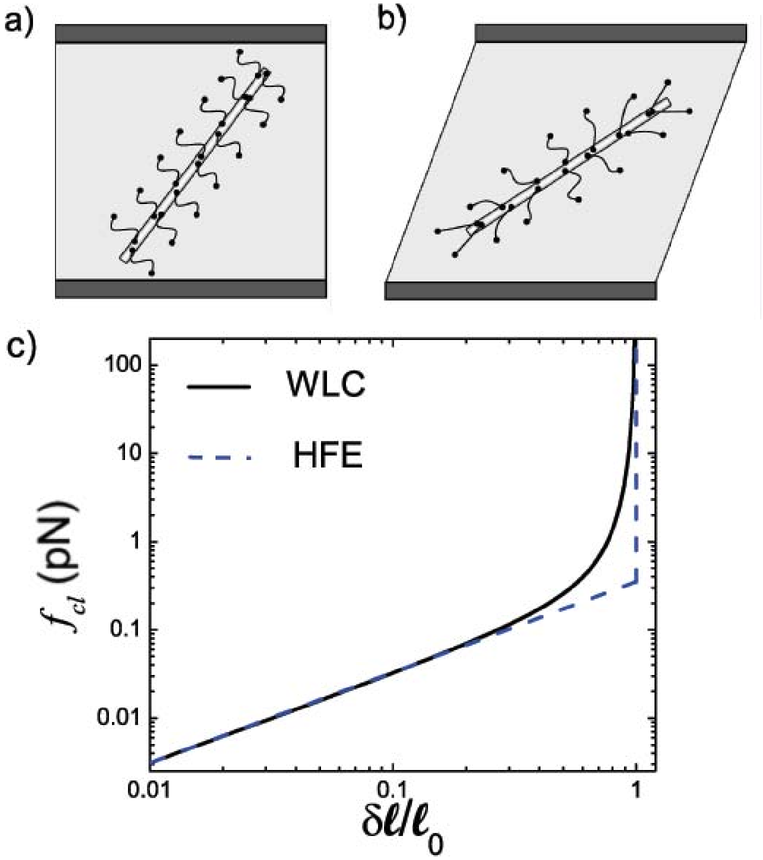

Figure 3.2 – (Color online) a) a single filament connected by *n* flexible cross-links to the surrounding network, which we model as an effective elastic continuum (shown here as a grey background) and b) illustrates the proposed nonuniform deformation of the cross-linkers on a single filament in a sheared background medium. c) Force-extension curve of a Hookean Finite Extendable (HFE) cross-linker (dashed blue curve) and of a WLC cross-linker (solid black curve).

found by replacing the lower limit of the integration by x

$$\tau(\epsilon,x)=\frac{n}{L}\int_{x}^{L/2} dx' f_{cl}\big(u_{cl}(x',\epsilon)\big) \tag{3.3}$$

3.3.1 Hookean Finite Extendable cross-linkers

We can solve Eqns. (3.1) and (3.2) to compute the midpoint tension in a rod for a specific force-extension curve for the cross-links. In the absence of unfolding or unbinding, we can describe the force-extension behavior of a flexible cross-linker such as filamin with the WLC model, as depicted with the black solid line in Fig. 3.2 c). It is instructive to simplify the WLC force-extension curve by assuming a Hookean response with a spring constant k_{cl} up to an extension ℓ_0, which is the molecular weight of the cross-linker. The spring constant $k_{cl} = \frac{2}{3}\frac{k_B T}{\ell_p \ell_0}$ is found from the WLC model for small extensions in the limit $\ell_p \ll \ell_0$ [18], where $k_B T$ is the thermal energy. Beyond an extension ℓ_0, the cross-linker becomes infinitely stiff. The force-extension curve of these Hookean Finite Extendable (HFE) cross-links is shown as a blue dashed curve in Fig. 3.2 c). The finite extensibility of the cross-links implies a critical strain $\epsilon_c = \frac{\ell_0}{L/2}$ at which the cross-linkers at the boundaries of the rod reach full extension. Since the linkers are placed in series with the medium the elastic constants add; thus, for strains $\epsilon \leq \epsilon_c$

$$\tau_0(\epsilon)=\frac{n}{L}\int_{0}^{L/2} dx' \,\frac{k_{cl}K_{EM}}{k_{cl}+K_{EM}}\epsilon x'. \tag{3.4}$$

Thus, the midpoint tension depends linearly on strain for $\epsilon \leq \epsilon_c$. For larger strains, the expression for the midpoint tension in the rod in Eq. (3.2) reads

$$\begin{aligned}\tau_0(\epsilon) &= \frac{n}{L}\int_{0}^{\ell_0/\epsilon} dx' \,\frac{k_{cl}K_{EM}}{k_{cl}+K_{EM}}\epsilon x' \\ &+ \frac{n}{L}\int_{\ell_0/\epsilon}^{\frac{L}{2}} dx' \left[\frac{k_{cl}K_{EM}}{k_{cl}+K_{EM}}\ell_0 + K_{EM}(\epsilon x' - \ell_0)\right].\end{aligned} \tag{3.5}$$

The expression has separated into two integrals, representing a sum over the cross-links with an extension $< \ell_0$ and a sum over the cross-links that have already reached full extension. We also note that beyond ϵ_c, the midpoint tension depends nonlinearly on strain. Using Eq. (3.5) we compute the 1D modulus $G_{1D} = \tau_0/\epsilon$, as shown in Fig. 3.3. Below the critical strain, the response is dominated by the linear elasticity of the cross-links $G_{1D} \approx \frac{1}{8} n k_{cl} L$. The cross-links at the edge of the rod become rigid at a strain threshold $\epsilon_c = 2\ell_0/L$. As the strain is further increased, the cross-links stiffen consecutively (inwards from the edge of the rod), resulting in a sharp increase of G_{1D}. At large strains, G_{1D} asymptotically approaches a second linear regime $\sim \frac{1}{8} n K_{EM} L$.

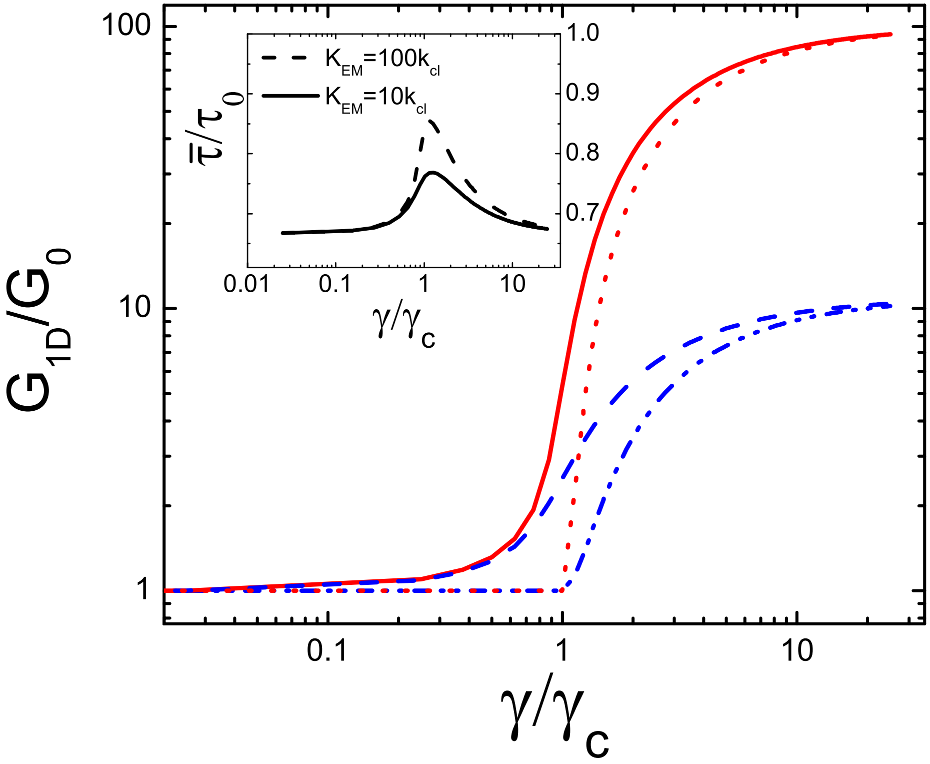

Figure 3.3 – (Color online) a) The modulus $G_{1D} = \tau_0/\epsilon$ for the 1D representation of the linear medium model with HFE cross-links with $K_{EM} = 10k_{cl}$ (blue dash dotted curve) and $K_{EM} = 100k_{cl}$ (red dotted curve). We also show G_{1D} for the model with WLC cross-links with $K_{EM} = 10k_{cl}$ (blue dashed curve) and $K_{EM} = 100k_{cl}$ (red solid curve). The inset shows the ratio of the average tension $\bar{\tau}$ and the midpoint tension τ_0.

3.3.2 Worm Like Chain cross-Linkers

We now consider flexible cross-linkers described by the more realistic WLC force-extension curve, as depicted by the solid line in Fig. 3.2 c. The force-extension relation is well described by the interpolation formula [18]

$$f_{cl}(u) = \frac{k_B T}{\ell_p} \left(\frac{1}{4\left(1 - \frac{u}{\ell_0}\right)^2} - \frac{1}{4} + \frac{u}{\ell_0} \right), \tag{3.6}$$

where k_B is Boltzmann's constant and T is the temperature. This interpolation formula captures the linear and asymptotic stiffening regimes. More detailed theoretical work on WLC polymers in this limit can be found in [19–23]. Using Eqs. (3.1) and (3.2), the 1D modulus G_{1D} is calculated for cross-linkers with this force-extension curve, as shown in Fig. 3.4. The force-extension curve of the WLC cross-linker is linear up to extensions very close to ℓ_0, upon which a pronounced stiffening occurs, as shown in Fig. 3.2 c). We can use these features, together with the property that for a dense network the medium is much stiffer than the flexible cross-linkers $K_{EM} \gg k_{cl}$, to write an approximate expression for the tension in a rod in a closed form analogous to Eq. (3.5).

$$\begin{aligned} \tau_0(\epsilon) \quad &\approx \frac{n}{L} \int_0^{\ell_0/\epsilon} dx' \int_0^{\epsilon x'} du \frac{k_{cl}(u) K_{EM}}{k_{cl}(u) + K_{EM}} \\ + \quad &\frac{n}{L} \int_{\ell_0/\epsilon}^{\frac{L}{2}} dx' \left[\int_0^{\ell_0} du \frac{k_{cl}(u) K_{EM}}{k_{cl}(u) + K_{EM}} + K_{EM}(\epsilon x' - \ell_0) \right], \end{aligned} \tag{3.7}$$

where $k_{cl}(u)$ is the differential stiffness df_{cl}/du of the WLC cross-linker. This equation states that the BEU deforms essentially affine up to the critical strain. Beyond ϵ_c, those cross-links that have reached full extension are no longer compliant and start to pull back on the surrounding medium. The approximate calculation of $d\tau_0/d\epsilon$ using Eq. (3.7) is shown together with the exact calculation performed with Eq. (3.2) in Fig. 3.4. This graph demonstrates that the approximation captures the essential behavior of the exact curve, and results only in a minor quantitative difference in the cross-over regime. Therefore, we will continue constructing our model using this more convenient approximate form.

The 1D modulus calculated with Eq. (3.7) is shown for the WLC cross-links together with the results of the HFE cross-links in Fig. 3.3. Although the main behavior is very similar to that of the HFE cross-linker model, the use of the more realistic WLC force-extension curve has introduced a considerable smoothing of the cross-over. The nonlinear behavior in the WLC force-extension curve initiates slowly well before full extension, resulting in a more gradual onset of nonlinear behavior of the model with

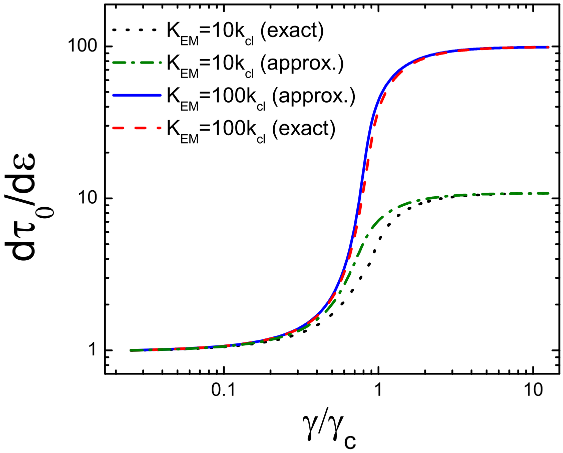

Figure 3.4 – (Color online) The 1D differential modulus $d\tau_0/d\epsilon$ of the rod with WLC cross-linkers as a function of the extensional strain ϵ imposed on the medium parallel to the orientation of the rod. The red dashed and black dotted curves show exact calculations using Eqs. (3.1) and (3.2) and the solid blue and green dash-dotted curves show approximate calculations using Eq. (3.7).

WLC cross-linkers. Importantly, the characteristic strain ϵ_c for the nonlinear behavior is proportional to ℓ_0/L, independent of the exact nonlinear response of the linkers.

For a calculation of network mechanics the average tension $\bar{\tau}$ in a filament is more relevant than the midpoint tension [35]. $\bar{\tau}$ is found by averaging the tension profile given by Eq. (3.3) along the backbone of the filament. The ratio $\bar{\tau}/\tau_0$ is shown in the inset of Fig. 3.3. We find that over a broad range of strains $\bar{\tau} = 3/2\tau_0$. During the cross-over regime the ratio exhibits a peak with an amplitude that depends on the exact ratio of K_{EM} and k_{cl}.

3.4 Self-Consistent medium model

The linear treatment of the effective medium breaks down at large strains; here the network exhibits a nonlinear response as the cross-linkers get extended into their nonlinear regime. Thus, it is no longer appropriate to describe that the effective medium, which should reflect the network elasticity, as linear. In this section we extend our model by requiring that the elasticity of the background medium *self-consistently* represents the nonlinear elasticity of the constituent BEU's. Within this approach, the elasticity of the medium depends on the density of filaments and on the elasticity of a BEU averaged over all orientations. The stiffness of the effective medium K_{EM} that couples to a single cross-link is determined by the stiffness of a BEU

$$K_{EM} = \frac{\alpha}{nL}\frac{d\tau_0}{d\epsilon}. \tag{3.8}$$

The proportionality constant α may depend on the detailed structure of the network, and may be considered as a phenomenological coupling parameter between a linker and the surrounding network. In section 3.4.1 we estimate α using a continuum approach. The midpoint tension in a rod can be written in a similar form as Eq. (3.7)

$$\tau_0(\epsilon) = \frac{n}{L}\int^{\frac{L}{2}} dx'\, x' \int^{\epsilon} d\epsilon' \frac{k_{cl}(x'\epsilon')\frac{\alpha}{nL}\frac{d\tau}{d\epsilon}(\frac{x'\epsilon'}{L/2})}{k_{cl}(x'\epsilon') + \frac{\alpha}{nL}\frac{d\tau}{d\epsilon}(\frac{x'\epsilon'}{L/2})}, \tag{3.9}$$

where $k_{cl}(u)$ is the derivative of the force-extension relation of the cross-linker. Note that we have applied the same approximation as in Eq. (3.7). Eq. (3.9) can be simplified to the following differential equation for $\tau_0(\epsilon)$

$$2\frac{d\tau_0}{d\epsilon} + \epsilon\frac{d^2\tau_0}{d\epsilon^2} = \begin{cases} \frac{nL}{4}\frac{k_{cl}(\epsilon L/2)\frac{\alpha}{Ln}\frac{d\tau_0}{d\epsilon}}{k_{cl}(\epsilon L/2)+\frac{\alpha}{Ln}\frac{d\tau_0}{d\epsilon}} & \text{if } \epsilon < \frac{\ell_0}{L/2} \\ \frac{\alpha}{4}\frac{d\tau_0}{d\epsilon} & \text{if } \epsilon \geq \frac{\ell_0}{L/2} \end{cases} \tag{3.10}$$

We find the following behavior of this model with WLC cross-linkers. Below the characteristic strain for nonlinear response $\epsilon_c = 2\ell_0/L$, the tension in a rod depends approximately linearly on strain. This linearity will be reflected in the self-consistent effective medium, and the model will exhibit a behavior similar to the linear medium model up to the critical strain. By solving Eq. (3.10) we find the midpoint tension τ_0 in a rod as a function of extensional strain ϵ. Beyond the critical strain the tension depends highly nonlinearly on strain, with a derivative that increases as

$$\frac{d\tau_0}{d\epsilon} \sim \epsilon^{\frac{\alpha}{4}-1}. \tag{3.11}$$

Note that unlike in the linear medium model, where the derivative asymptotes to a final value set by K_{EM}, here $d\tau_0/d\epsilon$ increases indefinitely. For the HFE cross-linkers we find similar behavior, although in that case the cross-over between the linear regime and the asymptotic stiffening regime is more abrupt.

3.4.1 Continuum elastic limit

Here we derive an expression for the coupling parameter α in the continuum elastic limit. Note that this will only be a good approximation for a dense, isotropic network.

The modulus of the medium G_{EM} can be expressed in terms of the stiffness $\frac{d\tau_0}{d\epsilon}$ of a BEU by averaging over rod orientations [36]

$$G_{\text{network}} = \frac{1}{15}\rho\frac{d\bar{\tau}}{d\epsilon}, \tag{3.12}$$

where ρ is the length of filament per unit volume. ρ can also be expressed in terms of the mesh-size $\rho = 1/\xi^2$. In the linear medium treatment in section 3.3 we found that $\bar{\tau} = \frac{2}{3}\tau_0$. Thus, the network modulus reads

$$G_{\text{network}} = \frac{2}{45}\frac{1}{\xi^2}\frac{d\tau_0}{d\epsilon}. \tag{3.13}$$

We proceed by relating K_{EM} to G_{network}, which enables us to find an expression for α. Consider a rigid rod of diameter a and length L, which we use as a microrheological probe in an effective elastic medium with a shear modulus G_{EM}. If the rod is displaced along its axis, it will induce a medium deformation $\delta\ell$ that leads to a restoring force acting along its backbone. The restoring force per unit length is given by $2\pi G_{EM}/\log(L/a) \times \delta\ell$. Here we ignore the log term, which is of order 2π. Thus, the stiffness of the medium per cross-link K_{EM} is related to G_{EM} by

$$K_{EM} = \frac{L}{n}G_{EM}. \tag{3.14}$$

By requiring $G_{EM} = G_{network}$ we find α from Eqns. (3.13) and (3.14)

$$\alpha = \frac{2}{45}\left(\frac{L}{\xi}\right)^2. \tag{3.15}$$

Note that for a dense network $\alpha \gg 1$.

3.5 3D Network calculation

In this section we describe in detail how the macroscopic mechanical properties of a uniformly deforming network can be inferred from single filament properties. This procedure has been used to describe the viscoelastic [36] and nonlinear elastic properties [4, 5, 8] of semiflexible polymer networks with point-like rigid cross-links; here we present a detailed derivation of this theory. The main assumption of this calculation is a uniform, or affine deformation of the network. An affinely deforming polymer chain of length ℓ will stretch or compress, depending on its orientation, by an amount that scales as $\sim \ell\gamma$. The validity of the affine treatment of cross-linked semiflexible polymer networks has been subject to much debate. Simulations of networks in 2D demonstrate that the deformation can be both affine and non-affine depending on the density of the network and filament rigidity [32, 33]. Here we derive the affine theory for the case of a filamentous network with point-like rigid cross-links. Then we show how this framework can be used together with the effective medium approach to describe the mechanics of stiff polymer networks with flexible cross-links.

Consider a segment of a filament between two cross-links with an initial orientation $\hat{n}$. When subjected to a deformation described by the Cauchy deformation tensor Λ_{ij}, this filament segment experiences an extensional strain directed along its backbone

$$\epsilon = |\Lambda\hat{n}| - 1. \tag{3.16}$$

As before, we denote a 1D extensional strain with ϵ and a 3D strain with γ. This extensional strain leads either to compression or extension in the polymer segment depending on its orientation, and thus results in a tension $\tau(|\Lambda\hat{n}| - 1)$. The contribution of this tension to the macroscopic stress depends also on the orientation of the polymer segment. By integrating over contributions of the tension over all orientations accordingly, we can compute the macroscopic stress tensor σ_{ij}. The contribution of the tension in a polymer segment with an initial orientation $\hat{n}$ is calculated as follows. The deformation Λ_{ij} transforms the orientation of the segment into $n'_j = \Lambda_{jk}n_k/|\Lambda\hat{n}|$. Thus, the length density of polymers with an orientation $\hat{n}$ that cross the j-plane is given by $\frac{\rho}{\det\Lambda}\Lambda_{jk}n_k$, where the factor $\det\Lambda$ accounts for the volume change associated with the deformation. For the network calculations in this chapter we consider only simple shear, which conserves volume ($\det\Lambda = 1$). The tension in the i-direction in a filament with an initial orientation $\hat{n}$, as it reorients under strain, is $\tau(|\Lambda\hat{n}| - 1)\Lambda_{il}n_l/|\Lambda\hat{n}|$. Thus, the (symmetric) stress tensor reads [5]

$$\sigma_{ij} = \frac{\rho}{\det\Lambda}\left\langle \tau(|\Lambda\hat{n}| - 1)\frac{\Lambda_{il}n_l\Lambda_{jk}n_k}{|\Lambda\hat{n}|}\right\rangle. \tag{3.17}$$

The angular brackets indicate an average over the initial orientation of the polymer chains.

One important feature follows directly from Eq. (3.17). A nonlinear force extension curve for the filaments is not strictly required for a nonlinear network response. The extensional strain of a filament depends nonlinearly on the macroscopic strain of the network,

$$\epsilon = \sqrt{1 + 2\gamma_{kl}\hat{n}_k\hat{n}_l} - 1. \tag{3.18}$$

Furthermore, the reorientation of the filaments under strain leads to an increasingly more anisotropic filament distribution. These geometric effects result in a stiffening of the shear modulus under shear strains of order 1, even in the case of linear Hookean filaments. At large strains all filaments are effectively oriented in the strain direction, which limits the amount of stiffening to a factor of 4 (2D networks) and 5 (3D networks) over the linear modulus in the large strain limit. Thus the stiffening due to this effect occurs only at large strains and is limited. Therefore, we expect this mechanism to have a marginal contribution to the more dramatic stiffening that is observed in biopolymer gels at strains < 1 [4,5]. We would like to stress that the geometric stiffening discussed above has a different nature than the geometric stiffening discussed by [29,37]. In their case, the stiffening is attributed to a cross-over between an elastic response dominated by soft bending modes in the zero strain limit and a stiffer stretching mode dominated regime at finite strains. In the affine calculation described here, only stretching modes are considered.

By limiting ourself to a small strain limit, we exclude the geometric stiffening effects discussed above. This is instructive, since it allows us to study network stiffening due to filament properties alone, and it is a good approximation for most networks since the nonlinear response typically sets in at strains < 1. For a volume conserving deformation ($\det\Lambda = 1$) in the small strain limit the stress tensor in Eq. (3.17) reduces to [36]

$$\sigma_{ij} = \rho \left\langle \tau(\gamma_{kl}\hat{n}_k\hat{n}_l)\hat{n}_i\hat{n}_j \right\rangle , \tag{3.19}$$

In this limit the geometric stiffening mechanism discussed above is absent. Next we show explicitly how to calculate the shear stress σ_{xz}, in the z-plane for a network, which is sheared in the x-direction. A filament segment with an orientation given by the usual spherical coordinates θ and φ undergoes an extensional strain

$$\begin{aligned} \epsilon &= \sqrt{1+2\gamma\cos(\varphi)\sin(\theta)\cos(\theta)+\gamma^2\cos^2(\theta)} - 1 \\ &\approx \gamma\cos(\varphi)\sin(\theta)\cos(\theta), \end{aligned} \tag{3.20}$$

where we have used a small strain approximation in the second line. The tension in this segment contributes to the xz-component of the stress tensor through a geometric multiplication factor $\cos(\phi)\sin(\theta)\cos(\theta)$, where the first two terms are due to a projection of the forces in the x-direction and the second term is due to a projection of the orientation of the filament into the orientation of the z-plane. The stress in the xz-direction is thus given by

$$\sigma_{xz} = \frac{\rho}{4\pi}\int_0^{\pi}\int_0^{2\pi} d\theta d\varphi\ \sin(\theta)\tau\left[\gamma\cos(\varphi)\sin(\theta)\cos(\theta)\right]\cos(\varphi)\sin(\theta)\cos(\theta). \tag{3.21}$$

Since we limit ourselves to the small strain limit, we do not account for a redistribution of the filament orientations by the shear transformation in this equation.

3.5.1 Semiflexible polymer networks with rigid point-like cross-links

In this section we discuss how the affine framework can be used to compute the elastic response of a network with inextensible semiflexible polymers connected by point-like rigid cross-links.

Consider a segment of an inextensible semiflexible polymer of length ℓ_c between two rigid cross-links in the network. Thermal energy induces undulations in the filament, which can be stretched out by an applied tension. Within the WLC model in the semiflexible limit $\ell_c \gtrsim \ell_p$, the force-extension relation of this segment has been shown to be given implicitly by [28]

$$\delta\ell = \frac{\ell_c^2}{\pi^2 \ell_p} \sum_{n=1}^{\infty} \frac{\phi}{n^2(n^2+\phi)}, \tag{3.22}$$

where ϕ is the tension τ normalized by the buckling force threshold $\kappa\frac{\pi^2}{\ell_c^2}$. This relationship can be inverted to obtain the tension as a function of the extension $\delta\ell$:

$$\tau = \kappa \frac{\pi^2}{\ell_c^2} \phi \left(\delta\ell / \delta\ell_{\max}\right), \tag{3.23}$$

where $\delta\ell_{\max} = \frac{1}{6}\ell_c^2/\ell_p$ is the total stored length due to equilibrium fluctuations. This is also the maximum extension, which can be found from Eq. (3.22) as $\phi \to \infty$. For small extensions $\delta\ell$ this reduces to

$$\tau = 90 \frac{\kappa^2}{k_B T \ell_c^4} \delta\ell. \tag{3.24}$$

This result can be inserted into Eq. (3.19) to find the linear modulus of the network

$$G_0 = 6\rho \frac{\kappa^2}{k_B T \ell_c^3}. \tag{3.25}$$

For a network in either two or three dimensions, the maximally strained filaments under shear are oriented at a 45 degree angle with respect to the shear plane, implying that the maximum shear strain is

$$\gamma_{\max} = \frac{1}{3}\frac{\ell_c}{\ell_p}. \tag{3.26}$$

Using the small strain approximation(as in Eq. (3.19)), we can calculate the nonlinear network response

$$\begin{aligned} \frac{\sigma}{\sigma_c} \quad = \quad & \frac{1}{4\pi} \int_0^{\pi} \int_0^{2\pi} d\theta d\varphi \, \sin(\theta) \{ \\ & \phi \quad [\tilde{\gamma} \cos(\varphi) \sin(\theta) \cos(\theta)] \cos(\varphi) \sin(\theta) \cos(\theta) \} \end{aligned} \tag{3.27}$$

where we define the critical stress to be $\sigma_c = \rho\frac{\kappa}{\ell_c^2}$. We have also defined $\tilde{\gamma} = \gamma/\gamma_c$, where the critical strain for the network is given by

$$\gamma_c = \frac{1}{6}\frac{\ell_c}{\ell_p}. \tag{3.28}$$

Eq. (3.27) demonstrates that the nonlinear response of a network of inextensible semiflexible polymers with rigid cross-links is universal for small strains [4]. Note, however, that this would not hold if we would use the full nonlinear theory from Eq. (3.17), valid for arbitrarily large strains. Thus, geometric stiffening effects may lead to small departures from universality. Alternatively, universality may break down as a result of enthalpic stretching of the polymer backbone [5]. The universal nonlinear elastic response for a semiflexible polymer network with rigid cross-links is shown in Figs. 3.5 and 3.6. The divergence of the differential modulus beyond the critical strain is of the form $\sim \frac{1}{(1-\gamma_{\max})^2}$, as depicted in Fig. 3.5. This results into a powerlaw stiffening regime of the form $K \sim \sigma^{3/2}$, as shown in the inset of Fig. 3.6. This prediction is consistent with experiments on actin gels with the rigid cross-linker scruin [4].

In this section we have assumed that at zero strain all filament segments are at their equilibrium zero-force length. However, cross-linking of thermally fluctuating polymers will result in cross-linking distances both smaller and greater than their equilibrium length. This effect, which is ignored in our discussion here, leads to internal stresses build into the network during the gelation [5].

3.5.2 Stiff polymer networks with highly flexible cross-links

For a network with flexible cross-links we do not consider the tension in filament segments, but rather the average tension $\bar{\tau}$ in the whole filament. By using the effective medium approach we can compute the average tension in a filament as a function of the orientation of the rod and the macroscopic shear strain γ. Contributions to the stress from the average tension in the rods are integrated over all orientations according to Eq. (3.21). In our description we thus assume affine deformation of the network on length scales $> L$. Note, however, that we do not assume that the cross-links deform affinely.

We find both from the linear medium model and the self-consistent model for a network with highly flexible cross-links that the linear modulus is approximately given by

$$G_0 \approx \frac{1}{8} \rho n k_{cl} L. \tag{3.29}$$

The appearance of the filament length L in this equation is remarkable, and is due to the non-uniform deformation profile of the cross-links, which leverages the forces applied by the cross-links further from the midpoint of the filament. The onset of nonlinear elastic response occurs at a critical strain

$$\gamma_c = 4\frac{\ell_0}{L}. \tag{3.30}$$

The full nonlinear response as predicted by our model is shown in Figs. 3.5 and 3.6. The results of the linear medium model with WLC cross-links, as shown with a green dotted line, are qualitatively similar to the results of the 1D model (see Fig. 3.3). For the self-consistent model we find that beyond γ_c the differential modulus increases as a powerlaw, as shown in Fig. 3.5. There appears to be only a small quantitative difference between the model with HFE and WLC cross-links.

The differential modulus $K = d\sigma/d\gamma$ is plotted as a function of stress in Fig. 3.6. The stress is normalized by the critical stress σ_c, which we define here as

$$\sigma_c = G_0\gamma_c = \frac{1}{2}\rho n k_{cl}\ell_0. \tag{3.31}$$

We find a sharp increase in stiffness beyond the critical stress, which quickly asymptotes to a powerlaw regime, where the exponent is given by $1 - 1/(\frac{1}{60}(L/\xi)^2 - 1)$. Interestingly, this exponent does not depend on the exact form of the nonlinear response of the cross-linkers. This exponent emerges as a consequence of the finite extendability of the cross-links and the non-uniform deformation profile along the backbone of the filament. In the dense limit we consider in our model, the deviation from an exponent of 1 is small and depends only weakly on the ratio L/ξ. As an example, we consider a typical *in vitro* network for which $\xi = 0.3$ μm and the average filament length $L = 15$ μm, for which we find an exponent of 0.98. The asymptotic powerlaw regime with an exponent ≈ 1, as predicted by our model is consistent with recent experimental data on actin networks cross-linked by filamin [11, 16]. Finally, the inset of Fig. 3.6 shows the rigid linker model together with the self-consistent model for a network with flexible cross-links. In this case the stress is normalized by a stress σ_0, which marks the knee of the curve.

3.6 Tension profiles and single cross-linker force estimate

Recently, there has been much debate on the mechanical response of actin binding proteins such as filamin. Specifically, it is discussed whether the cross-links stiffen, unfold or unbind under tension in both physiological or *in vitro* conditions. The precise response of the linkers may have implications for the dynamical and mechanical properties of the cytoskeleton. The discussion has been partially resolved recently by single molecule [27] and bulk rheology [16] experiments on the actin-filamin system. These experiments indicate that cross-links unbind at forces well below the force required for domain unfolding. It is helpful for the interpretation bulk rheology experiments to be able to infer the forces experienced by a single cross-linker from the measured mechanical stress. In this section we show that by using the shape of

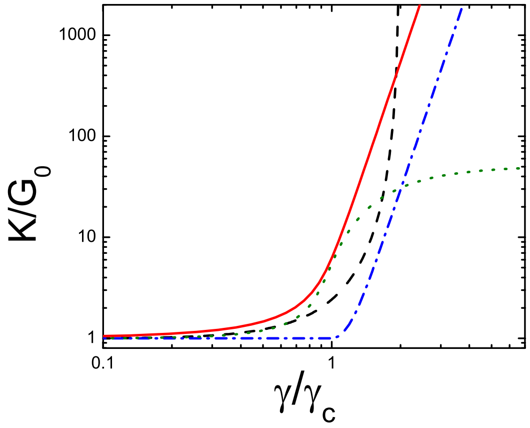

Figure 3.5 – (Color online) The differential modulus $K = d\sigma/d\gamma$ normalized by the linear modulus G_0 as a function of strain normalized by the critical strain γ_c. The universal curve for a semiflexible polymer network with rigid cross-links is shown as a black dashed curve. We also show the results of the self-consistent model with WLC cross-links (red solid curve) and simple cross-links (blue dash-dotted curve), the linear medium model with WLC cross-links with $K_{EM} = 100k_{cl}$ (green dotted curve).

the tension profile, we can relate a macroscopic quantity such as the stress to the maximum force experienced by a single cross-linker in the network.

The tension along a single filament is not uniform in networks of stiff finite length filaments and incompliant cross-links [32, 38]. It was found in simulations that in the affine regime the tension profile is flat close to the midpoint and the tension decreases exponentially towards the boundaries of the filament. In the non-affine regime a different tension profile has been reported, in which the tension decreases linearly towards the ends [38]. In the case of a flexibly cross-linked network of stiff polymers we also expect a non-uniform tension profile, although in this case the underlying physics is different. The deformation of a cross-linker at a distance x from the midpoint of the rod is $u_{cl} \sim x\gamma$; thus, cross-links further away from the midpoint exert larger forces on the rod, resulting in a non-uniform tension profile.

We can calculate the tension profile for a given rod using Eq. (3.3). In the limit of highly flexible cross-linkers, the tension profile in the linear elastic regime is given by

$$\tau(\epsilon, x) = \frac{n}{L}\frac{k_{cl}K_{EM}}{k_{cl}+K_{EM}}\frac{1}{2}\left(x^2 - \left(\frac{L}{2}\right)^2\right)\epsilon. \tag{3.32}$$

The tension profiles as computed with the self-consistent model with WLC cross-links are shown for various strains in Fig. 3.7. For low strains we find a parabolic profile, which flattens out towards the edges for larger strains.

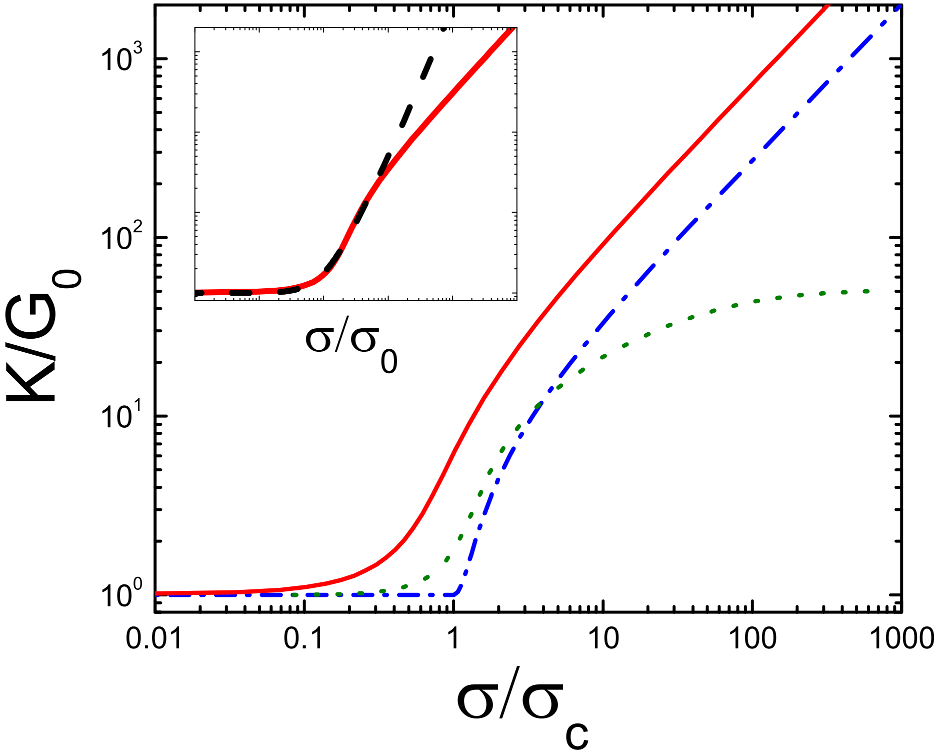

Figure 3.6 – (Color online) The differential modulus $K = d\sigma/d\gamma$ normalized by the linear modulus G_0 as a function of stress normalized by the critical stress σ_c for the self-consistent model with WLC cross-links (red solid curve), HFE cross-links (blue dash-dotted curve) and the linear medium model with WLC cross-links with $K_{EM} = 100k_{cl}$ (green dotted curve). The inset shows the rigid linker model together with the self-consistent model for a network with flexible cross-links. In this case the stress is normalized by a stress σ_0, which marks the knee of the curve.

We now proceed to estimate the force experienced by a single cross-linker. For an affinely deforming network in the linear response regime Eq. (3.17) simplifies to

$$\sigma = \frac{1}{15}\rho\bar{\tau}(\gamma). \tag{3.33}$$

Filaments at a 45° angle with respect to the stress plane bear the largest tension $\bar{\tau}_{max}$ and experience a strain along their backbone of $\gamma/2$. Assuming linear response we find $\bar{\tau}_{max}(\gamma) = \bar{\tau}(\gamma)/2$. In the case of a parabolic tension profile, the average tension $\bar{\tau}$ in a filament is related to the largest force f_0 experienced by a cross-linker at the boundary of the rod by $\bar{\tau} = \frac{1}{6}nf_0$. Thus, we can express the macroscopic stress in terms of the maximum forces experienced by cross-linkers on the filaments under the greatest load

$$\sigma = \frac{1}{45}\rho n f_{max}. \tag{3.34}$$

For the derivation of this equation we have assumed to be in the linear response regime. In the nonlinear regime we expect the expression to still hold approximately, although the prefactor will change.

Recently, Kasza et al. [16] found that the failure stress of the network σ_{max} is proportional to the number of cross-links per filament n in actin networks with the flexible cross-linker filamin. This suggests that filamin failure, rather than rupture of single actin filaments is the cause for network breakage. In contrast, for actin networks with the rigid cross-linker scruin, which binds more strongly to actin than filamin, rupture of actin was found to be the mechanism for network failure [4]. On the basis of our model and the experimental data from Ref. [16] we estimate filamin failure forces of order $1 - 5$ pN, far below the unfolding force 100 pN. This suggests that network failure is due to filamin unbinding. This is consistent with recent single molecule experiments, which show that filamin unbinding is favored over unfolding of the Ig-domains for low loading rates [27].

These numerical estimates for the force experienced by a single filamin cross-linker are for *in vitro* conditions. Under such conditions actin is present with a concentration of ~ 1 mg/ml and filamin is present at an actin to filamin ratio of ~ 100. *In vivo* the concentration of actin is believed to be an order of magnitude larger [16]. Living cells are, however, under stresses which in some cases are found to be of order 1000 Pa [42], more than an order magnitude larger than in the *in vitro* systems [11, 16]. Hence, the forces experienced by an individual cross-linker *in vivo* will be of the same order of magnitude as under *in vitro* conditions. Therefore, we do not expect a significant amount of domain unfolding of filamin to occur *in vivo* under typical conditions.

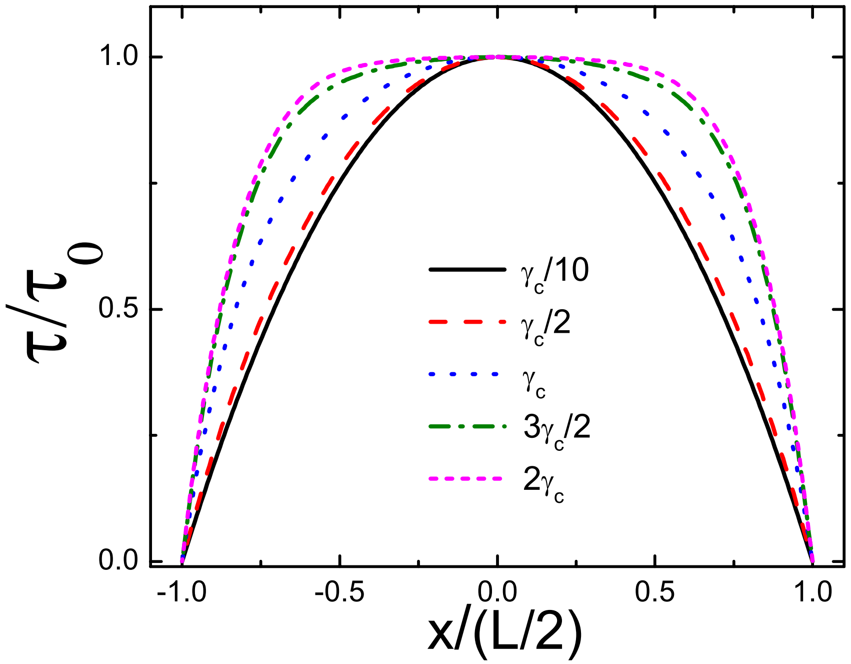

Figure 3.7 – (Color online) The reduced tension profile along the rod, normalized by the midpoint tension τ_0. This profile is calculated with the self-consistent model with WLC cross-links.

3.7 Implications and discussion

We have studied the nonlinear elasticity of stiff polymer network with highly flexible cross-links. We find that the mechanics of such a network is controlled by network connectivity expressed in terms of the number of cross-links per filament n. This was found earlier in experiments on actin-filamin gels [16], providing strong experimental evidence for cross-link dominated mechanics in these networks. Within this picture, stiffening occurs at a strain where the cross-links are stretched towards their full extension. As a result, we expect γ_c to be proportional to the molecular weight of the cross-linker ℓ_0. This prediction is consistent with the results of Wagner et al. [12], where cross-link length was varied, while keeping the average filament length fixed. Interestingly, they observed larger values of γ_c than expected either from our model or based on Refs [11, 12, 16].

In addition, we find here that the filament length L plays an important role in the nonlinear elasticity of these networks. In particular, the onset of nonlinear response $\gamma_c \sim \ell_0/L$ depends crucially on filament length. This has been confirmed by recent experiments on actin-filamin gels, showing an approximate inverse dependence of the γ_c on actin filament length [16]. The sensitivity of network response to filament length, both in experiments and in our model, appears to be one of the hallmarks of actin-filamin networks. On the one hand, this may explain the apparent difference between the critical strains reported in Refs. [11, 12, 16]. On the other hand, this also suggests that it may be even more important in such flexibly cross-linked networks to directly control and measure the filament length distribution than for other *in vitro* actin studies [39]. Our model does not account for filament length polydispersity. A distribution in filament length is expected to smooth somewhat the sharp stiffening transition predicted by our model.

The dependence of the critical strain for networks with flexible cross-links observed in experiments and predicted by our model is in striking contrast with the behavior found for rigidly cross-linked networks. In the latter case, theory predicts $\gamma_c \sim \ell_p/\ell_c$ (see Eq. (3.28)) consistent with experimental observations [4]. The insensitivity of the nonlinear elasticity of dense networks cross-linked with rigid linkers to filament length would suggest that network mechanics cannot be effectively controlled by actin polymerization regulation. We have shown here that the filament length plays a crucial role for networks with flexible cross-links, which are abundant in the cellular cytoskeleton. Thus regulating actin length by binding/capping proteins such as gelsolin may enable the cell not only to sensitively tune its linear elastic modulus, but also the onset of the nonlinear response of its cytoskeleton.

In the nonlinear regime we expect the differential modulus to increase linearly with stress for a dense flexibly cross-linked network. This behavior is a direct consequence of the non-uniform deformation profile along a filament and the finite extendability of the cross-links, although it is independent of the exact shape of the force-extension behavior of the cross-links. The powerlaw stiffening $K \sim \sigma^y$ with $y \approx 1$ is consistent with recent experiments on actin-filamin gels [11,16]. This stiffening behavior is very different from the nonlinear response observed for actin gels with rigid cross-links for which a powerlaw exponent of 3/2 is observed [4], consistent with theory for an affine response governed by the stretching out of thermal fluctuations of the actin filaments. Interestingly, *in vivo* experiments show that cells also exhibit power-law stiffening with an exponent of 1 [40].

In this chapter we examined a limit in which the stiffness of the cross-links is small compared to the stiffness of an F-actin segment between adjacent cross-links. For a large flexible cross-linker such as filamin this is clearly a good approximation in the linear regime. However, as the cross-links stiffen strongly they could, in principle, become as stiff as the actin segment. This would affect the nonlinear response of the network. To investigate this we calculated the differential stiffness df/du as a function of force f for a filamin cross-linker and an actin segment with a length 0.5 to 2 μm, spanning the range of typical distances between cross-links in dense and sparse networks respectively. This result is shown in Fig. 3.8. We that find the differential stiffness of a filamin cross-link is always smaller than for an F-actin segment, even at large forces in the nonlinear regime. This justifies our approach, in which we ignored the compliance of the actin, for a broad range of experimentally accessible polymer/cross-linking densities. However, at sufficiently high filamin concentrations, it may be possible that individual network nodes involve multiple cross-linkers, in which case the actin filament compliance may also become relevant. Thus the effect of the compliance of F-actin remains an interesting topic for further research.

We also use our model to study these networks on a more microscopic level, such as the non-uniform tension profiles along the filament backbone. These profiles can be used to establish a relation between the macroscopic stress and the largest force experienced by a single cross-linker in the network. This allows us to estimate the forces experienced by filamin cross-links under typical *in vitro* and *in vivo* conditions. We find that the load on these cross-links is not sufficiently high to lead to significant domain unfolding of the filamin Ig-domains, even at stresses large enough to rupture the network. Indeed both rheology experiments on actin filamin gels and single molecule experiments indicate that unbinding occurs well before domain unfolding.

In other large flexible cross-links such as spectrin [41], domain unfolding occurs at lower, more relevant forces. In this case the domain unfolding could have a dramatic effect on the nonlinear viscoelasticity of such networks. In previous work, DiDonna and Levine simulated 2D cross-linked networks, where they assumed a sawtooth force-extension curve for the cross-linkers to mimic domain unfolding [13]. Their model, however, does not include the dramatic stiffening that is known to occur before unfolding in filamin cross-links. They observe a fragile state with shear

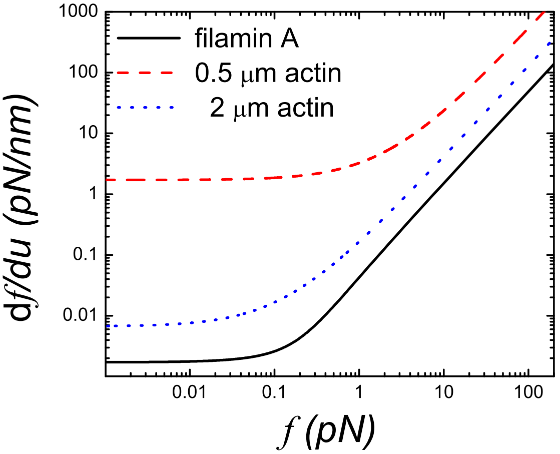

Figure 3.8 – (Color online) The differential stiffness df/du as a function of force f for a filamin cross-linker (solid line) and for several F-actin polymer segment lengths.

softening when an appreciable number of cross-linkers are at the threshold of domain unfolding. Our model is based on the stiffening of the cross-linkers, which initiates at forces far below those required for domain unfolding. This leads to strain stiffening at a point where only a fraction of cross-linkers are at their threshold for nonlinear response. Thus in both our model and that of Ref. [13] the network responds strongly to small strain changes, though in an opposite manner: stiffening in the present case vs softening in Ref. [13].

In related work, Dalhaimer, Discher, and Lubensky show that isotropic networks linked by large compliant cross-linkers exhibit a shear induced ordering transition to a nematic phase [14]. It would be interesting to investigate the effect of the nonlinear behavior of the cross-links on this transition. In the present calculation we have assumed an isotropic network. An ordering transition, which results in a strong alignment of filaments will dramatically affect the nonlinear elasticity of the network.

In this article we have studied networks of stiff polymers linked by highly flexible cross-links. Both experiments [11, 16] and our model [15] indicate that these networks have novel nonlinear rheological properties. We find that the network mechanics is highly tunable. By varying filament length, cross-linker length and network connectivity we can sensitively regulate the linear and nonlinear elasticity over orders of magnitude. These unique properties can be exploited in the design of novel synthetic materials.

3.8 Acknowledgments

This work was performed in collaboration with C. Storm. We thank K. Kasza, G. Koenderink, E. Conti and M. Das for helpful discussions.

Bibliography

[1] P. A. Janmey, U. Euteneuer, P. Traub, M. Schliwa. *Viscoelastic properties of vimentin compared with other filamentous biopolymer networks.* J. Cell Biol. **113**, 155 (1991).

[2] F. C. MacKintosh and P. A. Janmey. *Actin Gels*. Curr. Opin. Solid State Mater. Sci. **2**, 350 (1997).

[3] J. Y. Xu, D. Wirtz, T. D. Pollard. *Dynamic cross-linking by alpha-actinin determines the mechanical properties of actin filament networks*. J. Biol. Chem. **273**: 9570 (1998).

[4] M. L. Gardel, J. H. Shin, F. C. MacKintosh, L. Mahadevan, P. A. Matsudaira, and D. A. Weitz. *Elastic behavior of cross-linked and bundled actin networks*. Science **304**:1301-1305 (2004).

[5] C. Storm, J. Pastore, F. C. MacKintosh, T. C. Lubensky and P. A. Janmey. *Nonlinear elasticity in biological gels*. Nature **435**:191 (2005).

[6] A. R. Bausch and K. Kroy. *A bottom-up approach to cell mechanics*. Nature Phys. **2**, 231 (2006) .

[7] O. Chaudhuri, S. H. Parekh and D. A. Fletcher. *Reversible stress softening of actin networks*. Nature **445**: 295 (2007).

[8] P. A. Janmey, M. E. McCormick, S. Rammensee, J. L. Leight, P. C. Georges, and F. C. MacKintosh. *Negative normal stress in semiflexible biopolymer gels*. Nature Materials **6**, 48 (2007).

[9] F. Gittes, B. Schnurr, P. D. Olmsted, F. C. MacKintosh, and C. F. Schmidt. *Microscopic Viscoelasticity: Shear Moduli of Soft Materials Determined from Thermal Flucuations*. Phys. Rev. Lett. **79**, 3286 (1997).

[10] K. E. Kasza, A. C. Rowat, J. Liu, T. E. Angelini, C. P. Brangwynne, G. H. Koenderink and D. A Weitz. *The cell as a material*. Curr. Opin. Cell Biol. **19**:101-7 (2007).

[11] M. L. Gardel, F. Nakamura, J. H. Hartwig, J. C. Crocker, T. P. Stossel, and D. A. Weitz. *Prestressed F-actin networks cross-linked by hinged filamins replicate mechanical properties of cells*. Proc. Natl. Acad. Sci. **103**:1762-1767 (2006);
M. L. Gardel, F. Nakamura, J. Hartwig, J. C. Crocker, T. P. Stossel, and D. A. Weitz. *Stress-dependent elasticity of composite actin networks as a model for cell behavior*. Phys. Rev. Lett. **96**:088102 (2006).

[12] B. Wagner, R. Tharmann, I. Haase, M. Fischer and A.R. Bausch. *Cytoskeletal polymer networks: The molecular structure of cross-linkers determines macroscopic properties*. Proc. Nat. Acad. Sci. USA **103**, 13974 (2006).

[13] B. A. DiDonna, and A. J. Levine. *Filamin Cross-Linked Semiflexible Networks: Fragility under Strain*. Phys. Rev. Lett. **97**, 068104 (2006).

[14] P. Dalhaimer, D. E. Discher and T. C. Lubensky. *Crosslinked actin networks show liquid crystal elastomer behaviour, including soft-mode elasticity* Nature Phys. **3**, 354 (2007).

[15] C. P. Broedersz, C. Storm, and F. C. MacKintosh. *Nonlinear elasticity of composite networks of stiff biopolymers with flexible linkers*. Phys. Rev. Lett. **101**:118103 (2008);
C. P. Broedersz, C. Storm, and F. C. MacKintosh. *Effective-medium approach for stiff polymer networks with flexible cross-links*. Phys. Rev. E **79**:061914 (2009).

[16] K. E. Kasza, C. P. Broedersz, G. H. Koenderink, Y. C. Lin, W. Messner, E. A. Millman, F. Nakamura, T. P. Stossel, F. C. MacKintosh, D. A. Weitz. *Actin filament length tunes elasticity of flexibly crosslinked actin networks*. Biophys. J. **99**, 1091 (2010)

[17] C. Bustamante, J.F. Marko, E.D. Siggia and S. Smith. *Entropic elasticity of lambda-phage DNA*. Science **265**, 1599 (1994).

[18] J. F. Marko and E. D. Siggia. *Stretching DNA*. Macromolecules **27**, 981 (1995).

[19] J. Wilhelm and E. Frey. *Radial Distribution Function of Semiflexible Polymers*. Phys. Rev. Lett. **77**, 2581 (1996).

[20] A. Dhar and D. Chaudhuri. *Triple Minima in the Free Energy of Semiflexible Polymers*, Phys. Rev. Lett. **89**, 065502 (2002).

[21] J. Samuel and S. Sinha. *Elasticity of semiflexible polymers*. Phys. Rev. E **66**, 050801(R) (2002).

[22] S. Stepanow and G. M. Schutz. *The distribution function of a semiflexible polymer and random walks with constraints*. Europhys. Lett. **60**, 546 (2002).

[23] A. Ghosh, J. Samuel, and S. Sinha. *Elasticity of stiff biopolymers*. Phys. Rev E **76**, 061801 (2007).

[24] I. Schwaiger, A. Kardinal, M. Schleicher, A. Noegel and M. Rief. *A mechanical unfolding intermediate in an actin-crosslinking protein*. Nat. Struct. Biol. **11**, 81 (2003).

[25] S. Furuike, T. Ito, and M. Yamazaki. *Mechanical unfolding of single filamin A (ABP-280) molecules detected by atomic force microscopy*. FEBS Lett. **498**:72-75 (2001).

[26] Y. Tsuda, H. Yasutake, A. Ishijima, and T. Yanagida, Proc. Nat. Acad. Sci. USA **93**, 12937 (1996).

[27] M. Ferrer, H. Lee, J. Chen, B. Pelz, F. Nakamura, R. D. Kamm, and M. J. Lang *Measuring molecular rupture forces between single actin filaments and actin-binding proteins*. Proc. Natl. Acad. Sci. **105**, 9221-9226 (2008).

[28] F. C. MacKintosh, J. Käs, and P. A. Janmey. *Elasticity of semiflexible biopolymer networks*. Phys. Rev. Lett. **75**:4425-4428 (1995).

[29] P. R. Onck, T. Koeman, T. van Dillen, and E. van der Giessen. *Alternative explanation of stiffening in cross-linked semiflexible networks*. Phys. Rev. Lett. **95**, 178102 (2005).

[30] R. Tharmann, M. M. Claessens, and A. R. Bausch. *Viscoelasticity of isotropically cross-linked actin networks*. Phys. Rev. Lett. **98**:088103 (2007).

[31] J. S. Palmer and M. C. Boyce. *Constitutive modeling of the stress-strain behavior of F-actin filament networks*. Acta Biomaterialia, **4**, 597-612 (2008).

[32] D. A. Head, A. J. Levine, and F. C. MacKintosh. *Distinct regimes of elastic response and deformation modes of cross-linked cytoskeletal and semiflexible polymer networks*. Phys. Rev. E **68**:061907 (2003). (2003).

[33] J. Wilhelm and E. Frey. *Elasticity of Stiff Polymer Networks*. Phys. Rev. Lett. **91**, 108103 (2003).

[34] J. Liu, G. H. Koenderink, K. E. Kasza, F. C. MacKintosh, and D. A. Weitz. *Visualizing the Strain Field in Semiflexible Polymer Networks: Strain Fluctuations and Nonlinear Rheology of F-Actin Gels*. Phys. Rev. Lett. **98**, 198304 (2007).

[35] D. C. Morse. *Viscoelasticity of Concentrated Isotropic Solutions of Semiflexible Polymers. 1. Model and Stress Tensor*. Macromolecules **31**, 7030-7043 (1998).

[36] F. Gittes and F. C. MacKintosh. *Dynamic shear modulus of a semiflexible polymer network*. Phys. Rev. E **58**, R1241 (1998).

[37] C. Heussinger, B. Schaefer and E. Frey. *Nonaffine rubber elasticity for stiff polymer networks*. Phys. Rev. E **76**, 031906 (2007)

[38] C. Heussinger and E. Frey. *Force distributions and force chains in random stiff fiber networks*. Eur. Phys. J. E **24**, 47-53 (2007).

[39] P. A. Janmey , J. Peetermans, K. S. Zaner, T. P. Stossel, and T. Tanaka. *Structure and mobility of actin filaments as measured by quasielastic light scattering, viscometry, and electron microscopy*. J. Biol. Chem. **261**:8357-8362 (1986).

[40] P. Fernández, P. A. Pullarkat and A. Ott. *A Master Relation Defines the Nonlinear Viscoelasticity of Single Fibroblasts*. Biophys. J. **90**, 3796 (2006).

[41] M. Rief, J. Pascual, M. Saraste, H. E. Gaub. *Single molecule force spectroscopy of spectrin repeats: low unfolding forces in helix bundles*. J. of Mol. Biol. **286**, 553-561, (1999)

[42] N. Wang, I. M. Tolic-Norrelykke, J. Chen, S. M. Mijailovich, J. P. Butler, J. J. Fredberg and D. Stamenovic. *Cell Prestress. I. Stiffness and Prestress are Closely Associated in Adherent Contractile Cells*. Am. J. Physiol. **282**, C606 (2002).

4

Filament length tunes elasticity in flexibly crosslinked actin networks

- K. E. Kasza, C. P. Broedersz, G. H. Koenderink, Y. C. Lin, W. Messner, E. A. Millman, F. Nakamura, T. P. Stossel, F. C. MacKintosh and D. A. Weitz
  Actin filament length tunes elasticity of flexibly crosslinked actin networks,
  Biophysical Journal **99**: 1091 (2010)

- K. E. Kasza, G. H. Koenderink, Y. C. Lin, C. P. Broedersz, W. Messner, F. Nakamura, T. P. Stossel, F. C. MacKintosh and D. A. Weitz
  Nonlinear elasticity of stiff biopolymers connected by flexible linkers,
  Physical Review E **79**, 041928 (2009)

Abstract

Networks of the cytoskeletal biopolymer actin crosslinked by the compliant protein filamin form soft gels that stiffen dramatically under shear stress. We demonstrate that the elasticity of these networks shows a strong dependence on the mean length of the actin polymers. This behavior is in agreement with a model of rigid filaments connected by multiple flexible linkers (see chapter 3). This model allows us to estimate loads on individual cross-links, which we find to be less than 10 pN. We contrast the filament length dependence we observe in actin-filamin gels with the behavior of actin networks with short rigid linkers.

4.1 Introduction

The actin cytoskeleton is a composite intracellular biopolymer network. To tune the mechanical properties of the cytoskeleton for such diverse processes as cell division, locomotion, and shape change, a large number of actin binding proteins organize network structure [1]. Nucleating and capping proteins regulate the polymerization of monomeric actin into filamentous actin (F-actin). Crosslinking proteins bind the actin filaments together to form elastic gels or bundle structures, such as in stress fibers and filopodia. Motor protein assemblies control tension within the networks by pulling on actin filaments crosslinked to the network [2–4]. Even though the important molecular components are known, relatively little is understood of how this large ensemble of proteins collectively contributes to the mechanical response of the cytoskeleton.

Investigating the origins of the mechanical response of the complex and composite structure of the cytoskeleton presents a major challenge in biophysics. One approach has been to study reconstituted *in vitro* F-actin networks in the presence of purified binding proteins [3, 5–9]. Reconstituting the network allows precise control of its chemical composition and systematic investigation of its properties. A ubiquitous feature of these networks is that they stiffen strongly with increasing applied shear [5, 10]. When F-actin is crosslinked by small rigid crosslinks, the stiffening arises from the properties of the filaments themselves. F-actin is a semiflexible polymer with a persistence length of 17 μm [11]. Thermal bending undulations in the F-actin give rise to a decrease in its end-to-end distance; application of a force stretches out these undulations. For small extensions the force is proportional to the extension, whereas for large extensions approaching the contour length, the force diverges, leading to strain-stiffening [12]. Both the linear and nonlinear network elasticities are consistent with the theoretical predictions for a network of semiflexible polymers, provided the deformation is affine [5,7,13]. However, this picture of network mechanics implicitly assumes that the elasticity is controlled by one component, the actin filaments. It ignores any contribution of the crosslinking proteins; these can be both large and compliant, and therefore can themselves contribute to the elasticity.

One example of a large and flexible crosslink is filamin (Fig. 4.1B), which is abundant in cells. Filamin crosslinks F-actin into orthogonal networks in the cortex, connects F-actin to integrins, and may play a role in mechanotransduction [14–18]. Reconstituted actin networks with filamin can form isotropic networks mimicking the actin cortex of living cells, as shown in Fig. 4.1A,C, or (partially) bundled networks at high filamin concentrations (Fig. 4.1D,E). Actin-filamin networks exhibit a mechanical response that is qualitatively different from networks formed with rigid crosslinks [6,8,19,20]. Filamin-F-actin networks are compliant, weakly elastic solids. Nevertheless they can support large shear stresses because of their pronounced nonlinear strain-stiffening. Their nonlinear behavior is inconsistent with predictions for an affinely deforming network with rigid crosslinks [5,6,20]. In comparison to networks with rigid crosslinks, networks crosslinked by filamin exhibit mechanical properties that more closely mimic the properties of cells [3,6,19]. Recent experimental reports show that the unusual nonlinear elasticity of these networks is consistent with a model of rigid polymers connected by multiple flexible crosslinks [20–22]. The rigid polymer of length L constrains the deformation profile of the n flexible crosslinks bound along its length, as illustrated in Fig. 4.2; thus, polymer length is predicted to be an important parameter controlling the linear and nonlinear properties of the network [22]. Indeed, the linear viscoelasticity and rupture stress of F-actin networks crosslinked by filamin are sensitive to the addition of gelsolin [20,23], an actin capping and severing protein that shortens the average filament length. While these previous data support the view that F-actin length affects the rheology of these networks, fully elucidating the physical principles of this mechanism demands a more systematic investigation of the linear and nonlinear behavior of filamin-gelsolin-F-actin networks.

In this chapter, we investigate the mechanical response of networks of F-actin cross-linked by filamin as we systematically decrease L by adding gelsolin. Using bulk rheology we show that the linear modulus increases proportional to L^2. The critical strain, which marks the onset of stiffening, decreases with increasing L. In the nonlinear regime, the maximum stress before breaking is proportional to L. These results are contrasted with the rheology of networks formed with rigid crosslinks to demonstrate that these behaviors are unique features of the filamin-F-actin system. Thus, we show that the linear and nonlinear elastic behavior of F-actin crosslinked by filamin is indeed tuned by varying L, in a manner that is consistent with the theoretical predictions for a network of stiff polymers connected by flexible linkers (see chapter 3).

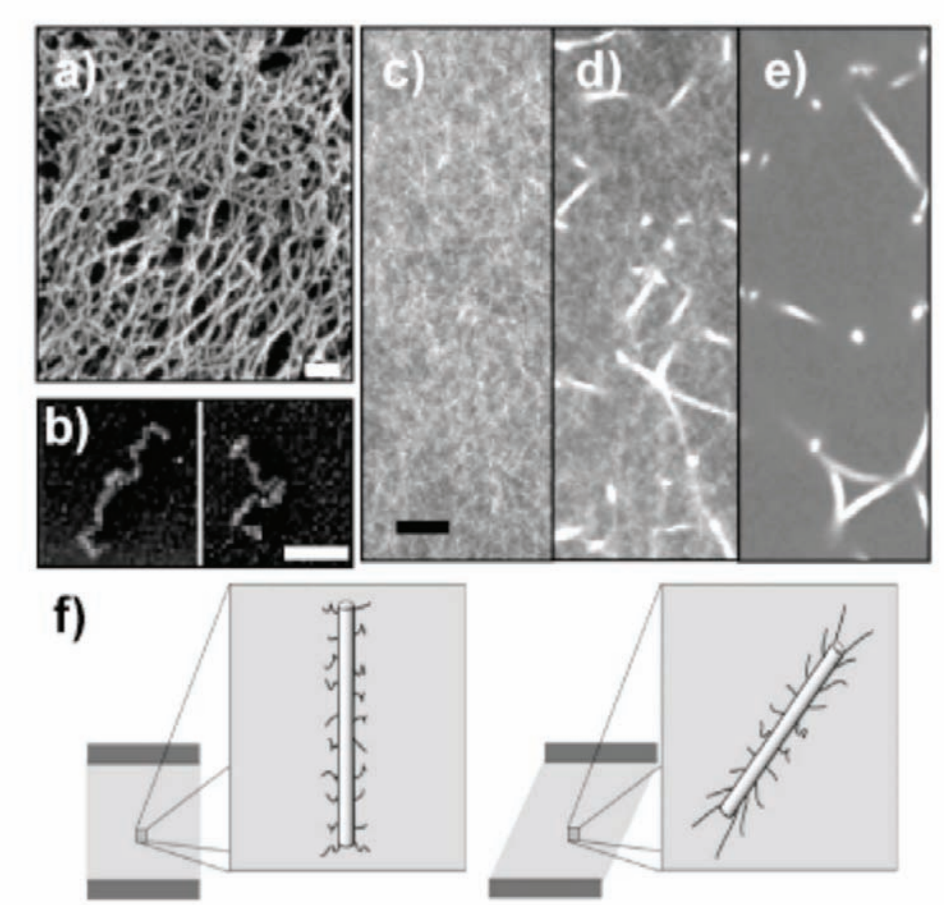

Figure 4.1 – (a) Electron micrograph of a fixed and rotary-shadowed filamin-F-actin network at $c_A = 1$ mg/ml, $L = 15$ μm, and $R_F = 0.005$. Scale bar= 100 nm. (b) Electron micrograph of rotary-shadowed filamin molecules. Scale bar= 50 nm. (c)-(e) Confocal images of various networks. Scale bar= 5 μm. $c_A = 0.5$ mg/ml with $L = 15$ μm and (c) $R_F = 0.002$ or (d) $R_F = 0.01$, or (e) $L = 1$ μm and $R_F = 0.04$.

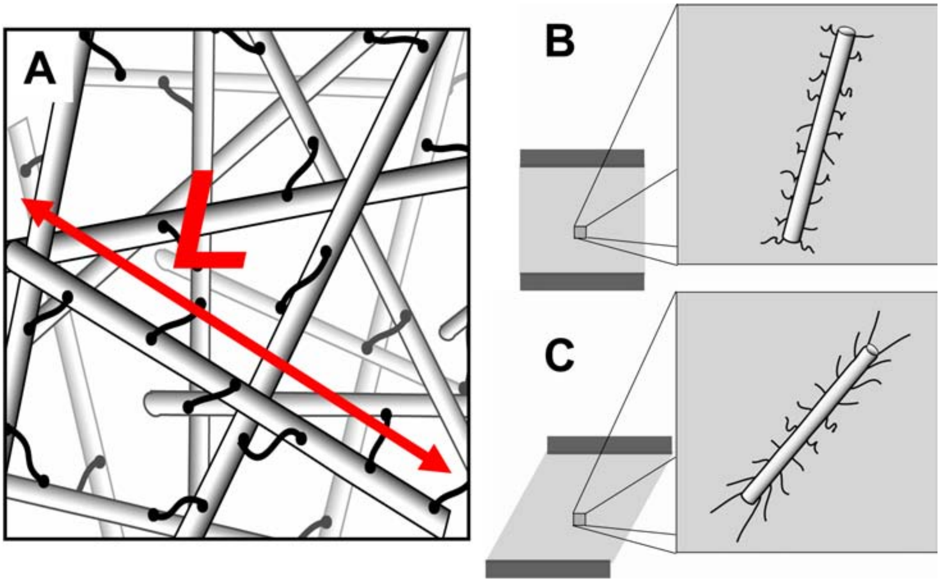

Figure 4.2 – (Color online) (A) Schematic of network of stiff polymers of mean length L connected by flexible crosslinks. (B-C) Schematic of stiff polymer and attached crosslinks in a network before (B) and after (C) shear.

The model quantitatively explains the dramatic nonlinear stiffening of filamin-F-actin networks, providing fundamental insight into its origins. In addition, this model provides an estimate of the maximum load experienced by individual filamin cross-links, which is less than 10 pN, too small to result in significant unfolding of filamin Ig-like domains.

4.2 Materials and methods

4.2.1 Proteins

We purify monomeric (G) actin from rabbit skeletal muscle [24], followed by gel-filtration (HiLoad 16/60 Superdex 200pg, GE Healthcare). Aliquots of purified G-actin in G buffer (2 mM Tris HCl, 0.2 mM ATP, 0.2 mM CaCl2, 0.2 mM DTT, 0.005% NaN_3, pH 8.0) are frozen in liquid nitrogen and stored at −80°C. Recombinant human filamin A is purified from Sf9 cell lysates [25]. Recombinant human plasma gelsolin is purified [26] or purchased (Biogen, Cambridge, MA). For rigidly crosslinked networks, we incorporate biotinylated actin monomers (Cytoskeleton, Denver, CO) that can be crosslinked by NeutrAvidin protein (Pierce, Rockford, IL).

4.2.2 Network formation

We form networks with an actin concentration, $c_A = 0.5$ mg/ml, unless otherwise noted, and control network microstructure by varying the molar ratio of filamin dimers to actin monomers, R_F. We regulate the actin filament length distribution with gelsolin. The molar ratio of gelsolin to actin monomers, R_G, sets the mean actin filament length [27]. Samples are prepared by mixing solutions of $10x$ polymerization buffer (20 mM Tris-HCl, 20 mM $MgCl_2$, 1 M KCl, 2 mM DTT, 2 mM $CaCl_2$, 5 mM ATP, pH 7.5), gelsolin, filamin, and G-actin.

For rigidly crosslinked networks, biotinylated actin monomers are incorporated in actin filaments at a molar ratio of biotinylated G-actin to non-biotinylated G-actin, R_B. Crosslinking is mediated by NeutrAvidin protein. Samples are prepared by mixing $10x$ polymerization buffer, gelsolin, biotinylated G-actin, and G-actin. After 3 min NeutrAvidin at a 1:1 molar ratio to biotinylated actin is gently mixed in.

The sample is loaded into a microscopy chamber, consisting of two cover slips with a 1 mm spacer, or between rheometer plates and polymerized for 1 hour at 25°C.

4.2.3 Characterization of f-actin length distribution

To characterize the actin filament length distribution, we polymerize 0.3 mg/ml F-actin in the presence of gelsolin. After 1 hour, the filaments are labeled and stabilized with a 1:1 molar ratio of Alexa-488 phalloidin and incubated at 25°C for 30 min. The filaments are diluted to a concentration of 2 nM, and 5 μL of the suspension is pipetted onto a cover slip functionalized with poly(acrylamide-co-diallyldimethylammonium chloride). A second coverslip is placed on top and the sample sealed. Nearly all filaments stick to the coated coverslip. Immobilized filaments are imaged using a confocal microscope (Leica SP5); image pixel size is 160 nm. Filament contour lengths, l, are measured manually in ImageJ; the minimum distance measurable using this method is 0.5 μm. For each gelsolin concentration, the width of the distribution of filament lengths is nearly equivalent to the mean (data not shown).

For network formation, we polymerize F-actin in the presence of gelsolin and filamin. In previous work, addition of alpha-actinin to gelsolin-regulated F-actin narrowed the width of the length distribution without significantly affecting the mean length L [28]. Similarly, we expect that filamin should not significantly change the values of L we measure here.

4.2.4 Imaging

For confocal microscopy, samples are fluorescently labeled by polymerizing in the presence of 0.6 μM Alexa-488 phalloidin and examined (Leica, TCS SP5). For transmission electron microscopy a 10 μL drop of assembled network is applied to a 400

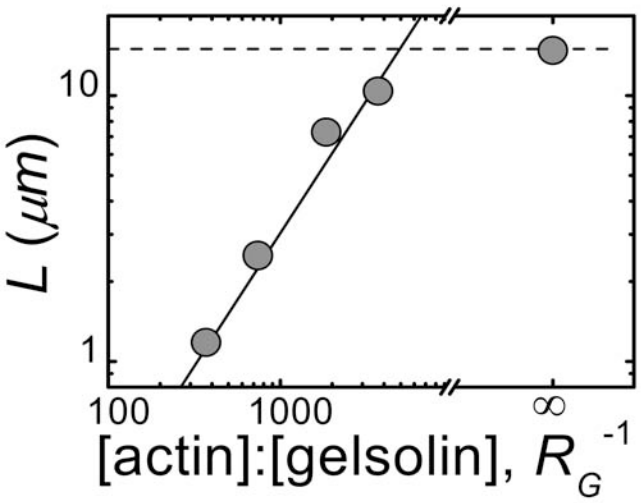

Figure 4.3 – Mean F-actin length L as a function of the molar ratio of actin to gelsolin, R_G^{-1}. L decreases from its unregulated value (dashed line) as gelsolin is added. The solid line denotes linear scaling.

mesh carbon-coated nickel grid and incubated for 30 s, stained with 1% uranyl acetate, rinsed by passing a drop of distilled water over the grid, air dried, and imaged (JEOL 2100).

4.2.5 Rheology

We use a stress-controlled rheometer with 40-mm stainless steel parallel plates and a 160 μm gap (AR-G2, TA Instruments or C-VOR, Bohlin Instruments). We polymerize samples *in situ* and use a solvent trap and apply a thin layer of low viscosity mineral oil around the sample to minimize evaporation. We confirm that the results are independent of gap and reproducible within and between different protein preparations.

The linear viscoelastic response is measured by applying a frequency-dependent, sinusoidal stress, $\sigma \sin(\omega t)$, and measuring the strain, $\gamma \sin(\omega t + \delta)$. We maintain $\gamma < 2\%$ to ensure linear response. The elastic modulus is

$$G'(\omega) = \frac{\sigma}{\gamma} \cos(\delta); \tag{4.1}$$

the viscous modulus

$$G''(\omega) = \frac{\sigma}{\gamma} \sin(\delta). \tag{4.2}$$

We measure the response in the nonlinear regime with a differential or "prestress" measurement; a small amplitude oscillatory stress, $\delta\sigma$, is superposed on a steady prestress, σ_0, to measure the differential modulus,

$$K^*(\sigma_0, \omega) = \left.\frac{\delta\sigma}{\delta\gamma}\right|_{\sigma_0}. \tag{4.3}$$

The elastic and viscous components are K' and K'', respectively. We confirm there is no time dependence in K' at various levels of prestress and minimal hysteresis in $K'(\sigma_0)$ (see chapter 5), as shown in Fig. 4.4. In a complementary strain ramp approach, we increase the strain at a fixed rate and measure the resulting stress. Both $\sigma(t)$ and $\gamma(t)$ are smoothed using a cubic spline algorithm to compute the differential modulus

$$K = \frac{\mathrm{d}\sigma}{\mathrm{d}\gamma}, \tag{4.4}$$

by applying a numerical derivative to the stress-strain curve.

4.3 Results and discussion

4.3.1 F-actin length distribution in the presence of gelsolin

Within the cell, the contour lengths, ℓ, of actin filaments are highly regulated. Typical lengths range from a hundred nanometers to a few microns [29, 30]. *In vitro*, high enough concentrations of pure monomeric actin will polymerize spontaneously in the presence of divalent salt and ATP. Yet, these *in vitro* filaments are typically much longer than those in the cell, with contour lengths that can be up to 50 μm (data not show).

To better mimic the conditions in cells, we use the F-actin capping and severing protein gelsolin to vary the mean length, $L = \langle \ell \rangle$, of our *in vitro* actin filaments. To characterize the filament length distribution in the presence of gelsolin, we image a diluted sample of F-actin stabilized with fluorescent phalloidin. For the ratio of gelsolin to actin, $R_G = 0$, the unregulated F-actin has a mean length of $L = 14.8$ μm. Upon adding a small amount of gelsolin, $R_G = 1 : 3700$, the length distribution is dominated by the presence of the gelsolin and L decreases to 10.4 μm. Increasing R_G decreases L further. We find that L scales linearly with R_G^{-1}, as shown in Fig. 4.3; it varies as $L = (330R_G)^{-1}$, with L measured in microns. This is consistent with a model where each gelsolin molecule associates with one actin filament. Each actin monomer adds 2.7 nm to the filament length [31], so that one micron of filament is composed of 370 monomers, predicting $L = (370R_G)^{-1}$. Some inactivation of gelsolin during storage may account for the slightly larger observed filament lengths compared to the prediction. These findings are consistent with previous studies of actin filament length distributions [27, 28, 32].

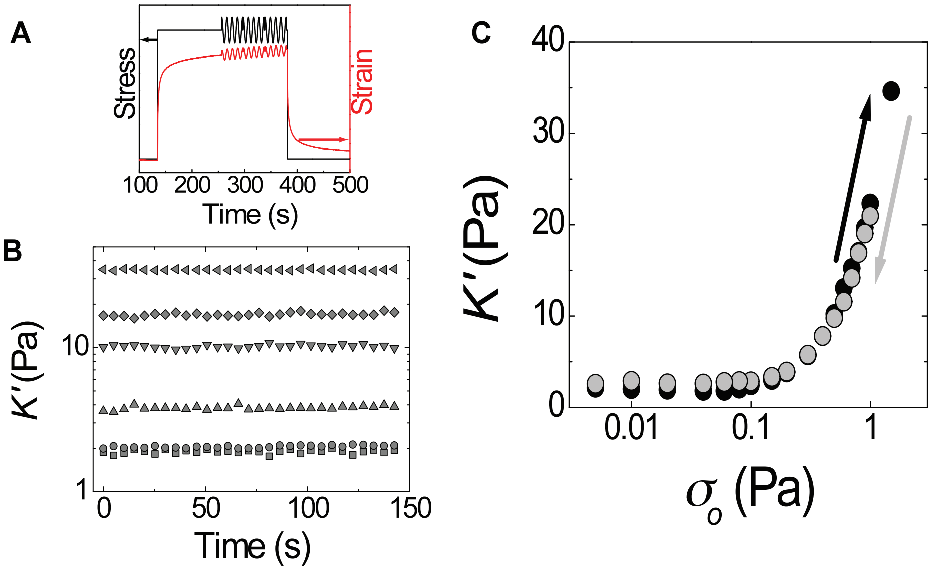

Figure 4.4 – (Color online) (A) To measure the nonlinear differential elastic response at a particular prestress, σ_0, a small, oscillatory stress is superposed on a static stress σ_0 and the resulting oscillatory strain is measured. (B) For a typical actin-filamin network with $c_A = 0.5$ mg/ml, $R_F = 0.005$, and $L = 15$ μm we show that there is no time dependence in K' at various levels of prestress σ_0, which are shown in panel (C). σ_0 can be increased to just below the maximum stress supported by the network and decreased again with minimal hysteresis in the differential elastic modulus, $K'(\sigma_0)$.

4.3.2 Microstructure of filamin-gelsolin-F-actin networks

We form *in vitro* networks of actin filaments whose lengths are regulated with gelsolin and which are crosslinked by filamin. *In vitro*, filamin efficiently crosslinks F-actin into orthogonal networks, which are soft but support large stresses [6,14]. These networks mimic several key features of cell mechanical properties [3,6,19]. The microstructure of these networks varies as we change L and the molar ratio of filamin to actin, R_F.

For $R_F \lesssim 0.01$ the networks are a homogeneous mesh of F-actin as seen by electron microscopy (Fig. 4.1A) and confocal microscopy (Fig. 4.5A and B). For $R_F > 0.01$ large bundles appear within the mesh (Fig. 4.5C-D). The value of $R_F \approx 0.01$ above which bundles appear is roughly independent of L [20]. From electron microscopy, the bundles appear as loose, branching structures with diameters ~ 100 nm (Fig. 4.5C, inset). These observations are consistent with reports for networks with filamin from chicken gizzard [23,33,34]. We confirm this bundling transition by tracking the thermal motion of particles within the networks (data not shown). Varying L has little effect on the visual appearance of the non-bundled networks (Fig. 4.5A-B). However, in the bundled networks, F-actin partitions more readily into the bundles at high R_G, forming networks of pure bundles without a background F-actin mesh, as visible in confocal microscopy (Fig. 4.5D) or detectable by particle tracking. This may be due to increased diffusion and decreased entanglements for shorter filaments, allowing them to more easily associate into bundles [33].

4.3.3 Linear response

To probe the mechanical properties of the filamin-gelsolin-F-actin networks, we use a stress-controlled rheometer. For an actin concentration $c_A = 0.5$ mg/ml and $L = 15$ μm, a weakly crosslinked network having $R_F = 0.001$ is a soft, viscoelastic solid (Fig. 4.6A, squares). The elastic modulus G' is two- to three-fold larger than the viscous modulus G'', and $G'(\omega)$ increases as a weak power-law with the frequency, ω, over a broad frequency range. This network is only slightly stiffer than purely entangled actin (triangles). Increasing R_F further to 0.01 only modestly increases G' and has little impact on the frequency response. This is in contrast to F-actin with rigid crosslinking induced by addition of NeutrAvidin to networks with a small fraction, R_B, of biotinylated actin monomers incorporated into the F-actin. Increasing R_B leads to a drastic increase in the stiffness of the network, as shown in Fig. 4.6B; this is accompanied by a decrease in the slope of the weak power-law frequency response of $G'(\omega)$, consistent with more solid-like behavior.

In the filamin networks, as we systematically decrease the mean filament length L from 10 to 2 μm by adding increasing amounts of gelsolin, G' decreases from 1 to 0.2 Pa (Fig. 4.6C). For rigidly crosslinked networks, G' also decreases with L (Fig. 4.6D). For both types of crosslinks, the slope of $G'(\omega)$ does not vary drastically

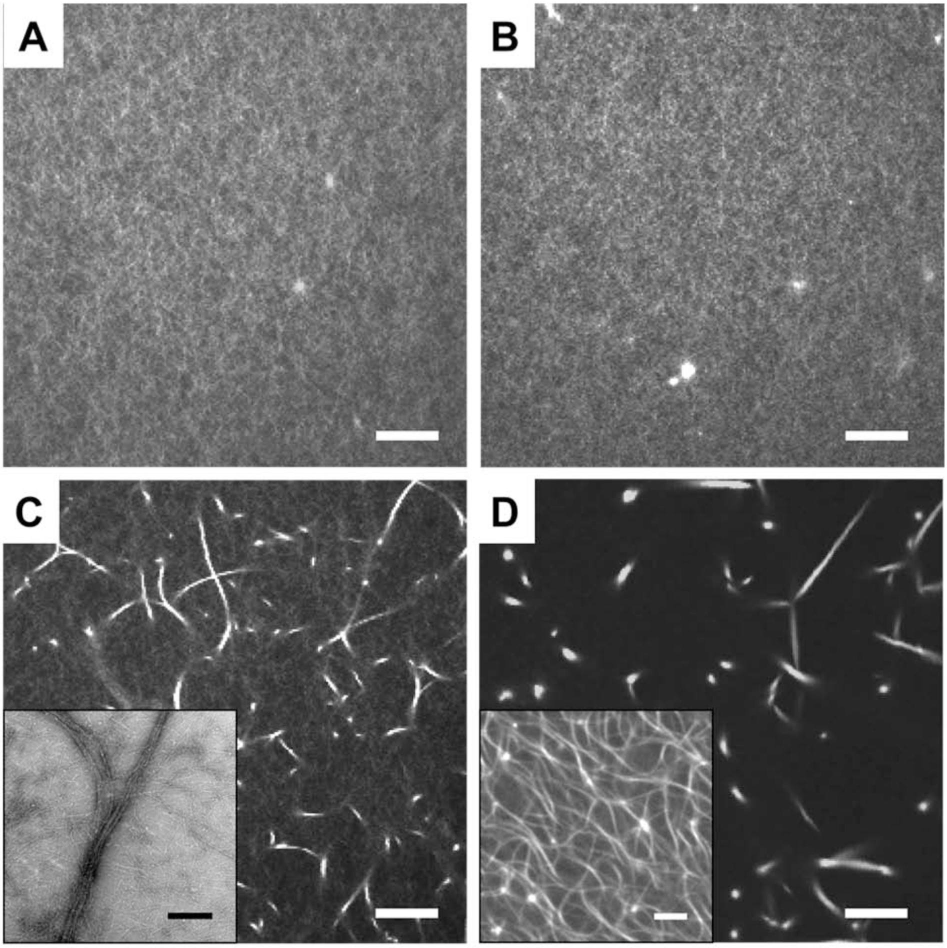

Figure 4.5 – Microstructure of filamin-gelsolin-F-actin networks. (A-B) For $R_F \lesssim 0.01$ networks are a homogeneous mesh of F-actin. (C-D) Large bundles are present at high R_F. A) Confocal image, $R_F = 0.002$, $R_G = 0$ ($L = 15$ μm). B) Confocal image, $R_F = 0.01$, $R_G = 1 : 370$ ($L = 1$ μm). C) Confocal image, $R_F = 0.01$, $R_G = 0$. Inset: TEM image. D) Confocal image, $R_F = 0.04$, $R_G = 1 : 370$. Inset: Confocal image at lower magnification to show network connectivity. Scale bars are 10 μm for confocal images and 0.5 μm for TEM image.

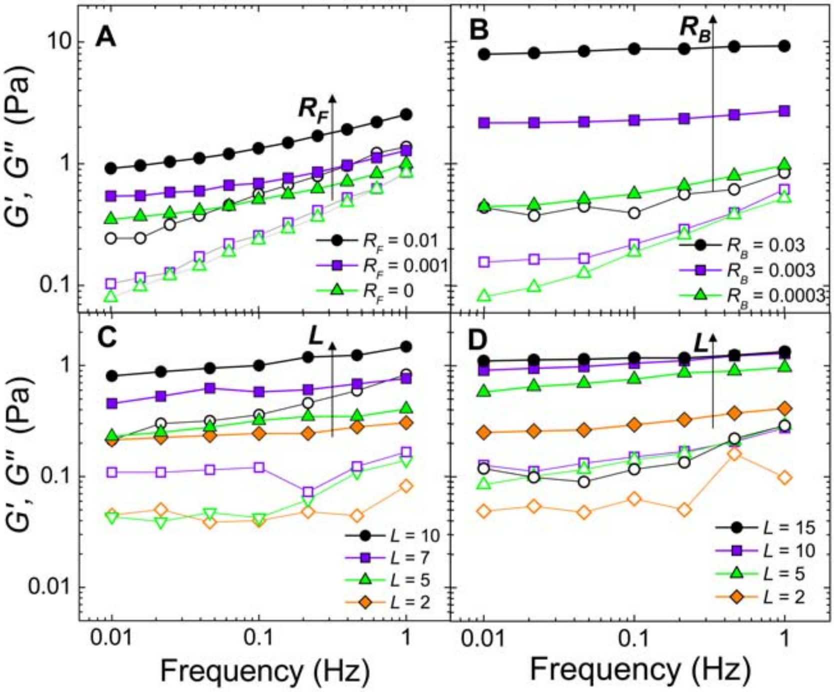

Figure 4.6 – (Color online) Linear viscoelasticity of crosslinked F-actin networks. Elastic moduli G' (solid) and viscous moduli G'' (open). Filamin crosslinked networks are soft, viscoelastic solids that become stiffer with increasing R_F or L: A) $L = 15$ μm with various R_F and C) $R_F = 0.01$ with various L (in μm). Rigidly crosslinked networks become stiffer with increasing L and significantly stiffer and more solid-like with increasing R_B: B) $L = 15$ μm with various R_B, and D) $R_B = 0.01$ with various L.

with L.

4.3.4 Dependence of the modulus on filament length

To quantify the changes in the elasticity of these networks as we decrease L, we plot G_0, defined as $G_0 = G'\big|_{\omega=0.1\ \mathrm{Hz}}$, as a function of L (Fig. 4.7A). For $R_F = 0.001$, G_0 is 0.2 Pa for the networks with the shortest filaments, $L = 1 - 2$ μm. As we increase L to 15 μm, G_0 increases to 0.5 Pa. For increasing values of R_F, G_0 starts out at roughly the same value for short filaments, but increases more strongly with L. Interestingly, at each R_F, G_0 increases stronger than linearly with L.

This strong dependence on L is not expected from an affine theory [12] that has been used to describe the linear and nonlinear elasticity of actin crosslinked with point-like rigid crosslinks such as heavy meromyosin and scruin [5, 7, 13]. In this theory network elasticity is governed by the thermal compliance of the semiflexible F-actin polymers; thermal fluctuations of the F-actin get stretched out as the network is deformed [12]. This model predicts:

$$G_0 = 6\rho k_{\mathrm{B}} T \frac{\ell_p^2}{\ell_c^3} \tag{4.5}$$

where ρ is the linear density of polymer, k_{B} is Boltzmann's constant, T is the temperature, ℓ_p is the persistence length of F-actin, and ℓ_c is the distance between crosslinks. Thus, in this theory the network elasticity is controlled by the distance between crosslinks rather than the length of the actin filaments, in disagreement with our results for filamin-F-actin.

Alternatively, the elasticity of our networks can originate from the compliant nature of the filamin crosslinks. The large 160 nm chain between the actin binding domains of a filamin protein is quite flexible and can be modeled as a linear polymer with $\ell_p = 20$ nm [35]. As a result, a filamin crosslink is soft compared to an F-actin segment of length ℓ_c, which ranges from 0.3 to 2 μm. This suggests that the compliance of the network is governed by the flexible crosslinks. Thus, we propose a model in which the actin polymers are treated as rigid rods linked by many flexible linkers (see chapter 3), as depicted in Fig. 4.2A. When the network surrounding a rigid rod is deformed, the linkers get stretched by an amount that increases linearly in the distance from the center of the rod, as shown in Fig. 4.2C. Provided the network deformation is uniform on the length scale of L:

$$G_0 = \frac{1}{8}\rho n k L \sim R_F L^2, \tag{4.6}$$

with k the stiffness of the flexible crosslinks and n the average number of crosslinks per actin filament [22]. The explicit L dependence arises as a direct result of the non-uniform deformation profile of the crosslinks. The average number of crosslinks per actin filament is proportional to both R_F and L and is given by $n = 370 R_F L$; thus, the overall prediction is that G_0 will increase proportional to $R_F L^2$.

To test this mechanism, we plot G_0 as a function of $R_F L^2$ (Fig. 4.7C). The data for different crosslinking densities collapses onto a single curve. For $R_F L^2 \geq 0.1$, G_0 scales nearly linearly with $R_F L^2$, consistent with the prediction. This supports the model of crosslink dominated elasticity. Below $R_F L^2 = 0.1$, which corresponds to $n = 7$ crosslinks for a 5 μm filament, the values of G_0 are roughly equivalent to the elasticities we measure for F-actin solutions in the absence of crosslinking, as shown by the gray bar in Fig. 4.7C. This suggests that the linear elasticity of these weakly crosslinked networks is dominated by the solution elasticity, not by the crosslinks. The threshold of $R_F L^2 = 0.1$ corresponds to typical physiological conditions ($L =$ 2 μm, $R_F = 0.02$) [36, 37], suggesting that by spatially or temporally regulating L,

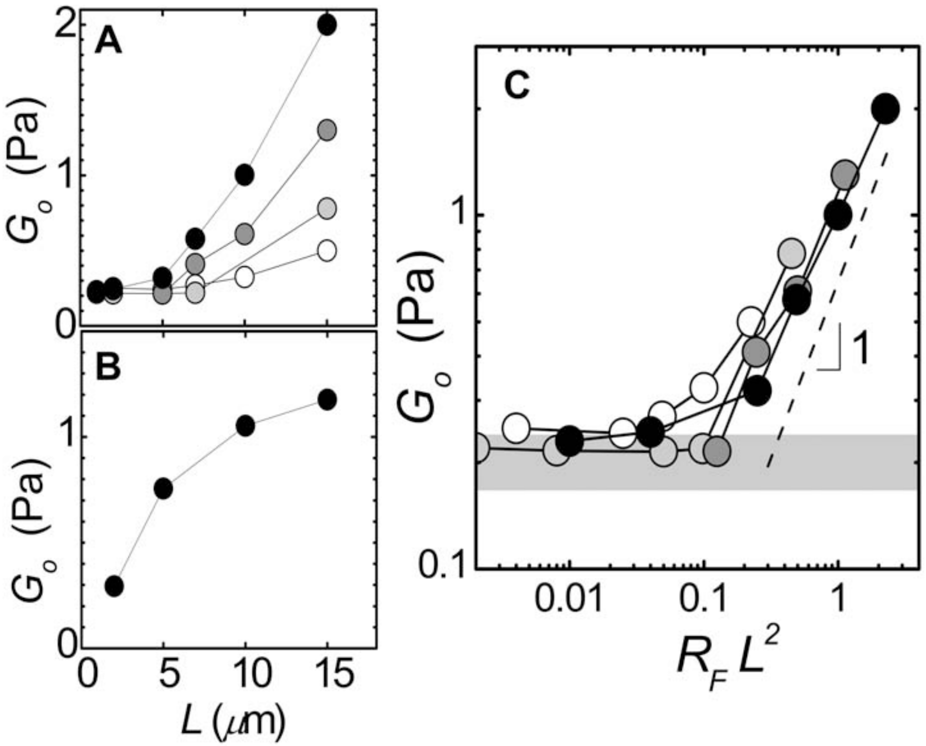

Figure 4.7 – Dependence on L of the linear elastic modulus measured at a frequency of 0.1Hz, G_0. A) For filamin networks G_0 increases stronger than linearly with L. $R_F = 0.001$ (white), 0.002 (light gray), 0.005 (gray), 0.01 (black). B) Rigidly crosslinked networks show qualitatively different behavior. $R_B = 0.01$. C) G_0 for networks crosslinked with filamin at different R_F collapse onto a single curve when plotted vs. $R_F L^2$ with nearly linear scaling above $R_F L^2 = 0.1$. The shaded bar represents the range of moduli measured for F-actin solutions with $2 < L < 7$ μm.

cytoskeletal elasticity could be adjusted from essentially that of entangled F-actin to a network with tunable stiffness. By contrast, the dependence of G_0 on L for the rigidly crosslinked networks is of a qualitatively different form; G_0 increases linearly with L for small L but approaches a plateau for large L (Fig. 4.7B). Simulations of 2D [38] and 3D [39] stiff polymer networks reveal a dependence on L qualitatively similar to our results. The departure from the plateau for decreasing L in simulations has been attributed to an increase in the non-affinity in the deformation of the network, where the affine thermal theory is expected to break down.

4.3.5 Nonlinear response

The dependence of G_0 on R_F and L is consistent with network elasticity that is governed by the filamin crosslinks. We further test the origin of the elasticity by measuring the nonlinear elastic properties of the filamin-F-actin gels with two complementary techniques: strain ramps and prestress measurements.

Strain ramps

In the first approach, we increase the strain, γ, at a fixed rate and measure the resulting stress, σ. From the derivative of the stress-strain curve, $K = \mathrm{d}\sigma/\mathrm{d}\gamma$, we quantify the nonlinear behavior. This technique has been used to study nonlinear behavior of both entangled and crosslinked F-actin networks [40–42]. For a filamin crosslinked network with $L = 15\ \mu$m and $R_F = 0.01$, K normalized by its initial value, K_0, is equal to 1 for small strains (Fig. 4.8A). At the critical strain, $\gamma_c = 0.06$, K/K_0 increases above 1, and the network begins to stiffen. It stiffens 30-fold before breaking at $\gamma_m = 0.9$. Networks with shorter filaments initially display weakening behavior, where K/K_0 decreases below 1, due to their lower network connectivity, but eventually stiffen. As we decrease L, γ_c increases markedly, as shown in Fig. 4.8A.

By contrast, rigidly crosslinked networks with $L > 5\ \mu$m stiffen at small strains, independent of L (Fig. 4.8B). Networks with $L \leq 2\ \mu$m do not stiffen and display weakening behavior. This is consistent with a transition from stiffening behavior arising from pulling out fluctuations in F-actin filaments, where

$$\gamma_c = \frac{1}{6}\frac{\ell_c}{\ell_p} \tag{4.7}$$

is set only by ℓ_c and ℓ_p, to weakening behavior, where the network becomes too sparsely connected to stiffen. However, the strong dependence of γ_c on L for filamin-F-actin gels is inconsistent with such a nonlinear response arising from thermal fluctuations of the actin filaments being stretched out. We propose instead that the nonlinear response for filamin-F-actin originates from the stiffening behavior of the crosslinks. Single molecule experiments indicate that filamin proteins stiffen markedly

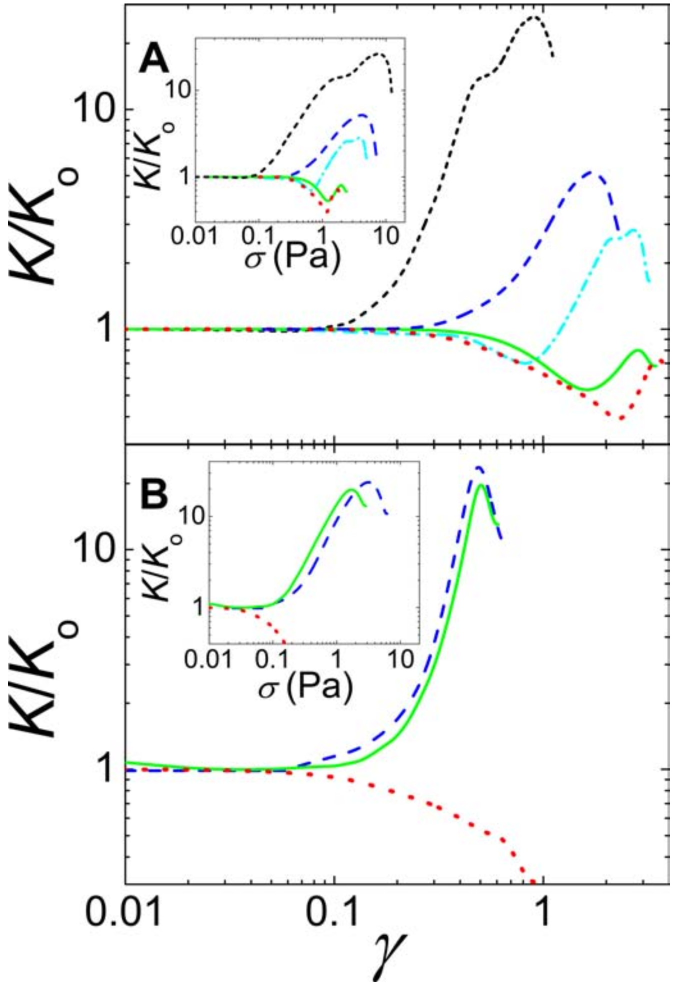

Figure 4.8 – (Color online) Nonlinear stiffening in strain ramps with a rate of $0.1s^{-1}$. The derivative of the stress-strain curve, K, normalized by its initial value, K_0, as a function of strain. A) Filamin with $R_F = 0.01$ and $L = 15$ (short dash), 10 (long dash), 7 (dash-dot), 5 (solid), 2 (dot) μm. For the network with $L = 15$ μm, $K/K_0 = 1$ at small strains before beginning to stiffen above $\gamma_c = 0.06$. Networks with shorter filaments initially display weakening behavior, where K/K_0 decreases below 1, due to their lower network connectivity, but stiffen at higher strains where the slope of the curve becomes positive. γ_c increases with decreasing L. B) Rigid crosslinks with $R_B = 0.01$ and $L = 10$ (dash), 5 (solid), 2 (dot) μm. Networks with long filaments display stiffening behavior that is independent of L, while networks with short filaments display weakening behavior. Insets: Same data plotted vs. stress.

as they are stretched towards their contour length ℓ_0 [47]. When the network surrounding a rigid rod is deformed strongly, linkers bound at the ends of the polymers are stretched most, as depicted in Fig. 4.2C. These linkers will be the first to reach full extension and stiffen, setting the critical strain at which the network begins to stiffen. These end-bound linkers reach full extension at a strain [22]:

$$\gamma_c = 4\frac{\ell_0}{L}. \tag{4.8}$$

The L-dependence arises because the amount an end-bound crosslink must stretch to accommodate a given macroscopic network strain increases with the length of the rigid rod to which it is bound.

Plotting γ_c as a function of L^{-1} in Fig. 4.9A, the dependence of γ_c on L^{-1} is in stark contrast to the stiffening behavior of rigidly crosslinked networks, which display no dependence of γ_c on L. The increase of γ_c with increasing L^{-1} is qualitatively consistent with the prediction of the model. We see similar behavior for γ_m (Fig. 4.9B), suggesting that the non-uniform deformation profile of the linkers prevails up to large strains. Interestingly, the γ_c data from the two systems coincide at small L^{-1} (Fig. 4.9A). In this limit of large L the model of rigid rods with flexible linkers predicts that the smallest of strains would lead to stiffening. However, this model relies on the linkers being the softest mode in the system. When the prediction for stiffening by the linkers would yield a lower γ_c than by the F-actin segments themselves, this picture breaks down, and it is no longer valid to assume the F-actin behave as rigid rods. In this limit, the compliance of the F-actin would contribute to the stiffening behavior of the system, consistent with our observation.

Prestress measurements

In our second technique for probing nonlinear response, we apply a steady prestress, σ_0, and probe the differential elastic modulus, $K'(\sigma_0, \omega)$, with a small oscillatory stress. This technique has been used in crosslinked F-actin networks to study nonlinear stiffening behavior [5, 6, 13, 42]. Rigidly crosslinked F-actin networks display stiffening with $K' \sim \sigma_0^{3/2}$ [5]; we see the same behavior for networks crosslinked by biotin-NeutrAvidin (Fig. 4.10B). This is consistent with the predictions for the affine thermal model in which the nonlinear response is due to pulling out thermal bending fluctuations in the semiflexible actin filaments within the network [5, 12].

Our model of rigid filaments connected by multiple flexible linkers predicts a different stiffening behavior that arises from the stiffening of the filamin crosslinks. The theoretical model is extended to the nonlinear regime by employing a self-consistent effective medium approach [20–22]. In this approach, the linkers are bound on one side to the rigid rod and on the other to an elastic continuum with a nonlinear elasticity that is required to self-consistently represent a uniform and isotropic collection

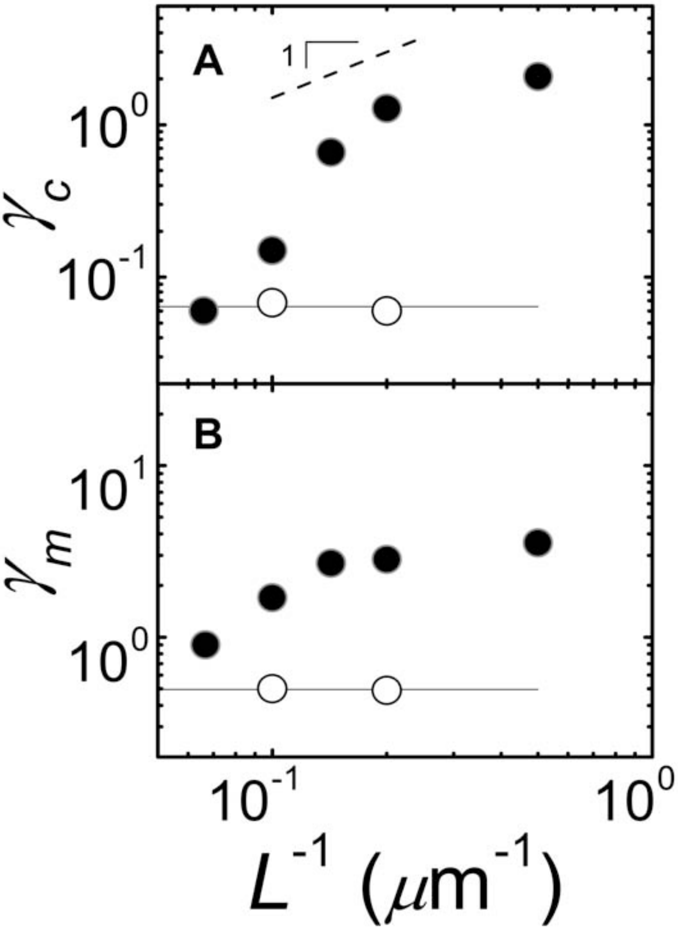

Figure 4.9 – Dependence of the critical and maximum strains on L. Filamin with $R_F = 0.01$ (solid), rigid crosslinks with $R_B = 0.01$ (open). A) γ_c of the filamin networks increases with increasing L^{-1}. In contrast, γ_c for rigidly crosslinked networks is independent of L with mean value denoted by the solid line. B) γ_m vs. L^{-1}.

of such elements. As the network is deformed the linkers get stretched and stiffen one-by-one as they approach full extension and start pulling back on the effective medium. This model predicts $K' \sim \sigma_0$ in the limit of a dense network.

To test this prediction, we measure $K'(\sigma_0)$ for the networks crosslinked by filamin. For a network with $R_F = 0.003$ and $L = 15$ μm (solid circles, Fig. 4.10A), K' increases with σ_0 above a critical stress, $\sigma_c = 0.1$ Pa, and reaches a stiffness, $K'_m = 10$ Pa, before breaking at $\sigma_m = 1$ Pa. Networks with higher R_F and L stiffen more and support larger stresses. For these networks, K' increases more strongly than linear in σ_0 just above σ_c, whereas at high σ_0, $K' \sim \sigma_0$ (Fig. 4.10A). This unusual stiffening behavior is in agreement with the prediction of the model. Rescaling K' by its initial value and σ_0 by σ_c, the $K'(\sigma_0)$ data for networks formed with different R_F and L collapse onto a single curve, provided the network is not highly bundled [20]. Our rescaled data agrees well with the nonlinear response calculated with the effective medium model (Fig. 4.11), with only one fit parameter that represents the coupling of a rigid rod to the effective medium. In contrast, the rescaled data from networks rigidly crosslinked by biotin-NeutrAvidin fall on a separate curve, which is well described by the prediction of the affine thermal theory of crosslinked semiflexible networks (Fig. 4.11). These data support the model of crosslink dominated elasticity in the filamin-F-actin networks.

Interestingly, although the filamin-F-actin networks are all quite compliant, the maximum stiffness before breaking, K_m , increases strongly with R_F, suggesting that network failure is due to filamin unbinding [20, 45]. Thus, the overall magnitude of stiffening, K'_m/G_0, increases with R_F (Figs. 4.10A and 4.12). Of these networks the highly bundled ones show the most dramatic stiffening (open symbols). The opposite behavior is observed for the rigidly crosslinked networks; G_0 increases significantly with R_B, while K'_m is nearly independent of R_B (Figs. 4.10B and 4.12), presumably because network failure is due to F-actin rupture [13].

4.3.6 Dependence of maximum stress on filament length

Assuming crosslink unbinding as the dominant failure mode for these networks, a scaling argument based on the theoretical model predicts how σ_m scales with c_A, R_F, and L. On the microscopic level, the crosslink will unbind from F-actin at a force, f_m. With multiple crosslinks per filament, the crosslinks act in parallel, and the total rupture force per filament increases linearly with n. From the density of filaments and assuming an isotropic orientation of filaments within the network, the maximum stress is [21, 22],

$$\sigma_m = \frac{1}{45}\rho n f_m \tag{4.9}$$

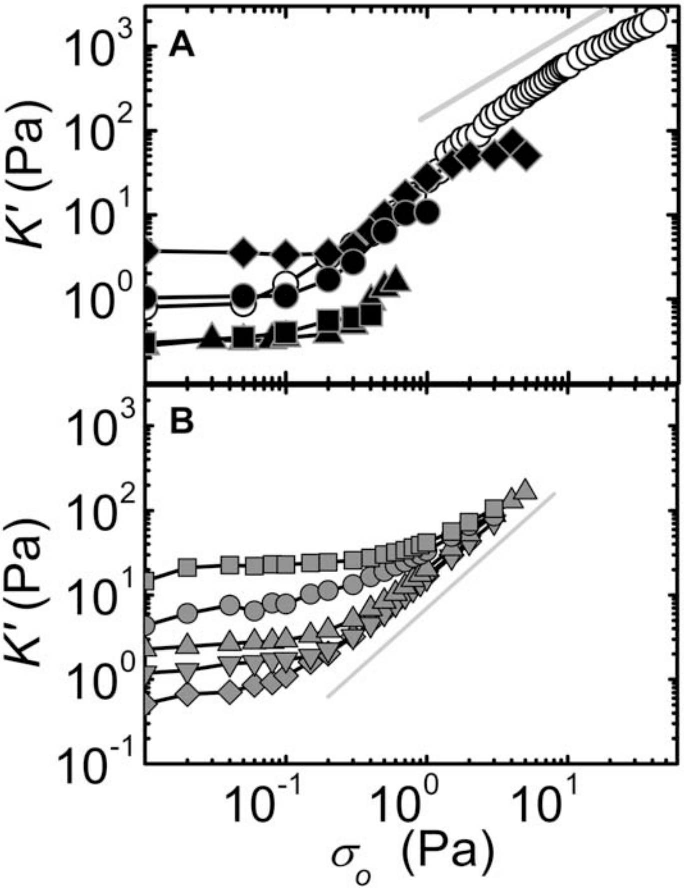

Figure 4.10 – Nonlinear stiffening in prestress measurements. A) Filamin networks with $R_F = 0.003$ and $L = 1$ (squares), 5 (triangles), 15 μm (solid circles); $R_F = 0.005$ with $L = 15$ μm (diamonds); $R_F = 0.01$ with $L = 15$ μm (open circles, bundled network). $K'(\sigma_0)$ is independent of prestress, σ_0, for small prestresses before beginning to increase with σ_0 at a critical stress, σ_c. Networks with higher R_F and L stiffen more and support larger stresses before breaking. Line denotes linear scaling predicted by the model. B) Rigidly crosslinked network with $L = 15$ μm and $R_B = 0.0003$ (diamonds), 0.001 (inverted triangles), 0.003 (triangles), 0.03 (circles), 0.3 (squares). These networks also display stiffening behavior, but the maximum stiffness and stress are roughly the same for every sample. Line denotes $K \sim \sigma^{3/2}$ scaling predicted by the affine thermal model.

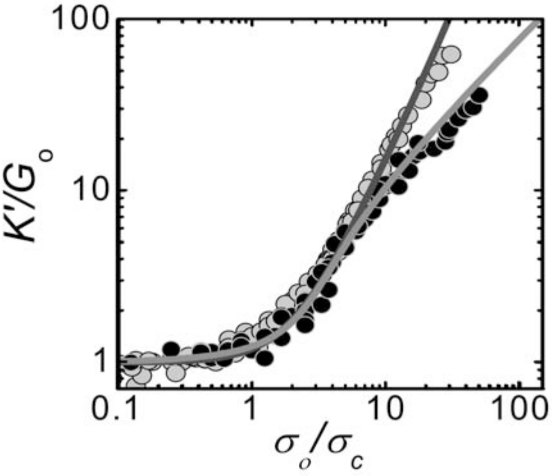

Figure 4.11 – Rescaled nonlinear stiffening of non-bundled networks with filamin (black) or rigid crosslinks (light gray) at various R_F or R_B, L, c_A. Filamin data is consistent with model of rigid rods connected by flexible linkers [21] (gray line), while rigid crosslinking data is consistent with model of semi-flexible filaments connected by rigid linkers [5] (dark gray line).

Thus, as we increase L at fixed R_F, the number of filamins per actin filament will increase, leading to a scaling prediction

$$\sigma_m \sim n \sim R_f L \tag{4.10}$$

We first look at σ_m measured in prestress experiments. In Fig. 4.10A, we see that σ_m supported by the $R_F = 0.003$ networks increases as we increase L. To quantify this, we plot σ_m as a function of L in Fig. 4.13A. Above a critical value of L, the maximum stress increases with L. This critical value of L decreases with increasing R_F. Similarly, for fixed L, σ_m increases roughly linearly with R_F over a broad range of R_F (Fig. 4.12). For the highest values of R_F, where the networks are highly bundled, σ_m increases dramatically (open symbols, Fig. 4.12). For R_F below a critical value, σ_m is roughly independent of R_F. This critical value of R_F decreases with increasing L [20].

We can collapse all the filamin data onto a single curve by plotting σ_m as a function of $R_F L$ [20], as shown in Fig. 4.13B. For $R_F L > 0.01$, σ_m grows nearly linearly with $R_F L$, consistent with the prediction of the model. For smaller values of $R_F L$, the network is rather weakly connected and breaks at very low levels of stress. The value of $R_F L \approx 0.01$ corresponds to $n \approx 4$. At physiological conditions $n \approx 15$—suggesting that the cytoskeleton operates in a regime where it has high enough connectivity to

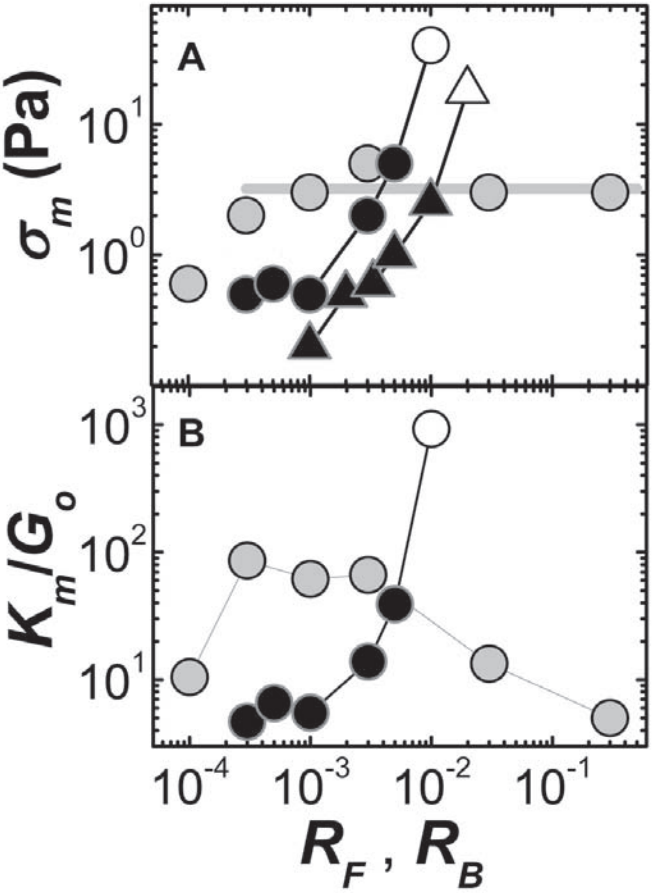

Figure 4.12 – Maximum stress and stiffening for crosslinked networks: A) Maximum stress as a function of R_F for filamin crosslinked networks with $L = 15$ μm (black circles) or $L = 5$ μm (black triangles) and as a function of R_B for rigidly crosslinked networks with $L = 15$ μm (gray circles). Gray line denotes mean maximum stress for rigidly crosslinked networks having $R_B > 0.001$. B) Magnitude of stiffening as a function of crosslinking ratios for networks with $L = 15$ μm. Filamin vs. R_F (black circles), rigid crosslinks vs. R_B (gray circles). (A-B) Non-bundled networks (solid symbols) and bundled networks (open symbols).

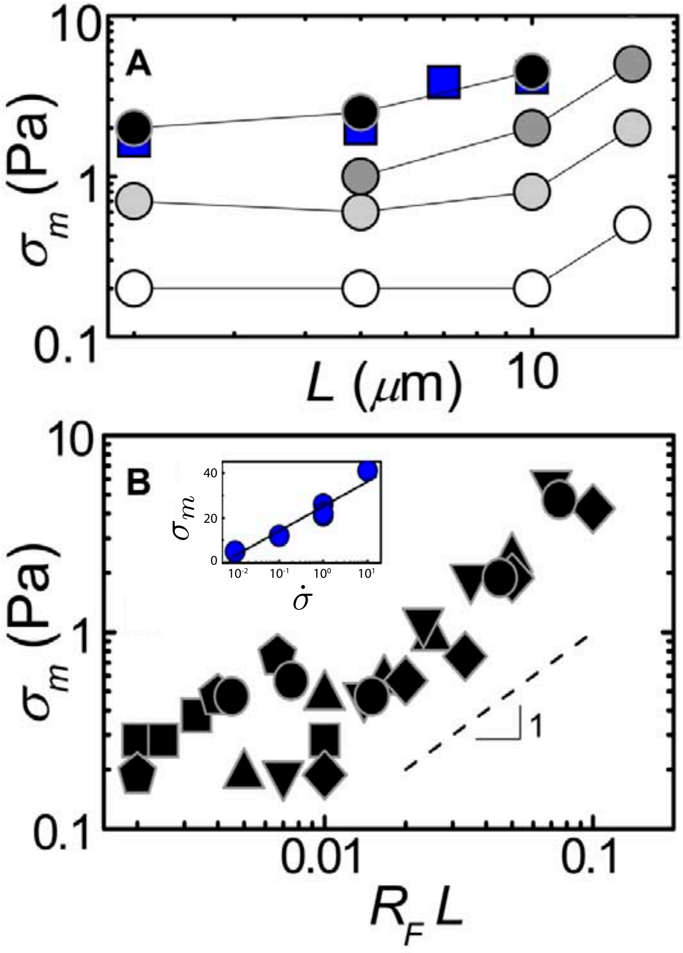

Figure 4.13 – (Color online) Scaling of the maximum stress, σ_m, with L for non-bundled filamin networks. A) The value σ_m increases with L. From prestress measurements (circles) or 0.1 s^{-1} strain ramps (squares): (white), 0.003 (light gray), 0.005 (gray), 0.01 (black). B) σ_m for samples of different compositions collapse onto a single curve when plotted vs. $R_F L$. Above $R_F L = 0.01$ the data scale roughly linearly with $R_F L$. $L = 15$ (circles), 10 (diamonds), 7 (inverted triangles), 5 (triangles), 2 (pentagons), 1 μm (squares). Inset: σ_m grows as the logarithm of loading rate in stress ramps for networks with $L = 15$ μm.

support large external stresses or internal tensions compared to purely entangled F-actin without rupturing. The linear scaling with $R_F L$ or n suggests that failure of these networks is indeed determined by unbinding of crosslinks [20,45]. In contrast, σ_m for rigidly crosslinked networks is nearly independent of R_B for $R_B > 0.001$ (Fig. 4.12); this is consistent with rupture of F-actin at network failure [13].

To further quantify the variations in the nonlinear response close to network failure, we investigate the dependence on *all* control parameters R_F, R_G, and c_A. For $c_A = 0.5$ mg/ml (black) and $L = 15$ μm (circles) with sparse cross-linking ($R_F = 0.0003$), σ_m is threefold larger than for purely entangled actin (Fig. 4.14a). The maximum stress is independent of R_F up to 0.001, as shown by the R_F dependence in Fig. 4.14a. Upon increasing R_F further, σ_m increases nearly linearly with R_F, up to a maximum of 5 Pa before the networks become bundled. Once bundles appear, σ_m continues to increase with R_F (open symbols, Fig. 4.14a). For $L = 7$ μm (inverted triangles), σ_m for all R_F is smaller than for the longer filaments. For $L = 1$ μm (squares), σ_m is 0.3 Pa and independent of R_F up to 0.01, before the network becomes bundled. Increasing c_A to 1.0 mg/ml (purple online) and further to 1.5 mg/ml (green online) at fixed R_F and L increases σ_m.

We first focus on low cross-linking densities, in the absence of bundles. Above, we found a naive estimate of the maximum stress at network failure would be $\sigma_m \sim nc_A$ (Eq. (4.9). However, this does not account for the three-body nature of filamin-F-actin cross-linking: the probability to form an effective cross-link requires binding to two actin filaments. This adds a factor of $\xi^{-1} \sim c_A^{1/2}$ which measures the linear density of neighboring actin filaments along a particular filament. The scaling prediction then becomes $\sigma_m \sim c_A^{3/2}$. To test this prediction, we scale σ_m from Fig. 4.14a by $c_A^{3/2}$, $\tilde{\sigma}_m = \sigma_m / c_A^{3/2}$. When plotted as a function of n, the data for the non-bundled networks do indeed collapse onto a single curve, as shown by the closed symbols in Fig. 4.14c. For $n \gtrsim 3$, $\tilde{\sigma}_m$ has a nearly linear dependence on n, in agreement with the prediction of the model. The somewhat stronger than linear scaling with n may indicate additional cooperativity beyond our simple model. For $n \lesssim 3$, the networks are weakly connected and support only very small shear stresses, nearly independent of n. The scaled data for the bundled networks also collapse, but onto a separate curve, which has a larger magnitude and somewhat weaker n dependence than the non-bundled networks (Fig. 4.14c, open symbols). A similar collapse is observed for $\tilde{K}'_m = K'_m / c_A^{3/2}$, when it is plotted as a function of n, as shown in Fig. 4.14d. These results further confirm our hypothesis that n is a key control parameter for the network mechanics.

The approximately linear dependence of σ_m on n in Fig. 4.14 suggests that network failure corresponds to a particular force per filamin cross-link. This failure is likely due to filamin unbinding from actin. From the schematic in Fig. 4.2, the maximum tension in a typical actin filament occurs at its mid-point, and is given by the

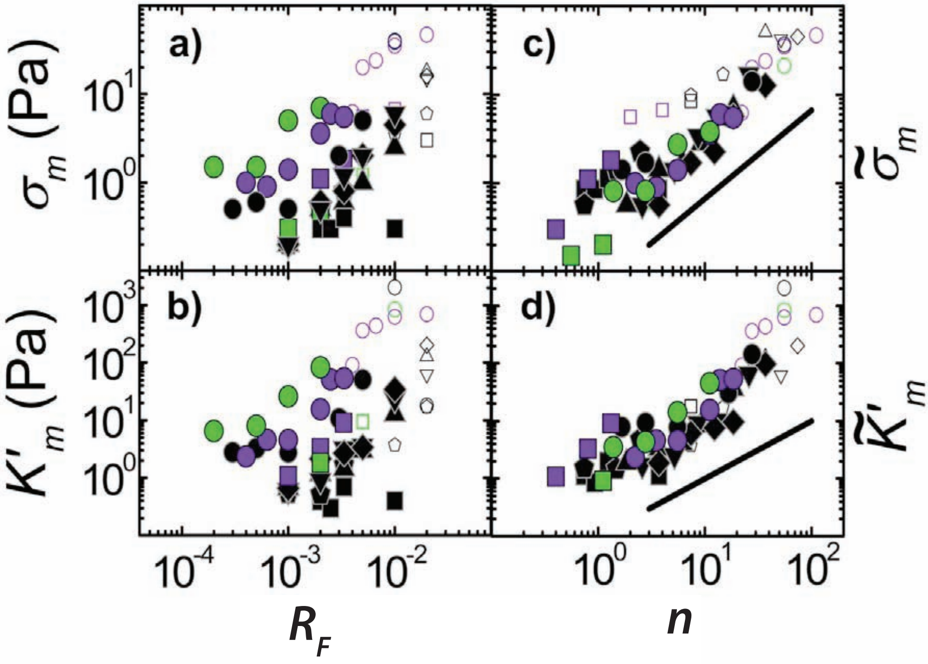

Figure 4.14 – (a) Maximum stress, σ_m, and (b) maximum differential modulus, K'_m, vs R_F. (c) Scaled maximum stress, $\tilde{\sigma}_m = \sigma_m/c_A^{3/2}$, and (d) maximum differential modulus, $\tilde{K}'_m = K'_m/c_A^{3/2}$, vs n. $c_A = 0.5$ mg/ml (black), $c_A = 1.0$ mg/ml (purple), and $c_A = 1.5$ mg/ml (green). $L = 1\mu$m (squares), $L = 2$ μm (pentagons), $L = 5$ μm (triangles), $L = 7$ μm (inverted triangles), $L = 10$ μm (diamonds), and $L = 15$ μm (circles). Lines denote linear scaling with n.

sum of forces applied by the filamins bound on each side of the mid-point. For large n, these forces should increase linearly away from this mid-point, which leads to an average tension $\langle\tau\rangle = nf_0/6$, where f_0 is the maximum force experienced by a filamin. For an isotropic network, the shear stress is given by $\sigma = \frac{2}{15}\rho\langle\tau\rangle_m$, where $\rho \sim \xi^{-2}$ is the density of polymer length per volume and $\langle\tau\rangle_m$ refers to the average tension along actin filaments oriented in the direction of maximal network extension. These are the filaments expected to be under the greatest tension. For a 1 mg/ml network, $\rho = 40\ \mu\text{m}^{-2}$, which sets $\langle\tau\rangle_m \approx 2$ pN for $\sigma_m = 10$ Pa. This force is the result of multiple filamins n, as noted above. Thus, the load on any individual filamin is less than 2 pN at network failure under the conditions of our experiments, corresponding to loading rates of $0.1 - 1$ pN/s. This is comparable to rupture forces for the actin-cross-linker bond measured for a number of actin binding proteins [7, 43–45], but is far below the $50 - 100$ pN forces required for full unfolding of individual Ig domains in filamin [47]. Indeed, recent single molecule studies indicate that filamin unbinding is favored over unfolding at loading rates below 50 pN/s [45]. Thus, we believe that network failure is a result of filamin unbinding and that filamin Ig domain unfolding is unlikely [46].

We can also determine σ_m from the strain ramp measurements. In the inset to Fig. 4.8A, we see that σ_m also increases with L for strain ramps conducted at a rate of 0.1 s^{-1}. Plotting σ_m determined in this way as a function of L (squares, Fig. 4.13A) for $R_F = 0.01$, we find that these measurements of σ_m show similar scaling as the prestress measurements do, and at this strain rate the values from the two methods nearly match. More generally, we expect that σ_m will depend on the rate of the measurement. The unbinding force for a single crosslink is expected to increase as the logarithm of the loading rate [41, 48]. Indeed, in an analogous macroscopic measurement, we find that σ_m increases as the logarithm of the loading rate on the network, again consistent with crosslink unbinding at network failure (inset, Fig. 4.13B).

4.4 Conclusions

The linear and nonlinear elastic behavior of filamin-gelsolin-F-actin networks support a model of crosslink dominated elasticity. The F-actin behaves as a rigid filament that constrains the deformation profile of the flexible crosslinks bound along its length; this leads to the unusual L dependence in the rheology of these networks. Our data suggest that the lengths of actin filaments within crosslinked cytoskeletal networks may be an important determinant of cell mechanics.

Large, flexible crosslinks like filamin form compliant gels that can nonetheless support stresses that are orders of magnitude larger than those of purely entangled F-actin. The stiffness of these networks can be tuned over a broad range by external stress or internal tension [3, 6, 20]. In contrast, rigid crosslinks form networks with a linear stiffness that is highly tunable by increasing the crosslink concentration, but show less dramatic nonlinear stiffening and tend to break at smaller strains [5, 7]. Interestingly, the mechanical response of F-actin networks can be tuned between these two cases by systematically varying the molecular weight of a crosslink [8].

Many physiological crosslinks are smaller and expected to be more incompliant than filamin; within the cell these crosslinks typically organize F-actin into bundles rather than orthogonal meshworks. For example, the α-actinin dimer forms an antiparallel rod of ≈ 30 nm, and fimbrin has two actin binding domains in tandem and is only ≈ 12 nm. Indeed, rheological studies show that α-actinin-F-actin networks have highly tunable linear stiffness [49], suggesting α-actinin behaves predominantly as a rigid crosslink. This also suggests that the cell may use large, compliant crosslinking proteins like the 160 nm long filamin dimers precisely because of the unique mechanical properties of the networks they form. In support of this view, filamin-F-actin networks mimic many key rheological features of cells [6, 19]. This highlights the potential value of these results in providing insight into the behavior observed in cells. Our results will serve as an important first step in developing more sophisticated models of cytoskeletal mechanics. Moreover, the model can be used to estimate the conditions required for forced unfolding of cross-links inside living cells [50]

4.5 Acknowledgements

This work was performed in collaboration with K. E. Kasza, G. H. Koenderink, Y. C. Lin, W. Messner, E. A. Millman, F. Nakamura, T. P. Stossel and D. A. Weitz. Most of the experiments were performed by K.E.K, some were performed by C.P.B.. C.P.B. gratefully acknowledges the hospitality of Harvard University where most of this work was performed. We thank C. Storm for helpful discussions.

Bibliography

[1] J. Stricker, T. Falzone, and M. L. Gardel. *Mechanics of the F-actin cytoskeleton*. J Biomech. **3** (2009).

[2] D. Humphrey, C. Duggan, D. Saha, D. Smith, and J. Kas. *Active fluidization of polymer networks through molecular motors*. Nature **416**:413-416 (2002).

[3] G. H. Koenderink, Z. Dogic, F. Nakamura, P. M. Bendix, F. C. Mackintosh, J. H. Hartwige, T. P. Stossele, and D. A. Weitz. *An active biopolymer network controlled by molecular motors*. Proc. Natl. Acad. Sci. **106**: 15192 (2009).

[4] D. Mizuno, C. Tardin, C. F. Schmidt, and F. C. Mackintosh. *Nonequilibrium mechanics of active cytoskeletal networks*. Science **315**:370-373 (2007).

[5] M. L. Gardel, J. H. Shin, F. C. MacKintosh, L. Mahadevan, P. Matsudaira, and D. A. Weitz. *Elastic behavior of cross-linked and bundled actin networks*. Science **304**:1301-1305 (2004).

[6] M. L. Gardel, F. Nakamura, J. H. Hartwig, J. C. Crocker, T. P. Stossel, and D. A. Weitz. *Prestressed F-actin networks cross-linked by hinged filamins replicate mechanical properties of cells*. Proc. Natl. Acad. Sci. **103**:1762-1767 (2006).

[7] R. Tharmann, M. M. Claessens, and A. R. Bausch. *Viscoelasticity of isotropically cross-linked actin networks*. Phys. Rev. Lett. **98**:088103 (2007).

[8] B. Wagner., R. Tharmann, I. Haase, M. Fischer, and A. R. Bausch. *Cytoskeletal polymer networks: the molecular structure of cross-linkers determines macroscopic properties*. Proc. Natl. Acad. Sci. **103**:13974-13978 (2006).

[9] K. M. Schmoller, O. Lieleg, and A. R. Bausch. *Cross-linking molecules modify composite actin networks independently*. Phys. Rev. Lett. **101**:118102 (2008).

[10] C. Storm, J. Pastore, F.C. MacKintosh, T.C. Lubensky and P.A. Janmey. *Nonlinear elasticity in biological gels*. Nature **435**:191 (2005).

[11] F. Gittes, B. Mickey, J. Nettleton, and J. Howard. *Flexural rigidity of microtubules and actin filaments measured from thermal fluctuations in shape*. J. Cell. Biol. 120:923-934 (1993).

[12] F. C. MacKintosh, J. Käs, and P. A. Janmey. *Elasticity of semiflexible biopolymer networks*. Phys. Rev. Lett. **75**:4425-4428 (1995).

[13] M. L. Gardel, J. H. Shin, F. C. MacKintosh, L. Mahadevan, P. A. Matsudaira., and D. A. Weitz. *Scaling of F-actin network rheology to probe single filament elasticity and dynamics*. Phys. Rev. Lett. **93**:188102 (2004).

[14] T. P. Stossel, J. Condeelis, L. Cooley, J. H. Hartwig, A. Noegel, M. Schleicher, S. S. Shapiro. *Filamins as integrators of cell mechanics and signalling*. Nat. Rev. Mol. Cell. Biol. **2**:138-145 (2001).

[15] K. E. Kasza, F. Nakamura, S. Hu, P. Kollmannsberger, N. Bonakdar, B. Fabry, T.P. Stossel, N. Wang, and D. A. Weitz. *Filamin A is essential for active cell stiffening but not passive stiffening under external force*. Biophys. J. **96**:4326-4335 (2009).

[16] F. J. Byfield, Q. Wen, I. Levental, K. Nordstrom, P. E. Arratia, R. T. Miller, P. A. Janmey. *Absence of filamin A prevents cells from responding to stiffness gradients on gels coated with collagen but not fibronectin*. Biophys. J. **96**:5095-5102 (2009).

[17] S. Gehler, M. Baldassarre, Y. Lad, J. L. Leight, M. A. Wozniak, K. M. Riching, K. W. Eliceiri, V. M. Weaver, D. A. Calderwood, P. J. Keely. *Filamin A-beta1 integrin complex tunes epithelial cell response to matrix tension*. Mol Biol Cell **20**:3224-3238 (2009).

[18] T. Kainulainen, A. Pender, M. D'Addario, Y. Feng, P. Lekic, and C. A. McCulloch. *Cell death and mechanoprotection by filamin a in connective tissues after challenge by applied tensile forces*. J. Biol. Chem. **277**:21998-22009 (2002).

[19] M. L. Gardel, F. Nakamura, J. Hartwig, J. C. Crocker, T. P. Stossel, and D. A. Weitz. *Stress-dependent elasticity of composite actin networks as a model for cell behavior*. Phys. Rev. Lett. **96**:088102 (2006).

[20] K. E. Kasza, G. H. Koenderink, Y. C. Lin, C. P. Broedersz, W. Messner, F. Nakamura, T. P. Stossel, F. C. MacKintosh, and D. A. Weitz. *Nonlinear elasticity of stiff biopolymers connected by flexible linkers*. Phys. Rev. E **79**:041928 (2009).

[21] C. P. Broedersz, C. Storm, and F. C. MacKintosh. *Nonlinear elasticity of composite networks of stiff biopolymers with flexible linkers*. Phys. Rev. Lett. **101**:118103 (2008).

[22] C. P. Broedersz, C. Storm, and F. C. MacKintosh. *Effective-medium approach for stiff polymer networks with flexible cross-links*. Phys. Rev. E **79**:061914 (2009).

[23] W. H. Goldmann, M. Tempel, I. Sprenger, G. Isenberg, and R. M. Ezzell. *Viscoelasticity of actin-gelsolin networks in the presence of filamin*. Eur J Biochem **246**:373-379 (1997).

[24] J. D. Pardee and J. A. Spudich. *Purification of muscle actin*. Methods Enzymol **85** Pt B:164-181 (1982).

[25] F. Nakamura, E. Osborn, P. A. Janmey, and T. P. Stossel. *Comparison of filamin A-induced cross-linking and Arp2/3 complex-mediated branching on the mechanics of actin filaments*. J. Biol. Chem. **277**:9148-9154 (2002).

[26] D. J. Kwiatkowski, P. A. Janmey, and H. L. Yin. *Identification of critical functional and regulatory domains in gelsolin*. J. Cell. Biol. **108**:1717-1726 (1989).

[27] P. A. Janmey , J. Peetermans, K. S. Zaner, T. P. Stossel, and T. Tanaka. *Structure and mobility of actin filaments as measured by quasielastic light scattering, viscometry, and electron microscopy*. J. Biol. Chem. **261**:8357-8362 (1986).

[28] D. Biron, and E. Moses. *The effect of alpha-actinin on the length distribution of F-actin*. Biophys. J. **86**:3284-3290 (2004).

[29] J. L. Podolski, and T. L. Steck. *Length distribution of F-actin in Dictyostelium discoideum*. J. Biol. Chem. **265**:1312-1318 (1990).

[30] T. M. Svitkina, A. B. Verkhovsky, K. M. McQuade, and G. G. Borisy. *Analysis of the actin-myosin II system in fish epidermal keratocytes: mechanism of cell body translocation*. J. Cell. Biol. **139**:397-415 (1997).

[31] J. Hanson, and J. Lowy. *The Structure of F-actin and of Actin Filaments Isolated from Muscle*. J Mol Biol **6**:46-60 (1963).

[32] S. Burlacu, P. A. Janmey, and J. Borejdo. *Distribution of actin filament lengths measured by fluorescence microscopy*. Am J Physiol **262**:C569-577 (1992).

[33] L. Hou, K. Luby-Phelps, and F. Lanni. *Brownian motion of inert tracer macromolecules in polymerized and spontaneously bundled mixtures of actin and filamin*. J. Cell. Biol. **110**:1645-1654 (1990).

[34] K. M. Schmoller, O. Lieleg, and A. R. Bausch. *Structural and viscoelastic properties of actin/filamin networks: cross-linked versus bundled networks*. Biophys. J. **97**:83-89 (2009).

[35] C. A. Hartemink. *The cross-linking mechanism of filamin A in the actin cytoskeleton*. Cambridge: Massachusetts Institute of Technology)(2005).

[36] J. H. Hartwig, and P. Shevlin. *The architecture of actin filaments and the ultrastructural location of actin-binding protein in the periphery of lung macrophages*. J. Cell. Biol. **103**:1007-1020 (1986).

[37] C. C. Cunningham, J. B. Gorlin, D. J. Kwiatkowski, J. H. Hartwig, P. A. Janmey, H.R. Byers, and T.P. Stossel. *Actin-binding protein requirement for cortical stability and efficient locomotion*. Science **255**:325-327 (1992).

[38] D. A. Head, A. J. Levine, and F. C. MacKintosh. *Distinct regimes of elastic response and deformation modes of cross-linked cytoskeletal and semiflexible polymer networks*. Phys. Rev. E **68**:061907 (2003).

[39] E. M. Huisman, C. Storm, and G. T. Barkema. *Monte Carlo study of multiply crosslinked semiflexible polymer networks*. Phys. Rev. E **78**:051801 (2008).

[40] C. Semmrich, R. J. Larsen, and A. R. Bausch. *Nonlinear mechanics of entangled F-actin solutions*. Soft Matter **4**:1675 (2008).

[41] O. Lieleg, and A. R. Bausch. *Cross-linker unbinding and self-similarity in bundled cytoskeletal networks*. Phys. Rev. Lett. **99**:158105 (2007).

[42] C.P. Broedersz, K.E. Kasza, L.M. Jawerth, S. Muenster, D.A. Weitz, F.C. MacKintosh. *Measurement of nonlinear rheology of cross-linked biopolymer gels*. Soft Matter, **6**: 4120 (2010).

[43] H. Miyata,, R. Yasuda, and K. Kinosita, Jr.. *Strength and lifetime of the bond between actin and skeltal muscle alpha-actinin studied with an optical trapping technique*. Biochim. Biophys. Acta. **1290**, 83)1996).

[44] T. Nishizaka, H. Miyata, H. Yoshikawa, S. Ishiwata, and K. Kinosita, Jr.. *Unbinding force of a single motor molecule of muscle measured using optical tweezers*. Nature **377**, 251 (1995).

[45] J. M. Ferrer, H. Lee, J. Chen, B. Pelz, F. Nakamura, R. D. Kamm, and M. J. Lang *Measuring molecular rupture forces between single actin filaments and actin-binding proteins*. Proc. Natl. Acad. Sci. **105**, 9221-9226 (2008).

[46] B. A. DiDonna, and A. J. Levine. *Filamin Cross-Linked Semiflexible Networks: Fragility under Strain*. Phys. Rev. Lett. **97**, 068104 (2006).

[47] S. Furuike, T. Ito, and M. Yamazaki. *Mechanical unfolding of single filamin A (ABP-280) molecules detected by atomic force microscopy*. FEBS Lett. **498**:72-75 (2001).

[48] E. Evans, and K. Ritchie. *Dynamic strength of molecular adhesion bonds*. Biophys. J. **72**:1541-1555 (1997).

[49] S. M. Ward, A. Weins, M. R. Pollak, and D. A. Weitz. *Dynamic viscoelasticity of actin cross-linked with wild-type and disease-causing mutant alpha-actinin-4*. Biophys. J. **95**:4915-4923 (2008).

[50] C. P. Johnson, H-Y. Tang, C. Carag, D. W. Speicher, and D. E. Discher. *Forced unfolding of proteins within cells.* Science **317**, 663 (2007).

5

Measurement of Nonlinear rheology of cross-linked biopolymer gels

- C. P. Broedersz, K. E. Kasza, L. M. Jawerth, S. Muenster, D .A. Weitz and F .C. MacKintosh
  Nonlinear rheology of cross-linked biopolymer gels,
  Soft Matter **6**, 4120 (2010)

Abstract

One of the hallmarks of biopolymer gels is their nonlinear viscoelastic response to stress, making the measurement of the mechanics of these gels very challenging. Various rheological protocols have been proposed for this; however, a thorough understanding of the techniques and their range of applicability, as well as a careful comparison between these methods are still lacking. Using both strain ramp and differential prestress protocols, we investigate the nonlinear response of a variety of systems ranging from extracellular fibrin gels to intracellular F-actin solutions and F-actin cross-linked with permanent and physiological transient linkers. We find that the prestress and strain ramp results agree well for permanently cross-linked networks over two decades of strain rates, while the protocols only agree at high strain rates for more transient networks. Surprisingly, the nonlinear response measured with the prestress protocol is insensitive to creep; although a large applied steady stress can lead to significant flow, this has no significant effect on either the linear or nonlinear response of the system. A simple model is presented to provide insight into these observations.

5.1 Introduction

The mechanical properties of cells depend largely on their cytoskeleton, an intracellular network consisting of various biopolymers such as F-actin and associated proteins for cross-linking and stress generation. At a larger scale, most tissue cells are not viable when suspended in a fluid, but depend on the stiff anchorage provided by the extracellular matrix [1], which also consists of filamentous protein polymers. Both intracellular and extracellular biopolymer networks exhibit remarkable mechanical properties, as demonstrated in numerous *in vitro* studies: their mechanical response is highly nonlinear, exhibiting both a pronounced elastic stiffening [2–12] and large, negative normal stress under applied shear [13–15]. This stiffening response is thought to moderate large deformations that endanger cellular and tissue integrity. However, during various essential cell-functions such as crawling, invasion and division the cytoskeleton must remodel, while simultaneously buttressing against external stress. The combination of these seemingly incompatible properties poses a significant experimental challenge for quantitative measurement of biopolymer gel mechanics. Traditional rheological methods are not sufficient for such systems and new methods are needed.

In many soft matter systems, a nonlinear response arises under flow conditions in the form of shear thickening or thinning. By contrast, the nonlinear response of reconstituted cross-linked biopolymer networks is largely elastic in nature. Many physiological cross-links are not permanent, however, and their transient nature complicates the mechanical response by enabling stress relaxation and network flow [16,17]. The typical unbinding time of a cross-linking protein for F-actin ranges from seconds to minutes [17–19]; thus cross-linker unbinding occurs on biological timescales and must be accounted for. This suggests various problems for the commonly used protocols [2, 3, 20–22]: during a strain ramp, in which the strain is the control variable that is increased linearly in time while the stress is measured, the elastic response and stress relaxation occur together, leading to an inevitable rate dependence of the measured elasticity [20, 23]. In a prestress measurement the stress is the control variable and an incremental response is measured in the presence of a constant applied prestress [3, 24]. However, concerns have been raised that a steadily applied prestress could also induce flow or restructuring of the sample, which is expected to affect the material properties [20]. A thorough understanding of the various measurement techniques is crucial to quantitatively explore the nonlinear mechanical response of biopolymer gels. Furthermore, a careful comparison between these protocols is needed to determine which protocol is most suitable to accurately measure the nonlinear mechanical response for different systems.

Here we study the nonlinear response of biopolymer gels with the prestress protocol and make a comparison with strain ramps, which we perform over a broad range of strain rates. We further study how the large stresses applied in the prestress protocol on timescales of minutes affect both the linear and nonlinear elastic response as determined when the applied pre-stress is the control variable; simultaneously we monitor the creep. To explore the generality of our results we investigate a range of systems: F-actin solutions and F-actin cross-linked with biotin-NeutrAvidin permanent rigid cross-links or physiological linkers, for which we use human filamin, a large flexible cross-linker. To extend the scope to extracellular fiber networks we also probe fibrin gels. The nonlinear response obtained with the prestress and strain ramp protocols agree well for permanent networks over two decades of strain rates. By contrast, the two protocols agree only at high strain rates for more transient networks. We further find that the prestress protocol is insensitive to creep; even when the applied stress leads to significant accumulated strain, we observe no significant effect on both the linear and the nonlinear response of the system, and the nonlinear response does not evolve significantly over time. We propose a simple yet general material model that includes the nonlinear elasticity of the network as well as network flow on long time-scales. This model can help to understand and account for our observations when applying the two different measurement protocols.

5.2 Materials and methods

G-actin is obtained from rabbit skeletal muscle and actin samples are prepared by mixing monomeric actin with solutions of 10x polymerization buffer (20 mM Tris-HCl, 20 mM $MgCl_2$, 1 M KCl, 2 mM DTT, 2 mM $CaCl_2$, 5 mM ATP, pH 7.5). The actin-filamin samples are prepared by gently mixing solutions of 10x polymerization buffer with a solution of recombinant human filamin A purified from Sf9 cell lysates and monomeric actin at a molar ratio of 0.003. For permanently cross-linked networks, biotinylated actin monomers are incorporated in actin filaments at a molar ratio of biotinylated monomers to non-biotinylated monomers $R = 0.003$. Cross-linking is mediated by NeutrAvidin proteins. Samples are prepared by mixing solutions of 10x polymerization buffer, biotinylated monomeric actin, and monomeric actin. After 3 minutes incubation, NeutrAvidin at a 1 : 1 molar ratio to biotinylated actin is gently mixed in.

Human fibrinogen (Enzyme Research Laboratories, South Bend, IN) is diluted in fibrin buffer (150 mM NaCl,20 mM TRIS, 20 mM $CaCl_2$, pH 7.4) to a final concentration of 0.8 mg/ml. The networks are cross-linked by fibrinoligase (FXIIIa), which is present in the fibrinogen stock solution. Polymerization is initiated by addition of human α-thrombin (Enzyme Research Laboratories, South Bend, IN) with a final concentration of 0.05 U/ml. After addition of thrombin, samples are pipetted briefly to mix and immediately pipetted into the rheometer. The networks are allowed to polymerize for two hours before all rheological tests.

The mechanical response is measured with a stress-controlled rheometer (Ares G2, TA Instruments), using a 40 mm diameter stainless steel parallel plate geometry with a gap of 160 μm for the actin samples and a 20 mm diameter stainless steel parallel plate with a gap of 500 μm for the fibrin samples. All samples are polymerized in situ at 25°C. We apply a thin layer of low viscosity mineral oil around the sample to minimize evaporation. Linear viscoelastic moduli are obtained by applying an oscillatory stress, $\sigma(t) = \delta\sigma \mathrm{e}^{\mathrm{i}\omega \mathrm{t}}$, and measuring the resulting strain, $\gamma(t) = \delta\gamma \mathrm{e}^{\mathrm{i}\omega \mathrm{t}}$; the complex modulus $G^* = G' + iG''$ is determined from $G^* = \delta\sigma/\delta\gamma$.

The nonlinear mechanical response is quantified using two distinct protocols: In the strain ramp protocol, the applied deformation of the sample is the control variable and the strain $\gamma(t)$ is steadily increased at a fixed rate, while the resulting stress $\sigma(t)$ is measured. Both $\gamma(t)$ and $\sigma(t)$ are smoothed using a cubic spline algorithm in Matlab to compute the differential modulus $K = \frac{\mathrm{d}\sigma}{\mathrm{d}\gamma}$ by applying a numerical derivative to the stress-strain curve. By contrast, in the prestress protocol, the applied stress is the control variable and we perform differential measurements to determine the materials' differential stiffness: A steady prestress, σ_0, is applied on which a small amplitude oscillatory stress, $\delta\sigma(t) = \delta\sigma \mathrm{e}^{\mathrm{i}\omega \mathrm{t}}$ is superposed at a frequency ω of 6.3 rad s^{-1}; we measure the total strain and determine the small oscillatory strain response,

$\delta\gamma(t) = \delta\gamma e^{i\omega t}$. The oscillatory stress amplitude used is at most 10 % of the steady prestress, and we confirm that the response is linear in $\delta\sigma$ for all σ_0. The complex differential or tangent viscoelastic modulus is determined from $K^* = \frac{\delta\sigma}{\delta\gamma}$.

5.3 Results

5.3.1 Linear mechanical response

To characterize the systems, we measure the frequency dependence of the linear viscoelastic moduli. When 0.5 mg/ml biotinylated actin (biotin:actin molar ratio of 0.003) is polymerized in the presence of NeutrAvidin it forms a soft, predominantly elastic gel. Within the frequency range we study here, $G' \approx 1$ Pa and appears to be virtually independent of frequency, as shown in Fig. 5.1a. At a frequency of 0.1 Hz, G'' is at least 10-fold smaller than G'. In the absence of cross-links polymerized actin forms an entangled solution. This soft viscoelastic material has an elastic modulus of only $G' \approx 0.5$ Pa at a frequency of 0.1 Hz and G' is larger than G'' (Fig. 5.2b). Consistent with previous studies [25–27], both viscoelastic moduli exhibit a weak frequency dependence, as shown in Fig. 5.2b. Interestingly, when actin is polymerized in the presence of filamin (filamin:actin molar ratio of 0.003), the viscoelastic response changes only marginally as compared to the pure F-actin solution. Although the linear elastic modulus increases to $G' \approx 1$ Pa , the G' to G'' ratio remains small and the moduli still exhibit a weak frequency dependence, as shown in Fig. 5.1c. Thus, in contrast to permanent biotin-NeutrAvidin linking, the filamin cross-links form a gel with a considerable viscous component.

The polymerization of fibrinogen is initiated by the addition of thrombin, inducing the formation of a network of thick fiber bundles with diameters on the order of hundreds of nanometers [28]. The presence of fibronoligase (FXIII) enzymatically promotes the formation of molecular bonds between protofibrils inside the bundle as well as between fiber bundles [29, 30]. The fibrin gels are stiffer than the actin gels studied here and have an elastic shear modulus of $G' \approx 16$ Pa, as shown in Fig. 5.1d. The elastic modulus G' is roughly 10-fold larger than G'' and appears to be independent of frequency in the range we probed, consistent with previous experiments [31]. The viscous modulus G'', however, exhibits a pronounced minimum at a frequency of 0.03 Hz; this together with the subsequent increase of G'' at lower frequencies may be indicative of a relaxation process at low frequencies.

5.3.2 Nonlinear response - Strain ramp protocol

To quantify the nonlinear mechanical response we first employ the strain ramp protocol. In principle, this represents the most direct method to probe the stress-strain

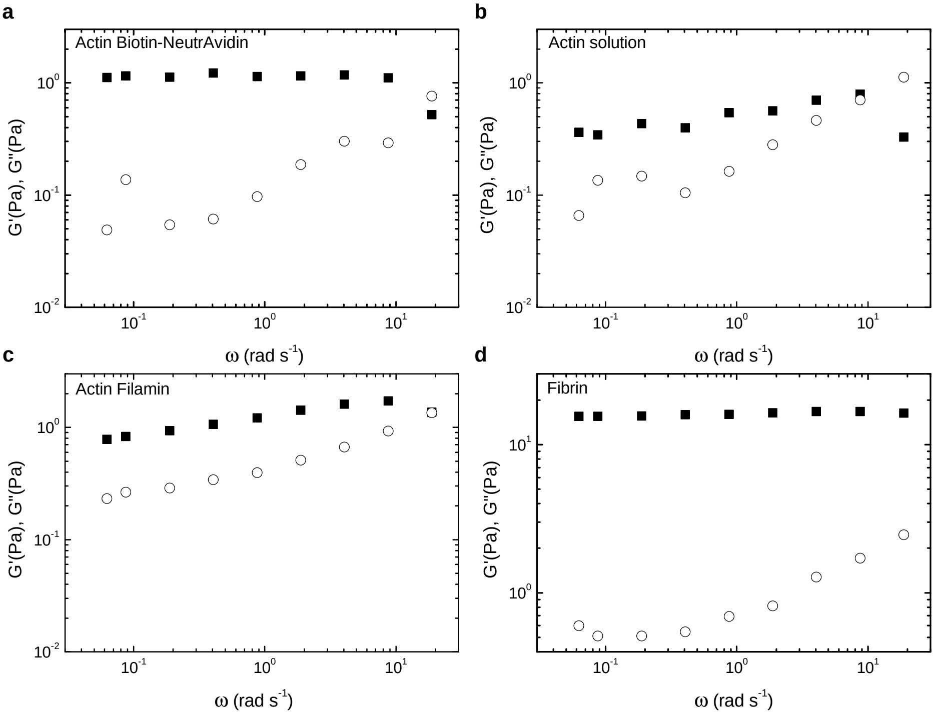

Figure 5.1 – The linear viscoelastic moduli G' (squares), G'' (circles) as a function of frequency for a) F-actin with a permanent biotin-NeutrAvidin cross-links. b) F-actin solution c) Actin cross-linked with the physiological linker protein filamin d) Fibrin with factor XIII.

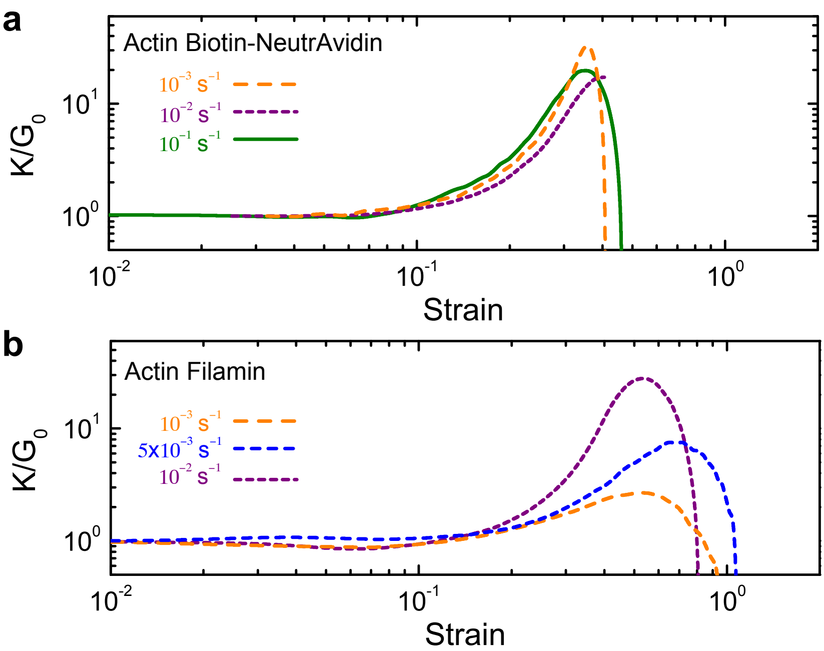

Figure 5.2 – (Color online) Strain ramp protocol: The tangent modulus $K = d\sigma/d\gamma$ normalized by the linear modulus G_0 as a function of strain for various strain rates $\dot{\gamma}$: 0.001 s^{-1} (orange), 0.005 s^{-1} (blue), 0.01 s^{-1} (purple) and 0.1 s^{-1} (green). a) F-actin cross-linked with biotin-NeutrAvidin. b) F-actin cross-linked with filamin.

behavior of a material, since the stress is measured as a function of an applied strain that increases linearly with time. It has been reported that pure F-actin solutions exhibit a nonlinear response that depends strongly on the strain rate $\dot{\gamma}$ [20]. By contrast, for actin networks with permanent biotin-NeutrAvidin cross-links the strain ramps exhibit no significant dependence on strain rate over two decades of $\dot{\gamma}$, as shown in Fig. 5.2a. Interestingly, the strain ramp measurements of F-actin networks cross-linked by filamin also depend strongly on $\dot{\gamma}$. The amount of stiffening becomes comparable to the biotin-NeutrAvidin cross-linked actin only at strain rates as high as $\dot{\gamma} = 0.01$ s^{-1}, as shown in Fig. 5.2b.

5.3.3 Nonlinear response - Prestress protocol

We also characterize the nonlinear, differential mechanical properties of biopolymer gels with the prestress protocol. Small stress oscillations are superimposed on a constant stress σ_0 to measure the elastic differential modulus K'; the shear direction of

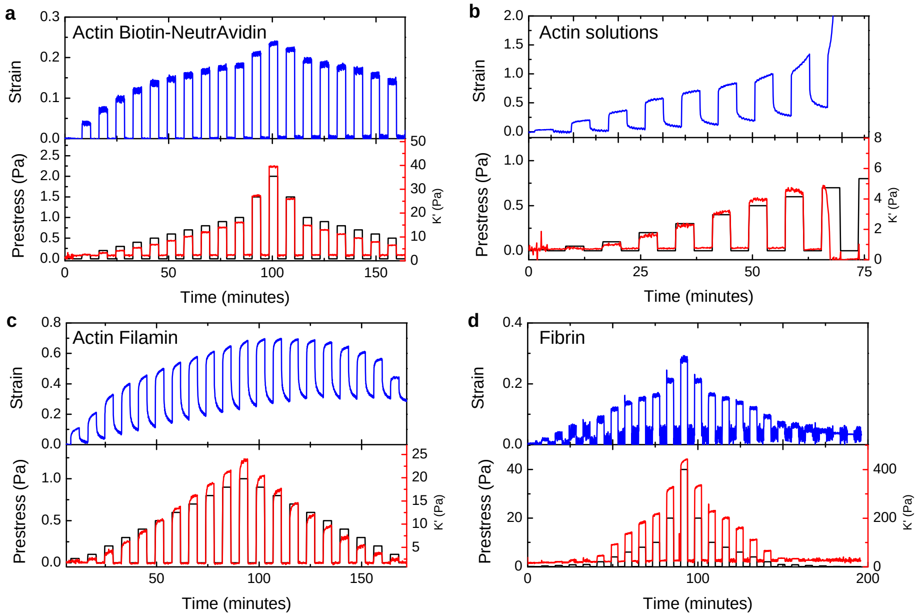

Figure 5.3 – Prestress protocol: The strain (blue curves) and the differential modulus K' (red curves) as a function of time during 4 minute prestress pulses (black curves) applied every 4 minutes of increasing and then decreasing magnitude. a) F-actin with permanent biotin-NeutrAvidin cross-links. b) F-actin solution. c) Actin cross-linked with the physiological linker protein filamin. d) Fibrin with factor XIII.

the small stress oscillation is chosen to be along to the same axis as the shear direction of the prestress [32]. To investigate the effect of the steady prestress on the linear and nonlinear mechanical properties as well as on the deformation of the material we employ the following detailed protocol. Each prestress measurement is held for 4 minutes at positive shear alternated with 4 minutes without load and subsequently repeated at higher prestress magnitude. The total strain and K' are monitored continuously throughout this protocol. After reaching a maximum value in the applied prestress we follow the same procedure in reverse to study possible hysteresis. In this reverse protocol the prestresses are applied in the same (positive) shear direction as in the forward protocol.

Both in permanent F-actin networks with biotin-NeutrAvidin cross-links as well as in pure F-actin solutions, K' responds to an applied prestress by a rapid increase, after which it exhibits no time-dependence, as shown in the lower panels of Figs. 5.3a-b. In the actin-filamin and fibrin systems, however, K' shows a relatively slower response

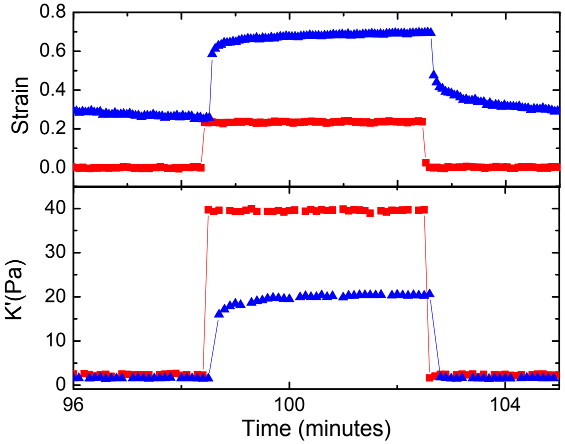

Figure 5.4 – (Color online) Close-up of the strain and differential modulus K' during the 13th prestress pulse of 2 Pa for actin with NeutrAvidin (red squares) and for actin with filamin (blue triangles).

to a step in the applied prestress (lower panel Figs. 5.3c,d and 5.4, although K' does appear to level off to a time-independent value. At the largest prestresses though this leveling off appears to occur more slowly. For the fibrin system we performed the same protocol with 16-minute prestress pulses and found that K' does level off within 16 minutes for prestresses as large as 40 Pa (data not shown). Remarkably, for all systems we observe that the mechanical response rapidly relaxes to the initial linear modulus as soon as the prestress is removed, unless the material breaks as demonstrated for an F-actin solution in the lower panel of Fig. 5.3b. We note that in the prestress protocol the materials state of stress is the control variable and unloading of the sample might result in a deformed state different from the initial one. However, the experiments here show that the linear mechanical properties measured at that unloaded state are unaffected by the previously applied large prestresses, even for large prestress to which the system responds nonlinearly.

To investigate to what extent the prestress affects the nonlinear mechanical properties, we reverse the protocol, moving from high to low prestress magnitude, after reaching the largest applied prestress. A potentially large effect could be anticipated in the cross-linked systems, since the applied prestress could lead to forced cross-link unbinding. Surprisingly, we observe no significant hysteresis for the cross-linked actin systems nor for the fibrin gels, as demonstrated by Figs. 5.3a,c-d. This observation indicates that, similar to the linear response, the nonlinear mechanical properties of these systems determined at a prescribed prestress are only weakly affected by large prestresses applied over several minutes.

The absence of any substantial hysteresis effects might be particularly surprising in the more transient actin-filamin network. The relatively large viscous component as well as the significant frequency dependence of the shear moduli (Fig. 5.1c) imply flow on long timescales. To investigate this flow we monitor the creep for all systems during the entire prestress protocol. As expected, the more permanent actin biotin-NeutrAvidin and fibrin systems accumulate little or no strain during the entire protocol (Fig. 5.3a). By contrast, both the pure F-actin and actin-filamin gels exhibit a significant accumulation of strain; this indicates that the sample is plastically flowing. The robustness of both the linear and nonlinear mechanical properties as measured with the prestress protocol in the presence of significant plastic flow is unexpected.

5.3.4 Protocol comparison

We further make a side-by-side comparison between the prestress measurements and the strain ramps at various strain rates. The prestress method measures the nonlinear mechanical response at a specific frequency, while the strain ramp probes the system at a specific rate, and it thus probes the response over a range of frequencies. For a system with a broad and flat elastic plateau, however, this difference is not expected to be significant. For actin networks cross-linked with the permanent biotin-NeutrAvidin links and the fibrin gels we find excellent agreement between the two protocols over two decades of strain rates, as shown in Fig. 5.5a,d. By contrast, for the actin-filamin system the strain ramp results exhibit a pronounced rate dependence (Fig. 5.5c). Interestingly, at large strain rates the strain-ramp results do show good agreement with the prestress results. For all systems we show both the prestress results using increasing levels of prestress (closed symbols) and the results obtained after this by using decreasing levels of prestress (open symbols). In all cases, even for the actin-filamin gels that exhibit creep, we find no significant hysteresis.

5.3.5 Simple model

To gain insight into the nonlinear rheological behavior of cross-linked biopolymer gels we propose a simple model that captures the main features observed experimentally. The nonlinear mechanical properties can arise through a variety of mechanisms, ranging from the nonlinear entropic elasticity of single polymer segments between rigid cross-links in F-actin [2, 3, 33] and intermediate filament [4, 34–36] networks, to the nonlinear response of the cross-links themselves, in the case of actin-filamin networks [37–40, 42]. In other systems, the nonlinear elasticity may be due to non-affine deformations [23, 43–45]. For the sake of generality of the model we do not make any assumptions about the underlying microscopic mechanism of strain stiffening. We do assume, however, that the elastic stiffness of the network responds

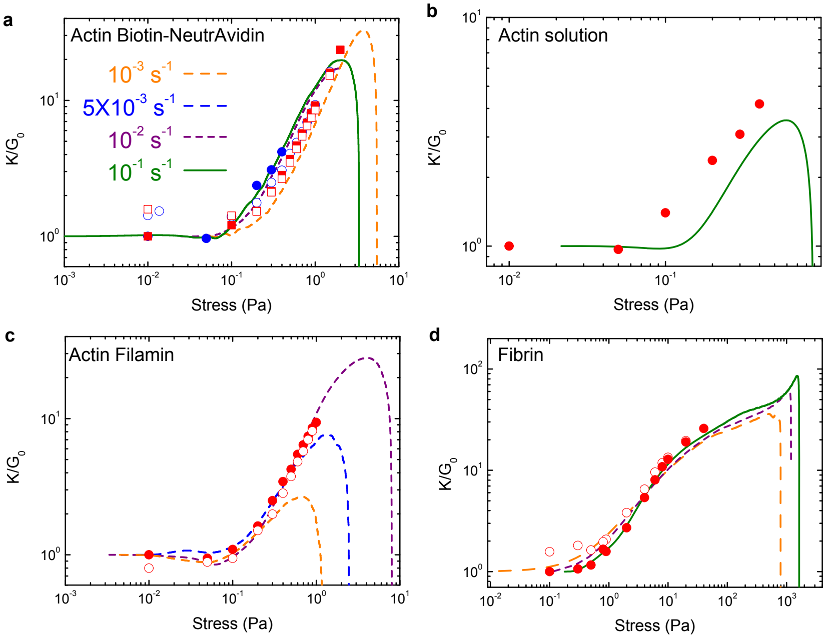

Figure 5.5 – (Color online) Protocol comparison: The tangent modulus (strain ramps) and differential modulus (prestress method) K normalized by the linear modulus G_0 as a function of stress σ (solid lines) for the prestress protocol with increasing prestress magnitude (closed symbols) and decreasing prestress magnitude (open symbols), and for the strain ramp protocol for various strain rates $\dot{\gamma}$: 0.001 s^{-1} (orange), 0.005 s^{-1} (blue), 0.01 s^{-1} (purple) and 0.1 s^{-1} (green). a) F-actin with permanent biotin-NeutrAvidin cross-links. b) F-actin solution. c) Actin cross-linked with the physiological linker protein filamin d) Fibrin with factor XIII.

instantaneously to an applied stress. Within this quasistatic approximation, the elastic stiffness of the network only depends on the current state of stress $k = k(\sigma)$. This approximation is easily justified on the long time-scales accessible by macrorheology for systems governed by the entropic elasticity of individual polymer segments. An applied tension extends a thermally contracted polymer strand; after a sufficiently large tension is applied, the entropic stiffness of this segment relaxes to a new increased equilibrium value. The time-scale for this process depends on the relaxation times of the thermally driven transverse fluctuations of the polymer segment. For a typical cross-linked F-Actin network this relaxation time can be estimated to be on the order of milliseconds [44] and can thus be considered instantaneous on the much longer timescales we probe with macrorheology. Even for non-affinely deforming networks, in which the nonlinearity can be associated with the buckling of filaments [6, 13, 44] this quasistatic approximation can be expected to be valid, provided that the spatial extent of such buckling is not too large.

In a transiently cross-linked network, the macroscopic strain is shared between two modes of deformation $\gamma = \gamma_e + \gamma_f$; the first mode γ_e consists of the reversible deformation of the network, whereas the second mode of deformation γ_f captures the flow of the network itself. Assuming that the strains in these two components are additive is equivalent to assuming that the stresses are always equal $\sigma_e = \sigma_f = \sigma$. It is convenient to set up a theoretical description of the nonlinear mechanical properties in terms of relations between small changes in stress $\mathrm{d}\sigma = \frac{\mathrm{d}\sigma}{\mathrm{d}t}\mathrm{d}t$ and the corresponding small changes in the strain $\mathrm{d}\gamma = \frac{\mathrm{d}\gamma}{\mathrm{d}t}\mathrm{d}t$. The reversible deformation of the network is described by a simple nonlinear viscoelastic model in which the elasticity $k(\sigma)$ and viscosity η contribute to the stress in parallel

$$\frac{\mathrm{d}\sigma}{\mathrm{d}t} = \left[k(\sigma) + \eta\frac{\mathrm{d}}{\mathrm{d}t}\right]\frac{\mathrm{d}\gamma_e}{\mathrm{d}t}. \tag{5.1}$$

The long-time flow of the network enables stress-relaxation. This relaxation may in general be governed by a spectrum of relaxation times. For simplicity, we here use a minimalistic approach that considers only a single relaxation time-scale, although the main qualitative behavior of this model does not depend on this assumption. In practice, this assumption implies that we treat the long-time flow of the network as a simple liquid with a viscosity , for which the stress relaxation is given by

$$\frac{\mathrm{d}\sigma}{\mathrm{d}t} = \zeta\frac{\mathrm{d}^2\gamma_f}{\mathrm{d}t^2}. \tag{5.2}$$

Eqs. (5.1) and (5.2) together describe the rheological behavior of this model. Eq. (5.1) can also be understood as a nonlinear generalization of the Kelvin-Voigt model in which a dashpot is placed parallel to a nonlinear spring, while Eq. (5.2) describes a Newtonian liquid-like stress relaxation. Equating the stresses represented in Eqs. (5.1) and (5.2) amounts to the assumption that the strain of the system has two contributions with additive compliance. This can also be understood as a second dashpot that is placed in series with the nonlinear Kelvin-Voigt element. Such a construction allows any stress stored in the spring to completely relax on long timescales at constant total strain. This addition to the Kelvin-Voigt element is essential for transient systems in which the stress can largely relax on long time scales [16, 17, 19].

In the prestress protocol a time-independent prestress σ_0 is imposed together with a small oscillatory stress $\delta\sigma(t)$ such that $\sigma(t) = \sigma_0 + \delta\sigma(t)$ and the resulting strain response $\gamma(t)$ is measured. This strain response can be decomposed as $\gamma(t) = \gamma_0(t) + \delta\gamma(t)$, where $\gamma_0(t)$ is the time-dependent creep response and $\delta\gamma(t)$ is a small-amplitude oscillatory strain, as illustrated in the inset of Fig. 5.6a. After an applied steady stress, $\gamma_0(t)$ increases rapidly after which it asymptotically approaches a regime in which $\gamma_0(t) \sim t$. Symmetry considerations imply that the network stiffness should be an even function of σ, and therefore to linear order in $\delta\sigma$, $k(\sigma) = k(\sigma_0)$. Thus, for the prestress protocol Eqs. (1) and (2) yield

$$\sigma_0 + \delta\sigma = \left[k(\sigma_0) + \eta\frac{\mathrm{d}}{\mathrm{d}t}\right]\gamma_{e,0} + \left[k(\sigma_0) + \eta\frac{\mathrm{d}}{\mathrm{d}t}\right]\delta\gamma_e = \zeta\frac{\mathrm{d}}{\mathrm{d}t}\gamma_{0,f} + \zeta\frac{\mathrm{d}}{\mathrm{d}t}\delta\gamma_f, \quad (5.3)$$

where $\gamma_0 = \gamma_{0,e} + \gamma_{0,f}$ and $\delta\gamma = \delta\gamma_e + \delta\gamma_f$. The creep strain γ_0 consists of both the network ($\gamma_{0,e}$) and flow ($\gamma_{0,f}$) response to a constant stress. After an initial relaxation, the former is expected to approach a constant, while the latter increases linearly with time. Remarkably, the differential components of the stress and strain are decoupled from the steady stress and creep strain in Eq. (5.3). This decoupling allows for a measurement of the differential response in parallel to a steady prestress, even when the sample is creeping. This result also holds when the long-time flow of the network is characterized by a spectrum of timescales. The in-phase differential response to an oscillatory stress is given by

$$K'(\omega) = \frac{k(\sigma_0)}{\left(1 + \frac{\eta}{\zeta}\right)^2 + \left(\frac{k}{\zeta\omega}\right)^2}. \quad (5.4)$$

At high frequencies there is a plateau $K' = k(\sigma_0)/(1 + \eta/\zeta)^2 \approx k(\sigma_0)$.

To demonstrate that this model qualitatively captures the experimentally observed strain response (upper panels Fig. 5.3), we compute the creep response to a series of increasing stress pulses alternated with zero stress periods, and its reverse order, as in the experimentally used protocol. For this calculation an interpolation formula is used for the dependence of the differential elastic stiffness $\sigma(k) \approx k_0 + k_1\sigma$, (with $\sigma > 0$) appropriate for an actin-filamin gel [37–40]. We find that during a prestress protocol strain accumulates, as depicted as a red line in Fig. 5.6a. Interestingly, the calculated response exhibits a remarkable resemblance with the creep response

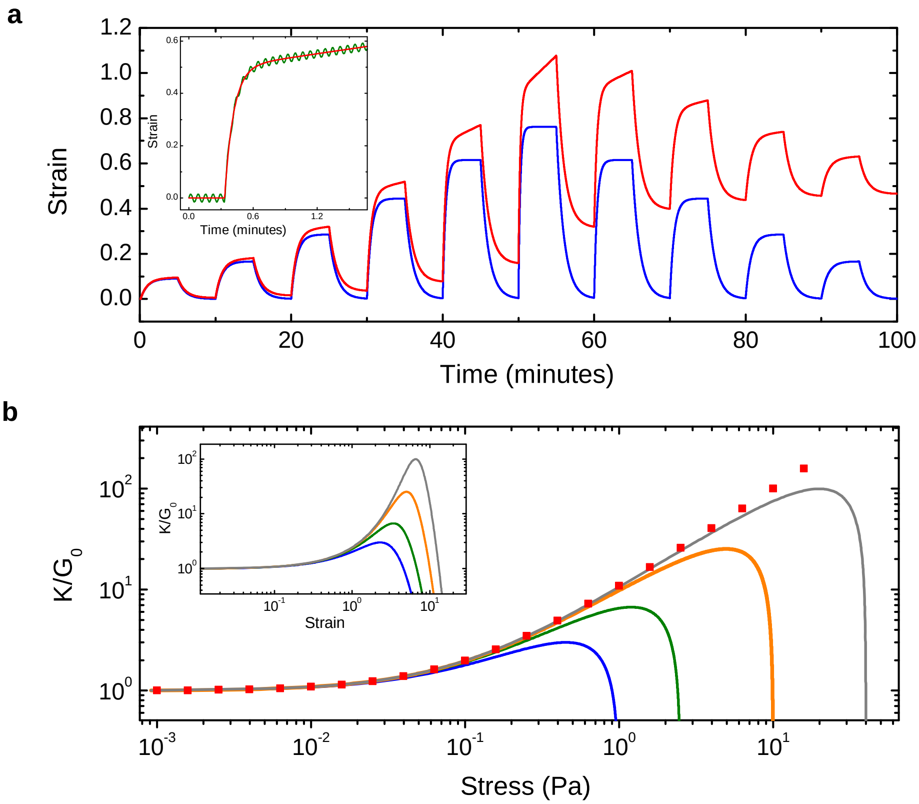

Figure 5.6 – Model: a) The calculated strain as a function of time during 4 minute prestress pulses applied every 4 minutes of increasing and then decreasing magnitude for a network ($\eta = 60$ Pa s, $k_0 = 1$ Pa, $k_1 = 0.6$, see main text) that is transient (red curve) and exhibits long-time flow ($\zeta = 6000$ Pa s), and a network that is permanent ($\zeta \rightarrow \infty$, blue curve).The inset shows the strain response $\gamma(t) = \gamma_0(t) + \delta\gamma(t)$ (green line) and the creep response $\gamma_0(t)$ (red line) to an applied steady stress superposed on a small oscillatory stress b) The calculated differential modulus as a function of stress for the prestress protocol (symbols) and the strain ramp protocol (solid lines with strain rates 10^{-3} s^{-1}, 5×10^{-3} s^{-1}, 10^{-2} s^{-1}, 5×10^{-2} s^{-1} increasing from blue to gray). The inset shows the differential modulus as a function of strain for the strain ramp protocol.

for the actin-filamin system (upper panel Fig. 5.3c). Permanent cross-links, however, inhibit network flow $\zeta \to \infty$, and as a result there is no strain accumulation during the prestress protocol in such a permanent network, as shown as a blue line in Fig. 5.6a. This is consistent with the experimental behavior we observe for F-actin networks with biotin-NeutrAvidin cross-links and fibrin (upper panel Figs. 5.3a,d).

To address the general nonlinear rheological response of this model we combine Eqs. (1) and (2) to obtain

$$\left(1+\frac{\eta}{\zeta}\right)\frac{\mathrm{d}^2\sigma}{\mathrm{d}t^2}+\frac{k(\sigma)}{\zeta}\left(1-(\eta+\zeta)\frac{\frac{\mathrm{d}}{\mathrm{d}t}k(\sigma)}{k(\sigma)^2}\right)\frac{\mathrm{d}\sigma}{\mathrm{d}t}=k(\sigma)\left(1-\eta\frac{\frac{\mathrm{d}}{\mathrm{d}t}k(\sigma)}{k(\sigma)^2}\right)\frac{\mathrm{d}^2\gamma}{\mathrm{d}t^2}+\eta\frac{\mathrm{d}^3\gamma}{\mathrm{d}t^3} \tag{5.5}$$

The initial conditions required to solve this differential equation can be found by inspecting the zero-stress linear limit of the model, in which $\frac{k(\sigma=0)}{\zeta}\sigma+(1+\eta/\zeta)\frac{\mathrm{d}\sigma}{\mathrm{d}t}=k(\sigma=0)\frac{\mathrm{d}\gamma}{\mathrm{d}t}+\eta\frac{\mathrm{d}^2\sigma}{\mathrm{d}t^2}$. For instance, in the case of a strain ramp the right hand side of Eq. (5.5) vanishes and the initial conditions become $\sigma(0)=0$ Pa, $\left.\frac{\mathrm{d}\sigma}{\mathrm{d}t}\right|_{t=0}=\frac{k(\sigma=0)}{1+\eta/\zeta}\frac{\mathrm{d}\gamma}{\mathrm{d}t}$. The calculated response to a strain ramp at a variety of strain rates is shown in Fig. 5.6b. Beyond a characteristic value for σ, K increases strongly with the applied stress. Interestingly, at slower strain rates the dependence of K with σ is weaker, while at large strain rates the response converges to a curve in which at large stresses $K \sim \sigma$, as can be expected for the nonlinear network elasticity we assumed for this example. Consistent with the measured behavior (Fig. 5.5), the high strain-rate limit curve coincides with the response as measured with a prestress protocol, as shown in Fig. 5.6b. At very high strain rates the quasistatic approximation will break down. In that case the strain ramp results can be expected to exceed the prestress results. Such high strain rates are, however, not accessible by most rheometers.

5.4 Discussion and implications

We have studied the nonlinear mechanical response of a range of biopolymer gels with both the strain ramp and the prestress protocols. The prestress and strain ramp results agree well over two decades in strain rate for biotin-NeutrAvidin cross-linked F-actin networks and cross-linked fibrin networks. For networks exhibiting creep such as the actin-filamin system, however, the two protocols agree only at high strain rates. The discrepancy in the results of the prestress and low-rate strain ramp protocols can be accounted for by the mode of stress relaxation in these systems; both the high-rate strain ramp and prestress protocols measure the fast nonlinear elastic response, while at low rates the stress measured during a strain ramp is the relatively fast elastic response convoluted with stress relaxation processes. These stress relaxation processes can be enabled by cross-linker unbinding events. Although, the rates of such cross-linker unbinding events can be force-dependent [23,37], this is not required to explain the experimental behavior we observe here.

We have developed a simple model, which accounts for the experimentally observed behavior. It captures the general nonlinear elastic response of a cross-linked biopolymer network, while allowing for simple flow of the network on long timescales. This model illustrates how the differential nonlinear elastic response can be measured with the prestress protocol, even while the system is creeping. A microscopic description of the long-time network flow is required to expand this model as to provide a quantitative description for the nonlinear rheology of cross-linked biopolymer gels.

It is important to monitor the strain during the prestress measurement to determine the extent of creep. Surprisingly, for systems that exhibit creep, the prestress method consistently yields results insensitive to this creep. By contrast, for the strain ramp technique, the elastic response and the creep are fundamentally coupled and cannot be separated because strain is the control variable; the results obtained with this technique are difficult to interpret for systems that creep. Thus, for systems that exhibit creep, the prestress method shows a clear advantage over the strain ramp method.

The prestress method is designed to quantify the nonlinear response of viscoelastic solids. This method, however, may not always be suitable for systems that exhibit a significant amount of creep; the flow induced by a steady stress can lead to restructuring, which might in turn affect the mechanical properties of the system. In this paper we have discussed a detailed protocol to test the applicability of the prestress method for a particular system. For all systems investigated here, the repeated large steady stresses applied over 4 minutes during the prestress protocol do not significantly affect either the linear or the nonlinear elastic properties; as measured with differential prestress experiments, the mechanical properties exhibit no significant time evolution, even if there is considerable creep. The results presented here demonstrate conclusively that the prestress method is a robust and reliable method for measuring the nonlinear viscoelastic properties of biopolymer gels, even for systems that exhibit creep. Furthermore, the protocol which we outline here, may be useful to investigate systems in which shear-induced restructuring leads to a change in the mechanical response.

5.5 Acknowledgements

This work was performed in collaboration with K. E. Kasza, L. M. Jawerth, S. Muenster and D.A. Weitz. C.P.B. acknowledges the hospitality of Harvard University where the experimental part of this work was performed. We thank F. Nakamura for the gift of

actin and filamin protein.

Bibliography

[1] A. L. Zajac and D. E. Discher. *Cell differentiation through tissue elasticity-coupled, myosin-driven remodeling*. Curr. Opin. Cell Biol. **20**, 609-615 (2008).

[2] C. Storm, J. Pastore, F.C. MacKintosh, T.C. Lubensky and P.A. Janmey. *Nonlinear elasticity in biological gels*. Nature **435**: 191 (2005).

[3] M. L. Gardel, J. H. Shin, F. C. MacKintosh, L. Mahadevan, P. A Matsudaira, D. A. Weitz. *Elastic Behavior of Cross-Linked and Bundled Actin Networks*. Science **304**, 1301 (2004); Phys. Rev. Lett. **93**, 188102 (2004).

[4] Y. C. Lin, N. Y. Yao, C. P. Broedersz, H. Herrmann, F. C. MacKintosh, D .A. Weitz. *Origins of elasticity in intermediate filament networks*. Phys. Rev. Lett. **104**, 058101 (2010).

[5] O. Lieleg, M. M. A. E. Claessens, C. Heussinger, E. Frey, and A. R. Bausch. *Mechanics of Bundled Semiflexible Polymer Networks*. Phys. Rev. Lett. **99**, 088102-4 (2007).

[6] O. Chaudhuri, S. H. Parekh and D. A. Fletcher. *Reversible stress softening of actin networks*. Nature **445**: 295 (2007).

[7] I. K. Piechocka, M. Bacabac, M. Potters, F. C. MacKintosh, G. H. Koenderink. *Structural hierarchy governs fibrin gel mechanics*. Biophys. J. **98**: 2281 (2010).

[8] K. E. Kasza, A. C. Rowat, J. Liu, T. E. Angelini, C. P. Brangwynne, G. H. Koenderink and D. A Weitz. *The cell as a material*. Curr. Opin. Cell Biol. **19**:101-7 (2007).

[9] A. R. Bausch and K. Kroy. *A bottom-up approach to cell mechanics*. Nature Phys. **2**, 231 (2006).

[10] J. Xu, Y. Tseng, and D. Wirtz. *Strain Hardening of Actin Filament Networks*, J. Biol. Chem. **275**, 35886-35892 (2000).

[11] A. E. X. Brown, R. I. Litvinov, D. E. Discher, Prashant K. Purohit, and J. W. Weisel. *Multiscale Mechanics of Fibrin Polymer: Gel Stretching with Protein Unfolding and Loss of Water*. Science **325**, 741-744 (2009).

[12] P. A. Janmey, S. Hvidt, J. Lamb, and T. P. Stossel. *Resemblance of Actin-Binding Protein/Actin Gels to Covalently Crosslinked Networks* Nature **345**, 89-92 (1990).

[13] E. Conti, F. C. MacKintosh. *Cross-Linked Networks of Stiff Filaments Exhibit Negative Normal Stress*. Phys. Rev. Lett. **102**, 088102 (2009).

[14] P. A. Janmey, M. E. McCormick, S. Rammensee, J. L. Leight, P. C. Georges, and F. C. MacKintosh. *Negative normal stress in semiflexible biopolymer gels*. Nature Materials **6**, 48 (2007).

[15] H. Kang, Qi Wen, P. A. Janmey, J. X. Tang, E. Conti, and F. C. MacKintosh, J. Phys. Chem. B **113**, 3799-3805 (2009).

[16] O. Lieleg, M. M. A. E. Claessens, Y. Luan, and A. R. Bausch. *Transient binding and dissipation in Cross-Linked actin networks*. Phys. Rev. Lett., **101**:108101–4 (2008).

[17] S. M. Volkmer Ward, A. Weins, M. R. Pollak, and D. A. Weitz. *Dynamic viscoelasticity of actin Cross-Linked with Wild-Type and Disease-Causing mutant alpha-Actinin-4*. Biophys. J., **95**:4915–4923 (2008).

[18] H. Miyata, R. Yasuda, and K. Kinosita. *Strength and lifetime of the bond between actin and skeletal muscle [alpha]-actinin studied with an optical trapping technique*. Biochimica et Biophysica Acta (BBA) - General Subjects, **1290**:83–88 (1996).

[19] D. Wachsstock, W. Schwarz, and T. Pollard. *Cross-linker dynamics determine the mechanical properties of actin gels*. Biophys. J., **66**:801–809 (1994).

[20] C. Semmrich, R. J. Larsen, and A. R. Bausch. *Nonlinear mechanics of entangled F-actin solutions*. Soft Matter **4**, 1675-1680 (2008).

[21] R. H. Ewoldt, A. E. Hosoi, and G. H. McKinley. *New measures for characterizing nonlinear viscoelasticity in large amplitude oscillatory shear*. J. Rheol. **52**, 1427-1458 (2008).

[22] R. H. Ewoldt, A. E. Hosoi, and G. H. McKinley. *Nonlinear viscoelastic biomaterials: meaningful characterization and engineering inspiration*. Integrative and Comparative Biology **49**, 40-50 (2009).

[23] O. Lieleg and A. R. Bausch. *Cross-Linker Unbinding and Self-Similarity in Bundled Cytoskeletal Networks*. Phys. Rev. Lett. **99**, 158105 (2007).

[24] M. L. Gardel, J. H. Shin, F. C. MacKintosh, L. Mahadevan, P. A. Matsudaira., and D. A. Weitz. *Scaling of F-actin network rheology to probe single filament elasticity and dynamics*. Phys. Rev. Lett. **93**:188102 (2004).

[25] B. Hinner, M. Tempel, E. Sackmann, K. Kroy, and E. Frey. *Entanglement, Elasticity, and Viscous Relaxation of Actin Solutions*. Phys. Rev. Lett. **81**, 2614 (1998).

[26] M. L. Gardel, M. T. Valentine, J. C. Crocker, A. R. Bausch, and D. A. Weitz. *Microrheology of Entangled F-Actin Solutions*. Phys. Rev. Lett. **91**, 158302 (2003).

[27] G. H. Koenderink, M. Atakhorrami, F. C. MacKintosh, and C. F. Schmidt. *High-Frequency Stress Relaxation in Semiflexible Polymer Solutions and Networks*. Phys. Rev. Lett. **96**, 138307-4 (2006).

[28] E. Distasio. *Cl^- Regulates the Structure of the Fibrin Clot*. Biophys. J. **75**, 1973-1979 (1998).

[29] G. W. Nelb, C. Gerth, and J. D. Ferry. *Rheology of fibrin clots. III. Shear creep and creep recovery of fine ligated and coarse unligated clots*. Biophys. Chem **5**, 377-387 (1976).

[30] C. Gerth, W. W. Roberts, and J. D. Ferry. *Rheology of fibrin clots. II. Linear viscoelastic behavior in shear creep*. Biophys. Chem **2**, 208-217 (1974).

[31] W. W. Roberts, O. Kramer, R. W. Rosser, F. H. M. Nestler, and J. D. Ferry. *Rheology of fibrin clots. I. : Dynamic viscoelastic properties and fluid permeation*. Biophys. Chem. **1**, 152-160 (1974).

[32] J. Vermant, L. Walker, P. Moldenaers, and J. Mewis. *Orthogonal versus Parallel Superposition Measurements* J. Non-Newtonian Fluid Mech. **79**, 173-189 (1998).

[33] F. C. MacKintosh, J. Käs, and P. A. Janmey. *Elasticity of semiflexible biopolymer networks*. Phys. Rev. Lett. **75**:4425-4428 (1995).

[34] N. Y. Yao, C. P. Broedersz, Y. C. Lin, K. E. Kasza, F. C. MacKintosh, D. A. Weitz. *Elasticity in ionically cross-linked neurofilament networks* Biophys. J. **98**: 2147 (2010).

[35] Y. C. Lin, C. P. Broedersz, A. C. Rowat, T. Wedig, H. Herrmann, F. C. MacKintosh and D. A. Weitz. J. Mol. Biol. **399**, 637-644 (2010).

[36] S. Rammensee, P. A. Janmey and A. R. Bausch. *Mechanical and structural properties of in vitro neurofilament hydrogels*. Euro. Biophys. J. **36**, 661 (2007).

[37] K. E. Kasza, G. H. Koenderink, Y. C. Lin, C. P. Broedersz, W. Messner, F. Nakamura, T. P. Stossel, F. C. MacKintosh, and D. A. Weitz. *Nonlinear elasticity of stiff biopolymers connected by flexible linkers*. Phys. Rev. E **79**:041928 (2009).

[38] K. E. Kasza, C. P. Broedersz, G. H. Koenderink, Y. C. Lin, W. Messner, E. A. Millman, F. Nakamura, T. P. Stossel, F. C. MacKintosh, D. A. Weitz. *Actin filament length tunes elasticity of flexibly crosslinked actin networks*. Biophys. J. **99**, 1091 (2010).

[39] C. P. Broedersz, C. Storm, and F. C. MacKintosh. *Effective-medium approach for stiff polymer networks with flexible cross-links*. Phys. Rev. E **79**:061914 (2009).

[40] C. P. Broedersz, C. Storm, and F. C. MacKintosh. *Nonlinear elasticity of composite networks of stiff biopolymers with flexible linkers*. Phys. Rev. Lett. **101**:118103 (2008).

[41] M. L. Gardel, F. Nakamura, J. H. Hartwig, J. C. Crocker, T. P. Stossel, and D. A. Weitz. *Prestressed F-actin networks cross-linked by hinged filamins replicate mechanical properties of cells*. Proc. Natl. Acad. Sci. **103**:1762-1767 (2006).

[42] B. Wagner, R. Tharmann, I. Haase, M. Fischer, and A. R. Bausch. *Cytoskeletal polymer networks: the molecular structure of cross-linkers determines macroscopic properties*. Proc. Natl. Acad. Sci. **103**:13974-13978 (2006).

[43] C. Heussinger and E. Frey. *Floppy Modes and Nonaffine Deformations in Random Fiber Networks*. Phys. Rev. Lett. **97**, 105501 (2006).

[44] P. R. Onck, T. Koeman, T. van Dillen, and E. van der Giessen. *Alternative explanation of stiffening in cross-linked semiflexible networks*. Phys. Rev. Lett. **95**, 178102 (2005).

[45] E. M. Huisman, T. van Dillen, P. R. Onck, and E. Van der Giessen. *Three-Dimensional Cross-Linked F-Actin Networks: Relation between Network Architecture and Mechanical Behavior*. Phys. Rev. Lett. **99**, 208103 (2007)

[46] F. Gittes and F. C. MacKintosh. *Dynamic shear modulus of a semiflexible polymer network* Phys. Rev. E **58**, R1241 (1998).

6

Criticality and isostaticity in fiber networks

- C. P. Broedersz, X. Mao, T. C. Lubensky and F. C. MacKintosh
  Criticality and isostaticity in fiber networks,
  arXiv:1011.6535 (Submitted)

- C. P. Broedersz, M. Sheinman and F. C. MacKintosh
  Elasticity of diluted super-isostatic lattices of stiff filaments in 2D and 3D,
  (To be submitted)

Abstract

It has been known since Maxwell that collections of particles interacting via central forces only become rigid above the isostatic threshold, where the constraints and internal degrees of freedom just balance [1,2]. However, such networks can be stabilized below this threshold by additional interactions [3–5]. Here we elucidate the relative roles of bending versus central force interactions in stabilizing fibrous networks [6–16]. We study disordered networks with variable connectivity that exhibit both bending rigidity and central-force thresholds. Although the former determines the true onset of rigidity, the latter controls a cross-over between various mechanical regimes exhibiting rich critical behavior, including an anomalous power-law dependence of the shear modulus on *both* stretching and bending rigidities, as well as a breakdown of mean field theory. At the central force isostatic point, we also find divergent strain fluctuations together with a divergent correlation length ξ, implying a violation of continuum elasticity in this simple mechanical system. These results may apply to systems ranging from bond-bending network glasses [2,17–19] to the cellular cytoskeleton [21,22].

6.1 Introduction

Soft materials, such as foams and granular packings attain mechanical rigidity when the connectivity exceeds the isostatic point. This isostatic point is captured by a classical argument introduced by Maxwell [1], which balances the degrees of freedom in the system against the number of constraints due to connectivity. Interestingly, stiff fiber network form a distinct class of systems that exhibit solid-like behavior at connectivities well below the isostatic point. There are numerous examples of stiff-fiber networks, ranging from carbon nanotube gels at the small scale to felt and paper at the macroscopic scale [23–25]. In addition, critical biological components such as the intra-cellular cytoskeleton and extra-cellular matrices of collagen and fibrin are composed of such networks [26]. Biological systems largely employ network architectures with a coordination number $z \leq 4$, which is far below the central force (CF) isostatic point in 3D. The mechanical stability of such networks depends in large part on the considerable bending rigidity of the constituting filaments. Intriguingly, however, the elastic moduli of these systems can be either bend or stretch dominated. Both numerical and analytical approaches have demonstrated the existence

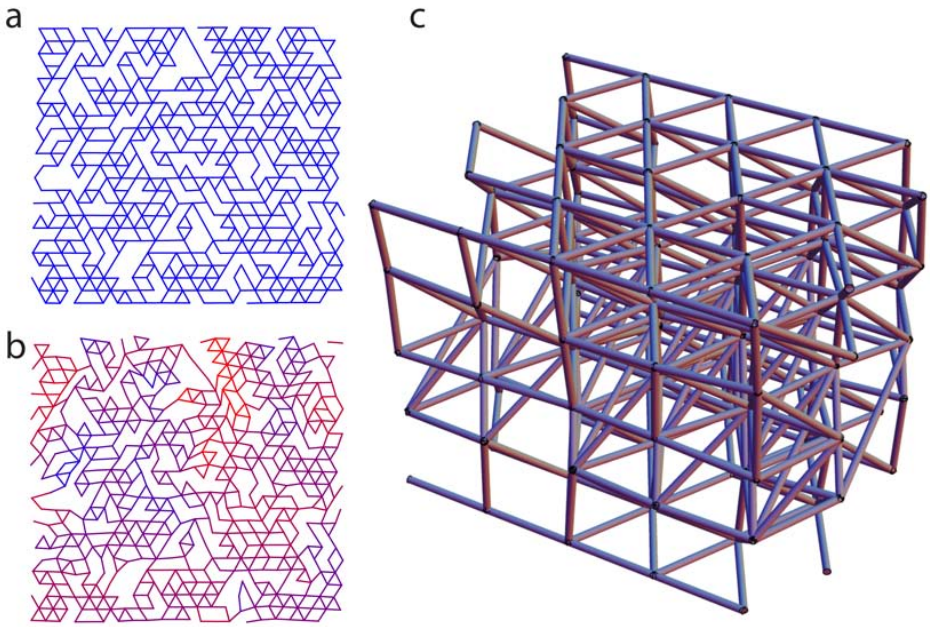

Figure 6.1 – Fiber networks arranged on 2D and 3D lattices A small section of a sheared diluted triangular network near isostaticity with relatively stiff filaments ($\kappa = 10^1$ in units of $\mu\ell_0^2$) (a) and floppy filaments ($\kappa = 10^{-5}$) (b). The deviation of the local deformation from a uniform deformation is indicated by color, where blue corresponds to a uniform or affine deformation and red corresponds to a highly non-affine deformation. (c) An example of a small section of the diluted FCC network at $p = 0.7$. To probe the mechanical properties of this network we shear the 111-plane (shown on top) along the direction of one of the bond angles in this plane.

of these distinct elastic regimes for such stiff polymer networks [6–8, 12, 13, 16, 27]. In addition, experimental studies on reconstituted cross-linked actin networks provide evidence for the existence of both stretching dominated and bending dominated elastic regimes [9, 14, 15, 28]. However, the physical principles governing these elastic regimes remain poorly understood. In particular, the role of connectivity in the mechanics of semiflexible polymer networks is not known [4, 5].

Here we study the elasticity of disordered fiber networks composed of straight, stiff filaments organized on a triangular lattice in 2D and on a face centered cubic (FCC) lattice in 3D, as illustrated in Fig. 6.1. Undiluted, these networks have a coordination number $z_m = 6$ (triangular lattice) and $z_m = 12$ (FCC), placing them well above the CF isostatic point $z_c = 2d$ in d dimensions [1]. There are physiological networks with such high connectivities, e.g. approximately 6-fold coordinated networks confined to 2D in the red blood cell [30], although most biological networks have lower connectivities. An important advantage of lattice based networks is their applications in various analytical effective medium approaches, which we will here compare to our numerical results [4,17,27,31–35]. We explore the effects of network connectivity—both above and below z_c—by removing filament segments between vertices with a probability $q = 1 - p$. In addition to lowering the connectivity, this also has the effect of introducing disorder in the networks. In the range of network connectivity spanning from the rigidity percolation point to the CF isostatic point, the average filament length remains approximately constant. Thus, in these networks we expect the network connectivity to be the major control parameter.

Our main results are summarized in a phase diagram shown in Fig. 6.2. This diagram maps the mechanical response of the diluted superisostatic networks in terms of two key variables: the connectivity z and the ratio of the bending rigidity κ and the stretching modulus μ of the fibers. An important difference with most prior work on subisostatic off-lattice networks [6–8] is that we here characterize the system in terms of connectivity [5] instead of filament length or line density. Consistent with these prior studies we identify two distinct elastic regimes: A stretching governed regime and a bending governed regime. In addition however, we find an intermediate broad cross-over regime in which the shear modulus scales simultaneously with κ and μ, $G \sim \kappa^{f/\phi}\mu^{1-f/\phi}$ where $f/\phi \approx 0.50 \pm 0.01$ (2D) and 0.40 ± 0.01 (3D). This regime extends over a remarkably broad range of z and κ/μ. Such a regime—characterized by a strong coupling between stretch and bend modes—has not been observed in prior theoretical work on fiber networks. This cross-over regime is a direct consequence of the critical behavior close to the CF isostatic point and similar regimes appear in random resistor network [3] with good and bad conductors and mechanical models for a spring network with strong and weak springs [4, 5].

In the bending dominated regime, we find that $G \sim \kappa|z - z_c|^{f-\phi}$ close to the CF isostatic point, where $f = 1.4 \pm 0.1$ (2D), $f = 1.6 \pm 0.2$ (3D) and and $\phi = 3 \pm 0.2$ (2D), $\phi = 3.6 \pm 0.3$ (3D). Above the CF isostatic point, the number of constraints on the lattice vertices provided by the stretching forces are sufficient to mechanically constrain the system. As a result, the system is necessarily dominated by stretching modes at superisostatic coordinations. This does not mean, however, that the bending rigidity does not play a role. For vanishing κ/μ, we find that the mechanical response above the isostatic point becomes $G \sim \mu|z - z_c|^f$ close to the CF isostatic point. In contrast, in the limit of large κ/μ the shear modulus is approximately $G \sim \mu z$.

The stretching governed regime extends all the way down to the rigidity percolation point for large values of κ/μ. This finding is in contrast with previous studies on off-lattice subisostatic networks that have reported that, upon dilution, the stretching governed regime crosses-over to a non-affine bending regime before losing rigidity [6, 7]. It is important to note that, although the mechanics is governed by stretching modes in this regime, the shear modulus drops substantially below the affine shear modulus, indicating that the deformation field contains a significant non-affine component.

The CF isostatic point plays a central role in determining the cross-over from the stretching dominated regime to the bending dominated regime [3–5, 31]. In the limit of vanishing κ/μ, the isostatic point is a true critical point. Indeed, we find for low κ/μ that the fluctuations, in the form of non-affine deformations, become large around the isostatic point, reminiscent of a second order phase transition [31]. The finite bending rigidity, however, suppresses this divergence. From the perspective of critical phenomena, the bending rigidity may be thought of as an applied field or coupling constant that leads to a crossover from one critical system to another, such as from the Heisenberg model to the Ising model [36]. In such systems, there is a continuous evolution of the critical point. Interestingly, we find no such continuous evolution, but rather a discontinuous jump in the critical point as soon as κ becomes nonzero.

We show that we can express the mechanical response around the cross-over between the stretching and the bending regimes in terms of a scaling function, which allows us to collapse all the data on to a universal curve that exhibits distinct branches above and below the critical point. This provides further evidence that the physics of the isostatic point controls the cross-over from the stretching to the bending regime. These results are qualitatively consistent with the results of an effective medium theory (EMT) using the coherent potential approximation (CPA) by Mao and Lubensky [31, 33]. Importantly, however, the exponents governing the transition at the CF isostatic we obtain numerically differ significantly from the EMT predictions, indicating a breakdown of meanfield theory. By contrast, there is evidence that such a breakdown of meanfield theory does not occur in spring networks in jammed configurations [5].

6.2 Model

The networks consist of stiff filaments organized on a triangular lattice in 2D and an FCC lattice in 3D. In both cases, a perfect lattice consists of straight filaments spanning the system. At each lattice vertex, a cross-link is formed between *all* intersecting filaments. Thus, this results in cross-links between 3 (triangular) or 6 filaments (FCC). These cross-links hinge freely and do not introduce additional rigidity. To reduce network connectivity, we randomly remove filament segments between vertices with a probability $q = 1 - p$. This procedure allows us to generate disordered lattice-based networks with a connectivity $z \approx 6p$ in 2D and $z \approx 12p$ in 3D. Cutting bonds also reduces the length of the polymer; the average filament length is given by $\langle L \rangle = \ell_0/q$ [31].

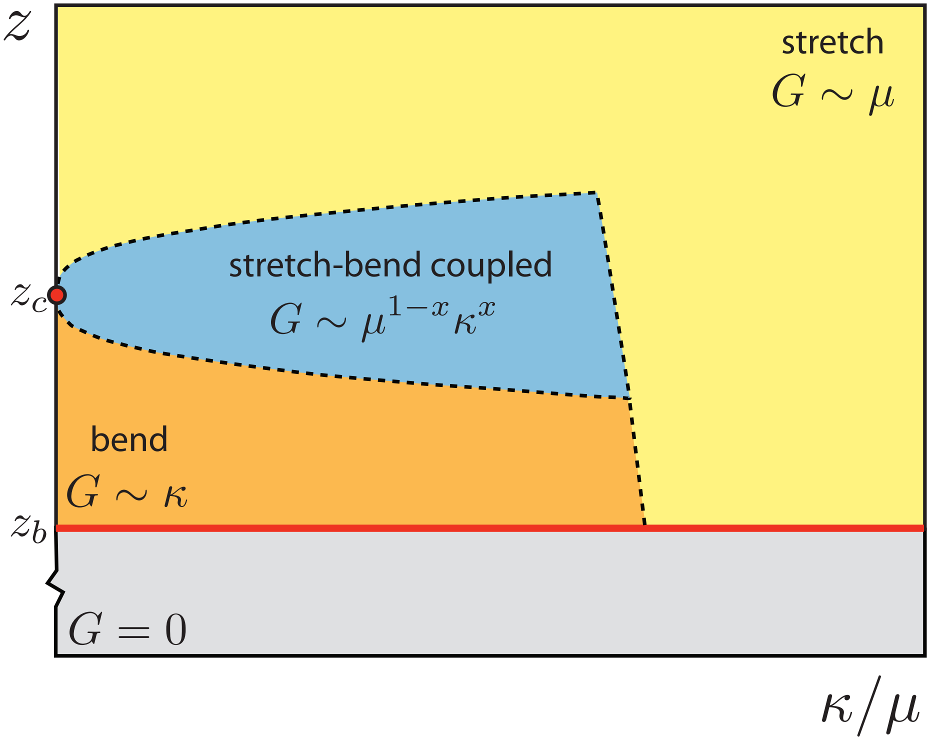
z
stretch
$G \sim \mu$
stretch-bend coupled
$G \sim \mu^{1-x}\kappa^{x}$
z_c
bend
$G \sim \kappa$
z_b
$G = 0$
κ/μ

Figure 6.2 – (Color online) **Phase diagram** The phase diagram for diluted super-isostatic networks. Above the rigidity percolation point z_b there are three distinct mechanical regimes: a stretching dominated regime with $G \sim \mu$, a bending dominated regime with $G \sim \kappa$ and a regime in which bend and stretch modes couple with $G \sim \mu^{1-x}\kappa^{x}$. Here x is related to the critical exponents $x = f/\phi$. We find here that $x = 0.50 \pm 0.01$ (2D triangular lattice) and $x = 0.40 \pm 0.01$ (3D FCC). The mechanical regimes are controlled by the isostatic point z_c, which acts as a zero-temperature critical point.

Semiflexible polymers are well described by the wormlike chain model. At finite temperature T, bending fluctuations are excited; such fluctuations generate *small* undulations in the polymer that are characterized by the persistence length $\ell_p = \kappa/k_\mathrm{B}T$. This length scale represents the decay length in tangent vector correlations along the polymer backbone. These thermal bending undulations contract the polymer longitudinally, and result in an entropic or thermal modulus $\mu_\mathrm{th} = 90\ell_p^2 k_\mathrm{B}T/\ell^3$ for a polymer segment of length ℓ [37]. In addition, the polymer exhibits an enthalpic or mechanical stretch modulus μ_mech. For simple elastic cylinders, this stretch modulus is related to κ through the radius r, by $\mu_\mathrm{mech} = 4\kappa/r^2$. Biopolymers typically have a large aspect ratio, in which r is much smaller than the other length-scales ℓ_c and ℓ_p. Thus, it is usually the case that $\mu_\mathrm{th} \ll \mu_\mathrm{mech}$, and the entropic stretch mode dominates the response to a longitudinal force, even when the network scale ℓ_0 is small compared to the persistence length [7].

Here we aim to capture the zero-frequency behavior of semiflexible polymer networks. On such timescales the polymer bending dynamics does not play a role. This allows us to integrate out these degrees of freedom. The resulting coarse grained Hamiltonian describes a descretized extensible worm like chain,

$$\mathscr{H} = \frac{\kappa}{2\ell_0}\sum_i |\Delta\hat{\mathbf{t}}_i|^2 + \frac{\mu}{2l_0}\sum_i \Delta\ell_i^2 \tag{6.1}$$

where $\Delta\hat{\mathbf{t}}_i$ is the change in the tangent vector between nodes i and $i-1$, and $\Delta\ell_i$ represents the change in length with respect to the restlength ℓ_0 between nodes i and $i-1$. The mechanical and thermal moduli add as springs in series and the full longitudinal compliance is given by $\mu^{-1} = \mu_\mathrm{mech}^{-1} + \mu_\mathrm{th}^{-1}$. With this, we have reduced the approach to a purely mechanical model in which the stretch modulus μ captures the entropic compliance. This model also captures the athermal limit in which the fibers can be considered to be simple elastic beams for which $\mu = \mu_\mathrm{mech}$.

The relative importance of the bending and the stretching term in Eq. 6.1 is captured by the length scale $\ell_b = \sqrt{\kappa/\mu}$, which forms one of the key control parameters for the network mechanics. For simple mechanical beams of radius r, $\ell_b = r/2$, while for a thermally excited semiflexible polymer of length ℓ, $\ell_b = \ell\sqrt{\ell/90\ell_p}$ [7]. For our networks, the characteristic polymer length is ℓ_0, and the most relevant values of ℓ_b/ℓ_0 for biopolymer systems are in the range $10^{-2} - 10^{-1}$, corresponding to systems ranging from actin filaments to the more flexible intermediate filaments; in systems where actin forms tightly coupled stiff bundles even lower values of ℓ_b/ℓ_0 may be reached. It is, however, instructive to explore limits of the model outside this range.

The mechanical response of the fibers in the network is determined by their bending rigidity κ and stretching modulus μ. For small deformations, the stretching and bending energy of the network can be expanded to quadratic order in the displacements $\mathbf{u}_i$ from the undeformed reference state at each vertex i,

$$E_{\text{stretch}} = \frac{1}{2}\frac{\mu}{\ell_0}\sum_{\langle ij\rangle} g_{ij}\left(\mathbf{u}_{ij}\cdot\hat{\mathbf{r}}_{ij}\right)^2 \tag{6.2}$$

$$E_{\text{bend}} = \frac{1}{2}\frac{\kappa}{\ell_0^3}\sum_{\langle ijk\rangle} g_{ij}g_{jk}\left[\left(\mathbf{u}_{jk}-\mathbf{u}_{ij}\right)\times\hat{\mathbf{r}}_{ij}\right]^2, \tag{6.3}$$

where ℓ_0 is the lattice spacing, $\mathbf{u}_{ij} = \mathbf{u}_j - \mathbf{u}_i$ and $\hat{\mathbf{r}}_{ij}$ is the unit vector oriented along the ij-th bond in the undeformed reference state. Here, $g_{ij} = 1$ for present bonds and $g_{ij} = 0$ for removed bonds. The summation extends over neighboring pairs of vertices in the stretching term [Eq. (6.2)], and over coaxial neighboring bonds in the bending term [Eq. (6.3)]. Thus, unlike bond-bending [20] and network glass models [2, 17–19], here the crosslinks at each vertex are freely hinged. In contrast to our model, network glasses and most prior models for stiff-fiber networks [6,8,11,12] have maximum coordination number 4. In this paper, all lengths are expressed in units of the lattice spacing ℓ_0, and all energies and moduli are measured in units of μ/ℓ_0. Thus, the bending rigidity κ is given in units of $\mu\ell_0^2$.

The mechanical response of the network is determined numerically in our simulations by applying a shear deformation with a strain γ. This is realized by translating the horizontal boundaries to which the filaments are attached, after which the internal degrees of freedom are relaxed by minimizing the energy using a conjugate gradient algorithm [38]. To reduce edge effects in our simulation, periodic boundary conditions are employed at all boundaries. The shear modulus of the network is related to the elastic energy through $G = \frac{2}{V_0 W^d}\frac{E}{\gamma^2}$ for a small strain γ, where V_0 is the area/volume of a unitcel. Here W^d is the system size, which in our simulations is $W^2 \approx 40000$ (2D) and $W^3 \approx 30000$ (3D), and we use strains no larger than $\gamma = 0.05$.

We probe mechanical the properties of diluted fiber networks on an FCC lattice by applying a shear on the 111-plane along one of the bond directions in the plane. An example of a small portion of the network is shown in Fig. 6.1. From this viewing angle the 111-plane lies on top. At $p = 1$, the cubic symmetry of the lattice allows us to express the mechanical response in terms of three components C_{11}, C_{12} and C_{44}. With a shear of the 111-plane we probe a combination of these components $G_{111} = (4C_{11} - 4C_{12} + C_{44})/12$.

6.3 Results

6.3.1 Elastic response

An example of a small portion of a diluted triangular lattice, to which a shear deformation is applied, is shown in Fig. 6.1. When the bending rigidity is high ($\kappa = 10$) the

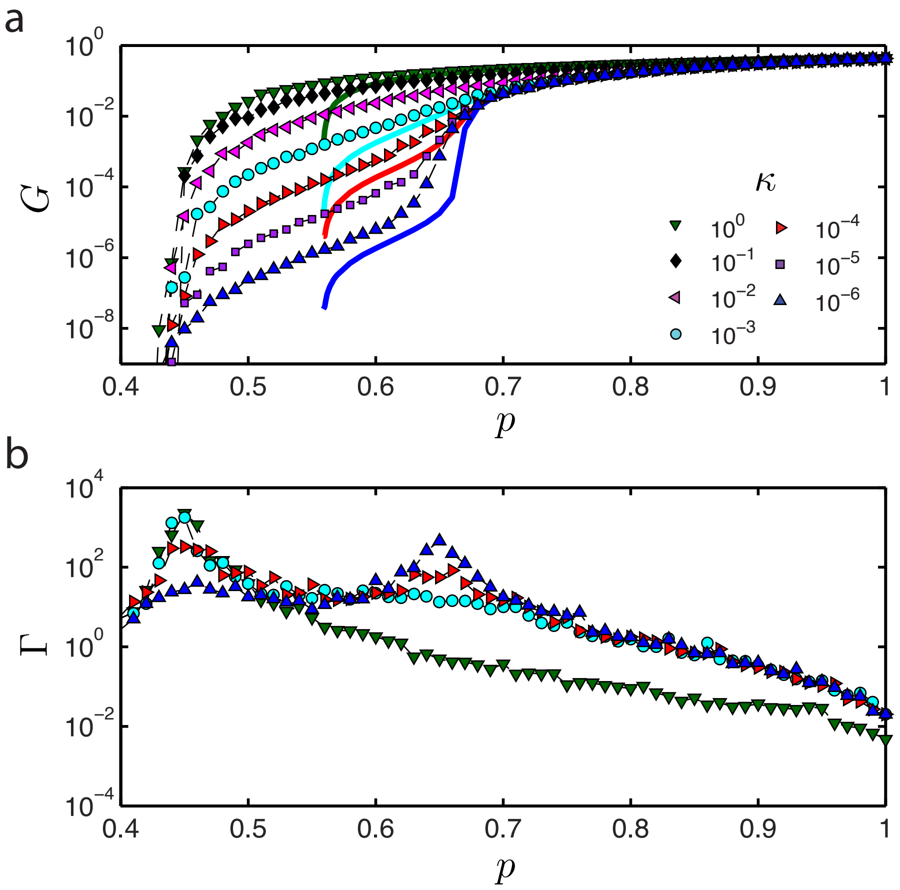

Figure 6.3 – (Color online) **Mechanics and non-affine strain fluctuations in a triangular lattice** a) The shear modulus G in units of μ/ℓ_0 as a function of p for a range of filament bending rigidities κ for the 2D triangular lattice The EMT calculations for the 2D triangular lattice are shown as solid lines for various values of κ. b) The non-affinity measure Γ is shown as a function of p for various values of κ for the 2D triangular lattice.

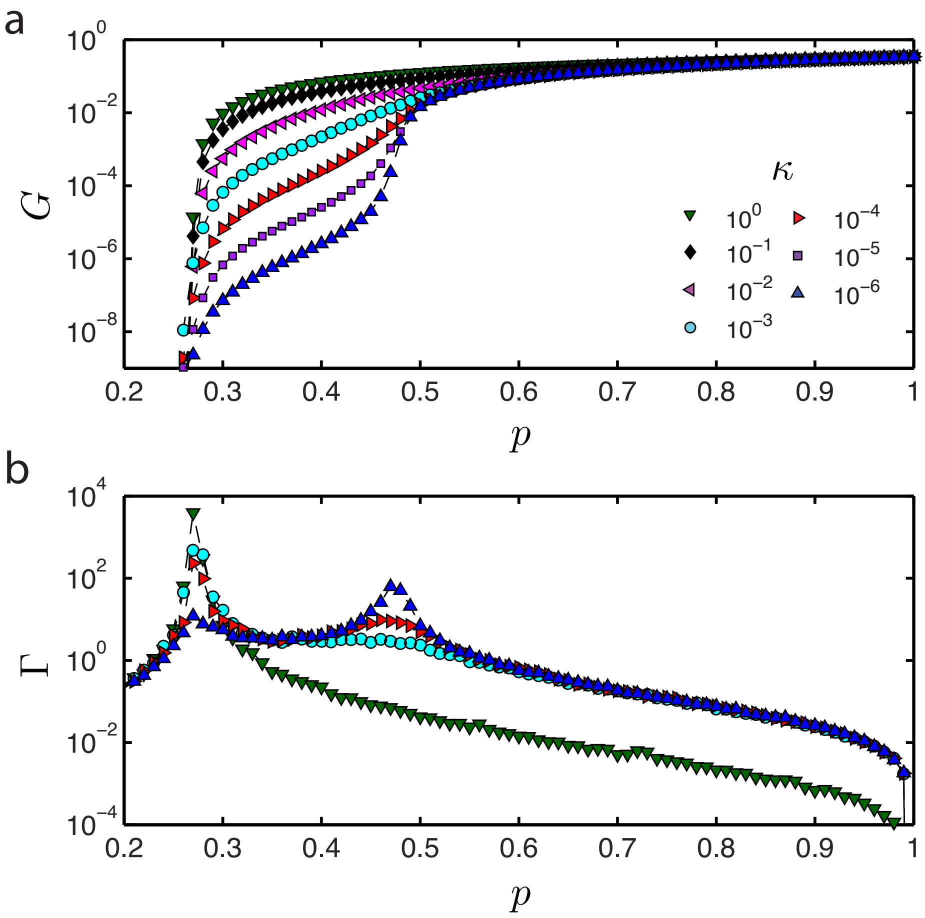

Figure 6.4 – (Color online) **Mechanics and non-affine strain fluctuations in an FCC lattice** a) The shear modulus G_{111} in units of μ/ℓ_0 as a function of p for a range of filament bending rigidities κ for the 3D FCC lattice. b) The non-affinity measure Γ is shown as a function of p for various values of κ for the 3D FCC lattice.

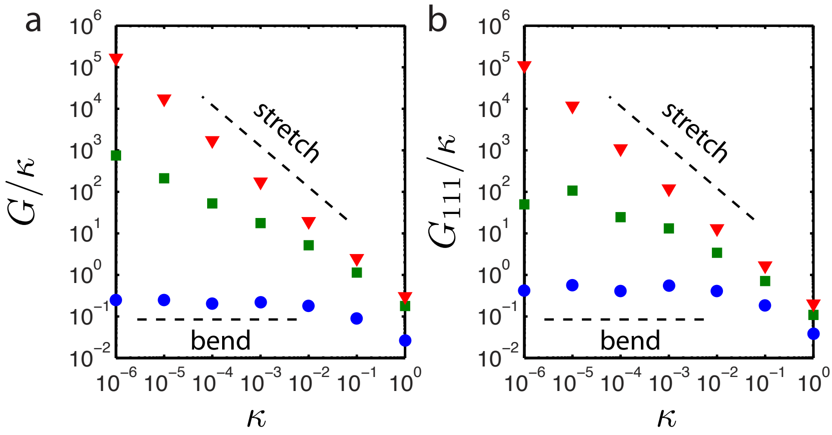

Figure 6.5 – (Color online) **Various elastic regimes in lattice-based fiber networks** The shear modulus G scaled by κ as a function of κ for various values of p for (a) the triangular lattice ($p = 0.5$ blue circles, 0.65 green squares, 0.8 red triangles) and (b) the FCC lattice ($p = 0.35$ blue circles, 0.47 green squares, 0.65 red triangles). The horizontal line indicates a bending dominated regime ($G \sim \kappa$) and a line with a slope of -1 indicates a stretching dominated regime ($G \sim \mu$).

deformation field is uniform or affine (Fig. 6.1a). In contrast, for low bending rigidity ($\kappa = 10^{-5}$), the deformation field is highly non-affine (Fig. 6.1b). This non-affine deformation field is clearly sensitive to the local disorder in the network; regions with a locally high connectivity appear to behave much more affinely in comparison with regions with a low connectivity. The deformation of the rigid network is clearly dominated by filament stretching. In comparison, large bending deformations are evident in the sheared floppy network.

To investigate the mechanical response of a network, we calculate its shear modulus G numerically. Plots of G versus p for different κ are shown for the triangular and FCC lattices in Figs. 6.3a and 6.4a, respectively. The diluted networks exhibit a finite shear modulus well below the CF isostatic point (expected at $p_c = 2/3$ in 2D and $p_c = 1/2$ in 3D); G vanishes at a κ-independent rigidity percolation point located at $p_b = 0.445 \pm 0.005$ (2D triangular lattice) and $p_b = 0.275 \pm 0.005$ (3D FCC lattice), consistent with a floppy mode counting argument that includes the bending constraints [31,33] (See section 6.5). For $p > p_c$, G approaches a nearly κ-independent stretching dominated limit with $G \sim \mu$. In contrast, between the rigidity percolation threshold and the isostatic point ($p_b < p < p_c$), we identify distinct stretching and bending dominated regimes. At high κ the shear modulus converges to a κ-independent curve, indicating that the stretching regime extends down to p_b for large bending rigidities. However, when the bending rigidity is reduced, the shear modulus adopts a strong κ dependence, indicating a bending governed regime. In this bending regime, the shear modulus scales directly with the bending rigidity $G_{\text{bend}} \sim \kappa$. To resolve the bending regime we plot the shear modulus scaled by κ as a function of κ for various values of p, as shown in Fig. 6.5. The bending dominated regions appear in this plot as horizontal lines, while a pure stretch region appears as a line with a slope of -1. The most interesting behavior occurs near p_c as a function of κ; close to the critical point the shear modulus scales as $G \sim \kappa^x$ with $x < 1$, suggesting a broad crossover regime with G depending simultaneously on both κ and μ.

To gain further insight into the mechanical behavior of our models, we compare our results with a new effective medium theory (EMT) or coherent potential approximation (CPA) [27, 35, 39] for lattices with bending forces developed by Mao and Lubensky [31,32], whose results for G for different κ are shown in Fig. 6.3a. These results overestimate the rigidity percolation point p_b. Although the EMT overestimates the rigidity percolation point p_b, it does capture the essential features of the mechanical behavior, including the existence of separate bending and CF rigidity thresholds and the crossover between stretching and bending dominated regimes close to p_c.

To investigate the role of the CF isostatic point in the cross-over between stretching and bending regimes we perform a scaling analysis. We motivate this analysis by drawing an analogy with second order phase transitions in thermal systems. In this analogy the shear modulus may be thought of as the order parameter in the system, which vanishes continuously as the system undergoes a critical phase transition at the CF isostatic point in the limit $\kappa \to 0$. Thus, in this zero-κ limit we expect a behavior $G \sim \mu|\Delta p|^f$ in the vicinity of the CF isostatic point, where $\Delta p = p - p_c$ and f is the rigidity exponent. However, when bending interactions are included, rigidity is restored below the CF isostatic point. Thus κ may be thought of as an effective applied field or a coupling parameter that brings the system away from criticality, resulting in a cross-over to a different elastic regime governed by bending interactions. To capture this cross-over we can express the shear modulus in terms of $\frac{\kappa}{\mu}|\Delta p|^{-\phi}$ when $\kappa/\mu \ll \Delta p$, where ϕ is the cross-over exponent. Taken together, these arguments suggest the following scaling ansatz,

$$G = \mu|\Delta p|^f \mathscr{G}_\pm\left(\frac{\kappa}{\mu}|\Delta p|^{-\phi}\right), \tag{6.4}$$

where $\mathscr{G}_\pm$ is a universal function where the two branches apply above and below the transition. When the argument of $\mathscr{G}_\pm(y)$, $y \ll 1$, $\mathscr{G}_+(y) \sim$ const. and $\mathscr{G}_-(y) \sim y$ such that $G \sim \mu|\Delta p|^f$ for $\Delta p > 0$ and $G \sim \kappa|\Delta p|^{f-\phi}$ for $\Delta p < 0$. In the opposite limit $(\kappa/\mu) \gg |\Delta p|^\phi$, G must become independent of Δp since it is neither zero nor infinite at $\Delta p = 0$. Equation (6.4) predicts $G \sim \kappa^{f/\phi}\mu^{1-(f/\phi)}$. The scaling form in Eq. 6.4 is analogous to that for the conductivity of a random resistor network [3] with bonds occupied with resistors of conductance $\sigma_>$ and $\sigma_<$ with respective probabilities p and

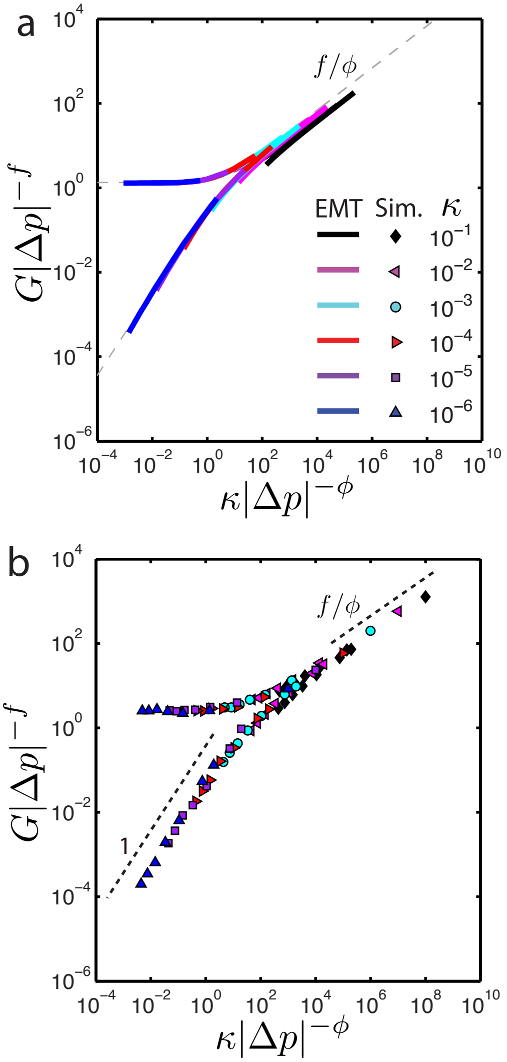

Figure 6.6 – Scaling analysis of the mechanics in the triangular lattice Scaling of the shear modulus in the vicinity of the isostatic point with the scaling form $G|\Delta p|^{-f} = \mathcal{G}_\pm\left(\kappa|\Delta p|^{-\phi}\right)$, with G in units of μ/ℓ_0, for the mechanical properties of the diluted triangular lattice for the EMT calculations (a) and the simulations (b) for a broad range of filament bending rigidities (κ in units of $\mu\ell_0^2$: 10^{-1} black, 10^{-2} magenta, 10^{-3} cyan, 10^{-4} red, 10^{-5} purple and 10^{-6} blue). The asymptotic form of the scaling function for low κ is shown as a dashed grey line in (a). The EMT exponents are $f_{\mathrm{EMT}} = 1$, $\phi_{\mathrm{EMT}} = 2$. In contrast, for the numerical data we obtain $f = 1.4 \pm 0.1$, $\phi = 3.0 \pm 0.2$ (2D). The scaling for the numerical data is performed with respect to the isostatic point of the finite system for which we find $p_c(W) \approx 0.651$ (2D, W=200).

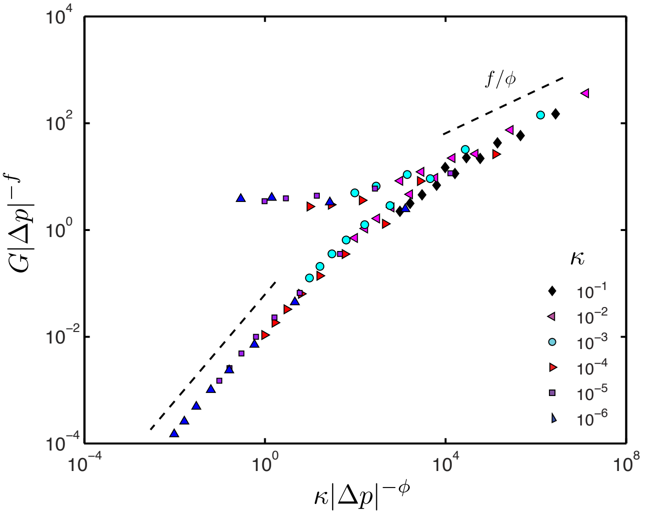

Figure 6.7 – (Color online) **Scaling analysis of the mechanics in the FCC lattice** Scaling of the shear modulus in the vicinity of the isostatic point with the scaling form $G|\Delta p|^{-f} = \mathcal{G}_{\pm}\left(\kappa|\Delta p|^{-\phi}\right)$, with G in units of μ/ℓ_0, for the mechanical properties of the FCC lattice for a broad range of filament bending rigidities (κ in units of $\mu\ell_0^2$: 10^{-1} black, 10^{-2} magenta, 10^{-3} cyan, 10^{-4} red, 10^{-5} purple and 10^{-6} blue). we obtain the exponents $f = 1.6 \pm 0.2$ $\phi = 3.6 \pm 0.3$ (3D). The scaling for the numerical data is performed with respect to the isostatic point of the finite system for which we find $p_c(W) \approx 0.473$ (3D, W=30).

Table 6.1 – Critical exponents

exponent	2D sim	2D EMT	3D sim
f	1.4 ± 0.1	1	1.6 ± 0.2
ϕ	3.0 ± 0.2	2	3.6 ± 0.3
ν	1.4 ± 0.2		
λ	2.2 ± 0.4		

$(1-p)$, as well as random spring networks with floppy and stiff springs [4, 5]. This scaling form is also predicted by the EMT theory when $\kappa/\mu \ll \Delta p$, with

$$\mathscr{G}_{\pm}(y) \quad \simeq \quad \frac{3}{2}\left(\pm 1 + \sqrt{1 + 4\mathscr{A}y/9}\right) \tag{6.5}$$

where $\mathscr{A} \simeq 2.413$, $f_{\text{EMT}} = 1$ and $\phi_{\text{EMT}} = 2$. Interestingly, these MF exponents are identical to those found in central-force networks with two types of springs [4, 5], which have been used to describe [5] bending models such as ours.

The full EMT results for G along with the scaling form valid at $\kappa/\mu \ll |\Delta p|^{\phi}$ are shown in Fig. 6.6a. Our simulation data for both 2D (Fig. 6.6b) and 3D networks (Fig. 6.7) are well described by the scaling hypothesis in Eq. (6.4), consistent with a second-order transition for $\kappa = 0$ in both cases [41]. Remarkably, however, the obtained numerical exponents ($f = 1.4 \pm 0.1$, $\phi = 3.0 \pm 0.2$) are significantly different from the EMT predictions, suggesting a breakdown of meanfield theory close to the CF isostatic point, in distinct contrast with the meanfield exponents observed for the jamming transition [5]. Importantly, we find that the bending stiffness κ is a relevant perturbation at p_c, which is reflected as a broad crossover regime with an anomalous scaling $G \sim \kappa^x \mu^{1-x}$ with $x = f/\phi$ (Fig. 6.8 where $x = 0.50 \pm 0.01$ (2D), consistent with the EMT prediction above, and $x = 0.40 \pm 0.01$ (3D). However, the precise nature of the interaction, such as the three-body bending interaction in our case, is expected to be irrelevant at p_c. Furthermore, our results for f are consistent with previous work on diluted periodic [40] and generic [41] lattices when $\kappa = 0$.

6.3.2 Non-affine deformations

To investigate the nature of the various mechanical regimes, we examine the local deformation field in our simulations. Several methods have been proposed to quantify the deviation from a uniform (affine) strain field [6,28,42]. Here we utilize a measure

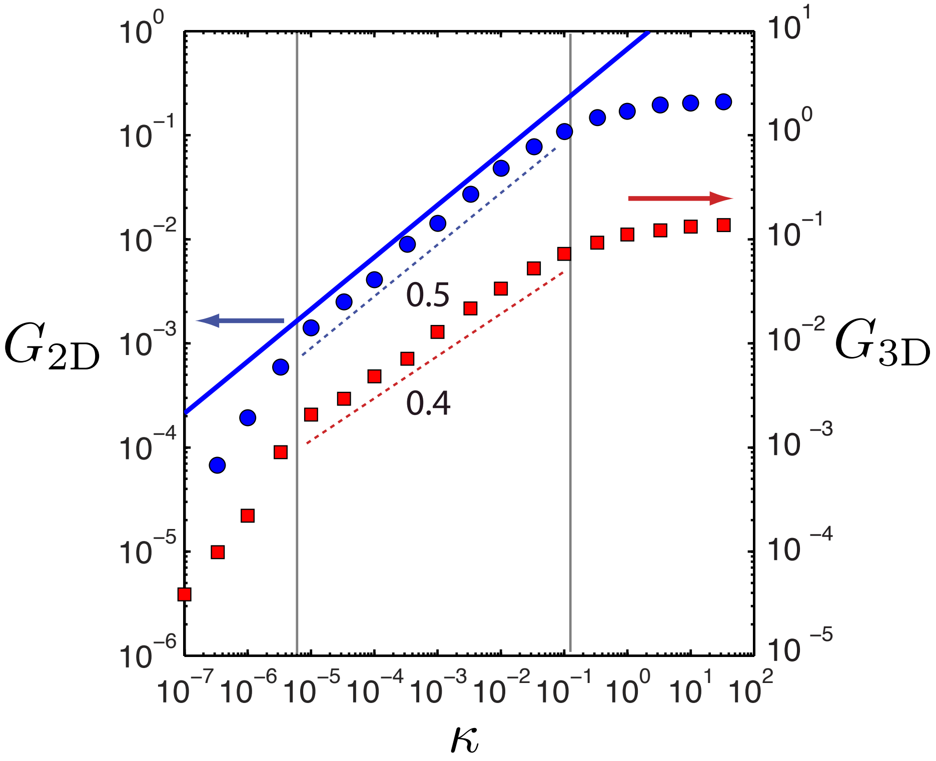

Figure 6.8 – (Color online) **Anomalous elasticity** The shear modulus as a function of κ close to the isostatic point for the triangular lattice ($p = 0.643$, blue circles) and the FCC lattice ($p = 0.47$, red squares). At low κ there is a bending dominated regime $G_{\text{bend}} \sim \kappa$, at intermediate κ there is a regime in which stretching and bending modes couple strongly with $G \sim \mu^{1-x}\kappa^x$, where $x = 0.50 \pm 0.01$ (2D) and $x \approx 0.40 \pm 0.01$ (3D). The EMT calculation for $\kappa/\mu \gg |\Delta p|^{\phi_{\text{EMT}}}$ is shown as a solid blue line.

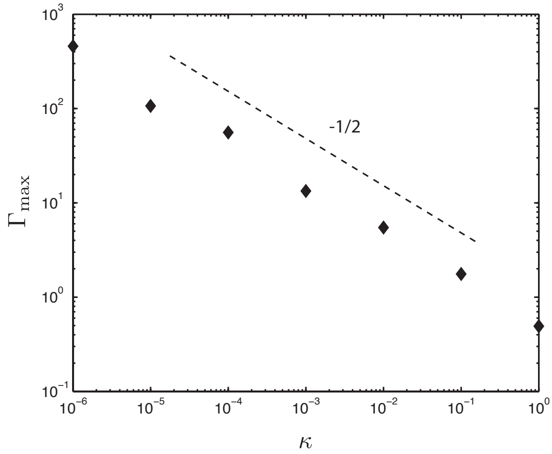

Figure 6.9 – Scaling of the non-affine fluctuations near isostaticity with bending rigidity. The amplitude of the non-affine fluctuations $\Gamma_{\max}$ near isostaticity at $p = 0.65$ as a function of the fiber bending rigidity.

for the non-affinity given by

$$\Gamma = \frac{1}{N\gamma^2} \sum_i \left[\mathbf{u}_i - \mathbf{u}_i^{(\mathrm{aff})}\right]^2, \tag{6.6}$$

where $\mathbf{u}_i^{(\mathrm{aff})}$ is the affine displacement of vertex i and N is the number of vertices. This quantity varies over eight orders of magnitude, indicating non-affine fluctuations that depend strongly on both κ and p, as shown in Figs. 6.3b and 6.4b. For stretch-dominated networks (high κ), we find a monotonic increase in non-affine fluctuations with decreasing p, which appear to diverge at p_b. In addition, for smaller values of κ, a second peak in Γ develops at p_c. The amplitude of the non-affine fluctuations at p_c scales with κ as $\Gamma_{\max} \sim \kappa^{-\beta}$, with $\beta \approx 0.5$, as shown in Fig. 6.9. The development of the peak in Γ around p_c coincides with the appearance of a crossover between the stretching and bending regimes (Figs. 6.3 and 6.4).

6.3.3 Finite size scaling

The critical phenomena we observe in the mechanical behavior suggests a divergence of the non-affine fluctuations according to $\Gamma = \Gamma_{\pm}|\Delta p|^{-\lambda}$, in a manner similar to that of spring networks in a jammed configuration [5], but with a non mean-field exponent. Moreover, we anticipate an associated divergent length-scale $\xi = \xi_{\pm}|\Delta p|^{-\nu}$ near the critical point P_c for vanishing κ. However, the divergence of ξ is limited by the system size W, which should suppress the divergence of Γ. Consistent with this

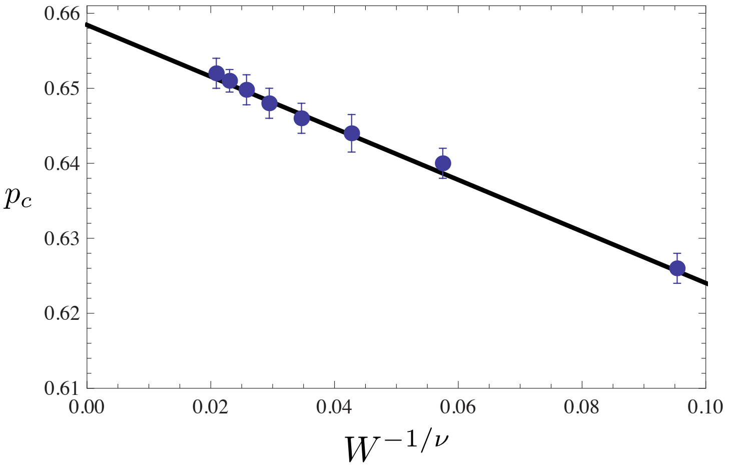

Figure 6.10 – (Color online) **Finite size scaling of the CF isostatic point** The finite size dependence of the central force isostatic point p_c. We performed a least square fit of the expected dependence $p_c(W) = p_c + bW^{-1/\nu}$, to the p_c determined from our simulations for a range of system sizes W. From this we obtain $p_c = 0.659 \pm 0.002$, $\nu = 1.4 \pm 0.2$ and $b = -0.3 \pm 0.1$.

picture, we find that the location of the cusp in the local fluctuations Γ shift towards higher p with increasing W. The system size dependence of $p_c(W)$ is expected to follow the behavior

$$p_c(W) = p_c + bW^{-1/\nu}, \tag{6.7}$$

where b is a coefficient and p_c is the central force isostatic point. We performed a least square fit of this dependence to $p_c(W)$ determined from our simulations for a range of system sizes (Fig. 6.10). From this we obtain $p_c = 0.659 \pm 0.002$, $\nu = 1.4 \pm 0.2$ and $b = -0.3 \pm 0.1$; these values are consistent with previous reports on generic CF networks [43], although, in contrast to those studies, we determine all exponents from the mechanics and deformation properties of the network. Generic lattices consist of slightly perturbed lattices and fall in a different universality class than the nongeneric perfect lattices. Although we start out with unperturbed lattices, we only determine the mechanical behavior using an imposed shear, which will induce lattice contortions at any finite strain, thereby avoiding the geometric singularities associated with the perfectly aligned bonds in the nongeneric lattices. Furthermore, the comparison of our exponent ν with the results on generic CF networks [43] may suggest that the divergent lengthscale ξ is associated to the size of rigid clusters in the network.

In addition, the amplitude of Γ increases with system size (Fig. 6.11a), in quantitative accord with the expected finite-size scaling. Specifically, we find a good collapse of the simulation data with $\Gamma = W^{\lambda/\nu}\mathscr{F}_{\Gamma,\pm}\left(|\Delta p|W^{1/\nu}\right)$ over a range of system sizes, with $\lambda/\nu = 1.6 \pm 0.2$ and $\nu = 1.4 \pm 0.2$, as shown in Fig. 6.11b. Similarly, the shear modulus exhibits finite-size scaling (Fig. 6.12a) according to $G = W^{-f/\nu}\mathscr{F}_{G,\pm}\left(|\Delta p|W^{1/\nu}\right)$, as shown in Fig. 6.12b. We obtain a good collapse of the elasticity data using $f/\nu = 0.9 \pm 0.1$, along with ν determined from the finite-size scaling of Γ (Fig. 6.11 and Fig. 6.10), consistent with the value of f obtained from the scaling in Fig. 6.6. In addition to a divergent Γ and ξ at p_c, we also find similar critical behavior at p_b, with $\lambda = 1.8$, $\nu = 1.3$, and rigidity exponent $f = 3.2$ for small κ. (This places our fiber model, along with Mikado models [6, 8] in a different universality class than bond-bending models, where $f = 3.97$ [20]). Thus, at both central-force and bending thresholds, we find critical behavior that is accompanied by divergent non-affine fluctuations and a scale-dependent shear modulus, implying a breakdown of continuum elasticity below the divergent length-scale ξ.

Finally, from the finite size scaling of the non-affine fluctuations at $\kappa = 0$ (Fig. 6.11) and the scaling of the elasticity data (Fig. 6.6), we can now predict the κ-dependence of Γ_{max}, which is shown in Fig. 6.9. Close to the CF isostatic point we expect a scaling behavior,

$$\Gamma \sim W^{\lambda/\nu}\left(|\Delta p|W^{1/\nu}\right)^{x'}\left(\frac{\kappa}{\mu}|\Delta p|^{-\phi}\right)^{y'}. \tag{6.8}$$

From this, we can determine the unknown exponents x' and y', by requiring that the W and Δp dependences cancel out. This leads to the prediction $\Gamma_{\text{max}} \sim \kappa^{-\lambda/\phi}$; similarly, $\xi \sim \kappa^{-\nu/\phi}$ at finit κ as $\Delta p \to 0$. Based on the exponents determined above (Table 1) we expect $\lambda/\phi = 0.7 \pm 0.2$, consistent with the observed scaling behavior $\lambda/\phi \approx 0.5$ for Γ_{max} in Fig. 6.9.

The simple one-point non-affinity measure we use here quantifies the average local deviation from the global shear profile. If we assume that the non-affine deformations associated to bending deformations in the filaments follow the same scaling dependence as Γ for $\kappa \to 0$, we expect a scaling for the shear modulus in the bending regime $< p_c$ of the form $G \sim \kappa\Gamma \sim \kappa|\Delta p|^{-\lambda}$ [5], implying $\lambda/\phi = 1 - f/\phi$. The most accurate and direct determinations of the ratios λ/ϕ and f/ϕ for the 2D triangular lattice are obtained from Figs. 6.9 and 6.8, $\lambda/\phi \approx 0.5$ and $f/\phi \approx 0.5$, consistent with the prediction of the scaling argument that relate these two ratios. This scaling argument also predicts the cross-over regime with anomalous elasticity. In this regime $\Gamma \sim \kappa^{-\lambda/\nu}$ and, thus $G \sim \kappa\Gamma \sim \kappa^{1-\lambda/\phi}$ consistent with our earlier results.

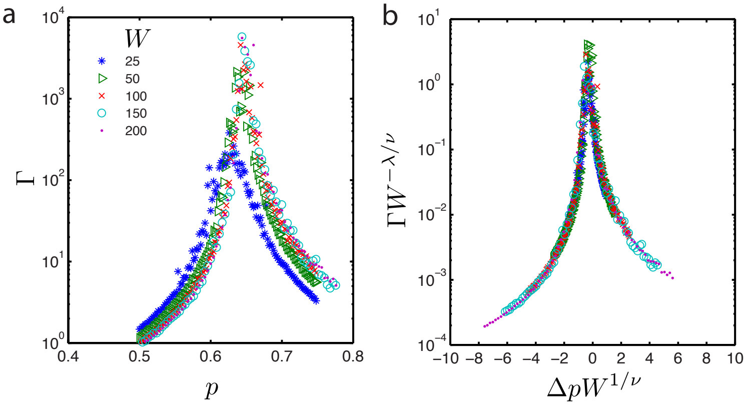

Figure 6.11 – Finite size scaling of the non-affine fluctuations (a) The non-affinity measure Γ for the 2D triangular lattice at $\kappa = 0$ for various systems sizes W (25 blue, 50 green, 100 red, 150 cyan and 200 purple). (b) Finite size scaling of the non-affinity measure Γ according to the scaling form $\Gamma = W^{\lambda/\nu}\mathscr{F}_{\Gamma,\pm}(\Delta p W^{1/\nu})$. The exponents we obtain are $\lambda/\nu = 1.6 \pm 0.2$, $\nu = 1.4 \pm 0.2$.

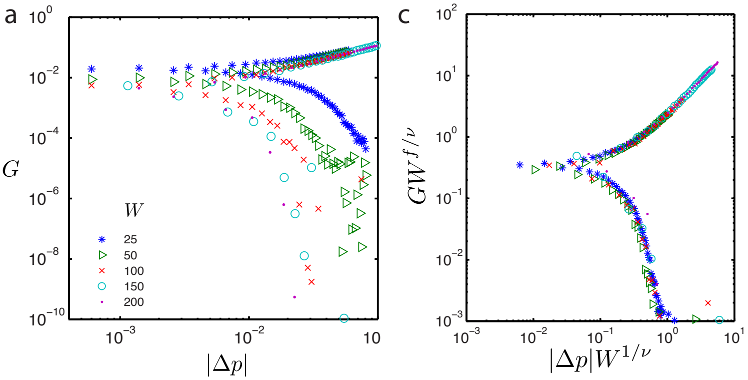

Figure 6.12 – Finite size scaling of the elasticity (a) The shear modulus G in units of μ/ℓ_0 as a function of $|\Delta p|$ of a 2D triangular network at $\kappa = 0$ for various systems sizes W (25 blue, 50 green, 100 red, 150 cyan and 200 purple). Finite size scaling of the shear modulus with the scaling form $G = W^{-f/\nu}\mathscr{F}_{G,\pm}(|\Delta p| W^{1/\nu})$. Here $\Delta p = p - p_c$, where $p_c = 0.659 \pm 0.002$. The exponents we obtain are $\nu = 1.4 \pm 0.2$ and $f/\nu = 0.9 \pm 0.1$.

6.4 Discussion and implications

In this chapter we studied the cross-over between bending and stretching behavior in lattice-based fiber networks. This cross-over is governed by the CF isostatic point, analogous to the behavior in multicomponent random resistor or spring networks [3–5], and bond bending networks [2, 17–19]. Interestingly, the critical behavior of weak-spring stabilized isostatic jammed packings is consistent with mean field predictions, while we observe a clear breakdown of mean field theory. It is interesting to compare the lattice based networks studied here with off-lattice random networks, also referred to as the mikado model. Prior studies [6–8] on that model have also identified both a stretching and a bending governed regime, consistent with our results. However, in the mikado model the cross-over between the two regimes has been argued to be governed by the filament length compared to a non-affinity length scale [6, 7]. This is in contrast with our results on superisostatic lattices. The range of p values between the rigidity percolation threshold and the isostatic point only result in a roughly 2-fold change in filament length. Therefore, we attribute the behavior we observe mostly to a change in the local coordination number.

The undiluted triangular and FCC lattices we study have an average coordination number greater than $2d$ and thus are above the Maxwell central-force isostatic threshold. These networks also consist of infinitely long filaments. Cutting bonds as we do introduces both finite length polymers, as well as lower connectivity, down to the CF threshold and below. As a result, the networks in our model exhibit two thresholds at p_c and p_b, in contrast to, e.g. the Mikado model in 2D [6, 8, 12] and network glass models [18] with only the bending rigidity threshold. Cytoskeletal and extracellular networks can have z as low as 3 (e.g., in branched networks) and as high as 6 (in the case of actin-spectrin networks), although they typically have a local connectivity $z \simeq 4$, where two filaments are connected by a cross-link. As a consequence, the CF isostatic point is expected to occur for high molecular weight in 2D. We conjecture that there is an analogous crossover behavior for such networks, including the anomalous scaling behavior for the elasticity. In addition, we expect that our results for the crossover behavior will apply to bond-bending models on similar lattices to ours [2, 17–19] for rigidity percolation and network glasses that include bending forces between bond pairs at each network node.

Interestingly, from the perspective of critical phenomena more generally, the kind of crossover behavior we find here is in contrast to most thermal systems, where a field or coupling constant leads to a crossover from one critical system to another, such as from the Heisenberg model to the Ising model [36]. In such systems, there is a continuous evolution of the critical point that is governed by the crossover exponent ϕ. Interestingly, we find no such continuous evolution, but rather a discontinuous jump in the critical point p_c as soon as κ becomes nonzero.

6.5 Appendix: Counting argument for rigidity threshold

The bend isostatic point p_b of lattice-based fibrous networks can be calculated using Maxwell counting and mean-field arguments. Isostatic conditions imply that the total number of the network constrains due to both stretching and bending are equal to the total number of degrees of freedom. In d dimension, the total number of the network degrees of freedom is equal to dN_c, where N_c is the number of network crosslinks. The number of the network constrains due to the stretching modulus of network filaments is $N_b p$, where N_b is the number of bonds in the undiluted network $(p = 1)$. In addition, the bending rigidity contributes $d - 1$ constraints at any pair of present neighboring coaxial bonds. The total number of such bonds is $N_b p^2$.

Thus, the rigidity percolation transition occurs when

$$dN_c = N_b \left(p + (d-1)p^2\right)$$

or

$$p_b = \frac{\sqrt{1 + \frac{4dN_c}{N_b}(d-1)} - 1}{2(d-1)}.$$

We now compute the rigidity percolation point for various cases. For the triangular and FCC networks we obtain values that are in reasonable agreement with our numerical results.

Triangular lattice

$$d = 2$$

$$\frac{N_c}{N_b} = \frac{1}{3}$$

$$p_b = \frac{\sqrt{\frac{11}{3}} - 1}{2} \simeq 0.4574$$

Kagome and square lattices

$$d = 2$$

$$\frac{N_c}{N_b} = \frac{1}{2}$$

$$p_b = \frac{\sqrt{5} - 1}{2} \simeq 0.618$$

FCC lattice

$$d = 3$$

$$\frac{N_c}{N_b} = \frac{1}{6}$$

$$p_b = \frac{\sqrt{5}-1}{4} \simeq 0.309$$

6.6 Acknowledgments

This work was performed in collaboration with X. Mao, T.C. Lubensky and M. Sheinman. X.M. and T.C.L. developed and executed the EMT and M.S. developed the counting argument. We thank M. Das and L. Jawerth for useful discussions.

Bibliography

[1] J. C. Maxwell. *On the calculation of the equilibrium and stiffness of frames*. Philos. Mag. **27**, 294 (1864).

[2] M. Thorpe. *Continuous deformations in random networks*. J. Non-Cryst. Solids **57**, 355 – 370 (1983).

[3] J. Straley. *Critical phenomena in resistor networks*. J. Phys. C: Solid State Phys. **9**, 783 (1976).

[4] E. J. Garboczi and M. F. Thorpe. *Effective-medium theory of percolation on central-force elastic networks. III. The superelastic problem*. Phys. Rev. B **33**, 3289 (1986).

[5] M. Wyart, H. Liang, A. Kabla and L. Mahadevan. *Elasticity of floppy and stiff random networks*. Phys. Rev. Lett. **101**, 215501 (2008).

[6] D. A. Head, A. J. Levine and F. C. MacKintosh. *Deformation of cross-linked semiflexible polymer networks*. Phys. Rev. Lett. **91**, 108102 (2003).

[7] D. A. Head, A. J. Levine, and F. C. MacKintosh. *Distinct regimes of elastic response and deformation modes of cross-linked cytoskeletal and semiflexible polymer networks*. Phys. Rev. E **68**:061907 (2003). (2003).

[8] J. Wilhelm and E. Frey. *Elasticity of stiff polymer networks*. Phys. Rev. Lett. **91**, 108103 (2003).

[9] M. L. Gardel, J. H. Shin, F. C. MacKintosh, L. Mahadevan, P. A. Matsudaira, D. A. Weitz. *Elastic Behavior of Cross-Linked and Bundled Actin Networks*. Science **304**, 1301 (2004); Phys. Rev. Lett. **93**, 188102 (2004).

[10] C. Storm, J. Pastore, F. C. MacKintosh, T. C. Lubensky and P. A. Janmey. *Nonlinear elasticity in biological gels*. Nature **435**: 191 (2005).

[11] P. R. Onck, T. Koeman, T. van Dillen and E. van der Giessen. *Alternative explanation of stiffening in cross-linked semiflexible networks*. Phys. Rev. Lett. **95**, 178102 (2005).

[12] C. Heussinger and E. Frey. *Floppy modes and nonaffine deformations in random fiber networks*. Phys. Rev. Lett. **97**, 105501 (2006).

[13] C. Heussinger, B. Schaefer and E. Frey. *Nonaffine rubber elasticity for stiff polymer networks*. Phys. Rev. E **76**, 031906 (2007)

[14] O. Lieleg, M. M. A. E. Claessens, C. Heussinger, E. Frey and A. R. Bausch. *Mechanics of Bundled Semiflexible Polymer Networks*, Phys. Rev. Lett. **99**, 088102 (2007).

[15] O. Chaudhuri, S. Parekh and D. Fletcher. *Reversible stress softening of actin networks*. Nature **445**, 295–298 (2007).

[16] G. A. Buxton and N. Clarke. *"Bending to stretching" transition in disordered networks*. Phys. Rev. Lett. **98**, 238103 (2007).

[17] L. M. Schwartz, S. Feng, M. F. Thorpe and P. N. Sen. *Behavior of depleted elastic networks - comparison of effective-medium and numerical-calculations*. Phys. Rev. B **32**, 4607–4617 (1985).

[18] H. He and M. F. Thorpe. *Elastic properties of glasses*. Phys. Rev. Lett. **54**, 2107–2110 (1985).

[19] M. Sahimi and S. Arbabi. *Mechanics of disordered solids. ii. percolation on elastic networks with bond-bending forces*. Phys. Rev. B **47**, 703–712 (1993).

[20] J. G. Zabolitzky, D. J. Bergman, and D. Stauffer. *Precision Calculation of Elasticity Percolation* J. Stat. Phys. **44**, 211 (1986).

[21] A. Bausch and K. Kroy. *A bottom-up approach to cell mechanics*. Nature Phys. **2**, 231–238 (2006).

[22] D. Fletcher and R. Mullins. *Cell mechanics and the cytoskeleton*. Nature **463**, 485–492 (2010).

[23] L. J. Hall *et al.* *Sign Change of Poisson's Ratio for Carbon Nanotube Sheets*. Science **320**, 504–507 (2008).

[24] L. A. Hough, M. F. Islam, P. A. Janmey and A. G. Yodh. *Viscoelasticity of single wall carbon nanotube suspensions*. Phys. Rev. Lett. **93**, 168102 (2004).

[25] A. Kabla and L. Mahadevan. *Nonlinear mechanics of soft fibrous networks*. J. R. Soc. Interface **4**, 99–106 (2007).

[26] J. Pedersen and M. Swartz. *Mechanobiology in the third dimension*. Ann. Biomed. Eng. **33**, 1469–1490 (2005).

[27] M. Das, F. C. MacKintosh and A. J. Levine. *Effective medium theory of semiflexible filamentous networks*. Phys. Rev. Lett. **99**, 038101 (2007).

[28] J. Liu, G. H. Koenderink, K. E. Kasza, F. C. MacKintosh, and D. A. Weitz. *Visualizing the Strain Field in Semiflexible Polymer Networks: Strain Fluctuations and Nonlinear Rheology of F-Actin Gels*. Phys. Rev. Lett. **98**, 198304 (2007).

[29] C. Heussinger and E. Frey. *Role of architecture in the elastic response of semiflexible polymer and fiber networks*. Phys. Rev. E **75**, 011917 (2007).

[30] T. J. Byers and D. Branton. *Visualization of the protein associations in the erythrocyte membrane skeleton*. Proc. Natl. Acad. Sci. USA **82**, 6153 (1985).

[31] C. P. Broedersz, X. Mao, F. C. MacKintosh, and T. C. Lubensky. *Criticality and isostaticity in fiber networks*. arXiv:1011.6535v1 (2010).

[32] X. Mao, N. Xu, and T. C. Lubensky. *Soft modes and elasticity of nearly isostatic lattices: randomness and dissipation*. Phys. Rev. Lett. **104**, 085504 (2010).

[33] X. Mao and T. C. Lubensky (to be published).

[34] A. Souslov, A. J. Liu, and T. C. Lubensky. *Elasticity and Response in. Nearly Isostatic Periodic Lattices*. Phys. Rev. Lett. **103**, 205503 (2009).

[35] S. Feng, M. F. Thorpe and E. Garboczi. *Effective-medium theory of percolation on central-force elastic networks*. Phys. Rev. B **31**, 276–280 (1985).

[36] M. E. Fisher, in *Proceedings of the School on Critical Phenomena, Stellenbosch, South Africa, 1982*, edited by F.J.W. Hahne (Springer-Verlag, Berlin, 1983), Vol. 186.

[37] F. C. MacKintosh, J. Käs, and P. A. Janmey. *Elasticity of semiflexible biopolymer networks*. Phys. Rev. Lett., **75**:4425 (1995).

[38] W. T. Vetterling and B. P. Flannery. *Numerical Recipes in C++: The Art of Scientific Computing, 2nd ed.* (Cambridge University Press, 2002).

[39] P. Soven. *Contribution to the theory of disordered alloys*. Phys. Rev. **178**, 1136–1144 (1969).

[40] S. Arbabi and M. Sahimi. Mechanics of disordered solids. I. percolation on elastic networks with central forces. *Phys. Rev. B* **47**, 695–702 (1993).

[41] M. V. Chubynsky and M. F. Thorpe. *Algorithms for three-dimensional rigidity analysis and a first-order percolation transition. Phys. Rev. E* **76**, 041135 (2007).

[42] B. A. DiDonna and T. C. Lubensky. *Nonaffine correlations in random elastic media*. Phys. Rev. E **72**, 066619 (2005).

[43] D. J. Jacobs and M. F. Thorpe. *Generic rigidity percolation in two dimensions*. Phys. Rev. E **53**, 3682–3693 (1996).

7

Molecular motors stiffen non-affine semiflexible polymer networks

- C. P. Broedersz and F. C. MacKintosh
  Molecular motors stiffen non-affine semiflexible polymer networks,
  arXiv:1009.3848, accepted for Soft Matter (2011)

Abstract

Reconstituted filamentous actin networks with myosin motor proteins form active gels, in which motor proteins generate forces that drive the network far from equilibrium. This motor activity can also strongly affect the network elasticity; experiments have shown a dramatic stiffening in *in vitro* networks with molecular motors. Here we study the effects of motor generated forces on the mechanics of simulated 2D networks of athermal stiff filaments. We show how heterogenous internal motor stresses can lead to stiffening in networks that are governed by filament bending modes. The motors are modeled as force dipoles that cause muscle like contractions. These contractions "pull out" the floppy bending modes in the system, which induces a cross-over to a stiffer stretching dominated regime. Through this mechanism, motors can lead to a nonlinear network response, even when the constituent filaments are themselves purely linear. These results have implications for the mechanics of living cells and suggest new design principles for active biomemetic materials with tunable mechanical properties.

7.1 Introduction

The mechanics of living cells is largely governed by the cytoskeleton, a complex assembly of various filamentous proteins. Cross-linked networks of actin filaments form one of the major structural components of the cytoskeleton. However, this cytoskeleton is driven far from equilibrium by the action of molecular motors that can generate stresses within the meshwork of filaments [1–3]. Such motor activity plays a key role in various cellular functions, including morphogenesis, division and locomotion. The nonequilibrium nature of motor activity has been demonstrated in simplified reconstituted filamentous actin networks with myosin motors [4–8]. Even in the absence of motor proteins, such *in vitro* networks of cytoskeletal filaments already constitute a rich class of soft matter systems that exhibit unusual material properties, including a highly nonlinear elastic response to external stress [9–15]. This nonlinear response can be exploited using molecular motors [4,7]; the network stiffness can be varied by orders of magnitude, depending on motor activity. A quantitative understanding of such active biological matter poses a challenge for theoretical modeling [3,16–21].

The nonlinear mechanical response of reconstituted biopolymer networks in many cases reflects the nonlinear force-extension behavior of the constituting cross-links or filaments [9–11,14,22]. For such networks, there is both theoretical and experimental evidence that internal stress generation by molecular motors can result in network stiffening in direct analogy to an externally applied uniform stress [4, 7, 18–20, 23]. However, the mechanical response of semiflexible polymers is highly anisotropic and is typically much softer to bending than to stretching. In some cases, this renders the network deformation highly non-affine with most of the energy stored in bending modes [24–28]. Such non-affinely deforming stiff polymer networks can also exhibit a nonlinear mechanical response, even when the network constituents have a linear force-extension behavior [29–32]. However, the effects of internal stresses generated by molecular motors in such networks are unknown.

Here we study the effects of motor generated forces on the network mechanics in 2D networks of athermal, stiff filaments using simulations. In the absence of motors, these networks can exhibit strain stiffening under an externally applied shear. This behavior has been attributed to a cross-over between two mechanical regimes; at small strains the mechanics is governed by soft bending modes and a non-affine deformation field, while at larger strains the elastic response is governed by the stiffer stretch modes and an affine deformation field [29]. We show that motors that generate internal stresses can also stiffen the network. The motors induce force dipoles leading to muscle like contractions, which "pull out" the floppy bending modes in the system. This induces a cross-over to a stiffer stretching dominated regime. Through this mechanism, motors can lead to network stiffening in non-affine stiff polymer networks in which the constituting filaments in the network are themselves linear elements. These results have implications for the mechanics of living cells and propose new design principles for active biomemetic materials with highly tunable mechanical properties.

7.2 The model

To study the basic effects of internal stress generated by molecular motors on the macroscopic mechanical properties of stiff polymer networks we employ a minimalistic model, which is illustrated in Fig. 7.1. Filamentous networks in 2D are generated by arranging filaments spanning the system size on a triangular lattice. Since physiological cross-linking proteins typically form binary cross-links, we randomly select two out of the three filaments at every vertex between which we form a binary cross-link. The remaining filament crosses this vertex as a phantom chain, without direct mechanical interactions with the other two filaments. The cross-links themselves hinge freely with no resistance. With this procedure we can generate disordered *phantom* networks, based on a triangular network, but with local 4-fold ($z = 4$) connectivity corresponding to binary cross-links. The use of a triangular lattice avoids, for example, well-known mechanical pathologies of the 4-fold square lattice. To create

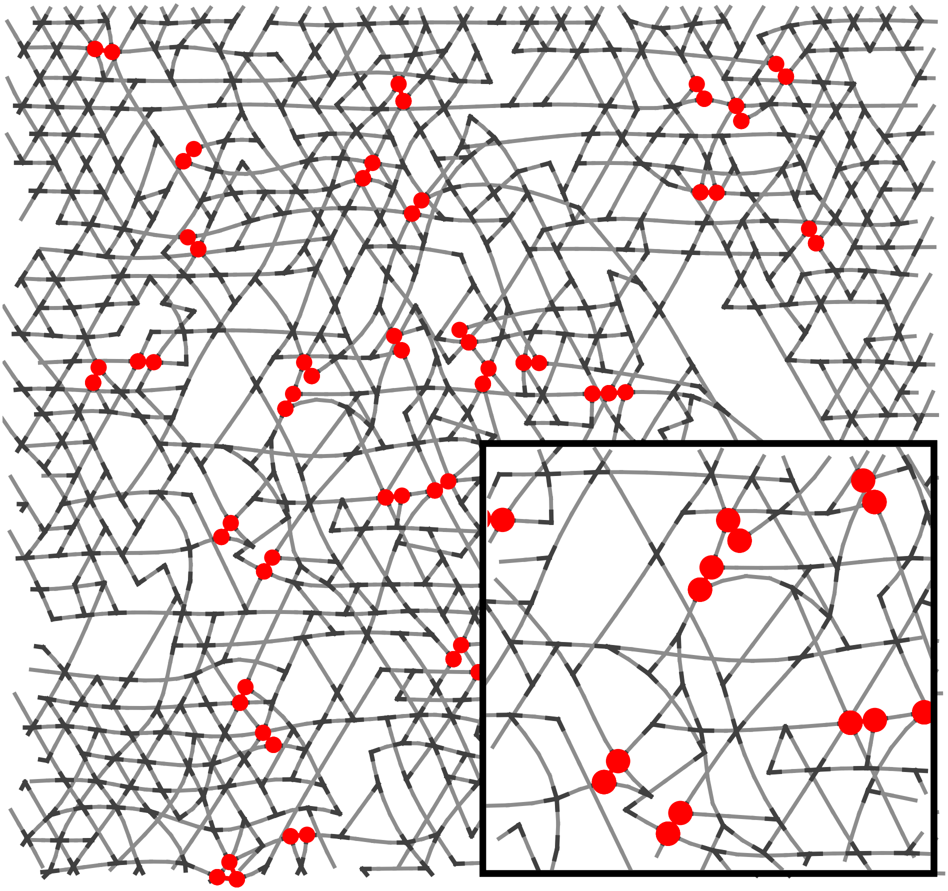

Figure 7.1 – (Color online) Example of a portion of the diluted 2D phantom triangular network at $q = 1/4$ and $\kappa = 10^{-3}$. The freely hinging binary cross-links are indicated in black. Motors generate muscle-like contractions, which we model with force dipoles. The segments along which these contractile force dipoles act are indicated with red dumbbells. The inset shows an enlargement of the network.

quenched disorder in the network, we cut and remove filament segments between vertices with a probability q. This also has the effect of shortening the filaments.

The filaments in the network are described by an extensible wormlike chain (EWLC) model with an energy

$$\mathscr{H} = \frac{1}{2}\kappa \int \mathrm{d}s \left(\frac{\mathrm{d}\hat{t}}{\mathrm{d}s}\right)^2 + \frac{1}{2}\mu \int \mathrm{d}s \left(\frac{\mathrm{d}\ell(s)}{\mathrm{d}s}\right)^2, \tag{7.1}$$

where κ is the bending rigidity, $\hat{\mathbf{t}}$ is the tangent vector at a position s along the polymer backbone and $\frac{\mathrm{d}\ell(s)}{\mathrm{d}s}$ is the local relative change in contour length, or longitudinal strain. We can quantify the relative importance of the stretch and bend contributions by the lengthscale $\ell_b = \sqrt{\kappa/\mu}$; this length scale forms one of the key control parameters for the network mechanics. For simple cylindrical beams with a radius r, the stretch modulus μ is related to κ through $\mu_{\mathrm{mech}} = 4\kappa/r^2$, and $\ell_b = r/2$. In contrast, a thermally fluctuating semiflexible polymer segment cross-linked in a network on a length-scale ℓ_c also has an entropic thermal stretch modulus $\mu_{\mathrm{th}} = 90\kappa^2/k_{\mathrm{B}}T\ell_c^3$ [33], where k_B is Boltzmann's constant and T is the temperature. In this case, $\ell_b = \ell_c\sqrt{\ell_c/90\ell_p}$, where $\ell_p = \kappa/k_{\mathrm{B}}T$ is the persistence length. The most relevant values of ℓ_b/ℓ_c for biopolymer systems range from $10^{-2} - 10^{-1}$. This range extends from relatively stiff actin filaments to the more flexible intermediate filaments. Various actin binding proteins are capable of forming tightly coupled stiff bundles of actin filaments, which further reduces ℓ_b. The mechanical and thermal moduli add as springs in series and the total modulus is given by $\mu^{-1} = \mu_{\mathrm{mech}}^{-1} + \mu_{\mathrm{th}}^{-1}$. In the remainder of this paper all lengths are determined in units of the distance between lattice vertices ℓ_0 and the bending rigidity κ is measured in units of $\mu\ell_0^2$. Here, we focus on nonlinearities arising in networks of purely linear elements. Thus, we do not include intrinsic nonlinearities associated with the force-extension curve of thermal filaments, which is examined theoretically in Refs. [18–20]

In our numerical simulations we use a discretized version of Eq. (7.1) with a node at and between every lattice vertex. The mid-node allows us to capture buckling down to the single segment length-scale. To model the effect of muscle like contractions induced by molecular motors, we introduce force dipoles in the network [4, 18, 19, 23]. These force dipoles are randomly placed at neighboring cross-links. The force dipoles f_{ij} only act along existing bonds and, therefore, do not introduce additional constraints in the network. The total energy of the system includes a sum of the EWLC Hamiltonian over all filament segments and the work extracted by the force dipoles

$$E = \sum_i \mathscr{H}_i - \sum_{<ij>} f_{ij} r_{ij}, \tag{7.2}$$

where r_{ij} is the distance between cross-link i and j. The force dipoles are numerically implemented by shortening the effective rest length of the bond along which the motors acts in the stretch term of the energy (Eq. 7.1). The rest length is reduced by an amount $\delta r_{ij}^{(0)}$; the resulting force is given by $\mu \delta r_{ij}^{(0)}/\ell_0 \leq \mu$. The effects of internal motor generated stresses modeled in this way is illustrated in Fig. 7.1.

To investigate the mechanical response of the network, an external strain γ is applied by translating one of the horizontal boundaries to which the filaments are attached. The internal degrees of freedom of the network are relaxed by minimizing the energy using a conjugate gradient algorithm [34]. To reduce edge effects periodic boundary condition are employed at all boundaries. The linear shear modulus of a network of size W^2 is related to the energy $G = \frac{2}{W^2 A_0} \frac{E}{\gamma^2}$ for small strains, where A_0 is the area of a unit cell. In the nonlinear regime it is common to determine the differential modulus $K = \frac{1}{W^2 A_0} \frac{\mathrm{d}^2 E}{\mathrm{d}\gamma^2}$, which reduces to G for small γ. Similarly, the stress can be calculated in the nonlinear regime through $\sigma_{\mathrm{ext}} = \frac{1}{W^2 A_0} \frac{\mathrm{d}E}{\mathrm{d}\gamma}$. These measurements allow us to quantify the mechanical response of the system. Here we use system sizes ranging from $W^2 \simeq 3000$ to 8000. In all cases W is always at least 4.5 times as large as $\langle L \rangle$ to avoid filaments that span the system between shear plates.

7.3 Results and discussion

7.3.1 Passive networks

We probe the 2D phantom triangular networks by determining both the linear and nonlinear elastic response of the networks in the absence of motors. The linear mechanical response of diluted networks ($q < 1$) exhibits two distinct mechanical regimes. At low κ, the shear modulus G scales directly with κ, as shown in the upper inset of Fig. 7.2. This demonstrates that in this regime the macroscopic mechanics is governed by filament bending deformation modes. By contrast, at large κ the shear modulus asymptotically approaches a limit in which G is independent of κ indicative of a stretching dominated regime. These result are consistent with previous observations on 2D mikado networks [24–26].

These mechanical regimes have important implications for the nonlinear elastic response. When a large external shear is imposed on a network that is initially in the bending dominated regime, the differential modulus $K = \frac{\mathrm{d}\sigma}{\mathrm{d}\gamma}$ increases strongly as a function of external stress σ_{ext}, as shown in Fig. 7.2 (The same data are shown as a function of the applied shear strain γ in the lower inset of Fig. 7.2) . Previous studies have observed similar stiffening in networks with strictly linear elements [29–32]. This remarkable behavior has been explained in terms of a *strain*-induced crossover from a bending to a stretching dominated regime. At low stresses the network mechanics is governed by bending modes, which for small κ constitute the softest modes in the system. However, when the stress is increased the deformations become

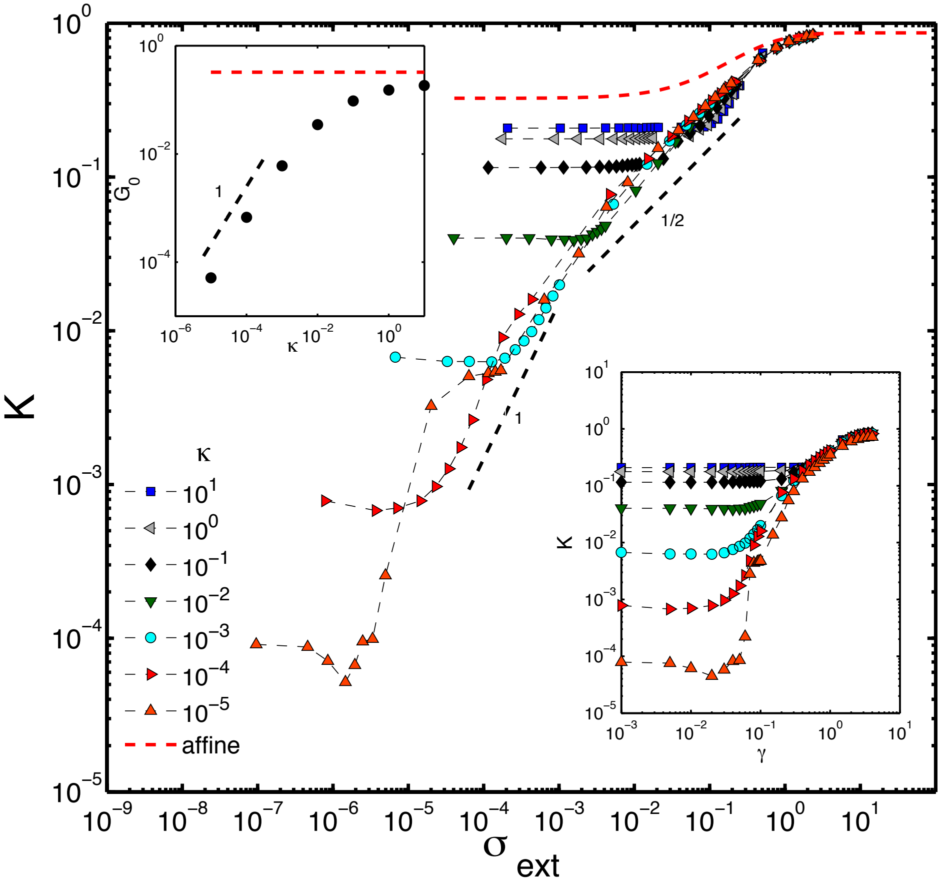

Figure 7.2 – (Color online) The differential shear modulus $K = \mathrm{d}\sigma/\mathrm{d}\gamma$ as a function of the applied external stress σ_{ext} for various ratios of bending rigidities κ and fixed $q = 1/4$. K and σ_{ext} are measured in units of μ/ℓ_0. The affine prediction is shown as a red dashed line, which constitutes an upper bound to the elastic response. Although definite powerlaw regimes appear to be absent, the stiffening curves for floppy systems with $\kappa \lesssim 10^{-3}$ initially show a stiffening behavior of approximately $K \sim \sigma$ that crosses over to a regime $K \sim \sigma^{1/2}$ at large stress, as shown by the dashed lines indicating slopes of 1 and 1/2. For stiffer systems with $\kappa \gtrsim 10^{-2}$, only the second of these regimes is apparent. The upper inset shows the linear shear modulus G as a function of κ, and the red dashed line indicates the affine prediction. The lower inset shows the same data as shown in the main figure as a function of the applied shear strain γ.

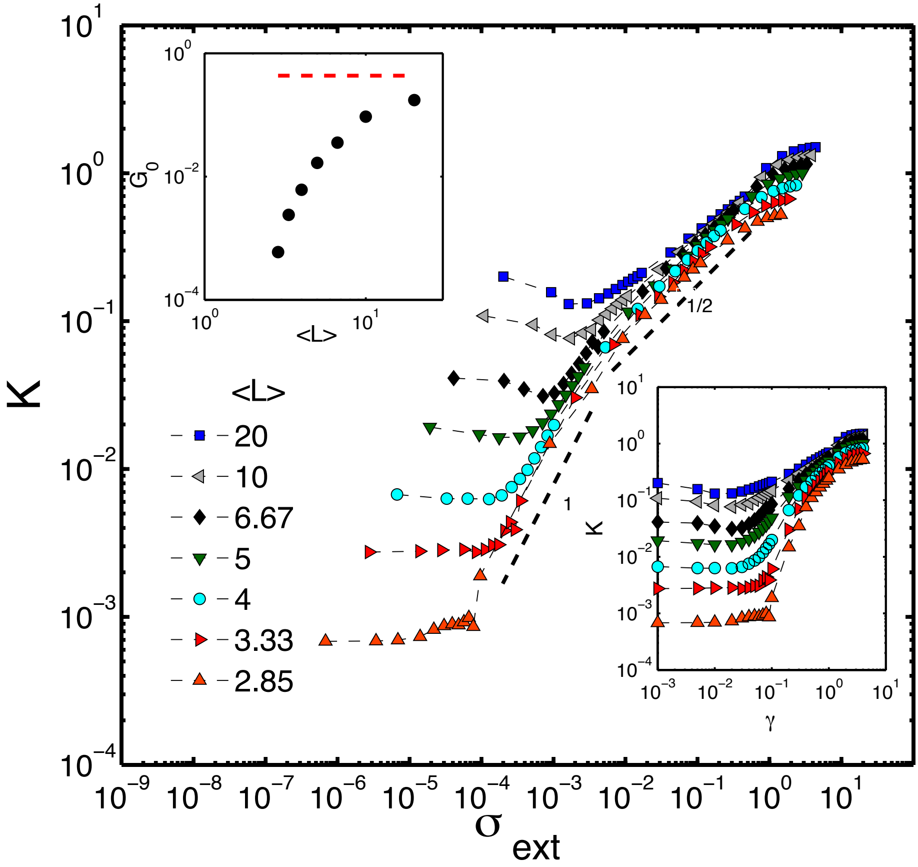

Figure 7.3 – (Color online) The differential shear modulus $K = d\sigma/d\gamma$ as a function of the applied external stress σ_{ext} for various values of $\langle L\rangle$ at fixed bending rigidity $\kappa = 10^{-3}$. K and σ_{ext} are measured in units of μ/ℓ_0. Although definite powerlaw regimes appear to be absent, the stiffening curves for $\langle L\rangle \lesssim 5$ initially show a stiffening behavior of approximately $K \sim \sigma$ that crosses over to a regime $K \sim \sigma^{1/2}$ at large shear, as shown by the dashed lines that indicate a slope of 1 and 1/2. For longer filaments, only the second, weaker stiffening response is apparent. The upper inset shows the linear shear modulus G as a function of the average filament length $\langle L\rangle$, and the red dashed line indicates the affine prediction in the high molecular weight limit. The lower inset shows the same data as shown in the main figure as a function of the applied shear strain γ.

correspondingly large and the stretching of filaments is no longer avoidable. This picture is consistent with our simulations. When a substantial shear is imposed the stiffening curves—over a large range of bending rigidities—converge to a single curve that is consistent with the affine prediction [10, 35], shown as a red dashed line in Fig. 7.2. This calculation also demonstrates that even an affinely deforming network of strictly linear elements stiffens under shear. This stiffening behavior is purely due to geometric effects; under shear the network becomes increasingly anisotropic and the filaments reorient to line up in the shear direction [35]. The extent of this purely geometric stiffening is, however, limited. Moreover, this geometrically-stiffened limit represents an upper bound on the stiffness of networks with purely linear elements.

In addition to κ, the average length of filaments in the system $\langle L \rangle$ constitutes an important control parameter for the linear response. We can probe this by varying q, since the average length of filaments is given by $\langle L \rangle = 1/q$ [36]. Consistent with previous work [24–26], a cross-over from a non-affine bending regime and an affine stretching regime can also be achieved by increasing $\langle L \rangle$, as shown in the upper inset of Fig. 7.3. In the high molecular weight limit, $\langle L \rangle \to \infty$, the connectivity in the system approaches the central force isostatic point in 2D above which the network is completely constrained by the filament stretching modes and will thus deform affinely [36, 37]. We estimate that in experimental biopolymer systems $\langle L \rangle$ varies a over a range of order 5-30, in units of the network mesh size. The strong dependence of the linear elastic response on $\langle L \rangle$ is also reflected in the nonlinear response (Fig. 7.3 and the lower inset of Fig. 7.3). Networks with shorter filaments are increasingly governed by soft bending modes and thus exhibit a greater degree of stiffening under shear.

In the absence of motors, we find that our diluted phantom triangular networks exhibit a linear and nonlinear response to external shear that is consistent with previous work on 2D off-lattice networks of stiff filaments [24–26]. Our phantom triangular networks thus provide a good model system to study the effects of internal stresses generated by molecular motors in athermal networks.

7.3.2 Active networks

To investigate the effect of motor generated stresses we introduce force dipoles in the network at various densities ρ_{M}. Here, ρ_{M} represents the effective density of motors generating contractile forces at any given time. Thus, ρ_{M} is directly proportional to the duty ratio of the motors, i.e. the fraction of the time that a motor is attached to a filament [38]. After introducing the motors, the network is relaxed after which we determine the shear modulus of the active network. The shear modulus G increases strongly when the force exerted by a single motor f_0 is increased beyond a threshold value, as shown in Fig. 7.4. Interestingly, the motor forces at

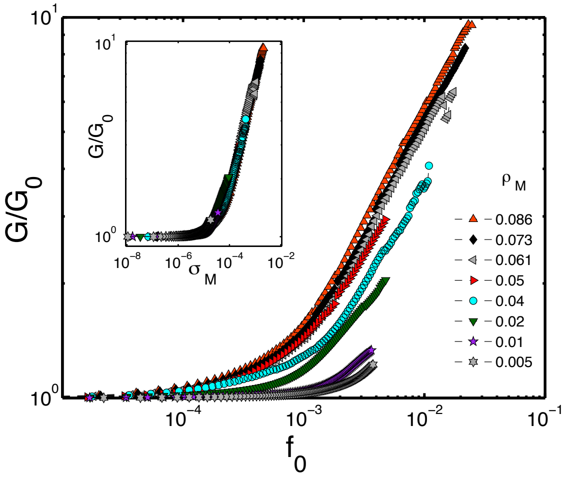

Figure 7.4 – (Color online) The shear modulus G as a function of force exerted per motor f_0 for various motor densities ρ_{M} at fixed $q = 1/4$ and $\kappa = 10^{-3}$. The shear modulus G is normalized by the shear modulus G_0 of the passive network. The inset shows the shear modulus G_0 as a function of the generated stress σ_{M}. The apparent collapse of these curves supports supports the hypotheses that σ_{M} is the appropriate control variable.

which the system becomes nonlinear for low motor densities is close to the buckling force threshold $f_b = \pi^2\kappa/\ell_c^2 \approx 2 \times 10^{-3}$. The buckling force threshold has been identified as an important force-scale for stiffening of these networks under external shear [29, 32]. In addition, these data imply that a minimum motor density is required for motor generated stiffening, consistent with recent experiments [7]. The characteristic motor-generated stress can be expressed as $\sigma_{\mathrm{M}} = \rho_{\mathrm{M}}\ell_0 f_0$. Remarkably, all stiffening curves can be collapsed by expressing the shear modulus as a function of σ_{M} (inset Fig. 7.4). This demonstrates that the characteristic motor generated stress σ_{M} is a useful quantity, even though the distribution of stress is likely to be highly heterogenous.

To explore the nature of the stiffening induced by motors we study the networks' response at various values of κ. We observe that motor activity dramatically increases the network stiffness over a range of κ values, as shown in Fig. 7.5. Interestingly, the degree of stiffening induced by motors stress is substantially larger for networks with lower κ, while for large κ we observe no stiffening at all. To compare the stiffening between the active and passive networks, we determine the critical stress for the onset of stiffening. When the linear mechanics of the networks is controlled by bending modes ($G \sim \kappa$) we find that σ_c scales linearly with κ for both active and passive networks, as shown in the inset Fig. 7.5. At larger bending rigidities σ_c saturates to

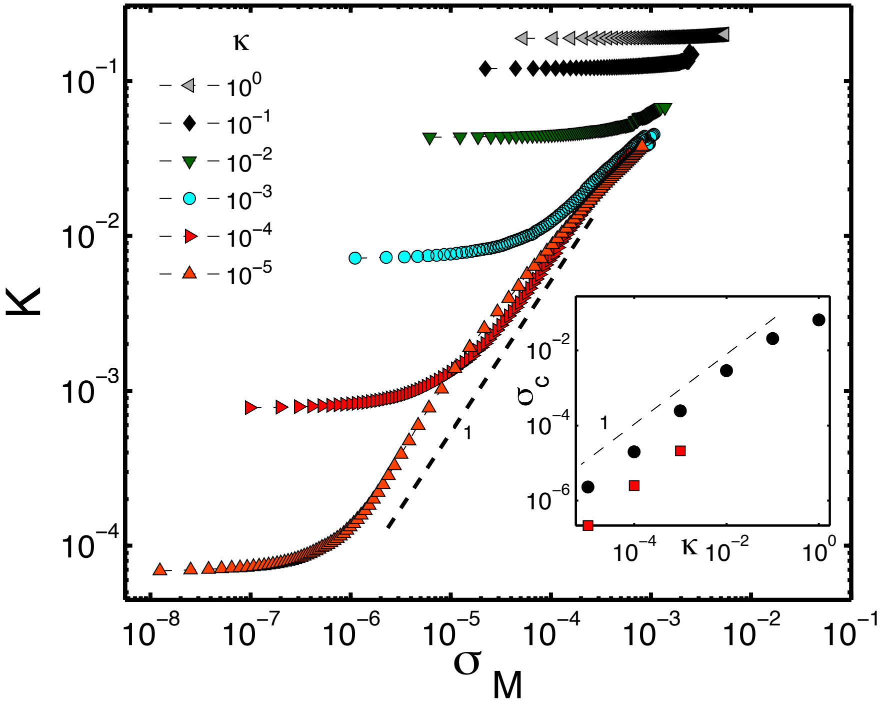

Figure 7.5 – (Color online) The linear shear modulus G as a function of motor generated stress σ_{M} for various of bending rigidities κ at fixed $q = 1/4$. The stiffening curves for networks with floppy filaments for $\kappa \lesssim 10^{-3}$ show an approximate scaling behavior given by $K \sim \sigma$, as shown by the dashed lines that indicate a slope of 1. The inset shows the critical stress for the onset of stiffening as a function of κ for both the active (red squares) and the passive (black circles) systems.

a value independent of κ. Interestingly, the values of σ_c for active floppy networks are substantially lower than for the passive networks. This indicates that internally generated motor stress is more effective in network stiffening than an external stress.

To identify the role of filament length in motor generated stiffening we vary q to tune $\langle L\rangle$. Interestingly, only networks with relatively short filaments stiffen strongly (Fig. 7.6). Networks with longer filaments are governed increasingly by the stretching modes in the system. This is consistent with the numerical data in Fig. 7.5, for which we observe that only bending dominated networks are capable of stiffening by motor activity. The critical stress for the onset of stiffening scales in the same way with $\langle L\rangle$ for the active networks as for the passive networks (inset Fig. 7.6), similar to what we observe for the scaling of σ_c with κ (inset Fig. 7.6). Taken together, these results provide evidence that the motor generated stiffening in the active networks derives from the same origin as the stiffening of passive networks under external shear.

The analogy between external stress and motor generated stress can be further explored by determining the effect of motor activity on the microscopic deformation field. The stiffening in passive networks has been attributed to a shear-induced cross-over between soft bending modes and stiffer stretching modes; concomitant with this cross-over the deformation becomes increasingly affine for larger strains [29]. Our simulations suggest that the same basic mechanism is responsible for the motor generated stiffening in non-affine networks. To further test this picture we investigate the microscopic deformation field of the these networks under a small external shear after they are relaxed in the presence of motors. We subtract the affine deformation $\delta\mathbf{r}_i^{(\mathrm{A})}$ of a cross-link i from the actual deformation $\delta\mathbf{r}_i$ to isolate the non-affine contribution,

$$\delta\mathbf{r}_i^{(\mathrm{NA})} = \delta\mathbf{r}_i - \delta\mathbf{r}_i^{(\mathrm{A})} \tag{7.3}$$

Consistent with prior work [24] for a passive networks deep in the bending dominated regime, we observe large non-affine deformations, as shown in Fig. 7.7a. In contrast, when motors are present the non-affine contribution to the deformation field is substantially reduced, as shown in Fig. 7.7b. Note, that the motors will initially generate highly non-affine deformations and large bends. These results show, however, that the subsequent deformation of this active network under a small external shear is considerably more affine than in the passive case. For small motor forces we do not expect to observe this effect; it was shown by Didona and Lubensky [39] that random stresses do not affect the non-affinity of the deformation in the linear regime. Our result provide insight into the motor induced stiffening we observe in our simulations (Figs. 7.5 and 7.6). Motor activity pulls out the floppy bend modes—thereby effectively constraining the network—which renders the network deformation more affine. This induces a cross-over from a response governed by bending modes to a response governed by stretching modes, which results in a stiffening of the networks response.

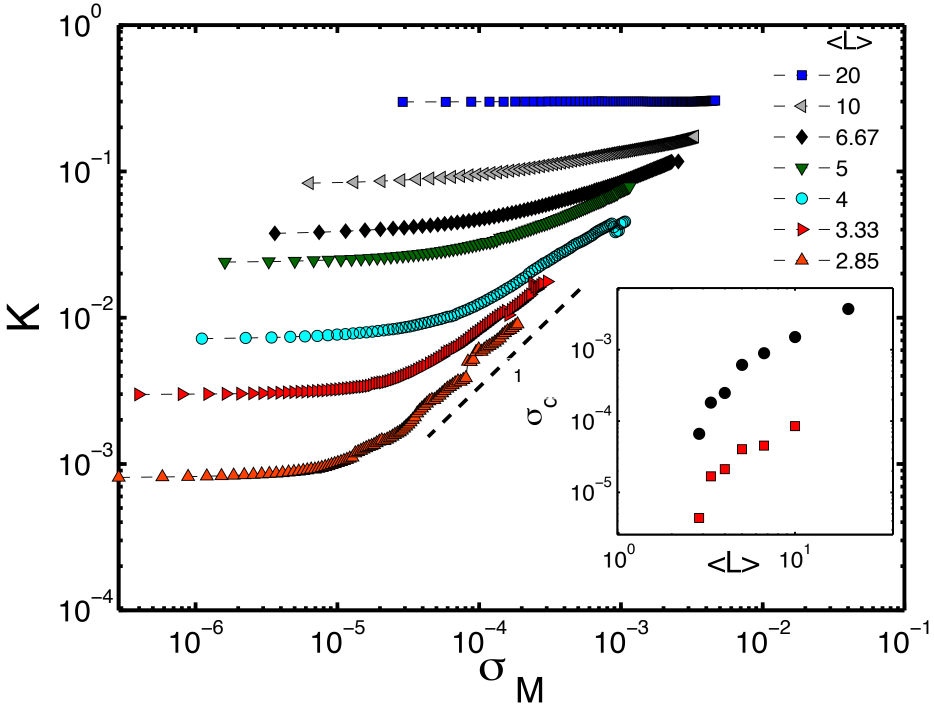

Figure 7.6 – (Color online) The linear shear modulus G as a function of motor generated stress σ_{M} for various values of $\langle L \rangle$ at fixes bending rigidity $\kappa = 10^{-3}$. The stiffening curves for $\langle L \rangle \lesssim 5$ show an approximate scaling behavior given by $K \sim \sigma$, as shown by the dashed lines that indicate a slope of 1. The inset shows the critical stress for the onset of stiffening as a function of $\langle L \rangle$ for both the active (red squares) and the passive (black circles) systems.

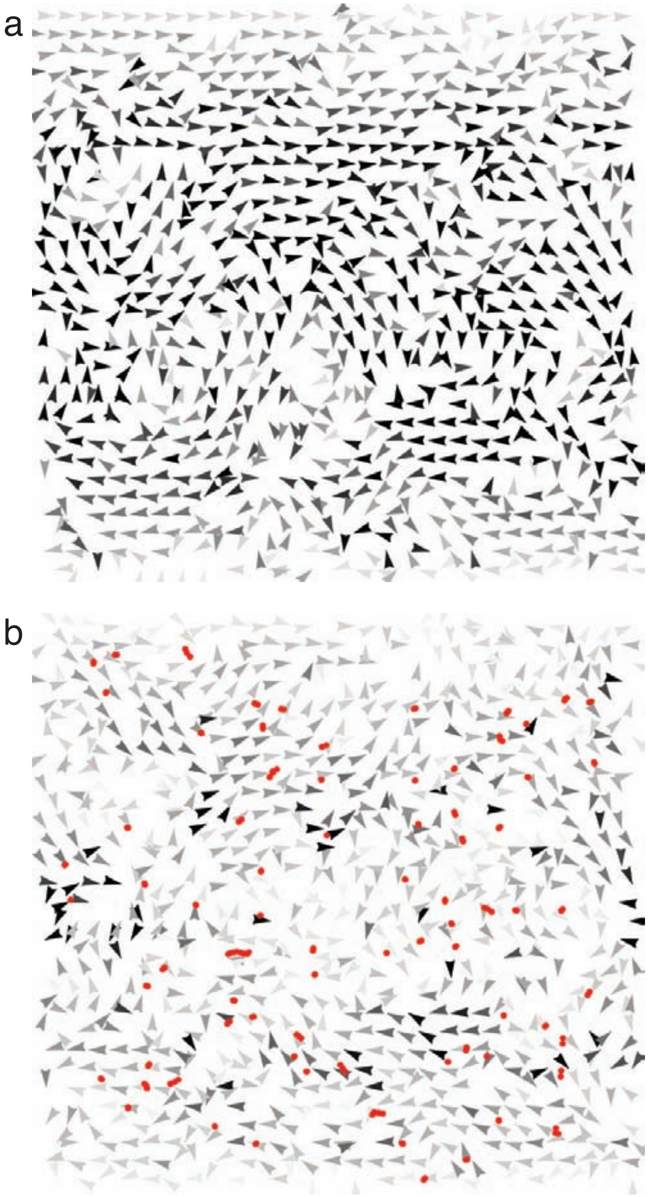

Figure 7.7 – The non-affine component of the deformation field under an external shear for a passive (a) network ($\kappa = 10^{-3}$ and $q = 1/4$) and for the same network with motors ($\rho_{\mathrm{M}} = 0.061$, $f_0 \sim 10^{-2}$) deep into the stiffened regime. The greyscale of the arrow heads indicate the magnitude of the non-affine deformation; black indicates a large magnitude (~ 0.01) and light grey a small magnitude (~ 0.001). The motors are shown as red dumbbells.

7.4 Conclusions

Here we have shown that molecular motors—modeled as force dipoles—stiffen non-affine networks. Interestingly, we find that only networks that are strongly governed by bending modes are capable of stiffening through motor activity. The internal stresses generated by the motors pull-out the floppy bending modes in the system, after which the network can only deform by means of the stiffer stretching modes. In this way, motors induce a cross-over to a stretching dominated regime, in analogy to prior results on externally-stressed networks [29, 32]. The absence of motor-induced stiffening of our networks in the stretching dominated regime can be attributed to the purely linear force-extension behavior of the filaments in our model. Analytical studies based on affine *stretching* dominated networks [18–20] and recent network simulations [40] have shown that motor activity can lead to stiffening when the expected non-linear force-extension relation of the network constituents is taken into account.

Nevertheless, within the model we consider, with purely linear elements, our results support the qualitative equivalence of external and internal stress in the non-linear network response [4, 7, 18]. So far, this correspondence has been understood in the context of stretching-dominated networks, with nonlinear filaments [18–20]. The present work shows that this analogy is more general. Interestingly, however, there are some quantitative differences between network stiffening by external load vs internal motor stresses. Specifically, our results support the idea that motor stresses can be more effective in generating stiffening, since they act in all directions [7]. By contrast, when a network is externally sheared, most stress is focussed on a small fraction of the filaments that are oriented the direction of extension. Furthermore, there are quantitative differences in the form of the stiffening response with stress in the present model. We find that motor contractility leads to an increase in the shear modulus with motor stress σ_M (Figs. 4, 5) that is approximately given by $G \sim \sigma_\mathrm{M}^x$, where $x \approx 1$. By contrast, the stiffening by external shear exhibits a more complex dependence on the stress, with two distinct regimes, corresponding to $x \simeq 1$ and $x \simeq 1/2$. One important difference that sets the passive networks apart, are the geometric effects that arise at large external shears through the collective alignment of filament in the direction of maximum extension.

The results presented here provide further insight into the mechanisms available for the active cellular cytoskeleton to regulate the mechanical behavior of the cell. Furthermore, these principles can inspire the design of novel active biomemetic materials with tunable elastic properties.

7.5 Acknowledgments

The authors thank I. Barmes, E. Conti, M. Das, M. Depken and L. Jawerth for fruitful discussions.

Bibliography

[1] B. Alberts, A. Johnson, J. Lewis, M. Ra, K. Roberts,and P. Walter, *Molecular Biology of the Cell* (Garland Science, 2002), 4th ed.

[2] C. P. Brangwynne, G. H. Koenderink, F. C. MacKintosh, and D. A. Weitz. *Cytoplasmic diffusion: molecular motors mix it up*. J. Cell Biol. **183**, 583 (2008).

[3] J. Joanny and J. Prost. *Active gels as a description of the actin-myosin cytoskeleton*. HFSP Journal **3**, 94 (2009).

[4] D. Mizuno, C. Tardin, C. F. Schmidt, and F. C. MacKintosh. *Nonequilibrium Mechanics of Active Cytoskeletal Networks*. Science **315**, 370 (2007).

[5] C. P. Brangwynne, G. H. Koenderink, F. C. MacKintosh, and D. A. Weitz. *Non-equilibrium microtubule fluctuations in a model cytoskeleton*. Phys. Rev. Lett. **100**, 118104 (2008).

[6] P. Bendix, G. Koenderink, D. Cuvelier, Z. Dogic, B. Koeleman, W. Brieher, C. Field, L. Mahadevan, and D. Weitz. *A quantitative analysis of contractility in active cytoskeletal protein networks*. Biophys. J. **94**, 3126 (2008).

[7] G. H. Koenderink, Z. Dogic, F. Nakamura, P. M. Bendix, F. C. MacKintosh, J. H. Hartwig, T. P. Stossel, and D. A. Weitz. *An active biopolymer network controlled by molecular motors* Proc. Natl. Acad. Sci. USA **106**, 15192 (2009).

[8] V. Schaller, C. Weber, C. Semmrich, E. Frey, and A. R. Bausch. *Polar Patterns of driven Filaments*. Nature **467**, 73 (2010).

[9] M. L. Gardel, J. H. Shin, F. C. MacKintosh, L. Mahadevan, P. A. Matsudaira, D. A. Weitz. *Elastic Behavior of Cross-Linked and Bundled Actin Networks*. Science **304**, 1301 (2004); Phys. Rev. Lett. **93**, 188102 (2004).

[10] C. Storm, J. Pastore, F. C. MacKintosh, T. C. Lubensky and P. A. Janmey. *Nonlinear elasticity in biological gels*. Nature **435**: 191 (2005).

[11] B. Wagner, R. Tharmann, I. Haase, M. Fischer and A. R. Bausch. *Cytoskeletal polymer networks: The molecular structure of cross-linkers determines macroscopic properties*. Proc. Nat. Acad. Sci. USA **103**, 13974 (2006).

[12] A. R. Bausch and K. Kroy. *A bottom-up approach to cell mechanics*. Nature Phys. **2**, 231 (2006) .

[13] R. Tharmann, M. M. Claessens, and A. R. Bausch. *Viscoelasticity of isotropically cross-linked actin networks*. Phys. Rev. Lett. **98**:088103 (2007).

[14] K. E. Kasza, G. H. Koenderink, Y. C. Lin, C. P. Broedersz, W. Messner, F. Nakamura, T. P. Stossel, F. C. MacKintosh, and D. A. Weitz. *Nonlinear elasticity of stiff biopolymers connected by flexible linkers*. Phys. Rev. E **79**:041928 (2009).

[15] C. P. Broedersz, K. E. Kasza, L. M. Jawerth, S. Münster, D. A. Weitz, and F. C. MacKintosh. *Measurement of Nonlinear rheology of cross-linked biopolymer gels*. Soft Matter **6**, 4120 (2010).

[16] K. Kruse, J. F. Joanny, F. Jlicher, J. Prost, and K. Sekimoto. *Generic theory of active polar gels: a paradigm for cytoskeletal dynamics*. Eur. Phys. J. E **16**, 5 (2005).

[17] J. F. Joanny, F. Jülicher, K. Kruse, and J. Prost. *Hydrodynamic theory for multi-component active polar gels*. New J. Phys. **9**, 422 (2007).

[18] F. C. MacKintosh and A. J. Levine. *Non-equilibrium mechanics and dynamics of motor-activated gels*. Phy. Rev. Lett. **100**, 018104 (2008).

[19] A. J. Levine and F. C. MacKintosh. *The mechanics and fluctuation spectrum of active gels*. J. Phys. Chem. **113**: 3820 (2009)

[20] T. B. Liverpool, M. C. Marchetti, J. Joanny, and J. Prost. *Mechanical response of active gels*. Europhys. Lett. **85**, 18007 (2009).

[21] F. C. MacKintosh and C. F. Schmidt. *Active cellular materials*. Curr. Opin. Cell Biol. **22**, 29 (2010).

[22] C. P. Broedersz, C. Storm, and F. C. MacKintosh. *Nonlinear elasticity of composite networks of stiff biopolymers with flexible linkers*. Phys. Rev. Lett. **101**:118103 (2008).

[23] D. A. Head and D. Mizuno. *Nonlocal fluctuation correlations in active gels*. Phys. Rev. E **8**, 041910 (2010).

[24] D. A. Head, A. J. Levine, and F. C. MacKintosh. *Distinct regimes of elastic response and deformation modes of cross-linked cytoskeletal and semiflexible polymer networks*. Phys. Rev. E **68**:061907 (2003).

[25] D. A. Head, A. J. Levine, and F. C. MacKintosh. *Deformation of crosslinked semiflexible polymer networks*. Phys. Rev. Lett. **91**, 108102 (2003).

[26] J. Wilhelm and E. Frey. *Elasticity of stiff polymer networks*, Phys. Rev.Lett. **91**, 108103 (2003).

[27] C. Heussinger and E. Frey. *Floppy modes and nonaffine deformations in random fiber networks*. Phys. Rev.Lett. **97**, 105501 (2006).

[28] M. Das, F. C. MacKintosh, and A. J. Levine. *Effective medium theory of semiflexible filamentous networks*. Phys. Rev.Lett. **99**, 038101 (2007).

[29] P. R. Onck, T. Koeman, T. van Dillen, and E. van der Giessen. *Alternative explanation of stiffening in cross-linked semiflexible networks*. Phys. Rev.Lett. **95**, 178102 (2005).

[30] O. Lieleg, M. M. A. E. Claessens, C. Heussinger, E. Frey and A. R. Bausch, *Mechanics of Bundled Semiflexible Polymer Networks*, Phys. Rev. Lett. **99**, 088102 (2007).

[31] E. M. Huisman, T. van Dillen, P. R. Onck, and E. Van der Giessen. *Three-Dimensional Cross-Linked F-Actin Networks: Relation between Network Architecture and Mechanical Behavior*. Phys. Rev. Lett. **99**, 208103 (2007).

[32] E. Conti, F. C. MacKintosh. *Cross-Linked Networks of Stiff Filaments Exhibit Negative Normal Stress*. Phys. Rev. Lett. **102**, 088102 (2009).

[33] F. C. MacKintosh, J. Käs, and P. Janmey. *Elasticity of Semiflexible Biopolymer Networks*. Phys. Rev. Lett. **75**, 4425 (1995).

[34] W. T. Vetterling and B. P. Flannery, Numerical Recipes in C++: The Art of Scientic Computing (Cambridge University Press, 2002), 2nd ed., ISBN 0521750334.

[35] C. P. Broedersz, C. Storm, and F. C. MacKintosh. *Effective-medium approach for stiff polymer networks with flexible cross-links*. Phys. Rev. E **79**:061914 (2009).

[36] C. P. Broedersz, X. Mao, F. C. MacKintosh, and T. C. Lubensky. *Criticality and isostaticity in fiber networks*. arXiv:1011.6535v1 (2010).

[37] M. Wyart, H. Liang, A. Kabla and L. Mahadevan *Elasticity of floppy and stiff random networks*. Phys. Rev. Lett. **101**, 215501 (2008).

[38] J. Howard. *Molecular motors: structural adaptations to cellular functions*. Nature **389**, 561 (1997).

[39] B. A. DiDonna and T. C. Lubensky, *Nonaffine correlations in random elastic media*. Phys. Rev. E **72**, 066619 (2005).

[40] P. Chen and V. B. Shenoy. *Strain Stiffening Induced by Molecular Motors in Active Crosslinked Biopolymer Networks*. Soft Matter **7**, 355 (2011).

8

Origins of elasticity in intermediate filament networks

- Y. C. Lin, N. Y. Yao, C. P. Broedersz, H. Herrmann, F. C. MacKintosh and D .A. Weitz
  Origins of elasticity in intermediate filament networks,
  Physical Review Letters, **104**: 058101 (2010)

- Y. C. Lin, C. P. Broedersz, A. C. Rowat, T. Wedig, H. Herrmann, F. C. MacKintosh and D. A. Weitz
  Divalent Cations Crosslink Vimentin Intermediate Filament Tail Domains to Regulate Network Mechanics,
  Journal of Molecular Biology **399**, 637-644 (2010)

- N. Y. Yao, C. P. Broedersz, Y. C. Lin, K. E. Kasza, F. C. MacKintosh and D. A. Weitz
  Elasticity in ionically cross-linked neurofilament networks,
  Biophysical Journal, **98** 2147-2153 (2010)

Abstract

Intermediate filaments are principal structural elements found in abundance in the cytosol of all metazoan cells, where they form networks that contribute to cellular elasticity. We measure the linear and nonlinear viscoelasticity of reconstituted networks of two distinct intermediate filaments, vimentin and neurofilaments. Each network exhibits predominantly elastic behavior and strong nonlinear strain stiffening. Divalent ions behave as effective cross-linkers for both networks. The network behavior is consistent with the affine thermal theory for networks of semi-flexible polymers.

8.1 Introduction

The mechanical response of cells depends largely on the structure and elasticity of their cytoskeleton, consisting of a variety of biopolymer networks, including filamentous actin, microtubules, and intermediate filaments (IFs) [1]. While filamentous actin and microtubules have been extensively studied, much less is known about IFs, although some key parameters such as their persistence length have been measured [2]. Compared to actin and microtubules, IFs are more varied and specialized. Their networks are cytoskeletal components contributing to the elasticity of the cell: there are five families of IFs found in a variety of cell types, ranging from muscles to neurons. Intermediate filament networks exhibit pronounced nonlinear elasticity similar to that observed in actin networks that are cross-linked. However, there are myriad associated actin-binding proteins that lead to this cross-linking; by contrast, fewer cross-linking proteins have been identified for IFs [3,4]. Thus, the origin of the nonlinear elasticity in IF networks has not been identified.

Here, we investigate the elasticity of two different IF networks, *vimentin* and *neurofilaments* (NFs). The networks exhibit remarkably similar mechanical properties: they are weak elastic solids even at the lowest frequencies probed and they exhibit strong nonlinear strain stiffening over several decades in stress. This behavior requires cross-linking of the network and we show that divalent ions act as effective cross-linkers. By comparing the linear and nonlinear macroscopic behavior, we extract microscopic network parameters. These observations suggest a general design principle for regulating the elasticity of intermediate filament networks even in the absence of specific cross-linking proteins.

To explore the generality of this behavior, we use NFs, found only in neurons, and vimentin, found in nearly all mesenchymal cells. The main difference between these

IFs lies in the length of their negatively charged carboxy terminal tail domains; NF tail domains are much longer than those of vimentin and appear as sidearms extending from the NFs enabling the formation of lateral bonds between NFs [6]. The tail domains of vimentin are also thought to be important for inter-filament interactions, although their precise role is not as clear as in the case of NFs [7, 8]. Furthermore, optimal assembly is obtained at different ionic conditions, with NFs favoring a pH of 6.2, where vimentin does not assemble properly [9].

8.2 Materials and methods

Neurofilaments are purified from bovine spinal cords [10–12]: fresh tissue is homogenized, then centrifuged, after which the crude neurofilament pellet is purified overnight on a discontinuous sucrose gradient with 0.8 M sucrose (5.9 ml), 1.5 M sucrose (1.3 ml) and 2.0 M sucrose (1.0 ml). The purified neurofilament is then dialyzed for 76 hours and afterwards 120 μl aliquots are flash frozen in liquid nitrogen and stored at -80 °C. Human vimentin protein is expressed in Escherichia coli and purified from inclusion bodies [13]. The protein is stored at -80 °C in 8 M urea, 5 mM Tris-HCl (pH 7.5), 1 mM DTT, 1 mM EDTA, 0.1 mM EGTA, and 10 mM methyl ammonium chloride. Twenty-four hours before use, we renature the protein from 8 M urea by stepwise dialysis (6 M, 4 M, 2 M) into a solution of 5 mM Tris-HCl, pH 8.4, 1 mM EDTA, 0.1 mM EGTA, and 1 mM DTT. The protein concentration is determined using a Bradford assay with bovine serum albumin (BSA) as a standard.

The mechanical response of intermediate filament networks is measured with a stress-controlled rheometer using a 2° 20mm cone-plate geometry (HR Nano, Bohlin Instruments). Before rheological testing, neurofilament samples are thawed on ice, after which, varying concentrations of Mg^{2+} are added. Vimentin polymerization is initiated by adding Mg^{2+} and 1/10 of the final sample volume of 10X polymerization buffer (0.2 M Tris-HCl, pH 7.0, containing 1.6 M NaCl). The samples are quickly loaded onto the rheometer and polymerized between the rheometer plates for one hour at 25 °C, using a solvent trap to prevent drying. We measure the linear viscoelastic moduli $G'(\omega)$, $G''(\omega)$. In addition, we use large amplitude oscillatory measurements to qualify the network's nonlinearity. However, to better quantify the network's nonlinear behavior we utilize a differential measurement [14, 15]. The system is held at a constant average (pre-)stress σ, while the differential response $d\gamma$ to a small additional oscillatory stress $d\sigma$ is measured. This measures the nonlinear tangent modulus $K = d\sigma/d\gamma$.

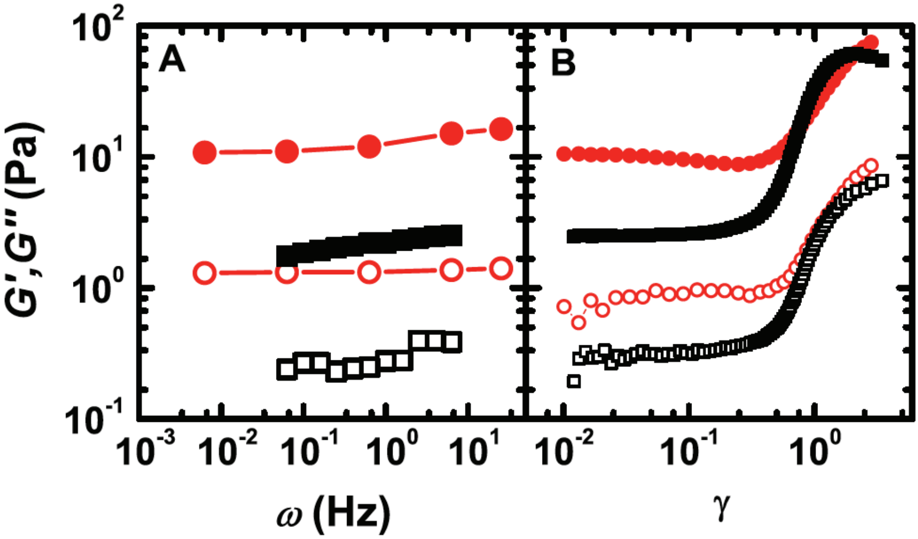

Figure 8.1 – (Color online). A) G' (solid symbols) and G'' (open symbols) as a function of frequency in the linear regime. B) G' (solid symbols) and G'' (open symbols) as a function of strain, γ. Samples of vimentin (squares) and neurofilaments (circles) are probed at a 2 mg/ml filament concentration and 5 mM Mg^{2+}.

8.3 Results and discussion

To investigate the origin of elasticity in intermediate filament networks, we probe the frequency dependence of the linear viscoelastic moduli. Consistent with other biopolymer networks, both G' and G'' depend weakly on frequency (from 0.01-10 Hz), with G' much larger than G'', as shown in Fig. 8.1A. This suggests the existence of soft cross-linked gels. We characterize the linear elasticity by the plateau modulus, G_0, the value of $G'(\omega)$ at 0.1 Hz. Interestingly, for purely entangled networks of similar concentration, we would expect the moduli of the two IF networks to be comparable; the fact that NFs are about an order of magnitude stiffer can be accounted for by cross-linking. The networks also exhibit dramatic strain stiffening above a critical strain γ_c, as shown in Fig. 8.1B.

For both IFs, the elasticity depends strongly on the polymer concentration and also on the concentration of Mg^{2+} added to the solution [16]. By analogy to prior studies of biopolymer networks [15, 17], we examine the dependence on IF concentration c_{IF}, at a fixed mole ratio, R of Mg^{2+} to IF. For both vimentin and NFs, the linear elastic modulus increases with filament concentration in a way similar to cross-linked F-actin networks, in that the modulus scales slightly stronger than quadratically with

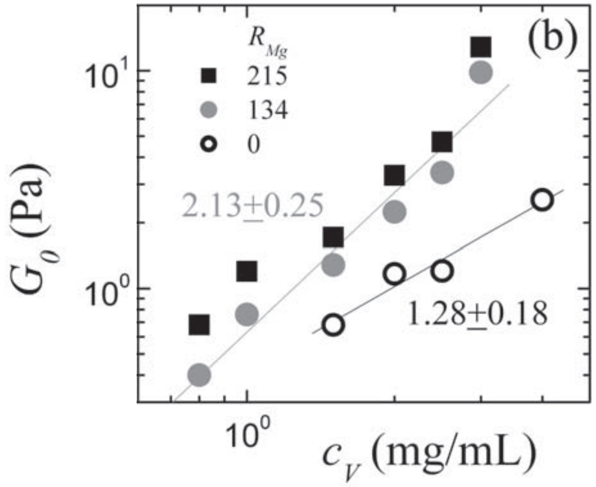

Figure 8.2 – Dependence of the linear elastic modulus, G_0, of vimentin with a concentration c_V. In the absence of divalent cations, $G_0 \sim c_V^{1.3}$, while in the presence of divalent cations, the concentration dependence becomes $G_0 \sim c_V^{2.1}$

filament concentration, as shown in Fig. 8.3A. This is consistent with a theoretical model for cross-linked semiflexible polymers, in which the elasticity is dominated by entropic filament stretching; in this affine thermal model, the filaments are considered to be entropic springs, leading to $G_0 \sim c_{\mathrm{IF}}^{11/5}$ [18]. In addition, we also find that G_0 scales directly with c_{Mg}, as shown in Fig. 8.3B, demonstrating the role of Mg^{2+} in the network elasticity for both IFs. Interestingly, in the absence of divalent cations, $G_0 \sim c_V^{1.28}$ (Fig. 8.2, open circles), which, within our measurement error, is consistent with $G_0 \sim c_V^{7/5}$, as expected for an entangled solution of semiflexible polymers [19–21]. Taken together, these findings suggest that divalent cations behave as crosslinkers for IF networks.

To elucidate the role of Mg^{2+} as a network cross-linker, we investigate the nonlinear elastic regime of IF networks by probing the differential moduli [15]. Above a critical stress σ_c, both IF networks display pronounced nonlinear stiffening with applied stress, exhibiting an approximate power law of 3/2, as shown in Fig. 8.4. This is consistent with theoretical expectations and previous experiments for cross-linked networks, where nonlinear elasticity results from the stretching out of thermal fluctuations of network strands between cross-links [15, 17, 18, 22]. Interestingly, the predictions of the affine thermal model apply for networks cross-linked by molecular linkers and experiments have focused on actin-linkers such as scruin. The absence

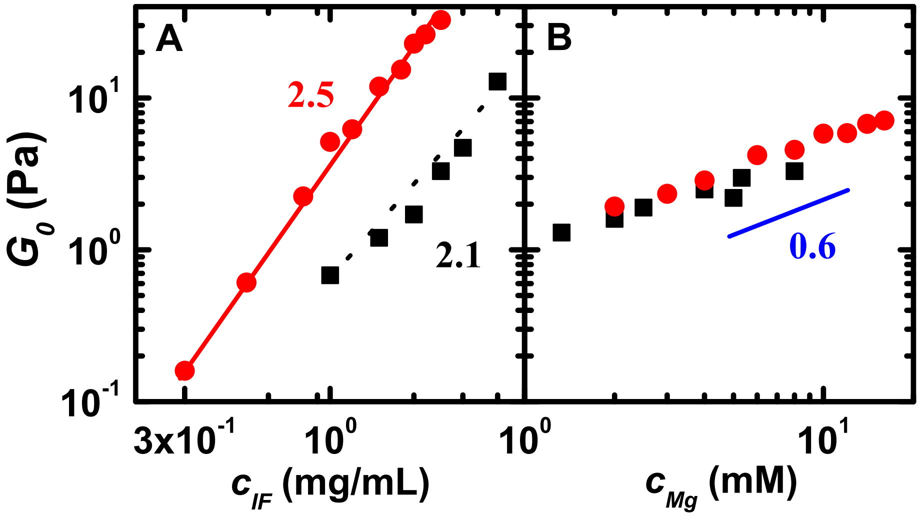

Figure 8.3 – (Color online). A) G_0 as a function of c_{IF} holding R constant, where $R = 1000$ for neurofilaments (circles) and $R = 215$ for vimentin (squares). The solid line is obtained using a regression fit and depicts $G_0 \sim c_{\mathrm{NF}}^{2.5}$ for neurofilaments, while the dashed line indicates $G_0 \sim c_{\mathrm{V}}^{2.1}$. B) G_0 as a function of c_{Mg} holding c_{IF} constant, where $c_{\mathrm{IF}} = 1$ mg/ml for neurofilaments (circles) and $c_{\mathrm{IF}} = 2$ mg/ml for vimentin (squares).

of molecular linkers in these IF networks suggests that ions may be playing the role of permanent effective molecular cross-links, lending insight into the nature of ionic interactions in IF networks. Previously, these ionic interactions have been understood within a framework of condensed counterions and salt-bridging on polyelectrolyte brushes [23–25]. We hypothesize that Mg^{2+} mediates attractive interactions between the negatively charged tail domains of the IFs thereby forming permanent cross-links analogous to molecular linkers. In particular, IF tail domains are likely collapsed flexible chains, and the cross-linking interactions would be mediated by a collection of divalent ions interwoven into the entangled tail domain structure. Although tail domains of a single chain will likely cross-link within themselves, only cross-linking between different chains will contribute to network elasticity. Theoretically we expect a universal form for the nonlinear elastic response of the networks for all protein and ion concentrations. The data sets from both neurofilament and vimentin networks can, indeed, be scaled onto a single master curve, which is in good agreement with the theoretical prediction shown by the solid line in the inset of Fig. 8.4 [15, 17]. Here, we fit each data set to the full theoretical curve, using two independent parameters: σ is scaled by σ_c, while K' is scaled by the linear elastic modulus G_0. For both networks, we find excellent agreement with the theoretical curve for approximately four decades in stress, although vimentin departs from the theoretical master curve at the highest stresses. This departure can be accounted for by considering the enthalpic contribution of filament backbone stretching [26], suggesting that the Young's modulus of vimentin is less than that of neurofilaments, as discussed further below.

To further probe the mechanism of the network elasticity, we test the predicted relationship between the scale factors used above, G_0 and σ_c. Assuming an affine deformation, theory predicts the curve shown in the inset of Fig. 8.4, with

$$G_0 = 6\rho k_B T \frac{l_p^2}{l_c^3} \tag{8.1}$$

$$\sigma_c = \rho k_B T \frac{l_p}{l_c^2} \tag{8.2}$$

Here, k_B is Boltzmann's constant, T is the temperature, ρ is the filament density in length per volume, l_p is the persistence length, and l_c is the average distance between cross-links [15, 17, 18, 28]. Since $\rho \propto c_{\mathrm{IF}}$, the model predicts that $c_{\mathrm{IF}}^{1/2} G_0 \sim \sigma_c^{3/2}$, where the pre-factor should depend only on $k_B T$ and l_p. In particular, this relationship is predicted to be independent of l_c, so that even data sets with different cross-link densities should collapse onto a single curve. Both vimentin and NF networks agree with this data collapse and scaling for a variety of different filament and Mg^{2+} concentrations, as shown in Fig. 8.5. In the case of NFs, the generality of this ionic cross-linking behavior is depicted by a qualitative collapse onto the same curve for other divalent ions such as Ca^{2+} and Zn^{2+}. This scaling relates the linear elasticity

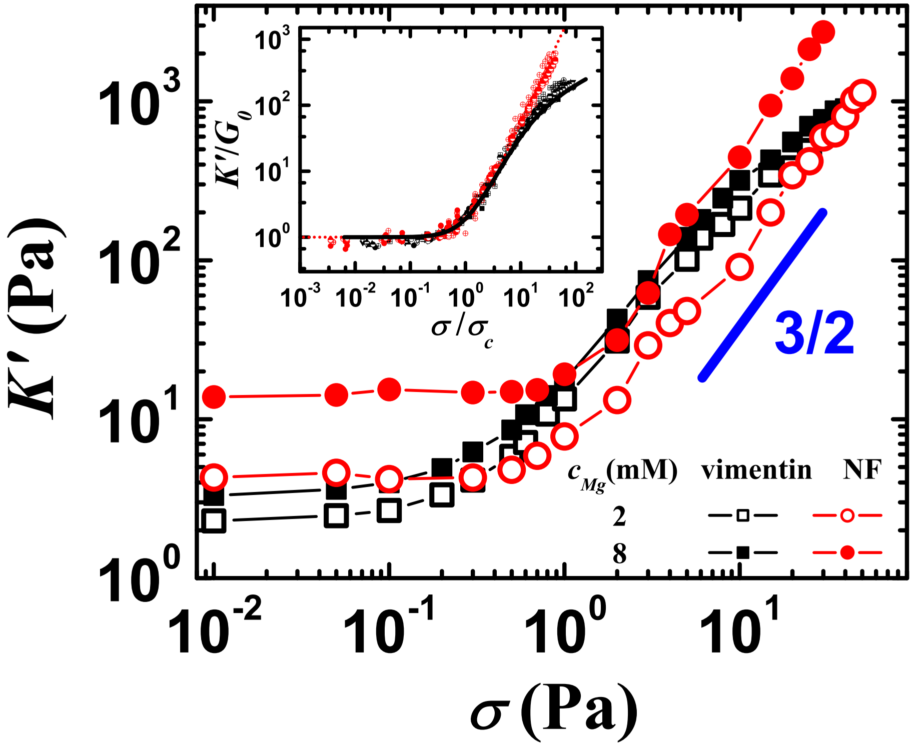

Figure 8.4 – (Color online). K' at 0.6 rad/sec as a function of σ for vimentin and neurofilament networks: [$c_{\mathrm{Mg}} = 2$ mM (open symbols), $c_{\mathrm{Mg}} = 8$ mM (solid symbols) and $c_{\mathrm{IF}} = 2$ mg/ml (all symbols)]. The solid line shows a 3/2 power law. The inset shows the data sets rescaled by σ_c and G_0 depicting the universal form of the stiffening response; the rescaled theory is indicated by the dashed red line, while the solid black line depicts the deviation due to enthalpic backbone stretching

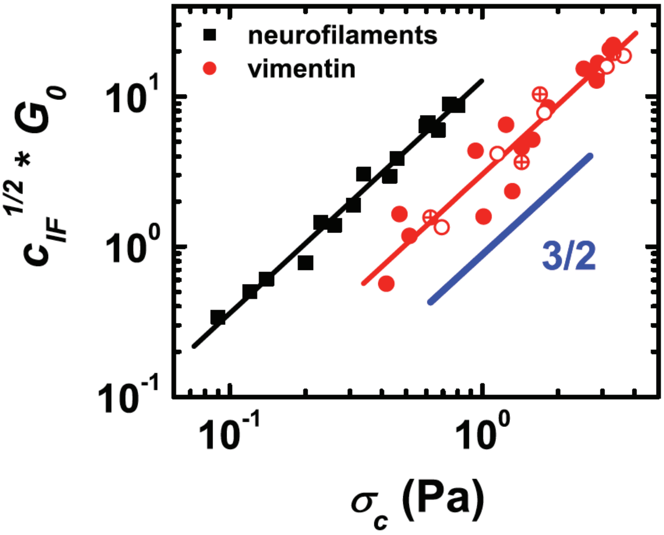

Figure 8.5 – (Color online). The dependence of $c_{\mathrm{IF}}^{1/2}G_0$ on σ_c. Vimentin data points are obtained with Mg^{2+}, while NF data points are obtained with Mg^{2+} (closed circles), Ca^{2+} (open circles), and Zn^{2+} (crossed circles). The solid lines reflect regression fits. The affine thermal model predicts a power law of 3/2, shown for reference.

of the networks to the stress at which nonlinear behavior begins as the filaments approach their full extension; therefore, it is independent of the scaling of K_0 with σ in Fig. 8.4. This provides strong evidence that the linear elasticity of IF networks is also governed by entropic stretching.

The relative shift between the two curves in Fig. 8.5. can be explained by a difference in persistence lengths of the filaments. Remarkably, we can precisely determine this persistence length directly from the macroscopic network behavior under shear. Using Eqs. (8.1) and (8.3) together with the bulk rheology yields

$$l_p = \frac{1}{36}\rho k_B T \frac{G_0^2}{\sigma_c^3}, \tag{8.3}$$

where $\rho \approx 0.5 \times 10^{13}$ m^{-2} for IF networks at a concentration of 4 μM. We find that for NFs, $l_p \approx 0.2$ μm, while for vimentin, $l_p \approx 0.5$ μm; both of these values are in good accord with previous experiments [2, 29–31]. Furthermore, we are also able to determine the cross-linking lengthscale,

$$l_c = 6 l_p \frac{\sigma_c}{G_0}, \tag{8.4}$$

where we have obtained l_p directly from bulk rheological parameters using Eq. (8.3). Direct determination of l_c is difficult and has rarely been made in such systems [32]. Here, we find that $l_c \approx 0.3$ μm for NFs and $l_c \approx 0.6$ μm for vimentin. This is consistent with our hypothesis that the filaments are cross-linked on the scale of their persistence length and thus the networks can be characterized as semiflexible.

To further examine the behavior of Mg^{2+} as a cross-linker, we consider the scaling of l_c as a function of both R and c_{IF} (Eq. (8.4)). Cross-linking occurs on the scale of the entanglement length l_e, which scales as $c_{\mathrm{IF}}^{-2/5}$ [18,33]. Since our data suggest that Mg^{2+} is effectively a cross-linker, we expect l_c to scale with R^{-x} for some exponent x [15,17]. Consistent with the theoretical prediction, the data do exhibit an approximate scaling, $l_c \sim R^{-x} c_{\mathrm{IF}}^{-y} = c_{\mathrm{Mg}}^{-x} c_{\mathrm{IF}}^{x-y}$; $x \approx 0.23$ for both IFs and $y \approx 0.4$ for vimentin and $y \approx 0.5$ for neurofilaments, measured at fixed R, as shown in Fig. 8.6. Interestingly, the larger value of y for NFs is consistent with the correspondingly stronger concentration dependence of G_0 as observed in Fig. 8.3. This may be a consequence of denser cross-linking; then we expect $G_0 \sim c_{\mathrm{NF}}^{5/2}$ [18]. Furthermore, as a consistency check for the value of x, we can also determine it directly from the c_{Mg} dependence of G_0. Inserting a scaling of $l_c \sim R^{-x}$ into Eq. (8.1) gives $G_0 \sim c_{\mathrm{Mg}}^{3x}$, holding c_{IF} fixed. Based on the scaling of G_0 in Fig. 8.3B, we find $x \approx 0.20$, in good accord with the value measured directly from the c_{Mg} dependence of l_c. Both the excellent agreement with theory and the internal consistency of our measurements provides convincing evidence that Mg^{2+} effectively cross-links IF networks. Moreover, we find similar behavior for Ca^{2+} and Zn^{2+}.

The values we observe for G_0 and the maximum stress are consistent with most previous experiments [1, 12], although one experiment with NFs yielded a smaller modulus and solution like behavior [34]. Remarkably, we can extract the microstructural parameters l_p and l_c directly from bulk rheology; values of l_p are consistent with previous measurements [29], while values of l_c are comparable to the expected mesh size $\xi \approx 1/\sqrt{\rho}$. Compared with vimentin, NFs consistently exhibit smaller values of l_c, suggesting a more densely cross-linked network; this may result from the longer NF tail domains and concomitantly stronger electrostatic interactions. Measurements based on probe particle motion in IF networks have suggested larger values of ξ [34]; however, recent measurements yield results which are more consistent with the expected value [35].

At the very highest stresses, $\sigma/\sigma_c > 10$, the experimental data deviate significantly from the theoretical prediction (inset Fig. 8.4). This deviation could result from irreversible network fracture or failure; however, we find that in the high stress regime just below σ_{max}, the elastic behavior is fully reversible on the timescales of our measurements (Fig. 8.7). Alternatively, the observed behavior could result from slippage between crosslinks, as can occur in a solution or transiently-crosslinked system, such as F-actin solutions without permanent crosslinks [37]; however, such a

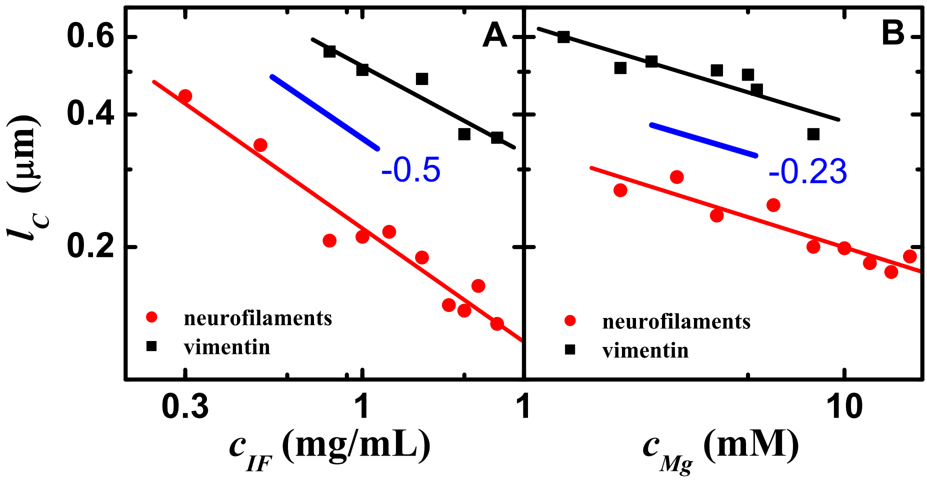

Figure 8.6 – (Color online). A: the dependence of l_c on c_{IF}. A power law of -0.5 is shown for reference. B: the dependence of l_c on c_{Mg}. A regression fit results in a power law of -0.23 for both vimentin and neurofilament networks.

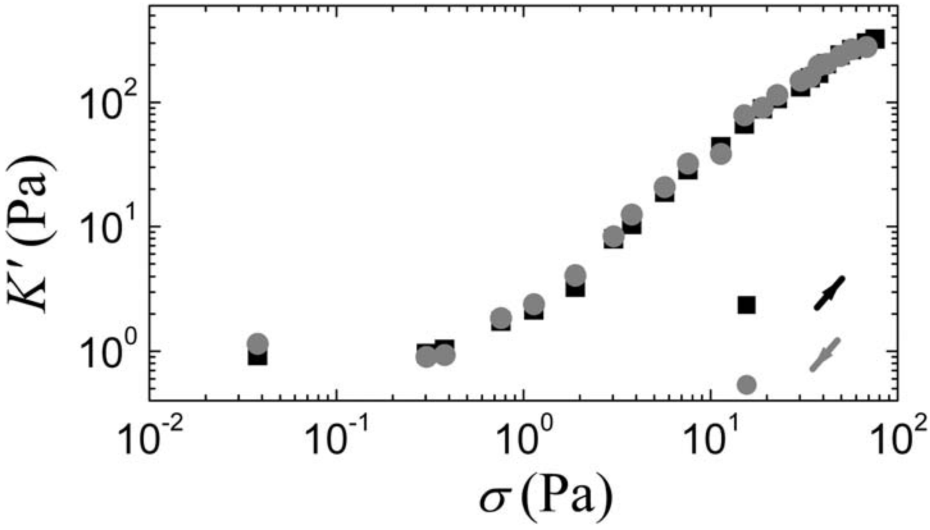

Figure 8.7 – Hysteresis test for vimentin networks at high applying stress. The entire linear and nonlinear elastic response of vimentin networks are highly reversible; the time between each data point is $1-2$ minutes.

data collapse (Fig. 8.4) is not possible when the stiffening exponent varies with protein concentration, as observed for F-actin solutions [37]. Instead, we include the consequences of the extensibility of individual filaments. This is motivated by observations that many types of intermediate filaments are highly extensible compared to actin [1, 36, 38] and appear straightened in human keratinocyte cells subjected to large uniaxial strains of 100% [38]. The extensional modulus depends on intrinsic properties of individual filaments, and should thus be independent of ℓ_c, whereas the linear entropic modulus scales as $1/\ell_c^3$ [18]. Thus network response should be increasingly dominated by the enthalpic stretching mode for smaller values of ℓ_c or for increasing values of σ, where thermal fluctuations are pulled out thereby increasing the effective spring constant of the entropic mode. Consistent with this, the deviation of the data from the universal curve at high stress increases as ℓ_c decreases, as seen more clearly in the inset of Fig. 8.8.

To make a more quantitative comparison, we extend the inextensible, entropic model by introducing an enthalpic stretch modulus, E [26, 33]; this parameter describes the resistance of the filament to changes in its contour length, and is related to its intrinsic structure and material properties; for a linear elastic rod E represents the force required to stretch the rod to twice its original length. A value for E can be estimated by assuming the filament behaves as a homogeneous elastic rod of diameter, ≈ 10 nm, for which $E \approx 4k_\mathrm{B}T\ell_p/r^2 \approx 463$ pN. Interestingly this is comparable to the force required to unfold coiled-coil domains of vimentin dimers [39], $200-300$ pN. However, at the point where we observe network failure, we estimate that the filaments are stretched to less than twice their length. Moreover, the resulting filament tension is borne by the 16 dimers in cross-section [40]. Thus, these networks break upon application of forces on a per dimer basis that are much lower than required to unfold the coiled-coil domains. The resulting predictions using this extended theoretical treatment require no further fitting parameters, and are in excellent agreement with each set of experimental data for the entire strain stiffening curves, as shown in the inset of Fig. 8.8. We also determine the Young's modulus $Y \approx 9$ MPa from the macroscoping rheological data using an affine theory for networks of extensible semiflexible polymers; this value is consistent with previously reported values of the keratin-like IF proteins from hagfish slime threads [3,41]. Thus, the full nonlinear behavior of vimentin networks is well described by this theory for crosslinked networks of stretchable, semiflexible polymers.

8.4 Conclusions

Vimentin and NF networks show striking similarity in their linear and nonlinear elastic behavior, both of which are governed by cross-linking due to divalent ions. Intrigu-

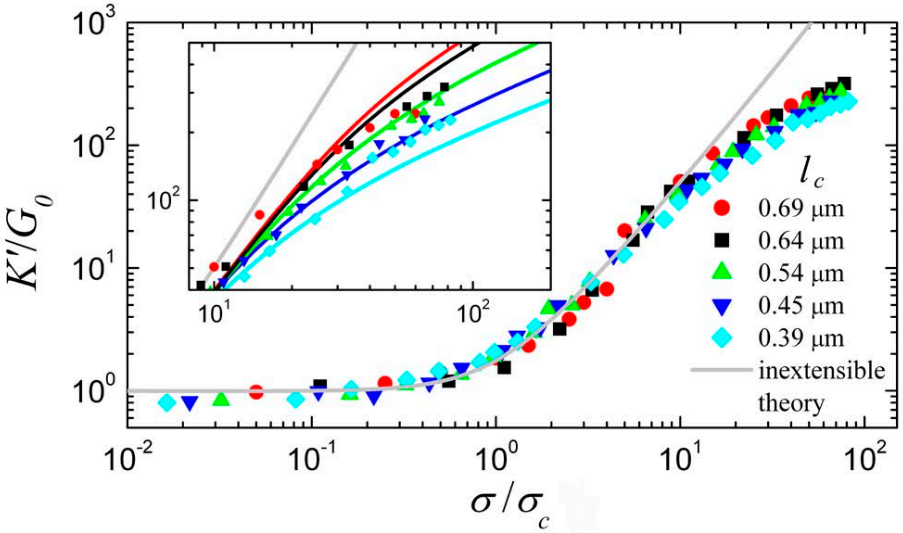

Figure 8.8 – Elastic response of vimentin networks results from stretching the entropic fluctuations of single semiflexible filaments at low to intermediate stresses; at high stress, enthalpic stretching of the individual filaments contributes to the nonlinear response. Each data set is rescaled by σ_c and G_0, revealing a data collapse which reflects the universal form of the entropic model or inextensible theory (grey line). The departure between the entropic model and our experimental data depends on the average cross-linking distance, ℓ_c: a larger departure is observed at high stress with decreasing ℓ_c. (Inset) A zoomed in version of the main graph showing each set of the experimental data (colored symbols), which are in agreement with the modified theory (colored lines) that captures the behavior of networks in all stress regimes. These theoretical curves are calculated directly using the values of ℓ_p and ℓ_c obtained by determining G_0 and σ_c together with Eqns. (8.3)-(8.4) and an extensional modulus for vimentin calculated from $E \approx 4k_\mathrm{B}T\ell_p/r^2$. Thus, this calculation requires no further fitting procedure.

ingly, divalent ions play a role nearly identical to that of molecular cross-linkers in F-actin networks. This suggests that there is a strong affinity of the divalent ions to the IFs; thus, a large fraction of the ions must be bound hence becoming effective molecular cross-links. Despite the similarities in their mechanical behavior, the nonlinear rheology of vimentin shows a clear departure from that of NFs at the highest stresses; this results from the enthalpic contribution of filament backbone stretching [26]. By contrast NFs do not exhibit a measurable filament compliance, implying that their Young's modulus is larger than that of vimentin; this is surprising given the similar molecular architecture of the backbone of the two IFs. This may reflect another important role of the tail domains: they might also affect the backbone stretching of filaments. However, this is based on macroscopic rheology, and direct force-extension measurements of individual filament stretching are needed to confirm this. Such filament extension experiments may also elucidate the nature of the electrostatic interactions that mediate effective molecular cross-linking between IFs.

8.5 Acknowledgements

This work was performed in collaboration with Y. C. Lin, N. Y. Yao, A. C. Rowat, T. Wedig, H. Herrmann, and D. A. Weitz. Y.C. Lin and N.Y. Yao contributed equally to this work. The authors acknowledge the insights of Fyl Pincus and discussions with P. Janmey on neurofilament rheology.

Bibliography

[1] O. I. Wagner, S. Rammenseec, N. Kordea, Q. Wena, J.-F. Leterrierd, and P. A. Janmeya. *Softness, strength and self-repair in intermediate filament networks* Exp. Cell. Res. **313**, 2228 (2007).

[2] N. Mücke, L. Kreplak, R. Kirmse, T. Wedig, H. Herrmann, U. Aebi and J. Langowski1. *Assessing the Flexibility of Intermediate Filaments by Atomic Force Microscopy*. Journal of Mol. Bio. **335**, 1241 (2004).

[3] M. Schaffeld, and J. Schultess. *Genes Coding for Intermediate Filament Proteins Closely Related to the Hagfish "Thread Keratins (TK)" Alpha and Gamma also Exist in Lamprey, Teleosts and Amphibians*. Exp. Cell. Res. **312**, 1447-1462 (2006).

[4] F.A. Steinbock, G. Wiche. *Plectin: a cytolinker by design*. Biol. Chem. **380** 151-158 (1999).

[5] K. Roper, S.L. Gregory, N.H. Brown. *The 'spectraplakins': cytoskeletal giants with characteristics of both spectrin and plakin families*, J. Cell Sci. **115**, 4215-4225 (2002).

[6] B. Alberts, A. Johnson, J. Lewis, M. Ra, K. Roberts,and P. Walter, *Molecular Biology of the Cell* (Garland Science, 2002), 4th ed.

[7] A. Eckelt, H. Herrmann, W. W. Franke. *Assembly of a tail-less mutant of the intermediate filament protein, vimentin, in vitro and in vivo*. Eur. J. Cell Biol. **58**, 319-330.

[8] M. B. McCormick, P. Kouklis, A. Syder, E. Fuchs *The roles of the rod end and the tail in vimentin IF assembly and IF network formation*. J. Cell Biol. **122**:395-407 (1993).

[9] H. Herrmann, and U. Aebi, *Guidebook to the Cytoskeletal and Motor Proteins*, Oxford University Press, (1999).

[10] A. Delacourte, G. Filliatreau, F. Boutteau, G. Biserte and J. Schrevel. *Study of the 10-nm-filament fraction isolated during the standard microtubule preparation*. Biochem. J. **191**, 543 (1980).

[11] J. F. Leterrier, and J. Eyer. *Properties of highly viscous gels formed by neurofilaments in vitro. A possible consequence of a specific inter-filament cross-bridging*. Biochem. J. **245**, 93 (1987).

[12] J. F. Leterrier, J. Käs, J. Hartwig, R. Vegners, and P. A. Janmey. *Mechanical Effects of Neurofilament Cross-bridges* J. Bio. Chem. **271**, 15687 (1996).

[13] H. Herrmann, I. Hofmann, and W. W. Franke. *Identification of a nonapeptide motif in the vimentin head domain involved in intermediate filament assembly*. J. Mol. Biol. **223**, 637 (1992).

[14] N. Y. Yao, R. Larsen, and D. A. Weitz. *Probing nonlinear rheology with inertio-elastic oscillations* J. Rheol. **52**, 13 (2008).

[15] M. L. Gardel, J. H. Shin, F. C. MacKintosh, L. Mahadevan, P. Matsudaira, and D. A. Weitz. *Elastic behavior of cross-linked and bundled actin networks*. Science **304**:1301-1305 (2004).

[16] J. Käs, H. Strey, J. X. Tang, D. Finger, R. Ezzell, E. Sackmann and P. A. Janmey. *et al*. *F-actin, a model polymer for semiflexible chains in dilute, semidilute, and liquid crystalline solutions*. Biophys. J. **70**, 609 (1996).

[17] M. L. Gardel, J. H. Shin, F. C. MacKintosh, L. Mahadevan, P. A. Matsudaira., and D. A. Weitz. *Scaling of F-actin network rheology to probe single filament elasticity and dynamics*. Phys. Rev. Lett. **93**:188102 (2004).

[18] F. C. MacKintosh, J. Käs, and P. Janmey. *Elasticity of Semiflexible Biopolymer Networks*. Phys. Rev. Lett. **75**, 4425 (1995).

[19] B. Hinner, M. Tempel, E. Sackmann, K. Kroy, and E. Frey. *Entanglement, elasticity, and viscous relaxation of actin solutions*. Phys. Rev. Lett. **81**, 2614 (1998).

[20] H. Isambert and A. C. Maggs. *Dynamics and rheology of actin solutions*. Macromolecules **29**, 1036-1040 (1996).

[21] D. C. Morse. *Viscoelasticity of concentrated isotropic solutions of semiflexible polymers: 2. Linear response*. Macromolecules, **31**, 7044-7067 (1998).

[22] M. Fixman and J. Kovac. *Polymer conformational statistics. III. Modified Gaussian model of stiff chains*. J. Chem. Phys. **58**, 4 1973.

[23] E. B. Zhulina and F. A. M. Leermakers. *A Self-Consistent Field Analysis of the Neurofilament Brush with Amino-Acid Resolution*. Biophys. J. **93**, 1421 (2007).

[24] S. Kumar, X. Yin, B. D. Trapp, J. H. Hoh, and M. E. Paulaitis. *Relating Interactions between Neurofilaments to the Structure of Axonal Neurofilament Distributions through Polymer Brush Models*. Biophys. J. **82**, 2360 (2002).

[25] J. C. Butler, T. Angelini, J. X. Tang, and G. C. L. Wong. *Ion Multivalence and Like-Charge Polyelectrolyte Attraction*. Phys. Rev. Lett. **91**, 028301 (2003).

[26] C. Storm, J. Pastore, F. C. MacKintosh, T. C. Lubensky and P. A. Janmey. *Nonlinear elasticity in biological gels*. Nature **435**:191 (2005).

[27] Y.-C. Lin, C. P. Broedersz, A. C. Rowat, T. Wedig, H. Herrmann, F. C. MacKintosh, D. A. Weitz. *Divalent Cations Crosslink Vimentin Intermediate Filament Tail Domains to Regulate Network Mechanics* J. Mol. Biol. **399**, 637-644 (2010).

[28] F. Gittes and F. C. MacKintosh. *Dynamic shear modulus of a semiflexible polymer network*. Phys. Rev. E **58**, R1241 (1998).

[29] Z. Dogic, J. Zhang, A. W. C. Lau, H. Aranda-Espinoza, P. Dalhaimer, D. E. Discher, P. A. Janmey, Randall D. Kamien, T. C. Lubensky, and A. G. Yodh. *Elongation and Fluctuations of Semiflexible Polymers in a Nematic Solvent*. Phys. Rev. Lett. **92**, (2004).

[30] P. A. Janmey, P. A. Janmey, U. Euteneuer, P. Traub, and M. Schliwa. *Viscoelastic properties of vimentin compared with other filamentous biopolymer networks*. J. Cell Bio. **113**, 115 (1991).

[31] M. Schopferer, H. Bär, B. Hochstei1, S. Sharma, N. Mücke, H. Herrmann and N. Willenbacher. *Desmin and Vimentin Intermediate Filament Networks: Their Viscoelastic Properties Investigated by Mechanical Rheometry* J. Mol. Bio. **388**, 133 (2009).

[32] R. Tharmann, M. M. Claessens, and A. R. Bausch. *Viscoelasticity of isotropically cross-linked actin networks*. Phys. Rev. Lett. **98**:088103 (2007).

[33] T. Odijk. *Stiff Chains and Filaments under Tension*. Macromolecules **28**, 7016 (1995).

[34] S. Rammensee, P. A. Janmey and A. R. Bausch. *Mechanical and structural properties of in vitro neurofilament hydrogels*. Euro. Biophys. J. **36**, 661 (2007).

[35] S. Koester, private communication (2009).

[36] L. Kreplak, H. Bar, J. F. Leterrier, H. Herrmann, U. and Aebi. *Exploring the Mechanical Behavior of Single Intermediate Filaments*. J. Mol. Biol. **354**, 569-577 (2005).

[37] C. Semmrich, R. J. Larsen, and A. R. Bausch. *Nonlinear Mechanics of Entangled F-actin Solutions*. Soft Matter **4**, 1675-1680 (2008).

[38] D. Fudge, D. Russell, D. Beriault, W. Moore, E.B. Lane, and A. W. Vogl. *The Intermediate Filament Network in Cultured Human Keratinocytes Is Remarkably Extensible and Resilient*. PLoS ONE **3**, e2327 (2008).

[39] Z. Qin, L. Kreplak, and M. J. Buehler. Hierarchical Structure Controls Nanomechanical Properties of Vimentin Intermediate Filaments. PLoS ONE **4**, e7294 (2009).

[40] A. C. Steven, J. Wall, J. Hainfeld, and P. M. Steinert. *Structure of Fibroblastic Intermediate Filaments: Analysis of Scanning Transmission Electron Microscopy*. Proc. Natl. Acad. Sci. USA **79**, 3101-3105 (1982).

[41] D. S. Fudge, K. H. Gardner, V. T. Forsyth, C. Riekel, and J. M. Gosline. *The Mechanical Properties of Hydrated Intermediate Filaments: Insights from Hagfish Slime Threads*. Biophys. J. **85**, 2015-2027 (2003).

Summary

In this thesis, we presented a study on the collective mechanical and dynamical behavior of biopolymer networks. The largest part of this work is dedicated to the development of theoretical models for these systems, although we have also included some experimental studies and an extensive discussion of the comparison between our theoretical predictions and experimental results. This work was part of a fruitful collaboration with various members of the lab of Dave Weitz at Harvard University.

My work is directly inspired by the cytoskeleton of living eukariotic cells. One of the major structural components of the cytoskeleton is actin, which forms several micrometers long filaments that are cross-linked into a network structure. The mechanical properties of the cytoskeleton are tightly controlled by a large number of actin binding proteins that enable diverse cellular behavior such as division, locomotion, and shape changes. Nucleating and capping proteins regulate the polymerization of monomeric actin into filamentous actin (F-actin). Crosslinking proteins bind the actin filaments together to form elastic gels and bundle structures, whereas motor protein assemblies control tension within these networks by internally straining the actin filaments. Even though the important molecular components are known, relatively little is understood of how this large ensemble of proteins collectively contributes to the mechanical response of the cytoskeleton. One approach to investigate the origins of the mechanical response of the complex and composite structure of the cytoskeleton has been to study reconstituted *in vitro* F-actin networks in the presence of purified binding proteins. These reconstituted networks form simplified modulus of the cytoskeleton and allow for a precise control of its biochemical composition, which enables a systematic investigation of its properties. Both on the theoretical and the experimental level, this thesis follows this approach to study biopolymer networks.

In chapter 2, we investigated the dynamics of semiflexible polymer networks with transient cross-links. The intrinsic dynamics of physiological actin cross-linkers may have important implications for the constantly remodeling internal networks of cells. Recent experiments on F-actin networks with transient linkers provide evidence of a complex viscoelastic behavior. We developed a microscopic model for the long time network relaxation governed by cross-link dynamics. This cross-link governed dynamics (CGD) model describes the structural relaxation that results from many independent cross-linker unbinding and rebinding events. We showed that this model provides a good quantitative description of the complex stress relaxation in these networks. Finally we discussed the effects of large stresses on the dynamic mechanical response of these networks. We observe that the unbinding rate of the linkers is dramatically reduced in networks that are subjected to a constant stress; this reflects a stabilization of the cross-linker-actin bond under an applied load. On the macroscopic scale, the applied stress enhances the solid-like nature of the gel.

In chapters 3 and 4, we investigated the nonlinear elasticity of stiff polymer networks with flexible cross-linkers. We quantitatively showed that the nonlinear elastic response of actin gels cross-linked with the physiological linker filamin can be accounted for by the highly flexible nature of the filamin cross-links. To describe these systems we developed a self-consistent mean field theory for the macroscopic nonlinear elasticity of these networks. The networks are modeled as a collection of randomly oriented rods connected by flexible linkers to a surrounding elastic continuum, which is required to self-consistently represent the behavior of the network. Using this model, we also showed that the dominating failure mode of these networks is due to the rupture of actin-filamin bonds.

In chapter 5, we examined various rheological protocols for the measurement of the nonlinear response of biopolymer gels. Using both strain ramp and differential prestress protocols, we investigated the nonlinear response of a variety of systems ranging from extracellular fibrin gels to intracellular F-actin solutions and F-actin cross-linked with permanent and physiological transient linkers. In particular, we designed a new experimental protocol to investigate how both the linear and nonlinear mechanical response changes as the system creeps and deforms plastically under a large applied shear stress. In this protocol the differential response is determined under steady shear stresses of varying magnitude alternated with periods without load. The total strain and differential response are monitored continuously. We found that the nonlinear response measured with the prestress protocol is remarkably insensitive to creep. This demonstrates that the nonlinear mechanical response of these biopolymer networks is robust, even when the network is flowing. By developing a simple, yet general phenomenological model that includes the nonlinear elasticity of the network as well as network flow on long timescales, we provided further insight into this behavior.

In chapter 6, we investigated the elasticity of random fiber networks. Fibrous networks, such as those that form the cellular cytoskeleton or the extracellular matrix, exhibit rigidity at remarkably low connectivity—well bellow the Maxwell central force isostatic point. This rigidity is due to additional constraints provided by the fibers' resistance to bending. We studied disordered fibrous networks with variable coordination number, both above and below the central-force isostatic point. This point controls a broad crossover from stretching- to bending-dominated elasticity. We showed that this crossover exhibits an anomalous power-law dependence of the shear modulus on both stretching and bending rigidities. At the central-force isostatic point—well above the rigidity threshold—we find divergent strain fluctuations together with an associated divergent correlation length, implying a breakdown of continuum elasticity. Thus, in this simple mechanical system we observe a remarkably rich demonstration of zero-temperature critical phenomena.

In chapter 7, we studied the effects of motor generated stresses on stiff polymer networks. Reconstituted *active* F-actin networks with motor proteins form a good model system for the study of cellular mechanics. The motor proteins generate forces that drive the network far from equilibrium and strongly affect the network mechanics. To elucidate the basic principles of the effects of force-generating motors on the mechanics of networks with the architecture of biopolymer networks with binary cross-links, we developed a lattice-based approach to design networks with a connectivity of 4 or less. We showed how heterogeneous internal stresses generated by motors can lead to stiffening in such networks that are governed by filament bending modes. The motors are modeled as force dipoles that cause muscle-like contractions. These contractions "pull out" the floppy bending modes in the system, which results in a dramatic stiffening of the networks' mechanical response.

In chapter 8, we investigated the origins of the elasticity of intermediate filament (IF) networks. Intermediate filament networks in the cytoplasm and nucleus are crucial for the mechanical integrity of metazoan cells. While filamentous actin and microtubules have been extensively studied, much less is known about IFs. In particular, the mechanism of cross-linking in these networks and the origins of their mechanical properties are not understood. In close collaboration with the experimental group of D. Weitz, we have shown that divalent ions can mediate a cross-linking interaction between the negatively charged tail domains of intermediate filaments. We used an affine model for the nonlinear elastic response of these systems, which includes both the entropic stiffening and the enthalpic stretching of the individual filaments, as well as geometric affects that arise in networks under large shear deformations. This model enabled us to extract microscopic parameters from the measured macroscopic rheological behavior, including the cross-linking lengthscale of the network as well as the Young's modulus and persistence length of the filaments.

Samenvatting

In dit proefschrift presenteren wij een studie naar het collectieve mechanische en dynamische gedrag van biopolymeernetwerken. Hoewel het grootste deel van dit werk gewijd is aan de ontwikkeling van theoretische modellen voor dit soort systemen, presenteren wij enkele experimentele studies en bespreken wij ook uitgebreid een vergelijking tussen onze theoretische voorspellingen en relevante experimentele resultaten. Dit werk maakt deel uit van een vruchtvolle samenwerkingen met meerdere leden van het laboratorium van Dave Weitz op Harvard University.

Het onderwerp van mijn onderzoek is grotendeels geïnspireerd door het cytoskelet van levende eukaryotisch cellen. Een van de belangrijkste structurele componenten van dit cytoskelet is actine. Dit eiwit vormt wormachtige vezels van enkele micrometers lang dat een verstrengelde netwerkstructuur vormt met talloze kruisverbindingen. Een grote verscheidenheid aan eiwitten wordt door de cel ingezet om de mechanische eigenschappen van het cytoskelet te reguleren voor diverse vitale processen zoals cel deling, cel beweging en cel vormveranderingen. Deze eiwitten organiseren de netwerkstructuur zoals bijvoorbeeld de nucleërende en afkappende eiwitten, die het polymeriseren van de actine monomeren in actine filamenten (F-actine) reguleren. Ook zijn er kruisverbindingvormende eiwitten die de actine filamenten aan elkaar linken om zo een elastische gel of bundel structuur te vormen, terwijl motoreiwitten een mechanische stress genereren in deze netwerken door te trekken aan de actine filamenten. Hoewel veel belangrijke moleculaire componenten inmiddels zijn geïdentificeerd, is er slechts weinig bekend over het collectieve gedrag van deze componenten en hoe dit leidt tot de mechanische respons van het cytoskelet als geheel. Een belangrijke benadering om de oorsprong van de mechanische respons van de complexe samengestelde structuur van het cytoskelet te achterhalen, is door gebruik te maken van gereconstrueerde *in vitro* F-actine netwerken met gepurificeerde bindende eiwitten. Deze methode maakt het mogelijk om de biochemische samenstelling van het netwerk heel precies te reguleren. Deze systemen vormen een vereenvoudigde module van het cytoskelet en ontlenen zich goed voor een systematische aanpak voor het onderzoeken van de fysische eigenschappen van deze netwerken. Zowel op een theoretisch als op een experimenteel niveau, hebben wij ons in dit proefschrift met name gericht op deze *in vitro* biopolymeernetwerken.

In hoofdstuk 2, hebben wij de dynamica van semiflexibele polymeernetwerken met kortlevende kruisverbindingen (linkers) bestudeerd. De intrinsieke dynamica van veel fysiologische linkereiwitten kan belangrijke implicaties hebben voor cellen, die voor een deel bestaan uit continu hervormende netwerken. Recente experimenten met F-actine netwerken met dynamische linkers hebben aangetoond dat deze systemen een complexe viscoelastische respons hebben. Om dit te beschrijven hebben wij een microscopisch model ontwikkeld voor de netwerkrelaxatie op langere tijdschalen die door de dynamica van de kortlevende linkers bepaald wordt. Dit "cross-link governed dynamics"(CGD) model beschrijft de structurele relaxatie die mogelijk gemaakt wordt door het continue formeren en verbreken van kruisverbindingen in het netwerk. We hebben laten zien dat dit model een goede kwantitatieve beschrijving geeft van het complexe viscoelastische gedrag van de actine netwerken met fysiologische linkereiwitten. Tot slot, hebben wij in dit hoofdstuk de gevolgen van grote mechanische stressen op de dynamische eigenschappen van het netwerk besproken. Deze stressen hebben een opmerkelijke invloed op de dynamica van de linkers. De frequentie waarmee kruisverbindingen in het netwerk verbroken worden, neemt af naarmate de stress opgevoerd wordt. Dit is een indicatie dat de stabiliteit van de kruisverbinding toe neemt als er een kracht op uitgeoefend wordt. Op de macroscopische schaal leidt dit ongewone gedrag er toe dat het netwerk zich in toenemende mate als een vaste stof gaat gedragen als er stress op uitgeoefend wordt.

In hoofdstukken 3 en 4, bestuderen we de niet-lineaire elastische eigenschappen van netwerken van stijve polymeren met flexibele linkers. We tonen aan dat de niet-lineaire eigenschappen van F-actine netwerken met de fysiologische linker filamine kan volgen uit het zeer flexibele gedrag van de filamine linkers. We ontwikkelen een kwantitatieve zelf-consistente mean-field model voor de macroscopische niet-lineaire elasticiteit van de netwerken. De netwerken worden beschreven als een verzameling van stijve fibers die verbonden zijn door flexibele linkers met een effectief medium dat op een zelf-consistente wijze de niet-lineaire eigenschappen van het netwerk bezit. Met behulp van dit model tonen wij tevens aan dat het breken van de experimentele netwerken veroorzaakt wordt door het verbreken van de actine-filamine verbindingen.

In hoofdstuk 5, bespreken we verschillende rheologische methoden om de niet-lineaire respons van biopolymeernetwerken te bepalen. Door gebruik te maken van de strain ramp en de differentiële prestress methode, onderzoeken wij de niet-lineaire respons van meerdere systemen, variërend van extracellulaire fibrine gels tot intracellulaire F-actine oplossingen en F-actine netwerken met zowel permanente als fysiologische kortlevende linkers. We hebben een nieuw protocol ontwikkeld om zowel de lineaire als de niet-lineaire mechanische eigenschappen van systemen te onderzoeken die plastisch deformeren of vloeien onder grote aangelegde stressen. In dit protocol wordt de differentiële respons bepaald in de aanwezigheid van een constante stress van variërende grote, afgewisseld met periodes zonder stress. Gedurende dit proces wordt de totale strain en de differentiële respons continu bepaald. Met dit onderzoek hebben we sterke aanwijzingen gevonden dat de differentiële response in het prestress protocol een opmerkelijk ongevoeligheid vertoond voor vloeistofachtige of plastische deformaties. Dit toont aan dat de niet-lineaire response van dit soort biopolymeernetwerken robuust is, zelfs als het netwerk vloeit. Om inzicht in dit gedrag te verkrijgen hebben wij een eenvoudig doch zeer algemeen fenomenologisch model ontwikkeld dat zowel de niet-lineaire als de vloeistofachtige eigenschappen van het netwerk bevat.

In hoofdstuk 6 bestuderen wij de elasticiteit van wanordelijke fiber netwerken. Dit soort netwerken, die onder andere het cellulaire cytoskelet of de extracellulaire matrix vormen, zijn ondanks hun opmerkelijk lage connectiviteit rigide. Deze mechanische stabiliteit valt ten dele te danken aan de weerstand van de fibers tegen verbuigingen. Wij hebben wanordelijke netwerken onderzocht met variabele connectivititeiten, zowel onder als boven het centrale-kracht isostatische punt. Dit is de minimale connectiviet waarbij een netwerk van elastische veren mechanische rigiditeit vertoond. Wij laten zien dat dit punt een overgang bepaald tussen elastische regimes die ofwel door filament buiging- of wel filament strek-deformaties gedomineerd worden. Deze overgang wordt gekenmerkt door een atypische afhankelijkheid van de stijfheid van het network op de rek en buig moduli van de fibers. Bij het centrale-kracht isostatische punt—dat veel hoger ligt dan de rigiditeitsdrempel—nemen wij divergerende relatieve deformaties waar met een bijbehorende divergente correlatielengteschaal. Dit impliceert dat op dit punt het systeem zich op de macroscopische schaal niet meer gedraagt als een continuüm elastisch lichaam. Kortom, in dit eenvoudige mechanische systeem nemen wij een opmerkelijk rijke diversiteit aan niet-thermische kritische fenomenen waar.

In hoofdstuk 7, bespreken wij de effecten van kracht genererende motoreiwitten op de mechanische eigenschappen van netwerken van stijve polymeren. Gereconstrueerde *actieve* F-actine netwerken met motoreiwitten vormen een goed modelsysteem voor cellulaire mechanica. Motoreiwitten genereren krachten die het netwerk uit thermisch evenwicht drijven en die de netwerkmechanica sterk beïnvloeden. Om de onderliggende principes die tot dit laatste gedrag leiden boven water te krijgen, hebben we een methode ontwikkeld die gebruik maakt van wanordelijke netwerken die op roosterstructuren geconstrueerd worden, met een connectivieit van 4 of minder, om de architectuur van biopolymeer netwerken met binaire kruisverbindingen na te bootsten. Hiermee hebben wij aangetoond dat heterogene stressen die door motors gegenereerd worden, leiden tot een sterke verandering in de stijfheid in netwerken die door filament buigdeformaties gedomineerd worden. De motoreiwitten worden gemodelleerd als krachtdipolen die spierachtige contracties teweegbrengen. Deze contracties trekken de zachte deformatie modes uit het systeem en zorgen er zo voor dat de stijfheid van het netwerk sterk toeneemt.

In hoofdstuk 8, onderzoeken wij de oorsprong van de elastische eigenschappen van netwerken van intermediate filamenten (IF). IF netwerken in het cytoplasma en de celkern zijn cruciaal voor de mechanische integriteit van metazoan cellen. Hoewel F-actine en microtubili uitgebreid onderzocht zijn, is er veel minder bekend over IFs. In het bijzonder is het mechanisme waarmee IF netwerk kruisverbindingen vormen en rigide worden slecht begrepen. In een nauwe samenwerking met de experimentele groep van Dave Weitz hebben wij aangetoond dat divalente ionen een kruisverbindingsinteractie mogelijk maken tussen de negatief geladen staartdomeinen van IFs. We maken gebruik van een affien model voor de niet-lineaire elastische respons van deze systemen dat zowel het niet-lineaire entropische rekgedrag als de enthalpische strek van de individuele filamenten omvat. Dit model heeft het mogelijk gemaakt om microscopische parameters te bepalen uit het macroscopische rheologische gedrag zoals de Young's modulus en de persistentie lengte van de filamenten en de lengteschaal van kruisverbindingen in het netwerk.

Acknowledgements

It is a great pleasure to finish this thesis by thanking the numerous people who I had the privilege to work with. I would need another two hundred pages of acknowledgments to do justice to all the help I received for my research. I will nonetheless try and keep it brief and limit it to the core group of people that contributed to this thesis and that provided some essential support along the way.

Fred, I would need a fair share of those two hundred pages to give a comprehensive account of all the things I should be thanking you for. To spare you some embarrassment, I will limit it to expressing my gratitude for your generosity in the broadest sense of the word. You have always encouraged and supported me to do whatever research I felt like, regardless of where or with whom. You encouraged me to go to an insane amount of international meetings and to spend a lot of time getting my hands dirty in Dave's lab. In matters concerning me, you always acted in my best interest, which I believe is a unique quality that I greatly appreciate. Thanks for letting me be a part of the diverse and inspiring research environment in your group and its links to, among others, the COSY group, the Koenderink group and the Weitzlab.

Moumita, Darina, Enrico, Kees, Chris, Martin, Albert, Misha and Fred, I would like to thank you for the great atmosphere in our "lab" and for being the colorful personalities that you are. We had such good times and the greatest scientific and nonscientific discussions. Enrico, your sense of humor, general enthusiasm and ideas live on in all of us. Mo, you inspired me with your enthusiasm for science, movies and books. Kees, even though you were largely located elsewhere and our overlap was brief, it was great fun and it had a large impact on my first endeavors in this field that lead to two chapters of this thesis. Special thanks also go out to Martin. We had/have such fruitful and brutally heated marathon blackboard discussions (sometimes going on for weeks on end) where you displayed your fearless and uncompromising attitude to any problem in physics. This work resulted in one of my favorite chapters of this thesis. Misha and Mo, although the fruits of our joint labor weren't finished in time to appear in this thesis, they will surely appear soon somewhere. Misha, the Russian-Israeli style you introduced to our group is wonderfully refreshing.

Dave, I would like to thank you for your hospitality and generosity in hosting me in your group. I think it is an essential part of the training of any serious theorist to spend some time in a real lab and there is really no better environment for that than the Weitzlab. If anything broke in the lab during this period - it wasn't me. I've got at least 200 people in the Weitzlab to thank but I would like to mention especially Karen, Norm, Yi-Chia, Lolo, Stefan, Hans, Kosta, Amy and Rodrigo (best barbecue on the northern hemisphere). Karen, thanks for introducing me to the mysterious arts of rheology and for the great collaboration on the filamin project that resulted in 2 chapters of this thesis. Yi-Chia and Amy, it was a great pleasure to work with you both on the intermediate filament projects, which resulted in one chapter of this thesis. Big Norm, apart from the great collaborations that lead to two thesis chapters, I would like to thank you for introducing me to the fine Chinese cuisine and for the epic adventures we had in Les Houches, New-York and Asiadam. You also provided a warm shoulder to cry on at the end of one of the darkest days in Dutch history - world cup finals 2010. Stefan and Lolo, thanks for always providing a warm home away from home when I am visiting the States. The discussions, the soccer games, the culinary delights we enjoyed and our road trips through the USA and Germany made up some of the best times of my PhD. Also, our scientific collaborations resulted in one chapter of this thesis and contributed to ideas and insights that are discussed in several other chapters.

I would also like to thank the Koenderink group. At times it felt like our group was partially entangled with yours, which lead to inspiring group meetings and many other fun interactions. Especially I would like to thank Iza, Karen, Bjorn, Marina, Jose and Gijsje for all our scientific and nonscientific interactions. I would also like to thank the COSY group for having us join in on your groupmeetings and for the good atmosphere and great coffee in the coffee room downstairs. The atmosphere upstairs in our corridor has also always been inspiring and lively thanks to our highly energetic fellow theorists. I would like to thank especially, Ted, Thijs, Jorn, Thomas, Wilco, Ben, Klaas, Taco, Daniel and Piet. Special thanks also go out to Marja for making VU bureaucracy seem simple and transparent. I would also like to thank Piet Blankert and the FEW for financial support that enabled various long research visits to the States. I've also very much enjoyed the interaction I had with the biophysics groups at Leiden University. I would like to thank Liesbeth for great chats about philosophy, life and the (non)affinity of biopolymer networks at the various meetings and schools we attended together. Tom and Xiaoming, our collaboration over the past year turned out to be very fruitful and inspiring and I thank you both for that.

I would like to thank my family and other friends. Itan and Sven, thank you for helping me out with programming problems and for the challenging, fun and inspiring discussions on any topic, especially the high-altitude discussions on the slopes of the Alps. Sven, the whole MacKintosh group is in your depth for helping us build up our computing facilities. Very warm thanks also go out to my parents, Barry, Anne, Sacha, Sterre, David, Hanneke, Niels, Trudy, Inge, Mathijs, Anna, Michiel and Raïna for their endless support and encouragement. I would like to thank Niels especially for designing the cool cover of my thesis.

Most importantly, I would like to thank Kirsten. You support me all the way from Amsterdam to Oslo, to Boston, to Princeton and beyond. I thank you for your sweetness, your encouragement, your fearless attitude in joining me in exploring the world, for your unconditional and endless patience to put up with me and the large amount of time and energy that I choose to dedicate to science and for so much more.

Curriculum Vitae

Chase Paul Broedersz was born on April 12, 1984 in Johannesburg, South Africa. He moved to the Netherlands at the age of three. After receiving his Atheneum high school degree (JSG Maimonides, Amsterdam, 2002) he started his physics studies at the Vrije Universiteit in Amsterdam. There, he performed his undergraduate research in the condensed matter physics group of prof. dr. Ronald Griessen (2005-2007) where he investigated hydrogen switchable mirrors. During this period, he contributed to the development of Hydrogenography, a high throughput optical screening method for metal based hydrogen storage materials. The theoretical component of this research was performed at the University of Oslo with Dr. Ole Martin Lovvik (2007). In Oslo, Chase performed density functional theory calculations to investigate the electronic properties and stability of complex metal hydrides. He received both his BSc (2005) and MSc (2007) degrees *Cum Laude*.

After completing his undergraduate studies in hard condensed matter physics, his interests shifted towards soft matter physics and the physics of life. He joined the group of prof. dr. Fred MacKintosh at the Vrije Universiteit as a PhD student in theoretical physics to study biopolymer gels (2007-2011). During this period he spent six months in the lab of prof. dr. Dave Weitz at Harvard University. There he performed experiments and worked closely with experimentalists to test and further develop theoretical models. His graduate research spans over a range of topics, from the dynamics and nonlinear elasticity of cytoskeletal biopolymer networks such as F-actin and intermediate filament networks to the basic properties of the elasticity of random fiber networks. The results of these studies have been described in this thesis and in various international peer-review journals.

In September 2011 Chase will take up a 5 year position as a theory fellow in the Lewis-Sigler Institute for Integrative Genomics and a lecturer in the Physics department at Princeton University.

List of publications

18 N. Y. Yao, D. Becker, C. P. Broedersz, M. Depken, M. R. Pollak, F. C. MacKintosh and D. A. Weitz
Nonlinear Viscoelasticity of Actin Cross-linked with Mutant α-Actinin-4
Under review (2011)

17 C. P. Broedersz, X. Mao, T. C. Lubensky and F. C. MacKintosh
Criticality and isostaticity in fiber networks
arXiv:1011.6535, under review (2011)

16 C. P. Broedersz and F. C. MacKintosh
Molecular motors stiffen non-affine semiflexible polymer networks
arXiv:1009.3848, accepted for Soft Matter (2011)

15 C. P. Broedersz, M. Depken, N. Y. Yao, M. R. Pollak, D. A. Weitz and F. C. MacKintosh
Cross-link governed dynamics of biopolymer networks
Physical Review Letters, **105**: 238101 (2010)

14 C. P. Broedersz, K. E. Kasza, L. M. Jawerth, S. Muenster, D .A. Weitz and F .C. MacKintosh
Nonlinear rheology of cross-linked biopolymer gels
Soft Matter **6**, 4120 (2010)

13 Y. C. Lin, C. P. Broedersz, A. C. Rowat, T. Wedig, H. Herrmann, F. C. MacKintosh and D. A. Weitz
Divalent Cations Crosslink Vimentin Intermediate Filament Tail Domains to Regulate Network Mechanics
Journal of Molecular Biology **399**, 637-644 (2010)

12 N. Y. Yao, C. P. Broedersz, Y. C. Lin, K. E. Kasza, F. C. MacKintosh and D. A. Weitz
Elasticity in ionically cross-linked neurofilament networks
Biophysical Journal **98**, 2147-2153 (2010)

11 Y. C. Lin, N. Y. Yao, C. P. Broedersz, H. Herrmann, F. C. MacKintosh and D .A. Weitz
Origins of elasticity in intermediate filament networks
Physical Review Letters **104**:058101 (2010)

10 K. E. Kasza, C. P. Broedersz, G. H. Koenderink, Y. C. Lin, W. Messner, E. A. Millman, F. Nakamura, T. P. Stossel, F. C. MacKintosh and D. A. Weitz
Actin filament length tunes elasticity of flexibly crosslinked actin networks
Biophysical Journal **99**: 1091 (2010)

9 R. Gremaud, C. P. Broedersz, A. Borgschulte, M. J. van Setten , H. Schreuders, M. Slaman , B. Dam and R. Griessen
Hydrogenography of $Mg_yNi_{1-y}H_x$ gradient thin films: Interplay between the thermodynamics and kinetics of hydrogenation
Acta Materialia **58**, 658-668 (2009)

8 C. P. Broedersz, C. Storm and F. C. MacKintosh
Effective medium approach for stiff polymer networks with flexible cross-links
Physical Review E **79**, 061914 (2009)

7 K. E. Kasza, G. H. Koenderink, Y. C. Lin, C. P. Broedersz, W. Messner, F. Nakamura, T. P. Stossel, F. C. MacKintosh and D. A. Weitz
Nonlinear elasticity of stiff biopolymers connected by flexible linkers
Physical Review E **79**, 041928 (2009)

6 C. P. Broedersz, C. Storm and F. C. MacKintosh
Nonlinear elasticity of composite networks of stiff biopolymers with flexible linkers
Physical Review Letters, **101**: 118103 (2008)

5 C. P. Broedersz, R. Gremaud, B. Dam, R. Griessen and O. M. Lovvik
The highly destabilized Mg-Ti-Ni-H system investigated by density functional calculations and hydrogenography experiments
Physical Review E **77**, 024204 (2008)

4 R. J. Westerwaal, C. P. Broedersz, R. Gremaud, M. Slaman, A. Borgschulte, W. Lohstroh, K. G. Tschersich, H. P. Fleischhauer, B. Dam and R. Griessen
Tuning the electrical, structural and optical properties of in-situ grown MgH2 thin films by activated reactive evaporation
Thin Solid Films **516**, 4351-4359 (2008)

3 R. Gremaud, C. P. Broedersz, D. Borsa, A. Borgschulte, P. Mauron, H. Schreuders, J. H. Rector, B. Dam and R. Griessen
Highly destabilized Mg-based hydrogen storage materials identified through combinatorial screening
Advanced Materials **19**, 2813 - 2817 (2007)

2 B. Dam, R. Gremaud, C. Broedersz and R. Griessen
Combinatorial thin film methods for the search of new light-weight metal-hydrides
Scripta Materialia **56**, 853-858 (2007)

1 R. J. Westerwaal, M. Slaman, A. Borgschulte, C. P. Broedersz, D. M. Borsa, W. Lohstroh, B. Kooi, G. ten Brink, K. G. Tschersich, H. P. Fleischhauer, B. Dam

and R. Griessen
Optical, structural, and electrical properties of Mg2NiH4 thin films in-situ grown by activated reactive evaporation
Journal of applied physics **100**, 063518 (2006)

Manuscripts in preparation

- *Stress enhanced gelation in cross-linked actin networks,*
  with N.Y. Yao, D.A. Weitz, M. Depken and F.C. MacKintosh.
- *Elasticity of sub-isostatic ordered and random polymer networks,*
  with M. Das and F.C. MacKintosh.
- *Mechanics and dynamics of transiently cross-linked biopolymer networks,*
  with M. Depken and F.C. MacKintosh.
- *Elasticity of diluted super-isostatic lattices of stiff filaments in 2D and 3D,*
  with M. Sheinman F.C. MacKintosh
- *Effective medium approach for the nonlinear elasticity of disordered networks,*
  with M. Sheinman F.C. MacKintosh